SPATIAL MODELLING IN PLANT ECOLOGY

Ruth Juliet Hendry B.A. (Cantab)

Thesis to be submitted for the degree of Doctor of Philosophy

University of Warwick

Ecosystems Analysis and Management Group

Department of Biological Sciences

and

Interdisciplinary Mathematics Research Program

Mathematics Institute

University of Warwick

Coventry CV4 7AL

September 199ff

Contents

List of Figures

List of Tables

Acknowledgements

I would like to thank my supervisors Jacquie McGlade and David Rand for the time they have devoted to me over the last three years.

I would also like to thank:

- John Marshall, Catherine Wattebot, Ros Ball and Steve Gaito - for all their support with the computing;
- Matt Keeling - for collaboration on the length scale technique of section 2.1.5;
- Laurence Benjamin and David Aikman - for providing the carrot data and for discussions on chapter 3;
- Jake Weiner - for discussions on plant monocultures and for co-authoring the paper based on chapter 3;
- Philip Bacon, Robert Moss and Xavier Lambin - for numerous discussions on grouse, both at Warwick and at ITE Banchory;
- Christian Wissel - for comments on the forest model;
- Igor Mezic - for discussion on the one-dimensional model in chapter 8;
- Alistair Jolliffe - for looking after the cat.

I would also like to thank my husband Jeremy, my parents, my sisters Helen and Katie, my parents-in-law and, finally, Pippa the cat for their support over the past three years.

Declaration

This thesis is the results of original research conducted by myself, unless stated otherwise in the text or acknowledgments, under the supervision of Professor Jacqueline M. McGlade and Professor David A. Rand. All sources of information have been specifically acknowledged.

No part of this thesis has been submitted for a degree at any other university.

Chapter 3 is soon to be published as:

Hendry, R.J., McGlade, J.M. & Weiner, J. A coupled map lattice model of the growth of plant communities. *Ecological Modelling* **(in press).**

Chapter 7 has been published as:

Hendry, R.J. & McGlade, J.M. 1995 Memory in ecological systems. *Proceedings of the Royal Society of London* **B 259:153-159.**

Parts of chapters 3 and 7 have been reproduced in:

McGlade, J.M. 1995 Dynamics of complex ecologies. In: Dynamical phenomena in living systems. ed. Mosekilde, E. & Mouritsen, O.G. pp. 251-268. Series on Synergetics, Springer, Berlin.

and chapter 7 is summarised in:

Rand, D.A. 1994 Measuring and characterizing spatial patterns, dynamics and chaos in spatially extended dynamical systems and ecologies. Philosophical Transactions of the Royal Society of London *A 348:497-514.*

Abbreviations

AE	artificial ecology
CA	cellular automaton
CLT	central limit theorem
CML	coupled map lattice
DNA	deoxyribonucleic acid
FRS	fighting rank strength
IBM	individual-based model
MRCI	mean relative clumping index
RCI	relative clumping index
RD	reaction-diffusion
RGR	relative growth rate
SEIR	susceptible-exposed-infectious-recovered
SIC	sensitivity to initial conditions
SIR	susceptible-infected-recovered
SIS	susceptible-infected-susceptible
SLA	specific leaf area
SVD	singular value decomposition
ULR	unit leaf rate
ZOI	zone of influence

Summary

In this thesis a range of lattice-based spatially explicit models of ecosystems are presented and their applicability to various ecological situations is demonstrated, with emphasis on plant communities. These mechanistic and individual-based models, which include coupled map lattices and cellular automata, aim to produce ecological insights and testable results. Models of both short and long term systems are developed, with the former being potentially testable in the field and the latter promoting understanding where experimentation is not feasible. A range of graphical and numerical techniques were developed to investigate both plant and animal model ecosystems.

The starting point is a short term single species coupled map lattice, which investigates population structure arising from local competitive interactions. The model concludes that increase of size variation with increasing density indicates the presence of competitive intraspecific asymmetry. This idea is applied to crop data, where considerable asymmetry is identified, emphasising the need for balancing crop yield and size consistency.

Multispecies extensions to this model focus on spatial patterning arising from biotic interactions and various numerical techniques underline the asymmetrical relationship between long- and short-lived species. Environmental heterogeneity is imposed on the plant species in a third version of the model via the incorporation of an explicit resource base. The complex interdependence of community and environment is highlighted and illustrated by a model of the evolution of seed sizes.

Through the application of cellular automata to forest and epidemiological systems, the concept of memory, such as age- or stage-structuring, is shown to be vital in the generation of spatial structure in long term ecological systems. Analytical investigations generate further insights and again emphasise the crucial role played by spatial extensiveness in the wide range of ecological situations considered here.

In conclusion, lattice models are ideally suited to the study of ecosystems.

1. Introduction to Ecosystem Modelling.

Chapter Summary

A brief historical overview is given of theoretical ecology and modelling in the twentieth century, which leads into a discussion on the subjects of scale, dynamics, nonlinearity and complexity. These are all considered to be fundamental features of ecological systems. A summary of modelling approaches used in the thesis is set out, which in particular addresses the importance of generality in modelling, the importance of individuals in ecology and the importance of the spatial dimension in ecology. A preference is stated for simple mechanistic models that promote understanding as opposed to detailed phenomenological models that are restricted to narrow predictive uses. A brief description is given of the models in chapters 3 to 7 and suitable theoretical approaches are outlined, in conjunction with a discussion on relevant spatial and temporal scales.

1.1. Overview of Descriptive Ecology.

'The aim of science is general statements' - Wissel 1992b

Ecology, as the study of the relationship of living organisms and their associated environments, has largely been dominated by descriptive techniques, empirical data collection and the classification of species and processes. As speculative hypotheses lacking support by extensive data were largely seen as controversial, most studies have demanded intensive experimental work, but the last few decades have witnessed the rise of theoretical ecology - recognition that models can be used to suggest fruitful empirical investigations. This contrasts with the classical ecological approach, where a model is purely phenomenological, constructed from pre-existing data; mathematical approaches being largely restricted to statistics.

The main focus in both empirical and theoretical ecology has been on the dynamics of single and multi-species populations and, more recently, as indicated in this thesis, of individual organisms. The original theoretical description of population growth was the *logistic equation*, by Pearl in 1920 (Kingsland, 1991), which described constrained exponential growth. This simple approximation of the development of single populations has remained central to theoretical ecology, despite being acknowledged as having restricted direct applicability. In particular it initiated a major revolution in scientific thought in the 1970s (section 2.2.2), following May's (1974) observation of complex behaviour or *chaos* arising from the logistic equation.

Multi-species population interactions were described quantitatively in the 1920s by Lotka (1920) and Volterra (1926). Both authors described predator-prey interactions which exhibited cycling (the Lotka-Volterra system) and Volterra also considered two-species competition. This system provided the basis for a large proportion of subsequent theoretical ecology and has over many years been endlessly refined and extended.

However, the constraints of such simple approaches have been increasingly pointed out in more recent years and the importance of spatial dimension has been highlighted, together with the associated issues of patterns and scaling[1].

Most organisms are profoundly influenced by the heterogeneity of the biotic and physical environment, especially in terrestrial ecosystems (Hanski, 1994a). Environmental heterogeneity is seen at all scales from microscopic to global so that any organisms have to respond to patterns over a range of scales.

Although many features vary gradually and boundaries between different regions are often highly diffuse, the heuristic term *patch* is usefully employed to describe an area of space that is different from the surrounding areas in some specified way. As discussed later in more detail in section 1.3.4, adequate spatial representation of patchiness, pattern and scale is now a central

[1] Clark & Evans, 1955; Levin & Segel, 1985; Huston et al., 1988; Wiens, 1989; Levin, 1990; Menge & Olson, 1990; Kolasa & Pickett, 1991; Bradshaw & Spies, 1992; Levin, 1992; Garcia-Moliner et al., 1993; Levin et al., 1993; Moloney et al., 1992; Hanski, 1994a; Steele & Henderson, 1994.

theme in ecological modelling research. Patchiness may be seen at any scale and assumptions concerning distributions and their underlying causal mechanisms cannot be inferred between scales. A system must therefore be studied across an entire range of scales before a complete understanding of its functioning can be obtained (Breckling, 1992). A region may, for example, be relatively homogeneous at an intermediate scale, yet simultaneously demonstrate fine scale patchiness and form one patch of a broad scale distribution of patches. Therefore assumptions must not be made about the behaviour of a system simply by noting the homogeneity or heterogeneity at one particular scale.

Ecological scale is a perceptual concept that is influenced by observation, by an ecologist or by any organism within an ecosystem (Levin, 1992). The response of an organism to environmental heterogeneity depends both on its size and behavioural repertoire. The relative sizes of organisms and environmental scales is termed *grain* or *resolution* and is the key to understanding the interaction of individuals with physical factors. The scales influencing species may vary within its life cycle. For example, some animals forage within small areas of relative homogeneity but move over large patchy landscapes to breed. In contrast, obtaining sufficient nutrition may depend on moving between isolated fertile patches scattered within hostile terrain. Even plant species operate over various scales: the sessile nature restricts adults to a single position, but dispersal of propagules and clonal spread may both integrate resources over patchy regions (chapter 5).

There is a complex interwoven relationship between organisms and environmental patterns, with animals and plants interacting with the environment to create or enhance patterns (Levin & Segel, 1985): ecological processes determine pattern and patterns determine process. Patterns can be generated from pure heterogeneity through biotic interactions - pattern or non-randomness is an *emergent phenomenon* (sections 1.2 and 2.1.6). Pattern is seen to emerge from a balance of ordering mechanisms with randomising processes (chapter 7).

There is also a two-way interaction between different scales: local mechanisms can produce emergent patterns at a broader scale, despite apparent microscale randomness (McCauley et

al., 1993). On the one hand, coarse-grained heterogeneity can impose constraints which cascade down to fine-scale processes. Alternatively, processes may act directly over a range of scales (Bak & Chen, 1990), which again highlights the need for multi-level analysis of ecosystems (Ricklefs, 1990; Moloney, 1993).

Temporal and spatial variation are hard to separate, so temporal scales must be also considered. Although patchy structures, especially at the landscape scale, may persist for centuries, many features at a variety of scales are ephemeral. Species are often adapted to compensate for temporal fluctuation of habitat quality by dispersal over spatially heterogeneous areas (section 5.4). Thus the environment and behaviour of organisms are strongly influenced by temporal as well as spatial variation and all of these factors are interdependent in a complex way.

The major challenge in theoretical ecology is the assessment and interpretation of the consequences of spatial and temporal variation on the distributions of resources and organisms. This has led to the developments of new methodologies, both experimental and analytical, which can address the issues of spatiotemporal heterogeneity and scaling. Such techniques are described and applied in chapters 2 to 7. Spatial heterogeneity is studied using the *clumping index* (section 2.1.6) which gives a dynamic quantification of the patchiness in a system. A second approach employs *multifractal theory* to identify complex scaling relationships within spatial distributions. Spatial scales are studied using the *coherence length scale*, which indicates the scale at which the dynamics in a model progress. These methods are all combined to described the patterns in communities and to elucidate the interactions between species.

In summary, there are two complementary challenges in ecology: the extraction of mechanisms from observed patterns and the prediction of patterns from known processes. Much classical ecology has tackled one or other of these aspects, but it is now recognised that pattern and function are so tightly coupled that they must be considered together.

1.2. Dynamics of Ecological Systems.

'...nonlinear systems are surely the rule, not the exception, outside the physical sciences' - May 1974

The traditional view of ecological systems was essentially static, in spite of the long history of 'population *dynamics*'. Most systems were assumed to either be at equilibrium or moving towards equilibrium; fluctuations were largely disregarded as being noise or measurement error (Turchin & Taylor, 1992). Dynamical aspects of theoretical ecology were primarily concerned with the speed of approach to equilibrium or the rate of recovery after disturbance. Species were assumed to grow until resource limitation set in or external perturbations took place. These sweeping assumptions held regardless of the long-standing empirical evidence of persistent fluctuations in population densities (such as lemmings (Finerty, 1980) or red grouse (Moss & Watson, 1994)), since these were viewed as anomalies by most ecologists.

Ecosystems possess a rich array of possible dynamical behaviours, ranging from the simplicity of a stable equilibrium to the complexity of quasiperiodic and chaotic behaviour. Now that it is generally held that *nonlinearity* or *density-dependence* is widespread in ecological systems, it is no longer assumed that ecosystems must be approaching stationary equilibria occurs.

This has important consequences for the analysis of real and model data, especially the assumption that populations always tend to stationary equilibria. The interpretation of apparently random dynamics must now be re-examined, because disorder is not necessarily the results of random processes such as environmental noise, but may arise from a mixture containing a significant deterministic component. Thus the traditional belief that all ecological processes may be predicted - given sufficient understanding of a system - has been destroyed: in fact, the behaviour of many ecosystems is unlikely to be predictable, even in principle.

this is typical of a chaotic system, which is characterised by limited predictability, an appearance of disorder and intricate geometric structures. A range of situations have been highlighted by theoretical studies which are particularly likely to lead to chaos and nonlinearity, many of which

apply to ecological systems and are discussed in section 2.2.2. Chaos is now a popular concept across a broad range of disciplines (Stewart, 1989a). However, in ecology, chaos theory has some of its harshest critics, as well as some of its most dogmatic sceptics and many enthusiasts (May, 1987).

The new theory has also had a profound impact on ecologists' view of complexity. Ecosystems have always been seen as complicated, often in the extreme, but complex outcomes have traditionally been attributed to complex causes (Procaccia, 1988). External influences have been sought to explain complicated dynamics, such as time lags, environmental stochasticity, population structure and interspecific interactions. Now the reverse is seen: very simple chaotic systems produce intrinsically complex and intricate dynamics and geometries (Green, 1991).

There has been increasing recognition that complex mechanisms can produce simple ordered structures at a larger scale, which contrasts with the complexity that is seen emerging from simple processes. Investigation of such *emergence* has recently become popular, as attempts are made to describe the development of simplicity from disorder. Thus observed simplicity and complexity can both arise from either simple or complex mechanisms - as Cohen & Stewart (1994) state: *'complexity is one of the least conserved properties in the universe'.*

1.3. Modelling Approaches Applied in this Thesis.

'The choice is always the same. You can make your model more complex and more faithful to reality, or you can make it simpler and easier to handle. Only the most naive scientist believes that the perfect model is the one that perfectly represents reality' - Gleick 1987

1.3.1. Introduction.

Before an ecological system is translated into a theoretical model or artificial system, an analysis of known system features must be carried out, along with the questions to be investigated The need for a spatial approach should also be assessed and, as with empirical studies, the relevant scales - both spatial and temporal - determined before a model can be constructed. In conjunction with identification of the scales of the system, the level of aggregation of organisms

in the model must also be chosen, such as individuals or populations. In all respects, the level of detail should be decided.

These issues are summarised in the following sections along with their impact upon individual models and, more broadly, on the field of theoretical ecology.

1.3.2. The Importance of Generality.

'Differences of opinion are obviously possible on the degree to which admittedly over-simplified theoretical models can explain some of the complex observational phenomena to be found in nature' - Bartlett 1957

'Whereas a good simulation should include as much detail as possible, a good model should include as little as possible' - Maynard Smith 1974

The optimal degree of generality in ecological modelling is a subject of considerable controversy. In general there are two possible approaches which are here termed *simulation* and *modelling* (May, 1981). A simulation involves condensing data to provide parameters for a detailed model of a specific situation. The results of the simulation are usually tested against experimental data and may then be used to predict future behaviour or examine other similar scenarios. In contrast, a model is more general and has the aim of investigating mechanisms behind empirical observations and providing a deeper understanding of the ecology.

Many terms are used to describe these alternative approaches. *Simulation* has been applied to both types of study; the terms *strategic*, *predictive* and *descriptive modelling* and *calculation tools* have been used for *simulation*, while *modelling* has been termed *tactical*, *simple*, *abstract*, *conceptual* and *general* [2].

There has been much discussion in the literature about the existence of generality in biology. (There have in fact been disputes about whether any search for generality in ecological studies is a valid enterprise (Bullock, 1994; Judson, 1994b).) The physical sciences are largely based

[2] Maynard Smith, 1974; Carter & Prince, 1988; Murdoch et al., 1992; Wissel, 1992b; Judson, 1994a; Weiner, 1995.

on general laws and the past few hundred years of modern science have involved the search for general and unifying concepts. The great physical laws of the seventeenth to nineteenth centuries, such as Newton's laws of motion and the gas laws, have all been succeeded by more detailed laws (relativity, quantum mechanics and statistical physics). However, they still hold as valid approximations under a wide range of circumstances.

It is not, however, immediately obvious that there are similar general laws governing ecological systems. Ecology is based on living entities: there is still a limited knowledge of the physiology of individual biological organisms; their behaviour and interactions with the biotic and abiotic environment.

Thus detailed mechanistic understanding is fundamentally harder to achieve in biological systems than in physics and chemistry. Nonetheless, the success of large scale physical approximations, such as Newton's laws, despite exclusion of microscopic details, leads to some hope that the equivalent holistic ecological laws, holding under 'normal' conditions and under certain approximations, might be discovered.

The existence of general concepts - at least as approximations - must be assumed, otherwise science itself is simply reduced to a colossal cataloguing endeavour. It is undeniable that some basic and precise rules do exist, for example as Judson (1994a) states, 'individuals always arise from individuals', but since there are more species and interactions than could ever be studied and catalogued, there is a overwhelming need for information about the best general rules that can be given.

There are many reasons for encouraging research into general ecological models. A general model can be simple and comprehensible, so that its results are applicable over a wide domain and provide deep understanding (Weiner, 1995). Models may can be used to investigate the factors causing systems to differ in their behaviours and impossible mechanisms can be quickly eliminated. Models sometimes produce counter-intuitive results and the subsequent investigations can often lead to novel insights into systems. Also, general models are usually straightforward to extend to alternative scenarios, as preliminary results provide new ideas and

insights.

Simulations, on the other hand, tend to be *phenomenological* with little reference to mechanisms. The inclusion of too many details may obscure understanding and restrict applicability to a narrow range of systems (Tilman, 1990; Wissel, 1992b). Thus the value of quantitative predictions from complex simulations must be questioned: highly-parameterised models are not powerful or reliable predictors (Levin, 1992), indeed a few dozen parameters (as is commonly found in ecology) can allow a mathematical prediction to be precisely fitted to almost any data. Thus the overwhelming enthusiasm of many theoretical ecologists for quantitative precision is often misplaced.

Detail in models is often confused with *testability*. Although fitting complicated equations to a data set may appear to be a rigorous methodology, it often only demonstrates the applicability of the mathematical representation, while providing no further biological insights and simple model is often highly testable. Much can be learned from the qualitative patterns produced by basic models (Bence & Nisbet, 1989) and it can sometimes be easier to validate a model in qualitative terms, that is, it is often easier to see that a pattern is intuitively incorrect, compared to assessing a certain error level, because the errors in a quantitative result vary continuously. Accurate prediction by a simulation should not, however, be undervalued; it tends to be clear when a simulation is providing a good description of a particular situation.

In spite of the fact that a model is simple, it may nonetheless capture a large proportion of the biological behaviour underlying an observed dynamic. A basic rule-based approach may offer a more direct and enlightening description of the essential functioning of a biological system than a complex equation-based representation which may be overly dependent on functional form and parametric detail.

On the mathematical side, it is certainly common for models to become highly detailed and involved in mathematical formalities. Although such cases may often have mathematical importance, the relevance to ecology is likely to be minimal (May, 1995). Indeed many of the criticisms of biological simulations also apply to the more mathematical end of the spectrum of

modelling.

Criticisms are also made of abstract biological modelling. Many experimentalists reject models because they have not been (or cannot be) tested in any satisfactory way or because parameters may not have been derived from data (Cousens, 1995). In some cases the variables or parameters of models are not properly defined and may be difficult to relate to actual ecological systems. A lot of the problems primarily arise from inadequate research and communication skills of theoreticians and lack of rigour of written publications. There is also frequent misunderstanding of the purpose of models, which often aim to investigate the impact of fundamental mechanisms. For example, values of certain parameters may not be significant if they do not critically affect dynamical behaviour. Models must not, however, be overly simplistic, as vital heterogeneities may not be observed, such as in the many model systems which change their behaviours substantially when spatial dimensions are added (as seen for example in chapter 7).

A balance must therefore be sought between simplicity and complexity in a model (Albrecht, 1992; Mauchamp et al., 1994). There is a role for detailed simulations in areas such as agriculture and conservation, where predictions to guide environmental intervention and management procedures are needed in the relatively short term. However, there is still a great need for deeper understanding of ecological principles, so that conceptual and abstract modelling has an important place in ecological research.

1.3.3. The Role of Individuals.

'Individual organisms hold, as basic units of ecological systems, more historical and biological relevance than ... more abstract entities' - Villa 1992

It has already been noted that it is possible to describe ecological structure and functioning on many levels, from individuals to the biosphere. Ecologists must select the scale and resolution most appropriate to the questions being asked of their observations and models. Classical ecological theory describes populations and, to a limited extent, multi-species communities. Structure, such as age or size and spatial dimensions has been incorporated in later work

(section 2.3), but the essential uniqueness of the individual is still not recognised fully.

Through theoretical and, more importantly, technological advances there has been an increase in the popularity of individual-based approaches and *individual-based models* (IBM) (DeAngelis & Gross, 1992), which allow the fate of individual organisms to be monitored over various time scales. The individuals may have a range of phenotypic and genotypic parameters and variables associated with them, such as age or size, behaviour and spatial location. Thus systems where the uniqueness of the characters of individuals may be important may be described in this explicit way.

The individual is an appropriate level for modelling for fundamental biological reasons, independent of technical arguments. Biologists know a lot about individual organisms, their behaviours and characteristics. In a simplistic way, the empirical study of individuals is more straightforward than populations and requires fewer initial assumptions prior to experimentation or observation. The advantages and disadvantages of the IBM approach are discussed in more detail later (section 2.3).

1.3.4. The Spatial Dimension.

'diversity in space is often overlooked by ecologists' - Gleason 1926

'most fundamental elements of ecology ... exhibit spatial variation' - Holmes et al. 1994

The overwhelming importance of space in ecology has long been recognised. The fundamental role of space in ecological interactions was first noted in plant ecology, as plants are most easily seen to influence the survival and growth of other nearby plants (Pielou, 1960; Kareiva & Andersen, 1988; Ford & Sorrensen, 1992). Gleason (1926), in a paper much ahead of its time, focused on the importance of both the individual plant and the significance of spatial interaction in plant communities.

Although spatial studies of plants have been carried out for many decades, the emphasis was long restricted to the classification of spatial distributions at fixed times as regular, random

or aggregated[3]. More wide-ranging experimental work and theoretical studies of plant populations eventually appeared, once suitable techniques, and in particular the computational power, became available[4]. The advances towards spatial treatment of plant ecology were followed by similar applications in other areas of ecology (Kareiva, 1990; Tilman, 1994; Kareiva, 1994) such as predator-prey systems[5], host-parasite systems[6] and various competition scenarios[7], as well as other areas of biology, notably physiology and development[8].

The ecological basis for spatial modelling is very strong. The spatial heterogeneity of the terrestrial environment is apparent to a casual observer on almost any scale (Kareiva, 1994).

[3] Thomas, 1951; Clark & Evans, 1955; Pielou, 1960; Mead, 1974; Diggle, 1977; Ripley, 1977; Simberloff, 1979; Ford & Diggle, 1981; Galiano, 1982; Heltshe & Ritchey, 1984; Sinclair, 1985; Sterner et al., 1986; Legendre & Fortin, 1989; Davis, 1993.

[4] Mead, 1966; 1967; Fischer & Miles, 1973; Ford, 1975; Diggle, 1976; Mack & Harper, 1977; Gates et al., 1979; Aikman & Watkinson, 1980; Gates, 1980a; 1980b; Ford & Diggle, 1981; Gates & Westcott, 1981; Waller, 1981; Weiner & Conte, 1981; Barkham & Hance, 1982; Gates, 1982a; Liddle at al., 1982; Weiner, 1982; Watkinson et al., 1983; Wixley, 1983; Cannell et al., 1984; Fowler, 1984; Mithen et al., 1984; Renshaw, 1984; Slatkin & Anderson, 1984; Weiner, 1984; Firbank & Watkinson, 1985; Hartnett & Bazzaz, 1985; Holsinger & Roughgarden, 1985; Pacala & Silander, 1985; Peart, 1985; Silander & Pacala, 1985; Weiner, 1985; Wu et al., 1985; Huston, 1986; Pacala, 1986; Penridge & Walker, 1986; Smith & Goodman, 1986; Schmid, 1986; Crawley & May, 1987; Firbank & Watkinson, 1987; Goldberg & Fleetwood, 1987; Hobbs & Hobbs, 1987; Lepš & Kindlmann, 1987; Mitchell-Olds, 1987; Bonan, 1988; Coffin & Lauenroth, 1988; Hara, 1988; Kenkel, 1988; Moloney, 1988; Robertson et al., 1988; Inghe, 1989; Kenkel et al., 1989a; Miller & Weiner, 1989; Crawley, 1990a; Galitsky, 1990; Gurevitch et al., 1990; Pacala & Silander, 1990; Weiner et al., 1990a; Bonan, 1991; Durrett & Swindle, 1991; Iwasa et al., 1991; Pacala & Weiner, 1991; Wissel, 1991; Czárán & Bartha, 1992; Ford & Sorrensen, 1992; Moloney et al., 1992; Silvertown et al., 1992; Armstrong et al., 1993; Bonan, 1993; Durrett, 1993b; Hochberg et al., 1994; Pacala & Tilman, 1994.

[5] Segel & Jackson, 1972; Comins & Blatt, 1974; Rothe, 1976; Hastings, 1977; Zeigler, 1977; Leung, 1978; Mimura & Murray, 1978; Kishimoto, 1982; Kareiva, 1987; Kareiva & Andersen, 1988; DeRoos et al., 1991; Solé & Valls, 1991; McCauley et al., 1993; Wilson et al., 1993.

[6] Hastings, 1978a; Ludwig et al., 1979; Pacala et al., 1990; Reeve, 1990; Sieburg et al., 1990; Hassell et al., 1991; Solé et al., 1992a; Kretzschmar & Adler, 1993; Hassell et al., 1994; May, 1995.

[7] Horn & MacArthur, 1972; Clifford & Sudbury, 1973; Slatkin, 1974; Shigesada et al., 1979; Mimura & Kawasaki, 1980; Kishimoto, 1981; Pacala & Roughgarden, 1982; Hanski, 1983; Solé & Valls, 1992a; Holmes et al., 1994; Pacala & Tilman, 1994.

[8] Lindenmayer 1968a; 1968b; Waddington & Cowe, 1969; Murray, 1981; Murray & Oster, 1984; Smith et al., 1984; Wolfram, 1984b; Cocho et al., 1987; Grindod et al., 1989.

The various classifications of ensembles of ecological entities, such as populations, communities and species, all frequently display heterogeneous distributions, on a range of scales (Moloney, 1988). The discrete character of individual organisms, together with their interactions, leads to a natural spatial of habitats and resources (Levin, 1992; Tilman, 1994). However, spatial effects extend beyond the biological world, to include geophysical features such as landscape topography, climatic variation and distribution of inorganic resources. These factors, while being essentially physical, are integral components of any ecosystem and are found to interact strongly with the living organisms in communities.

There are two facets of spatial heterogeneity in ecosystems: firstly patchiness or gradients of the external environment and secondly structure generated by intrinsic dynamics. 'Environment' usually refers to physical factors, but in some scenarios biotic features are treated externally, as when vegetation provides a background environment for animal communities. Intrinsic dynamics are concerned with interactions of species and behaviour of individual organisms (Ehrlich, 1961). The two types of spatial heterogeneity have been referred to respectively as *reactive* and *interactive* (Davis, 1993), or as *exogeneous* and *endogeneous* (Clark, 1991). Although the two categories involve different mechanisms, their development is highly interdependent, as shown in the relation of tree species, water distribution and fauna in the forest system described in chapter 7. Thus any ecosystem will be structured by a complex dynamical interweaving of environmental heterogeneity and intrinsic biotic heterogeneity (Ives, 1991; Jetschke, 1992).

The classification into exogeneous and endogeneous mechanisms helps to underline the inadequacies of much spatial ecology. Most ecological studies that claim to tackle space explicitly do so in a very restrictive way (Kareiva, 1990) and only emergent biotic patterns are considered. In a few examples environmental structure is imposed on communities, to study the effects of heterogeneity on the behaviour of organisms, but on the whole there has been negligible investigation of the inter-relationship of reaction and interaction in ecological space.

Shortcomings in theoretical spatial ecology are however far surpassed by those encountered in empirical studies. There is a natural obstacle to the collection of meaningful spatial data:

the amount of information required in most cases is prohibitively large (Kareiva & Andersen, 1988). However, the use of new techniques, including image processing of satellite data and a better understanding of sampling sparse or stochastic systems, will eventually improve not only the availability of data, but also its relevance. The gap between simulated and real data is highlighted in section 3.10.

Through the consideration of space in empirical and theoretical studies, many ecological ideas have had to be readjusted. One such concept is *stability*. Explicit inclusion of space in model systems has frequently been demonstrated to influence stability (Bascompte & Solé, 1994). For example, space has been shown to stabilise host-parasite and predator-prey systems (Pacala et al., 1990; Tilman, 1994). Although stability is a wide-ranging concept with a myriad of definitions (section 7.5.3), it is used here heuristically, in the sense of the ecological stability of real systems. Other concepts are also affected by considering explicitly spatial effects, for example, persistence is facilitated by spatial extensiveness, for example in insect populations; likewise the time to extinction of ultimately unsuccessful species is increased (Huston et al., 1988; May, 1995).

A second commonly-cited result of the addition of explicit spatial variation to models concerns *coexistence*. In Gause's exclusion principle it is stated that two species competing for the same resource cannot both persist; some degree of differential resource usage - *niche* or *resource partitioning* - is necessary for two species to occupy the same habitat. The superior competitor in a particular ecological niche will drive all others to extinction. Through spatial modelling, however, it has been demonstrated that coexistence is easily achieved in a spatially extensive situation[9]. A weaker species can persist by early colonisation in, or by superior migration across, a spatial domain: spatiotemporal heterogeneity can therefore be considered an effective strategy for survival (Müller et al., 1992). Thus space promotes competitive coexistence and hence diversity (Levin, 1974). However, if space is regarded as a *limiting resource* (Solé & Valls, 1992a), then coexistence in space is simply an extension of resource partitioning.

[9] Horn & MacArthur, 1972; Slatkin, 1974; Mimura & Kawasaki, 1980; Crawley & May, 1987; Chesson, 1991; Shorrocks, 1991; Nee & May, 1992; Pacala & Crawley, 1992; Solé et al., 1992b; 1992c.

In section 2.1, the different ways in which space may be represented in models in both the biological and physical sciences is considered in detail. Various labels and classifications of these models have been given in the literature: here the primary subdivision is into *implicit* and *explicit* models. In implicit or *patch* models, space is represented by subdivision of ecological systems as a representation of different regions of space. In contrast, in explicit models, fixed spatial locations are ascribed to individuals or populations. Explicit spatial models may be split into two subclasses: *continuous* and *discrete* models. Space is treated as a continuum in explicit continuous models and thus a partial differential equation representation is used, whereas in discrete models space is dealt with in discrete units. A further division of discrete models may be made into *cellular automata* (CA) and *coupled map lattices* (CML), in which discrete and continuous state variables (such as population size) are respectively used. The background and applications of implicit, explicit continuous and explicit discrete spatial models are described in chapter 2.

1.3.5. Summary.

'Knowledge is one. Its division into subjects is a concession to human weakness.' - Sir Halford John Mackinder 1887

The development of an ecological model depends on its purpose: the degree of generality must be assessed and the suitability of approach (such as individual-based) judged according to the system. The need for implicit or explicit spatial dimensions in a model must also be evaluated and the particular type of model chosen in line with its aims and the scales involved. For example, the scales involved in a boreal forest are represented in figure 1a, which is adapted from Schindler & Holling (1992). Different models will be needed to describe the key processes and phenomena, depending on the particular scales involved in the ecological problem being addressed.

In the case of an annual plant monoculture, described in chapter 3 the model operates over a single growing season, so that the relevant time scales lie between one day and one year. The sessile nature of terrestrial plants and the consequent locality of interactions, together with the

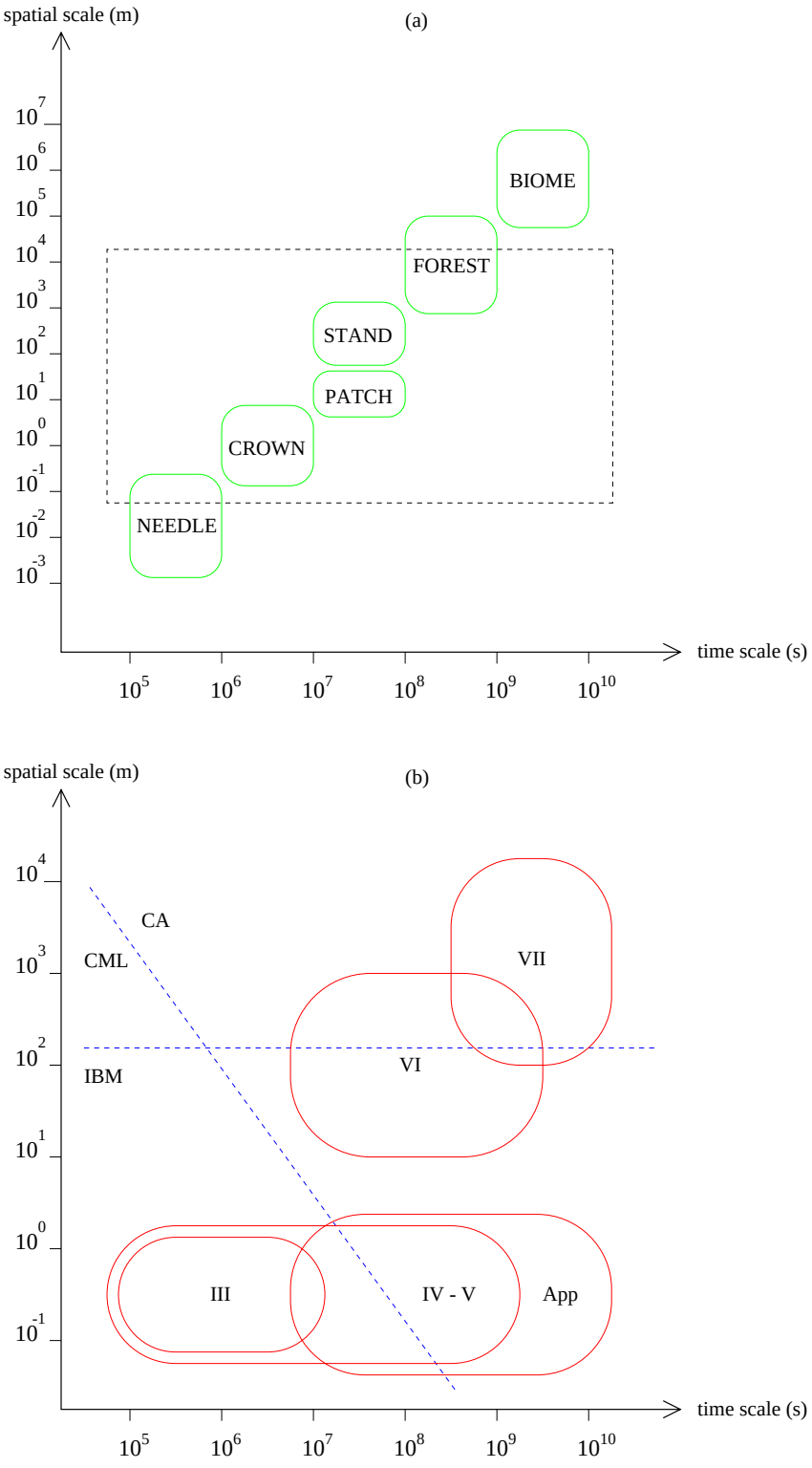

Figure 1: Representation of the spatial and temporal scales. (a) The key scales in a boreal forest ecosystem, adapted from Schindler & Holling (1992). (b) The key scales in the models presented here. The scope of these scales are indicated in (a) (- - -).

Chapter	**System**	**Spatial scale**	**Time scale**	**Species mobility**	**IBM**	**Model type**	**Computation intensity**
3	plant monoculture	small	small	sessile	yes	CML	moderate
4	two species plant mixture	small	large	sessile	yes	CML	high
5	plant monoculture/ mixture with explicit resource heterogeneity	small	small - large	sessile	yes	CML	moderate - high
6	red grouse population	medium	large	motile	yes	artificial ecology (extended CA)	high
7	forest mosaic cycle	large	large	sessile	no	CA	moderate
Appendix A	genetical plant model	small	large	sessile	yes	CA	moderate

Table 1: Summary of the key features of the model systems presented here.

aim of the model to explore the population structure, point to a spatial IBM. A CML allows the size of each individual to be found via a local mapping and the population structure thus quantified.

The annual monoculture model is extended to multiple seasons and two species in chapter 4. The computation is pushed to the limit of the available power by the extension of the time scale, but use of the CML does allow insights into spatial structure to be gained.

An explicit resource base is then added to the plant CML model in chapter 5 and the implications of resource heterogeneity is investigated for the system. The CML is again particularly suited to this, because of both its explicit and discrete treatment of space, which allows straightforward incorporation of environmental heterogeneity. Extension of the model to multiple years again relies on highly intense computation, illustrating the current limit of such modelling. The model is used to examine the correlation of seed size and nutrient availability and is shown to produce clear results in this controversial area.

Other more complex problems can be addressed using CA and their extensions, for example *artificial ecologies* (AE). This latter approach is used to study the territorial behaviour and resulting population dynamics of the red grouse (*Lagopus lagopus scoticus*) and is described in chapter 6. It has been strongly indicated by empirical observation that the spatial distribution of grouse territories is influential on population dynamics, so the grouse system is ideal for a spatial models. Also, since the purpose of the model is to study the territoriality of individual grouse, an IBM is required. The motile nature of grouse, however, requires more than a CA with simple static transition rules; the lattice cells contain individual birds, which can, naturally, move around.

A CA is also used to explore another phenomenon - a forest mosaic cycle, described in chapter 7. The mosaic cycle has local succession events, which point to a spatial model. This system involves far greater spatial and temporal scales than the other models presented here and therefore much less intensive computation per unit space and time is demanded. A CA is thus suggested which involves less computation given sufficiently simple rules. The large spatial

scales rule out an IBM, so the lattice cells of the CA represent particular local communities rather than individual trees.

A model of a plant community incorporating simple genetics is presented in appendix A, which aims to investigate selection operating at different stages of the life cycle. Although some results are spurious, the model provides good illustrations of some aspects of spatial modelling. For example, an AE is needed to enable the long time scales to be simulated, which are needed to allow the observation of the selection of different genotypes. However, the small spatial scales and simple rules allow the model to be an IBM.

The systems and their models are illustrated in figure 1b and are also summarised in table 1. Figure 1b is equivalent to the diagram of scales of Schindler & Holling (1992) (figure 1a) and illustrates the key scales involved in the models presented in this thesis.

The line separating CA and CML provides a good measure of computational intensity, with CML near the line being very intensive; a similar effect is seen for the IBM/non-IBM line. A CML can be used for the plant models of chapter 3 to res because the spatiotemporal scales are relatively short - these are situated near the origin of figure 1. In contrast, the large scales of the forest model of chapter 7and the genetic model of appendix A, which are situated well away from the origin of figure 1, mean that a simpler model must be used. In the case of the forest model, with its large spatial scales, it is not possible to use an IBM.

2. Techniques in Spatial and Nonlinear Ecological Modelling.

Chapter Summary

In this chapter, implicit and explicit models are discussed in more detail and applications of these types of models in ecology and other biological disciplines are reviewed.

The importance of spatial scales is addressed and the coherence length scale introduced, which provides the optimal scale for a lattice model, where maximum information is obtained about the dynamics. Various techniques for the quantification of spatial pattern are described, including the clumping index, a joint-count statistic, introduced as a dynamic measure of patchiness and multifractal theory, which provides a full quantification of complex geometric scaling relationships.

An overview is presented of chaos and nonlinearity theory applied to ecology and a method is described for measuring predictability in a chaotic system by identifying the maximum Lyapunov exponent.

Finally, it is argued that individuals fulfill a unique role in ecological systems and individual-based models are asserted to be important for overcoming unsuitable assumptions, such as perfect mixing in populations. Advantages and disadvantages of the individual-based approach are presented and the conclusion drawn that individuals should be modelled for a wide range of ecological situations.

2.1. Spatial Modelling in Ecology.

2.1.1. Introduction.

'spatial variation is as great or greater than temporal variation in most studies for which suitable

data are available' - Crawley 1990a

In chapter 1 the importance of space was discussed from an ecological perspective and some of the implications of incorporating spatial dimension into theoretical ecology were investigated.

The vital role played by space in modelling can be highlighted mathematically. A non-spatial model possessing a single globally stable equilibrium is clearly unlikely to produce any more interesting results in a spatial context than in the mean field. Once sufficient complexity is added to produce at least two equilibria in the mean field, a model is capable of intricate behaviour when it is extended spatially; the dynamics cannow have a range of possible outcomes, including uniform behaviour involving only one of the equilibria, a stationary pattern combining two or more equilibria and complex cyclic or chaotic spatiotemporal patterns of several equilibria. The existence of multiple equilibria gives an indication that a model should be extended and investigated over a spatial domain. Explicit spatial models exhibit an array of emergent phenomena, unattainable by classical mean field models (Durrett & Levin, 1994a). For example, increasing the spatial domain affects the rates of diffusion and as diffusion can be shown to be a bifurcation parameter, space itself can be viewed as a bifurcation parameter. Increasing the spatial extent of a model can produce bifurcations leading to chaos (Bascompte & Solé, 1994).

The construction and applications of the different types of spatial model introduced in section 1.3.4 are now discussed.

2.1.2. Implicit Space - Patch Models.

'space must be taken into account in all fundamental aspects of ecological organisation' - Solé & Valls 1992a

Patch, *metapopulation* or *island* models are an example of an early technique for representing a spatially extensive species or community[10]. This class of models contains no explicit spatial dimension, but rather consists of identical coupled patches within which subpopulations or subcommunities exist for majority of the time. The patches are linked by a pool of dispersers,

[10] Gadgil, 1971; Hanski, 1989; Hanski & Gilpin, 1991; Hanski, 1994b; Moilanen & Hanski, 1994.

which are extracted from the patches at a specified life stage (figure 2a). Spatial subdivision is thus implicit in the models. The models are based on the assumptions of total mixing and equal accessibility of all patches; fractions rather than distances of dispersal are monitored.

In basic patch models, simple maps or differential equations are applied to the subpopulations, describing average local birth and death rates, plus given levels of dispersal between all patches. Patch models represent ensembles of interacting populations, where global behaviour is governed by the balance between local extinction and establishment (Mangel & Tier, 1993). Dispersal acts to prevent extinction, initiate recolonisation of empty patches and damp global fluctuations. A huge variety of extensions of the basic scheme have been developed, for example where intricate details of local interactions (Hastings & Wolin, 1989; Chesson, 1981) and sophisticated mechanisms of dispersal are modelled (Levin et al., 1984; Cohen & Levin, 1991; Ludwig & Levin, 1991).

Although they can be criticised for being overly simplistic, patch models offer the advantage of being analytically tractable in general. Ecologically significant results have been obtained from patch models in a number of areas of interest, such as the stability of communities. Subdivision has been shown to have various effects on stability in different situations, for example: increased stability in patches[11], decreased stability[12] and stabilisation or destabilisation depending on system parameters (Vance, 1980) have been shown in many studies. For example, a subdivided system stabilises predator-prey interactions (Crowley, 1977) but patches need to fluctuate asynchronously, which requires avoiding very severe coupling. There must be high enough dispersal of both species, but not too high predator dispersal, as stability relies on the prey species avoiding predation when it is rare.

Persistence of species has also been studied with patch models (DeAngelis et al., 1979; Adler & Nuernberger, 1994). Sufficiently large patches are required for persistence (Hanski, 1994a), with enough migration between patches (Reeve, 1990), but not too much (Hanski & Zhang, 1993) -

[11] Crowley, 1977; Zeigler, 1977; Hastings, 1978b; Chesson, 1982; Hastings & Wolin, 1989; Gonzales-Andujar & Perry, 1993.

[12] Hastings, 1977; Kareiva, 1987; Reeve, 1990; Hastings, 1992; Wilson, 1992.

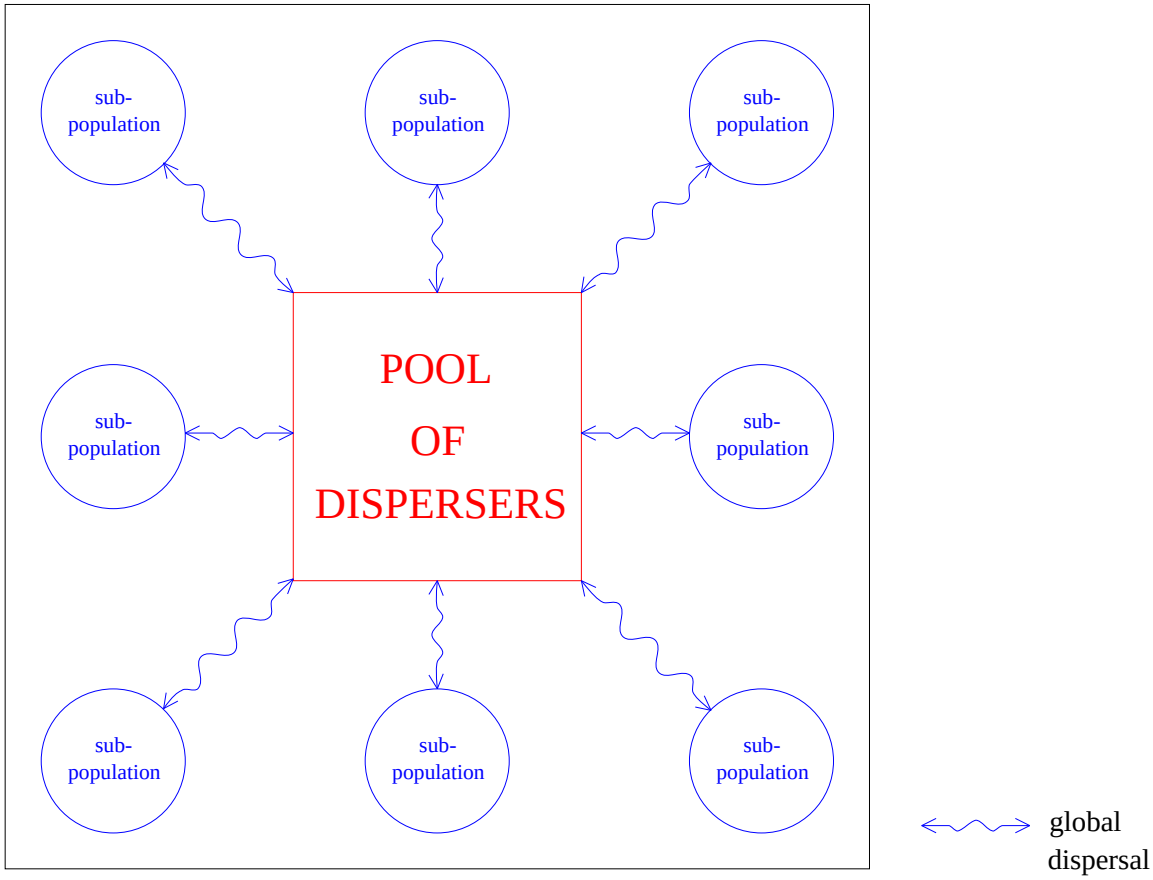
sub-
population
sub-
population
sub-
population
POOL
OF
DISPERSERS
sub-
population
sub-
population
sub-
population
sub-
population
sub-
population
global
dispersal

(a)

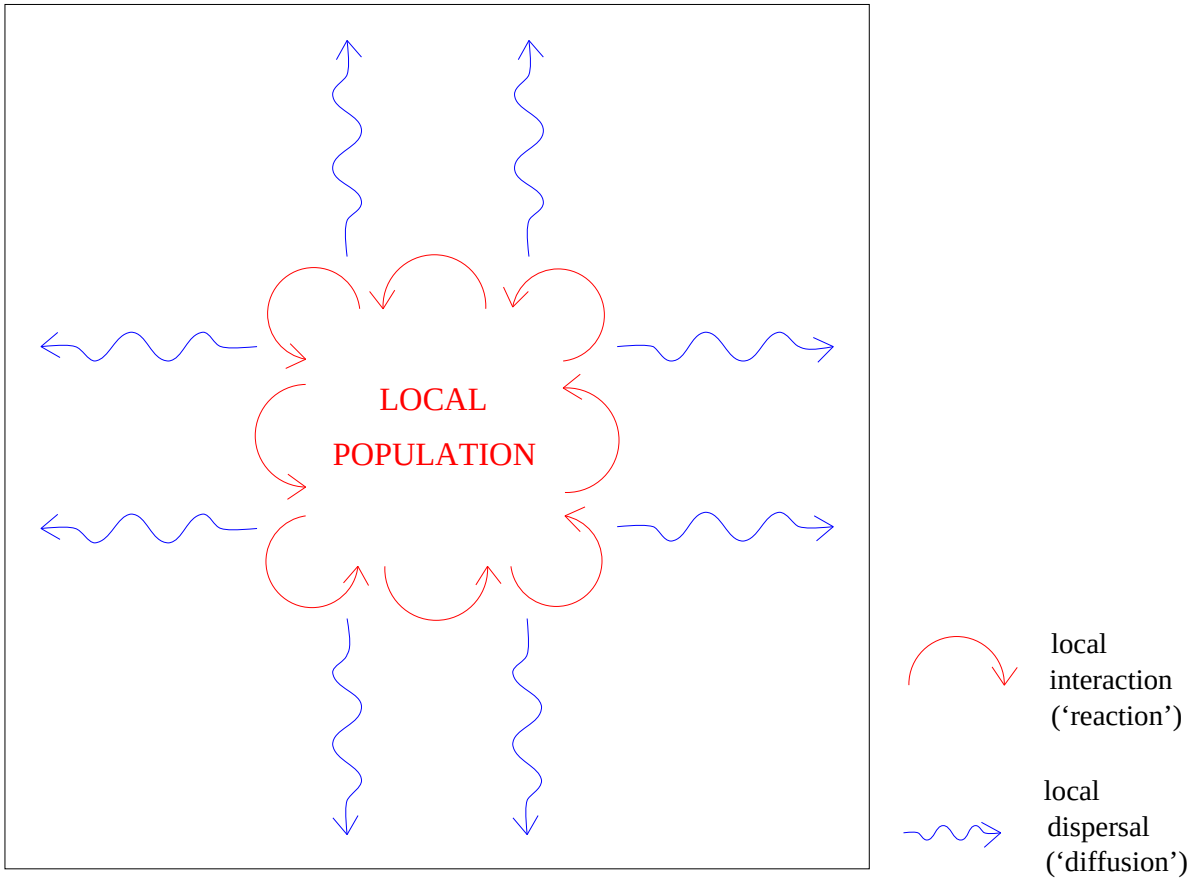
LOCAL
POPULATION
local
interaction
(‘reaction’)
local
dispersal
(‘diffusion’)

(b)

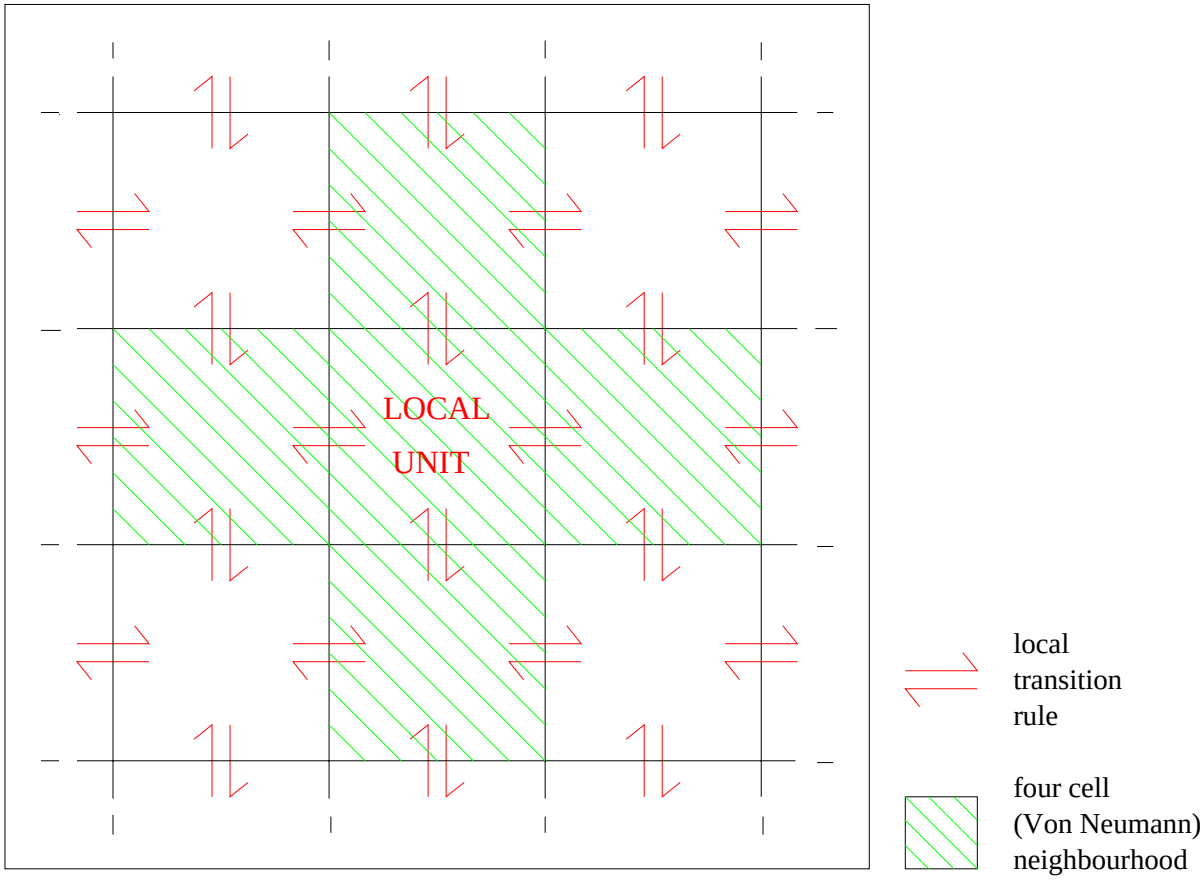
LOCAL
UNIT
local
transition
rule
four cell
(Von Neumann)
neighbourhood

(c)

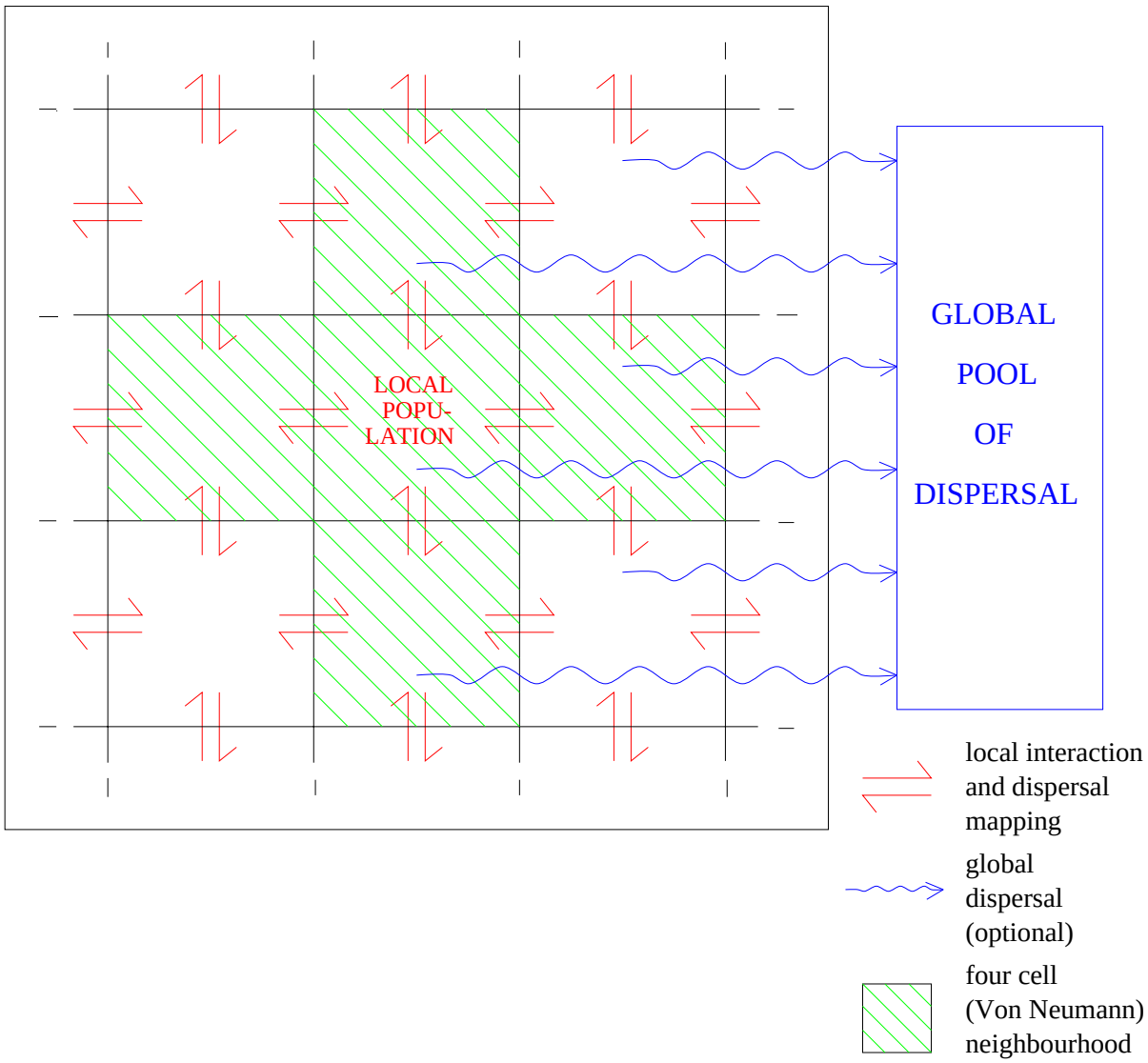

(d)

Figure 2: Representation of different types of spatial model. (a) Implicit or 'patch' model with global dispersal between local subpopulations. (b) Explicit continuous or 'reaction-diffusion' model with local interactions and dispersal. (c) and (d) Explicit discrete models. (c) Cellular automaton with local probabilistic transitions of the local unit type, which may be an individual, subpopulation or local community. (d) Coupled map lattice with a mapping of local interaction and dispersal and possible global dispersal.

corresponding to conservationists' intuition that spatial restriction leads to fragility in ecosystems. The greater tendency of laboratory populations to die while natural populations survive can also be explained by global stability arising through loosely-coupled replicate populations (Taylor, 1990).

Good examples of natural systems which have patchy distributions, such as the white-footed mouse of Fahrig & Merriam (1985), are often studied by conservation biology. this is probably because fragmented habitats - such as ponds and rock pools (Bengtsson, 1989), hill tops, islands (Holt, 1992) and patchy vegetation (Fahrig & Merriam, 1985; Kareiva, 1987) - provide particular challenges in conservation, as demographic stochasticity has a greater impact in subdivided populations and , as has been suggested, the low genetic variability in small populations might lead to greater risk of extinction (Caro & Laurenson, 1994). Patch models have also been used to show that lower collective risk of subdivided populations can in fact lead to more stable communities (Fahrig & Merriam, 1985; Doak et al., 1992).

Following on from the stability of communities is the subject of stable competitive coexistence, which is a popular application of patch models. It has been demonstrated in many spatial studies that an inferior competitor can survive if it is also a good colonisor (Hastings, 1980). Coexistence is allowed by subdivision of the population together with sufficient disturbance of the superior competitor and dispersal of the inferior competitor. It has been shown by single-species patch models that a non-zero proportion of patches may be vacant because of demographic stochasticity. Empty patches or *refuges* are then available for other species that are able to exploit them. Thus subdivision promotes coexistence, or can allow more species to coexist (Hastings, 1980; Wilson, 1992). Models that have been studied include those for predator-prey systems (Hastings, 1977; Leung, 1978), host-parasitoid systems (Pacala et al., 1990; Kretzschmar & Adler, 1993), fungi (Armstrong, 1976), plant systems (Elderkin, 1982; Motro, 1982a; 1982b; Kadmon & Schmida, 1990), competition with coexistence promoted by predation (Slatkin, 1974; Hastings, 1978a), competition with coexistence promoted by environmental heterogeneity (Horn & MacArthur, 1972; Chesson, 1982; Pacala & Tilman, 1994) and competition with coexistence promoted by spatial, temporal and spatiotemporal environmental

variation (Chesson, 1985) or disturbance (Levin & Paine, 1974).

A significant limitation of the patch model concerns scale effects. The construction of a patch model imposes a scale on the system, rather than allowing characteristic scales to emerge as an intrinsic feature (McCauley et al., 1993). The imposed scale may not be appropriate to the system so that intermediate scale effects may not be represented (Caswell & Etter, 1993). By using explicitly spatial models, heterogeneities can arise naturally and the scale of patchy phenomena is determined by the dynamics rather than by being specified.

2.1.3. Explicit Continuous Space - Reaction-Diffusion Models.

'space has a key effect in controlling the dynamics of the populations that diffuse in it' - Bascompte & Soleé 1994

While certain ecological systems are inherently patchy, others, especially marine systems, exist in relatively homogeneous environments or display continuous environmental gradients. Such situations motivate explicit treatment of spatial dimensions. Space as a continuum is modelled by partial differential equations, which are often referred to as reaction-diffusion (RD) systems (Levin & Segel, 1985; Holmes et al., 1994). In ecological terms, the reaction is the local population dynamic and the diffusion is the regional or global dispersal of populations (figure 2b).

The key result of RD theory is the emergence of spatiotemporal patterns by the mechanism of *dispersive* or *diffusive instability.* If a stable uniform equilibrium exists in the absence of diffusion, then spatially inhomogeneous patterns may arise through instabilities driven by diffusion[13]. The necessary conditions for the existence of non-uniform patterns have been addressed in many studies. A class of systems admitting such heterogeneities involve activator-inhibitors (Tsonis et al., 1989), which contain appropriate feedback mechanisms, where the activators and inhibitors are, for example, chemicals or competing species. The original paper addressing this phenomenon concerns morphogenesis (Turing, 1952) and much further work

[13] Segel & Jackson, 1972; Evans, 1980; Cohen & Murray, 1981; Murray, 1981; McLaughlin & Roughgarden, 1991; Maini, 1993a.

with spatial differential equations in developmental biology has subsequently been done[14].

Further applications in physiology include development of feather, shell and scale patterns (Murray et al., 1983; Murray & Oster, 1984; Meinhardt & Klingler, 1987; Cruywagen et al., 1994), animal coat markings[15], cell chemotaxis (Grindod et al., 1989; Murray, 1993a), modelling of the nervous system (Swindale, 1980) and tumour growth (Chaplain, 1993; 1994). Wound healing is also an interesting and highly applicable example of RD modelling. Understanding of the biochemical mechanisms by which wounds are dealt with by an animal has been increased and the optimal geometries for surgical incisions for minimal scarring have been explored with these approaches (Murray & Oster, 1984; Murray, 1993b).

Following on from the studies of spatiotemporal RD patterns in physiology have come ecological RD systems[16], where applications have included predator-prey, plant-herbivore and host-parasite systems[17]. As with patch models, continuum models have produced many results on competitive communities and in particular the promotion of coexistence and stability by spatial extensiveness[18], with results being sensitive to the size of spatial domains. Another example from physiology illustrates this domain dependence well. Pattern formation in mammalian coats has been shown to reflect the size of the animal. As the size increases a transition is seen between uniform colours and spots (Murray, 1993a). Similarly, postulated mechanochemical processes in the model explain the existence of animals with spotted bodies but striped tails, with the need for only a single mechanism acting in the different geometries (Murray, 1993c).

A second phenomenon concerns the existence of spatial wave solutions. These are of two types: travelling waves and kinematic waves (Murray, 1989). Travelling waves result from

[14] Maginu, 1975; Murray, 1982; Murray & Oster, 1984; Murray, 1989, Maini, 1993b; 1994.

[15] Bard, 1981; Murray, 1981; Murray & Oster, 1984; Murray, 1988; Savić, 1995.

[16] Levin & Segel, 1976; Rothe, 1976; Mimura & Murray, 1978; Shigesada et al., 1979; Evans, 1980; Mimura & Kawasaki, 1980; Cohen & Murray, 1981; Kishimoto, 1981; 1982; McLaughlin & Roughgarden, 1991.

[17] Segel & Jackson, 1972; Comins & Blatt, 1974; Levin & Segel, 1976; Rothe, 1976; Mimura & Murray, 1978; Ludwig et al., 1979; Kishimoto, 1982; McLaughlin & Roughgarden, 1991.

[18] Levin, 1974; Hastings, 1978b; Ludwig et al., 1979; Shigesada et al., 1979; Mimura & Kawasaki, 1980; Namba, 1980; Kishimoto, 1981; 1982; Shigesada & Roughgarden, 1982; Murray & Sperb, 1983.

the transition between two stable equilibria of a non-spatial model, which occurs as diffusion or convection is added; kinematic waves arise from coupling of oscillators. A travelling wave moves through space without changing shape, whereas a kinematic wave deforms through space and time. While simple diffusion leads to wave propagation at extremely slow speeds, which do not allow the level of information transfer observed in ecological or physiological systems, the addition of coupled local reaction dynamics increases wave speeds by many orders of magnitude, to realistic biological levels.

A wide range of wave solutions in spatial biological systems have been studied[19]: ecological applications generally concern waves of invasion of species or waves of pursuit and evasion in predator-prey systems, while epidemiology considers waves of disease or pathogens. The standard example of an oscillating system with spatial wave patterns is the Belousov-Zhabotinsky (BZ) reaction, a relatively straightforward chemical reaction which displays intricate spiral wave patterns (Zaikin & Zhabotinsky, 1970; Winfree, 1974; Hagan, 1982; Roux et al., 1981). Specific ecological examples include the spread of the grey squirrel (Okubo et al., 1989), the spread of rabies in foxes (Murray et al., 1986),waves of herbivores (Lewis, 1994). and the activities of colonies of social amoebae, such as the slime mold *Dictyostelium discoideium*, that exhibit spiral waves via chemotactic mechanisms[20].

While most models here involve the emergence of spatial patterns and other phenomena in homogeneous environments, a few studies have considered heterogeneous environments (McLaughlin & Roughgarden, 1991; Shigesada et al., 1979) and environmental gradients (Comins & Blatt, 1974). In addition to its role in the production of patterns in uniform environments, diffusion has been shown to be an amplifier of pre-existing heterogeneities (McLaughlin & Roughgarden, 1991).

[19] Skellam, 1951; Maginu, 1975; Murray, 1975; Britton, 1982a; Dunbar, 1983; Nagai & Mimura, 1983; Murray, 1989.

[20] Keller & Segel, 1970; Britton, 1982a; Hagan, 1982; Monk & Othmer, 1989; Goldbeter, 1993; Martiel, 1993; Höfer et al., 1995.

2.1.4. Explicit Discrete Space - Lattice Models.

'Knowledge of cellular automaton behavior may then yield rather general results on the behavior of complex natural systems' - Wolfram 1984b

RD techniques do, however, have some inadequacies, as local demographic stochasticity is ignored and densities are considered rather than individual organisms and their local spatial correlations. Also, although differential equation techniques can provide precise and sometimes analytically tractable descriptions of ecological systems, non-analytical cases can be computationally intensive. Environmental heterogeneities may be difficult to incorporate in models, even in purely numerical simulations. Often a discrete treatment of space is more appropriate. Any simulation using a digital computer naturally involves the discretisation of all variables, but solutions to a differential equation system aim to minimise effects of discretisation. An alternative approach is to treat discretisation as an intrinsic part of the model, enabling larger systems to be simulated at higher speeds.

As described in section 1.3.4, there are two main classes of such models: *cellular automata* (CA) where space, time and state variables are all discrete and *coupled map lattices* (CML) which have discrete space and time but continuous states. Each consists of a grid or lattice of cells (usually rectilinear, but occasionally triangular or hexagonal[21]) in one, two or more dimensions (Vicsek & Szalay, 1987; Langton, 1990; Solé et al., 1992b), with each cell having a specified state. The cells can represent any level in the hierarchy of biological organisation, from genes (Kauffman, 1969) and cells (Bignone, 1993) through individual organisms (Inghe, 1989) to communities and ecosystems (Wissel, 1991). The states change over discrete time steps, according to the local and global cell state configurations. Thus CML models are basically equivalent to CA models with an infinite number of states. However, the motivation behind the two types of model arise from different sources.

CA are fundamentally rule-based, with certain configurations of neighbouring cell types causing particular transitions of the focal cell state (figure 2c). Early CA were deterministic (Wolfram,

[21] Mead, 1967; Othmer & Scriven, 1971; Kitagawa, 1974; Diggle, 1976; Weiner & Conte, 1981.

1986), with all state transitions depending rigidly on the state space configuration. Later models have tended to be probabilistic, incorporating the demographic and environmental stochasticities of the natural world. Stochasticity in the dynamics is needed to give realistic modelling of ecological systems, but the required generation of random numbers is computationally intensive, so that probabilistic CA are intrinsically slower than their deterministic counterparts. CA rules may be abstractions from more complex mathematical models, via discretisation and aggregation, or alternatively, the rules may be a formalisation of verbal (or *linguistic* (Salski, 1992)) statements of mechanisms.

In contrast to CA, CML consist of local maps, relating a cell state at a given time step to the state of itself and neighbours (and perhaps the state of the whole lattice) at the previous time step (figure 2d). Such maps often arise as a discretisation of ordinary differential equations plus diffusive terms. Early examples of CML consist of small grids of ordinary differential equations or 'reaction and transport processes in groups of intercommunicating cells' (Othmer & Scriven, 1971).

Another source of discrete spatial models is the extension of patch models. In these cases subpopulations are given fixed coordinates in space and local exchanges of populations take place between nearby groups, in contrast to the global dynamics of the implicit patch models. Such models have been termed *stepping stone* models in various papers (Kareiva, 1990; Sawyer, 1979), but these are essentially CML. The state variables of the CML are generally the numbers or frequencies of certain species or other groups at each location. Thus CML are either spatially discrete versions of continuum systems or spatially explicit patch models, whereas CA can be often considered *heuristic* (Ermentrout & Edelstein-Keshet, 1993), being based on a few simple rules and a finite set of states.

Although in some respects lattice models are less precise than RD systems and are largely non-analytical (Caswell & Etter, 1993), they offer many advantages and have many uses. A simple lattice can be used, for example, to rule out impossible mechanisms; this is because a change in CA rules or CML maps may lead to significantly different spatial patterns. Such qualitative

differences may be sufficiently clear to allow identification of essential mechanisms and rejection of incorrect hypotheses. Similarly lattice models may be used for parameter testing, for quick identification of qualitative changes in system behaviour over a range of parameter values (Iwasa et al., 1991; Thi(e)ry et al., 1995). In the words of Caswell & Etter (1993) this type of model 'lays bare the factors determining the dynamics'.

Thus these models are important because they are easy to implement and fast to run, providing rapid feedback. Some authors, however, prefer to view CA and CML as the first stage in simulating complicated natural systems (Ermentrout & Edelstein-Keshet, 1993). Early use of lattices in modelling the physical world did indeed view the discretisation as a rapid approximation for continuum systems. Now lattices are seen as models in their own right and are used both to model specific systems and to promote general understanding (the *paradigm systems* of Hogeweg (1988)).

(a) Cellular Automata.

CA were originally conceived in the 1940s by Von Neumann and Ulam as idealisations of biological systems (Wolfram, 1983). Alternative terms for these models have included *cellular spaces* (Kitagawa, 1974), *tessellation automata*, *cellular structures*, *iterative arrays*, and *automata theoretical models* (Herman, 1969). Early research was focused on the possibility of the existence of self-reproduction and universal computation (Gardner, 1971).

The late 1960s saw the development of the automata game *Life* by Conway (Gardner, 1970). This simple CA consisted of only two states *(on/off)* and a small set of rules governing the birth and death of *on* states, but intricate patterns and complex dynamics were easily observed. These tied in with the concept of *self-organisation*, with simple local components resulting in the emergence of complex global structures (Wolfram, 1984b).

The popularity of automata models shadowed the increased accessibility of computing power. The personal computer revolution was accompanied by widespread interest by individuals in simple models such as *Life*, while the more recent development of supercomputers directed

research into massive CA with many states and complex rules.

By the 1980s the properties of general CA had been described and classified, chiefly by Wolfram and co-workers, first in one (Wolfram, 1984a) and later in two and more dimensions (Packard & Wolfram, 1984; Chaté & Manneville, 1992; Wolfram, 1986). Four universality classes were identified for one-dimensional CA: spatial homogeneity (independent of initial conditions), stable or periodic heterogeneous patterns (strongly dependent on initial conditions), chaotic (aperiodic) patterns and complicated localised patterns (Wolfram, 1984a; 1984b). Similar classifications applied in two dimensions (Packard & Wolfram, 1984).

The fourth universality class is particularly interesting. Also termed *crystal lattice patterns* (Hassell et al., 1991) or simply *complexity* (Judson, 1994a), this type of CA represents sophisticated self-organisation, where regular structures emerge from random initial conditions and complex patterns arise from simple rules. The realisation that CA can generate a 'rich array of complex spatiotemporally organized behaviors' (DeAngelis & Gross, 1992) or 'dramatic global spatiotemporal patterns' (Caswell & Etter, 1993) has led to a gradual increase of interest in CA for both abstract research and detailed ecological simulations.

Nowak and May have emphasised the aesthetic appeal of such lattice models: 'the patterns show every lace doily, rose window or Persian carpet you can imagine' (Nowak & May, 1992; May, 1995). Although undue enthusiasm for aesthetics should be avoided, it is perhaps the similarity of biological and computational patterns that may yet reconcile theory and simulation with empiricism and the natural world. The attraction to the field ecologist of patterns and intricacies in nature must surely arise from instincts similar to those causing geometric patterns in an artificial world to appeal to the theoretician.

The rules of CA are based on a cell *neighbourhood*, which consists of the neighbouring cells of a given *focal cell*. The simplest class of CA have rules which depend only on the sum of the states of the neighbourhood; such *totalistic* CA include *Life*. More complicated systems can involve directional rules, where transitions between states of the focal cell depend on the states of neighbours in specific directions (chapter 7and figure 52).

The neighbourhood used in a CA varies in shape and size. In a two-dimensional square lattice the basic *Von Neumann* neighbourhood consists of the four nearest neighbours (Cocho et al., 1987; Silvertown et al., 1992; figure 6). Several models use the extended *Moore* neighbourhood which contains the eight nearest neighbours (Gardner, 1971; Wissel, 1991; Solé & Bascompte, 1993; Hochberg et al., 1994; figure 52). More sophisticated models have used neighbourhoods with twelve or more cells (Inghe, 1989; Takahashi, 1990; Iwasa et al., 1991; Thiéry et al., 1995), or may even have random neighbourhoods (Keeling & Sheppard, 1994).

A generalisation of CA allows each lattice cell to represent an individual organism free to move around the lattice, interacting with other individuals. Such a model has been termed an *interacting particle system* (Durrett, 1988), a *lattice gas model* (Ermentrout & Edelstein-Keshet, 1993) or an *artificial ecology* (McGlade, 1993; McGlade et al., 1994; Rand & Wilson, 1995). Artificial ecologies are ideally suited to studies in behavioural ecology, for example foraging behaviours and insect movements (Rohlf & Davenport, 1969; Ermentrout & Edelstein-Keshet, 1993; Keeling, 1995).

Most CA have *synchronous* updating, which means that all lattice states are iterated at the same time, as functions of the previous time step's state. It should however be noted that a few systems are *asynchronous*, where the cells change at varying (perhaps random) times (Kitagawa, 1974; Gunji, 1990; Sieburg et al., 1990), but most systems are little affected by the method of updating (Keeling, 1995).

Except for a few simple analytical studies, most CA are run on finite lattices. This means that treatment of the lattice edges must be specified. There are several alternative scenarios (Haefner et al., 1991).

With *zero flux* boundary conditions, complete isolation of the system in a vacuum is assumed: no organisms, energy or information can flow across the boundaries. Such conditions are frequently used in plant studies, often with a *buffer zone* around the edge of the lattice (Davis, 1993). Dynamics and statistics are studied using the centre portion of the grid and a band of cells around the edge is excluded from consideration. However, it is sometimes of interest to study

explicitly the effects of edges and so the outer cells are intentionally included in all measurements of the grid.

A second possibility is *reflecting boundaries* (Mitchison, 1980), which assumes that the same states are present outside the grid as inside, as if reflected in each edge. These conditions are unlikely to be realistic in situations which involve either imposed or emergent heterogeneities, which will be most systems to which lattice models are applied.

A third and increasingly popular option is *periodic* or *toroidal* boundary conditions (Cox & Griffeath, 1986; Crawley & May, 1987; Inghe, 1989). Here the lattice forms a torus, with (in two dimensions) the left and right sides being joined and likewise the top and bottom. Edge effects can thus be eliminated, but only if the lattice is sufficiently large, This issue is investigated by the use of characteristic length scales in section 2.1.5. Toroidal boundaries are used here throughout.

In this thesis CA have been used to re-examine problems where other spatial modelling techniques have been previously employed, for example plant growth and competition[22], forest systems[23] and fungal communities (Halley et al., 1994). To help understand further the effects of space in ecological systems, various population dynamics have been modelled using CA (Molofsky, 1994), including predator-prey and host-parasite interactions[24], invasion dynamics (Clifford & Sudbury, 1973), Drosophila populations (Dytham & Shorrocks, 1992) and epidemics (Durrett, 1988; Yakowitz et al., 1990; Durrett, 1993a; 1993b). Other biological applications have included physiological pattern development such as mollusc patterns, genetics and immunology[25]. The topics of coexistence, stability and persistence all appear in many of

[22] Barkham & Hance, 1982; van Tongeren & Prentice, 1986; Crawley & May, 1987; Coffin & Lauenroth, 1988; Inghe, 1989; Durrett & Swindle, 1991; Silvertown et al., 1992; Colasanti & Grime, 1993; Dytham, 1994; Hochberg et al., 1994; Thiéry et al., 1995.

[23] Hogeweg, 1988; Bak & Chen, 1989; Iwasa et al., 1991; Wissel, 1991; Armstrong, 1993; Durrett & Levin, 1994b; Solé et al., 1994; Solé & Manrubia, 1995.

[24] DeRoos et al., 1991; Hassell et al., 1991; McCauley et al., 1993; Wilson et al., 1993; Satō et al., 1994; Keeling, 1995.

[25] Lindenmayer, 1968a; 1968b; Kauffman, 1969; Waddington & Cowe, 1969; Mitchinson, 1980; Burks & Farmer, 1984; Smith et al., 1984; Cocho et al., 1987; Coniglio et al., 1987; Gunji, 1990; Kougias & Schulte, 1990; Sieburg

the studies, as with the other types of spatial models.

In many CA studies the emphasis has been on the identification of patterns and qualitative behaviours (Wolfram, 1984b; DeRoos et al., 1991; Silvertown et al., 1992; Solé et al., 1994), including clustering effects[26], wave phenomena (Iwasa et al., 1991; Halley et al., 1994) and chaotic behaviour (Hassell et al., 1991). Responses to disturbances have been particularly widely studied in plant communities and in systems subject to fire or pest outbreaks[27].

(b) Coupled Map Lattices.

CML evolved in a much more gradual way than automata models, as they were not so much a new concept as a spatial extension of patch models. Small networks of ordinary differential equations were used in the 1960s and 1970s (Mead, 1967; Othmer & Scriven, 1971; 1974). In the 1980s the theory of finite and infinite lattices was developed, largely by Kaneko (1984; 1985; 1986; 1989) for simple examples such as the logistic map in one and two dimensions. In particular the existence of spatiotemporal chaos and other complex patterns in CML was demonstrated and the correspondence of such phenomena with structures in CA was shown in several studies (Kaneko, 1985; Hassell et al., 1991; Chaté & Manneville, 1992).

The geometric structure of CML is similar to that of CA and neighbourhoods of various sizes have been used, including Von Neumann (Chaté & Manneville, 1992) and Moore neighbourhoods (Solé & Bascompte, 1993). Some CML also involve global dynamics, for example organisms may sometimes disperse evenly over the entire grid. The same boundary conditions can be applied to CML as to CA; both periodic boundaries (Othmer & Scriven, 1971; Diggle, 1976; Kaneko, 1984; Solé & Valls, 1992b) and zero flux conditions (Mead, 1967; Kaneko, 1986; Solé & Valls, 1991; 1992a) are commonly used.

The sessile nature of plants, trees, algae and corals have made these communities suitable and

et al., 1990; Stauffer, 1991; Qi et al., 1993.

[26] Barkham & Hance, 1982; Weiner & Conte, 1981; Cox & Griffeath, 1986; Wissel, 1991; Hochberg et al., 1994.

[27] Coffin & Lauenroth, 1988; Bak & Chen, 1989; Inghe, 1989; Wissel, 1991; Hochberg et al., 1994; Rand et al., 1995.

popular subjects for CML techniques[28], but motile organisms have also been modelled, including Lotka-Volterra and host-parasitoid systems[29]. As with implicit and continuous models, CML results have been used to demonstrate spatial promotion of coexistence and stability[30]. Many CML studies have been focused on the formation of spatiotemporal patterns in the lattices, including spirals and chaotic structures[31].

2.1.5. Spatial Scales in Ecological Models - The Coherence Length Scale.

'Man masters nature not by force but by understanding' - Jacob Bronowski 1956

(a) Introduction.

Ecological processes in a finite region take place on many different spatial scales (section 1.1). The construction of discrete explicitly spatial models brings the issues of scaling to the forefront, as various scales are necessarily imposed on the system by the implementation of the model. Three imposed length scales arise from a discrete lattice. The smallest of these is the *cell size*, which may be related to the size, or area of direct influence of a sessile organism, or the space covered by a motile individual in a small time interval. Secondly, the *neighbourhood size*, usually defined in terms of the cell size, is the range over which biological interactions occur; this often consists of four or eight cells. The largest imposed scale is the *system length*, N, so that the total number of cells is N^2.

In addition to the imposed scales, there is an emergent length scale, at which the dynamics arising from the system progress. This is usually approximated by the classical *correlation length*, which is the separation distance at which any two sites are uncorrelated. Several techniques exist for determining correlation lengths, but these tend to be difficult and definite results are

[28] Mead, 1967; Diggle, 1976; Auld & Coote, 1980; Karlson & Jackson, 1981; Weiner & Conte, 1981; Gates, 1982; Hobbs & Hobbs, 1987; Green, 1989; Moloney et al., 1992; Pacala & Tilman, 1994.

[29] Hassell et al., 1991; Solé & Valls, 1991; Comins et al., 1992; Solé & Valls, 1992a; Solé et al., 1992a; 1992c; Solé & Bascompte, 1993; Hassell et al., 1994; Keeling, 1995.

[30] Karlson & Jackson, 1981; Hassell et al., 1991; Solé et al., 1992a; Solé & Bascompte, 1993; Bascompte & Solé, 1994; Hassell et al., 1994.

[31] Othmer & Scriven, 1971; 1974; Kaneko, 1986; 1989; Hassell et al., 1991; Solé & Valls, 1991; Moloney et al., 1992; Solé et al., 1992b; Bignone, 1993; Hassell et al., 1994; Bascompte & Solé, 1994; Solé & Bascompte, 1994.

not always forthcoming. Here a new length called the *coherence length scale*, n_c, is introduced. Within regions (or *subgrids*) of length significantly below n_c, the states of individual cells are strongly correlated. Disjoint regions of a size much larger than n_c are statistically independent.

It is usually desirable to perform computations using grids of around the coherence length for two reasons. Firstly, if the system is smaller than n_c, strong coupling obscures the true dynamics, particularly in a toroidal system; if a larger system is used, any dynamics will be averaged out and so more difficult to detect. Secondly very large grids will also inevitably be accompanied by excessive computational times. The length scale problem has been addressed by a few authors[32] but a widely applicable and robust technique has yet to be developed.

A method is presented here for determining the coherence length scale of a lattice-based model, using the analysis of errors arising from locally-coupled interactions.

(b) Mathematical Theory.

The identification of the coherence length scale, n_c, can be approached by analysing the errors arising from spatial aspects of a model. It is assumed here that the model is such that the dynamics tend towards a statistically stationary distribution. This means that on any subgrid of size n there is a time independent probability $\nu(\xi)$ that the configuration ξ will occur, after time t_0 when transients have passed. The state $x_i(\xi)$ of cell i can be mapped by an observable function $\mathcal{F}$ to a real number $\mathcal{F}(x_i(\xi))$. For any configuration ξ the spatial average of the observable on the subgrid, $\bar{\mathcal{F}}_n(\xi)$, is calculated at time t as:

$$\bar{\mathcal{F}}_n(\xi(t)) \quad = \quad \frac{1}{n^2} \sum_{\text{cells } i} \mathcal{F}(x_i(\xi(t))).$$

Assuming statistical stationarity, the long term time average $\langle \bar{\mathcal{F}} \rangle$ is given by:

[32] Wiens, 1989; DeRoos et al. 1991; Wissel 1991; Levin 1992; Rand & Wilson 1995.

$$\langle \bar{\mathcal{F}} \rangle \quad = \quad \sum_{\xi} \bar{\mathcal{F}}_n(\xi)\nu(\xi) = \lim_{T\to\infty} \frac{1}{T} \sum_{t_0+1}^{t_0+T} \bar{\mathcal{F}}_n(\xi(t)).$$

The infinite limit must, of course, be approximated, but a value of several thousand is usually sufficient for T. If an insufficient number of iterations is used then the error function, defined below, will not tend to zero as n tends to infinity. The *error function*, $\mathcal{E}_n$, is defined in terms of the fluctuations of $\bar{\mathcal{F}}_n$ about $\langle \bar{\mathcal{F}} \rangle$ (equation (1)).

$$\mathcal{E}_n^2 \quad = \quad \frac{1}{T} \sum_{t=t_0+1}^{t_0+T} \left(\bar{\mathcal{F}}_n(\xi(t)) - \langle \bar{\mathcal{F}} \rangle \right)^2 \tag{1}$$

It is postulated that $\mathcal{E}_n$ satisfies the *central limit theorem* (CLT) for large n. The CLT (Rosanov, 1977) is a fundamental theorem of probability theory and may be expressed as follows. Given ℓ random variables ζ_i $(i = 1, 2, \cdots, \ell)$ with finite means and variances, the sum:

$$S_\ell \quad = \quad \sum_{i=1}^{\ell} \zeta_i.$$

may be normalised to give the sum in equation (2), where $\mathbb{E}(\zeta)$ and $var(\zeta)$ are respectively the mean and variance of random variable ζ.

$$S_\ell^* \quad = \quad \frac{S_\ell - \mathbb{E}(S_\ell)}{\sqrt{var(S_\ell)}} \tag{2}$$

Then the random variables satisfy the CLT if:

$$\lim_{\ell\to\infty} S_\ell^* \quad \sim \quad N(0,1),$$

that is, S_ℓ^* approaches a standard normal distribution with mean 0 and variance 1 as ℓ becomes large. This may now be applied to $\mathcal{E}_n$ by identifying ζ_i with the scaled observable function:

$$S_{n^2} \quad = \quad \sum_{i=1}^{n^2} \frac{\mathcal{F}(x_i)}{n^2}.$$

The mean $\mathbb{E}(S_{n^2})$ of the sum S_{n^2} may be approximated by $\langle \bar{\mathcal{F}} \rangle$. Thus:

$$\mathcal{E}_n^2 \quad = \quad \left\langle \left(S_{n^2} - \mathbb{E}(S_{n^2}) \right)^2 \right\rangle,$$

which from equation (2) gives:

$$\mathcal{E}_n^2 \quad \simeq \quad \left\langle var(S_{n^2})\, {S^*_{n^2}}^2 \right\rangle.$$

Two simple lemmas give that $var(a\zeta) = a^2 var(\zeta)$ for constant a and $var(\zeta + \chi) = var(\zeta) + var(\chi)$ for independent random variables ζ and χ. From these results:

$$var(S_{n^2}) \quad = \quad var\left(\sum_{i=1}^{n^2} \frac{\mathcal{F}(x_i)}{n^2} \right) = \frac{1}{n^4} var\left(\sum_{i=1}^{n^2} \mathcal{F}(x_i) \right).$$

If the observables, $\mathcal{F}(x_i)$, are taken to be identical independent random variables with variance σ^2, then:

$$var(S_{n^2}) \quad = \quad \frac{1}{n^4} \sum_{i=1}^{n^2} var(\mathcal{F}(x_i)) = \frac{1}{n^4} n^2 \sigma^2 \sim \frac{1}{n^2}.$$

This arrives at the conclusion that:

$$\mathcal{E}_n^2 \quad \simeq \quad \left\langle \frac{\sigma^2}{n^2} {S^*_{n^2}}^2 \right\rangle$$

and hence:

$$\mathcal{E}_n \quad \sim \quad \frac{1}{n} N(0,1).$$

Given that the expected deviation from 0 of a $N(0,1)$ normal distribution is 1, the error varies as the inverse of the length scale, n (the size of the subgrid). This result can only be derived from the CLT by assuming n (and hence N) is large. However, the proof of the CLT depends on *Stirling's formula*:

$$z! \quad \sim \quad \sqrt{2\pi z} z^z e^{-z} \quad \text{as} \quad z \rightarrow \infty.$$

Through the examination of the higher order terms of Stirling's series for the factorial function (Arfken, 1970) the degree of inaccuracy for smaller z may be estimated (equation (3)). The derivation of the variation of $\mathcal{E}_n$ uses the CLT in terms of n^2. Putting $z = n^2$ in equation (3) shows that the inaccuracy is well below 1% for a subgrid as small as 5×5. Hence the error can be assumed to vary as $\frac{1}{n}$ at all but the very smallest scales. This theoretical error for random variables with given variance may now be denoted by $\mathcal{E}'_n$.

$$z! \quad = \quad \sqrt{2\pi z} z^z e^{-z} \left(1 + \frac{1}{12z} + \frac{1}{288z^2} + \cdots \right) \tag{3}$$

The error, $\mathcal{E}'_n$, applies to random variables with a distribution given by an infinite lattice. On small subgrids ($0 < n < n_c$), the absolute error $\mathcal{E}_n$ will be smaller or larger than $\mathcal{E}'_n$, but at large scales ($n > n_c$) the error will approach $\mathcal{E}'_n$ asymptotically. Thus, by fitting a $\frac{k}{n}$ curve to $\mathcal{E}_n$ (where k is a constant) for $n \sim N$, the coherence length scale n_c can be estimated as the value of n where $\mathcal{E}_n$ first meets the fitted curve.

If $\mathcal{E}_n > \mathcal{E}'_n$ for $n < n_c$ there is a greater error that that expected for the distribution on the infinite lattice, so there is aggregation of mass or individuals - *positive spatial coherence*. If $\mathcal{E}_n < \mathcal{E}'_n$ there is less aggregation; this situation is termed *negative spatial coherence* here. Further information is obtainable from the gradients of the error curve. If $\mathcal{E}_n$ does not decrease

as fast with n as does $\mathcal{E}'_n$, that is:

$$0 \quad > \quad \frac{\partial \mathcal{E}_n}{\partial n} \quad > \quad \frac{\partial \mathcal{E}'_n}{\partial n} \quad = \quad -1,$$

then there is a *aggregating* tendency, as mass or individuals accumulate in clumps. In contrast, if the interactions are such that mass or similar individuals tend to move apart (*disaggregation*), then:

$$-1 \quad = \quad \frac{\partial \mathcal{E}'_n}{\partial n} \quad > \quad \frac{\partial \mathcal{E}_n}{\partial n}.$$

Thus positive or negative coherence may be identified at scales below n_c, as well as aggregating or disaggregating tendencies as the scale of observation is varied. The error may alternatively be represented by a plot of $n\mathcal{E}_n$ against n (figures 23, 34 and 55). In these cases aggregating and disaggregating tendencies are represented respectively by:

$$\frac{\partial}{\partial n}(n\mathcal{E}_n) \quad > \quad 0$$

and

$$\frac{\partial}{\partial n}(n\mathcal{E}_n) \quad < \quad 0$$

and the fitted line will simply be a constant k. Detailed proofs of these results may be found in Keeling et al. (1995).

2.1.6. Measures of Spatial Pattern.

'spatial pattern is a conspicuous characteristic of any ecosystem' - Garcia-Moliner et al. 1993

(a) The Clumping Index.

A vital aspect of spatial heterogeneity is *pattern*, which can be defined as a departure from randomness (Galiano, 1982; Addicott et al., 1987). The character of the distribution of species and habitats is of fundamental ecological and sociobiological importance. The geometric shape of the constituents of an ecosystem, may, for example, affect the response to disease or parasites. For example a complex of small habitats will provide a physical barrier to the spread of an epidemic (Jetschke, 1992) and the destruction of fine-scale vegetational mosaics by fire management programs has created large patches through which fires spread rapidly (Minnich, 1983). Larger patches are, however, beneficial under other circumstances: predators are able to remove aphid clusters if they can move over sufficiently large areas, whereas a patchy environment inhibits predator movements and leads to pest outbreaks (Kareiva & Andersen, 1988). Thus the levels of *clumping* or *aggregation* of species, resources or features in the physical environment are important for understanding the functioning of systems and the response of individuals.

Many measures of aggregation have been developed in the biological and physical sciences (Legendre & Fortin, 1989). Biometricians have concentrated on statistical tests for distinguishing aggregated, random and regular patterns (Thomas, 1951; Diggle, 1977; Galiano, 1982; Perry, 1995). Many spatial models clearly produce clumped patterns, so that a statistical test to prove the presence of aggregation does not provide significant new information. More useful is the dynamical approach to the variation in the level of clumping which is developed here for discrete spatial models, which is also highly relevant to other lattice-based data, such as satellite images.

A simple parameter, the *clumping index* is based on the traditional joint-count statistics of Moran and others (Moran, 1948; Krishna Iyer, 1949; 1950; Ford & Diggle, 1981). The index C_i is defined for state i in a rectilinear grid by equation (4). n_{ij} is the number of interfaces

between a cell of type i and a cell of type j. Here the state variable i is discrete, such as a CA state. However, the state may be an aggregation of automata states (chapter 7), or a finite or infinite set of CML states (chapter 4).

$$C_i = \frac{n_{ii}}{\sum_{j \neq i} n_{ij}} \tag{4}$$

The significance of the value of C_i is now discussed. If the distribution of state i is random with density ρ, then the probability of two neighbouring cells being in state i is ρ^2. The probability that a state i cell has a neighbour in a different state is $2\rho(1-\rho)$. Thus the clumping index for a random distribution of density ρ is:

$$C_\rho = \frac{\rho}{2(1-\rho)}.$$

A *relative clumping index*, C_i^R can now be defined (equation (5)). This is greater or less than 1 according to whether the pattern is more or less clumped than a random distribution of density ρ. If N_i is the number of cells of type i and N is the grid size, then the density is $\frac{N_i}{N}$. Thus the clumping index for a distribution, relative to a random distribution of the same density, is given by equation (6).

$$C_i^R = \frac{2(1-\rho)n_{ii}}{\rho \sum_{j \neq i} n_{ij}} \tag{5}$$

$$C_i^R = \frac{2(N^2 - N_i)n_{ii}}{N_i \sum_{j \neq i} n_{ij}} \tag{6}$$

The standard and relative indices both have their uses. The clumping index can be plotted as a path through time as a function of density, with the random clumping curve, C_ρ, displayed on the same graph for comparison. In this way, increases and decreases in the degree of clumping over time can be displayed. Alternatively, the relative clumping index can be plotted as a

function of time. The effect of different mechanisms on spatial structure can be observed using either of the indices; the standard index plot allows density fluctuations to be observed at the same time. A second use of the indices is in the identification of transience, that is the dynamical behaviour of a system before it has 'settled down' (chapter 7).

Figure 3 shows the results of computing the clumping index C_i for random distributions of a particular cell state on a coupled map lattice, at different densities between 0 and 1, fitted to the curve C_ρ. These results verify the assumptions behind the derivation of the relative clumping index C_i^R. Additionally, the method can be used to indicate the effectiveness of the random number generator used, as the clumping indices should lie as near as possible to the curve C_ρ.

Regular $m \times m$ square clumps will have a clumping index of $\frac{m-1}{2}$ and an $n \times m$ rectangular clump will have index $\frac{n(m-1)+m(n-1)}{2(m+n)}$. Therefore an index of value C is equivalent to regular square blocks of size $(2C+1) \times (2C+1)$. This does not, however, indicate how much space there is between the clumps and illustrates the importance of the *relative* index C^R.

(b) Multifractal Theory Applied to Lattice Models.

Application of the theory of fractals provides another approach to the spatial structure of a lattice model. In particular, the recently-developed theory of multifractals can be used to consider the scales present in a spatial configuration. Multifractal theory was introduced in the basic form of an uncountably infinite number of *generalised fractal dimensions* by Hentschel & Procaccia (1983) and Grassberger (1983) and extended by Halsey et al. (1986) and Pawelzik & Schuster (1987). In recent years the theory has been developed further and applied to many areas of physics. Applications include percolation and random networks[33], clustering processes (Coniglio et al., 1987; Coniglio & Zannetti, 1989; Vicsek, 1990), wave phenomena (Shalev et al., 1992; Du & Ott, 1993; Grussbach & Schreiber, 1993), mechanics (Silberschmidt, 1993) and turbulence (Mandelbrot, 1974; Levi, 1986; Argoul et al., 1989).

Although there has been simple fractal analysis of vegetation and other spatial distributions in

[33] DeArcangelis et al., 1985; Blumenfeld et al., 1987; Coniglio et al., 1989; Aharony, 1990; Nagatani, 1993.

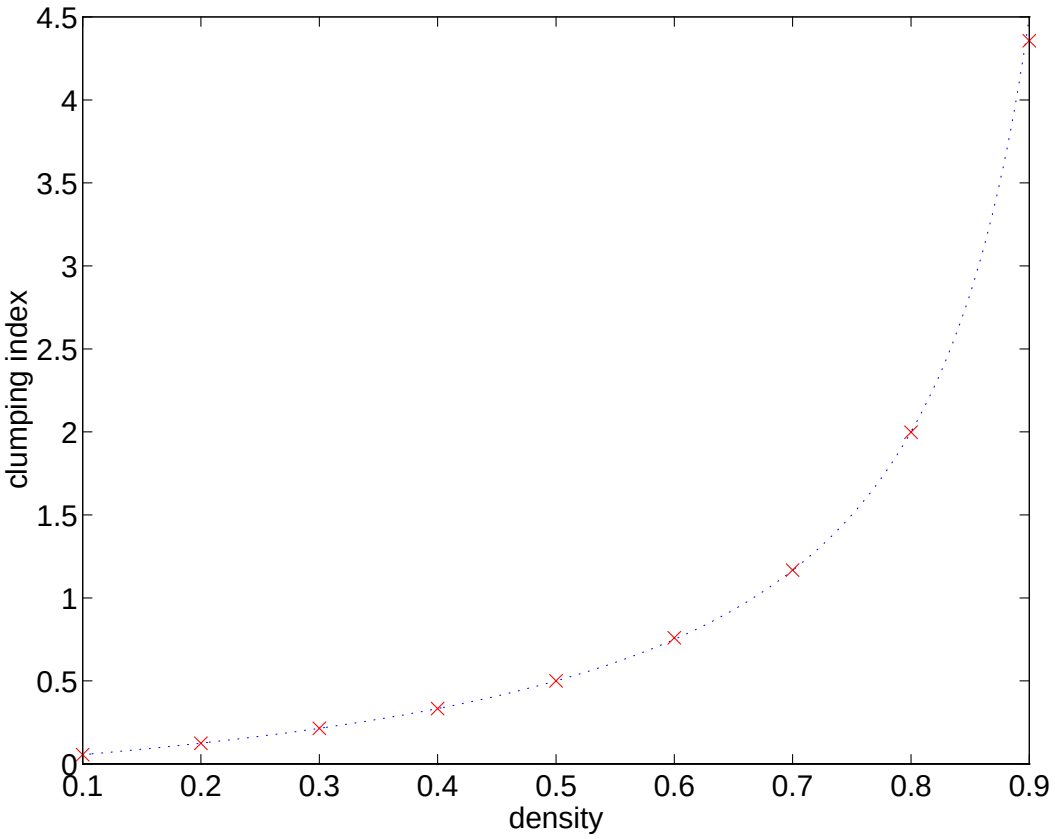

Figure 3: The clumping index for generated random distributions of cells at a range of densities (red $\times$). The fitted curve $(\cdots)$ is C_ρ.

ecology (Burrough, 1981; Morse et al., 1985), multifractals have yet to be applied in ecology. Multifractal analysis investigates distributions of measures on a geometric support and it is therefore easily applied to the square grid of a CML or CA. (While the finite nature of the lattice means that it is not fractal, it can be considered to be a 'truncated fractal'.)

The standard technique of *box counting* (Liebovitch & Toth, 1989; Block et al., 1990; Meisel et al., 1992) is used to determine a spectrum of fractal dimensions (Jensen et al., 1991), which provides a complete characterisation of the structure of the distribution. The grid is partitioned into boxes of length δ, where δ is here defined as the length divided by the grid size. Hence $\delta \leq 1$. The average mass in a δ-box defines a measure μ. A method of box counting is used which is weighted according to the measure of the boxes. A d-measure, $M_d(q,\delta)$, is defined as in equation (7), where the variables are as follows: D_δ is the set of boxes of size δ in the grid; μ_i is the measure on the box δ_i which is of size δ; $Z(q,\delta)$ is a partition function with moment of order q.

$$M_d(q,\delta) \quad = \quad \sum_{\delta_i \in D_\delta} \mu_i^q \delta^d = Z(q,\delta)\delta^d \tag{7}$$

A set of mass exponents $\{\tau(q)\}$ is defined such that $M_d(q,\delta)$ remains finite and non-zero as $\delta \rightarrow 0$ where $Z(q,\delta) \sim \delta^{-\tau(q)}$. Hence $\tau(q)$ is given by equation (8). By analogy with statistical physics, $\tau(q)$ is sometimes referred to in the literature as a fractal pressure and may be denoted by $P(q)$.

$$\tau(q) \quad = \quad \lim_{\delta \rightarrow 0} \frac{\log Z(q,\delta)}{-\log \delta} \tag{8}$$

The Lipschitz-Hölder exponent is defined such that the measure in a box scales with the α-power of the box size (equation (9)). Then the function $f(\alpha)$ is defined such that the number, $N(\alpha,\delta)$, of *α-boxes* where the measure scales in this way, scales with α (equation (10)).

$$\mu_i \quad \sim \quad \delta^\alpha \tag{9}$$

$$N(\alpha,\delta) \quad \sim \quad \delta^{-f(\alpha)} \tag{10}$$

A relationship can now be found between $(q,\tau(q))$ and $(\alpha,f(\alpha))$. A detailed proof may be found in, for example, Feder (1988) or Falconer (1990). The result can be quickly justified as follows. If $\rho(\alpha)$ is the density of α-boxes, then $\rho(\alpha)d\alpha$ is the number of boxes with measures scaling between δ^{α} and $\delta^{\alpha+d\alpha}$. Then, substituting $\mu_i = \delta^{\alpha}$, the following expression for the d-measure is obtained:

$$M_d(q,\delta) \quad = \quad \int \delta^{f(\alpha)}\delta^{\alpha q}\delta^{d}\rho(\alpha)d\alpha$$

which can be approximated by:

$$M_d \quad \sim \quad \delta^{\tilde{q}\alpha(\tilde{q})-f(\alpha(\tilde{q}))+d},$$

where $\tilde{q}$ maximises $q\alpha(q)-f(\alpha)$. This occurs where:

$$\frac{d}{dq}\left(q\alpha(q)-f(\alpha)\right) \quad = \quad \alpha(q)$$

which is when:

$$\frac{df}{d\alpha}(\alpha(q)) \quad = \quad q.$$

By comparison with the previous expressions for $M_d(q,\delta)$ (equation (7)) and $Z(q,\delta)$, the pair of equations (11) and (12) are obtained.

$$f(\alpha(q)) \quad = \quad \tau(q)+q\alpha(q) \tag{11}$$

$$\alpha(q) \quad = \quad -\frac{d\tau(q)}{dq} \tag{12}$$

Thus values for $\tau(q)$ can be found for specific ranges of $q \in \mathbb{R}$ using equation (8) and the definition of $Z(q,\delta)$. Then the exponents, $\alpha(q)$, can be found from (12) and the spectrum $f(\alpha)$ from (11). Heuristically, $f(\alpha)$ can be considered to be the fractal dimension of fractal subsets S_α of the geometric support S. These subsets can be thought of as having the same densities or measures (of order δ^α) and they cover the support ($S = \cup_\alpha S_\alpha$). Thus the size of the measure determines the scaling of the corresponding boxes.

A distribution is multifractal when there is a range of values of α and $f(\alpha)$. This can easily be seen from a graph of the pressure $\tau(q)$ against q (chapter 4). The gradient of the graph for any value of q is minus the value of α at that point. Hence a multifractal will have a nonlinear plot of $\tau(q)$, whereas it will be a straight line for a simple fractal. It is also generally observed that α approaches a finite constant as $q \rightarrow \infty$ and as $q \rightarrow -\infty$, which leads to a finite range for α and for $f(\alpha)$. $f(\alpha)$ is expected to be a concave curve within the finite range of α (chapter 4). The maximum of this spectrum corresponds to a sharp peak in the number of boxes in the fractal set S_α. In this way the scaling structure of a distribution on a grid can be analysed in a '*fully quantitative fashion*' (Stanley & Meakin, 1988).

2.1.7. Singular Value Decomposition as a Test for Robustness of Models.

'Wisdom is the principle thing; therefore get wisdom: and with all thy getting get understanding'
- Proverbs 4:7

(a) Introduction.

It is important in non-chaotic situations that the robustness of numerical models of ecological systems is determined over repeated runs; the same results should be produced for different simulations of the same dynamical system. Although a spatial model with local stochasticity will vary in its details, the statistically-averaged spatial structures and population compositions should usually remain constant. A simple technique is presented for assessing the robustness

of models in this context. The method is based on *singular value decomposition* (SVD) of a matrix containing model output data and involves comparison with *white* or *Gaussian* noise.

(b) Method.

This method relies on the generation of a *replication matrix* $\boldsymbol{X}$ from repeated runs of the model that is to be tested. Suitable model output must be chosen. It is important that a sufficient number of output variables is available, of the order of ten or more, so that a substantial matrix $\boldsymbol{X}$ can be formed. If n denotes the number of variables, then n replicated simulations should be carried out. If $\boldsymbol{x}_i = \{x_1^{(i)}, \cdots, x_n^{(i)}\}$ denotes the output vector for the model, with $x_j^{(i)}$ being the ith replicate of the jth variable, then the replication matrix is constructed as follows:

$$\boldsymbol{X} \quad = \quad \begin{pmatrix} \boldsymbol{x}_1 \\ \vdots \\ \boldsymbol{x}_n \end{pmatrix}.$$

The output vectors may correspond to the proportions of the state variables in a system. Alternatively, the vector may be a characterisation of the spatial structure of a system, such as a distribution of patch sizes. This allows the robustness of an emergent spatial pattern in a model to be assessed.

The standard technique of SVD is used to find the singular values of the replication matrix $\boldsymbol{X}$. The matrix is decomposed into the form:

$$\boldsymbol{X} = \boldsymbol{U}.\boldsymbol{S}.\boldsymbol{V}^T,$$

where $\boldsymbol{U}$ and $\boldsymbol{V}$ are orthogonal matrices and $\boldsymbol{S}$ is diagonal, with:

$$\boldsymbol{S} \quad = \quad \begin{pmatrix} e_1 & & \\ & \ddots & \\ & & e_n \end{pmatrix},$$

where $\{e_i\}$ are the singular values of $\boldsymbol{X}$. Standard computer algebra packages, such as Matlab (The Maths Works Inc., 1992) produce the singular values in descending order of magnitude: $\|e_1\| \geq \|e_2\| \geq \cdots \geq \|e_n\|$.

If the replicated runs are identical then rank($\boldsymbol{X}$) = 1 and hence $e_2 = e_3 = \cdots = e_n \equiv 0$. A stochastic model will always have some error in all of the output variables and thus rank($\boldsymbol{X}$) = n. However, if the replicates are accurate, then the vectors $\{\boldsymbol{x}_i\}$ will be similar and rank($\boldsymbol{X}$) will be *nearly* 1. This will be indicated by the presence of one dominant singular value, that is: $\|e_1\| \gg \|e_2\| > \|e_3\| > \cdots > \|e_n\|$. The following section quantifies this singular value difference, characterised by $\frac{\|e_2\|}{\|e_1\|}$, for different levels of noise.

(c) Application to Gaussian Noise.

Sample data can be generated to test the response of the singular value spectrum to varying levels of white (Gaussian) noise. A vector $\boldsymbol{x}$ is produced by assigning random values in the interval [0,100] to the elements $\{x_i\}$. Replicated 'output' values $\{\boldsymbol{x}_i\}$ are produced by adding Gaussian random variables of mean zero and specified standard deviation σ to $\boldsymbol{x}$:

$$\boldsymbol{x}_i \quad = \quad \boldsymbol{x} + \boldsymbol{\xi} \qquad (i = 1, \cdots, n)$$

where:

$$\boldsymbol{\xi} \quad = \quad (\xi_1, \cdots, \xi_n)$$

and:

$$\xi_j \quad \sim \quad N(0, \sigma).$$

The singular value spectrum may be found for a range of standard deviations σ. Here results are shown for $\sigma = \{1, 2, \cdots, 100\}$. Figure 4 shows sample replication matrices for $\sigma \in \{1, 5, 10, 25\}$

and $n = 20$. There is a clear dominant singular value in all cases, but the dominance decreases as noise increases. Figures 5a - b illustrate the relation between the Gaussian standard deviation σ and the ratio of the first two singular values. This demonstrates a linear relationship, although with increasing fluctuations at high σ. A standard linear regression (figure 5a) and a weighted regression (figure 5b) yield similar results. Weighting is achieved by using a factor of $\frac{1}{2^x}$ in the regression sums, which causes the linear fit to be biased towards the smaller noise levels.

The ratio of the first two singular values for the output from a model can be compared to the Gaussian results, specifically the gradient g of the fitted line, to obtain an estimate of the level of noise in the model. g represents the amount by which the ratio of the first two singular values increases for each 1% of noise. Therefore, the percentage Gaussian noise p_σ corresponding to a set of output data is given by:

$$p_\sigma = \frac{\|e_2\|}{g\|e_1\|}.$$

The effect of matrix size n must now be taken into consideration, as g may depend on n. The variation of $\frac{\|e_2\|}{\|e_1\|}$ with σ was found for a range of matrix sizes from 10×10 to 55×55. Figure 5a shows the plots of $\frac{\|e_2\|}{\|e_1\|}$ against σ aggregated to form a surface. The surface roughly takes the form of a flat plane. The important feature is the variation in the slope of lines in the plane as the matrix size varies, that is, the form of the function $g(n)$. The plane can be approximated by taking the slopes of the lines fitted for all of the sizes of matrix and fitting a line to these slopes (figure 5b). This demonstrates that g is linear in n. Thus the percentage of noise can be found by estimating $g(n)$ from figure 5b and using:

$$p_\sigma = \frac{\|e_2\|}{g(n)\|e_1\|}.$$

2.2. Chaos and Nonlinearity.

2.2.1. Introduction.

'...a rich variety of behaviour, some of it very bizarre...' - Cartwright & Littlewood 1945

'In view of the inevitable inaccuracy and incompleteness of weather observations, precise very-long-range forecasting would seem to be non-existent' - Lorenz 1963

Anomalies in the behaviour of nonlinear systems were noted in the last century by Poincaré, Kovalevskaya and Lyapunov (Percival, 1989) and later by Cartwright & Littlewood (1945). It was not until 1963 and the early days of digital computers, that Lorenz produced the first small illustration of a *strange attractor*, the finely-structured geometric shape on which the dynamics of a nonlinear system move in *phase space* (Lorenz, 1963). Working in a restricted area of meteorology, there was little attention given to the Lorenz system, until it was rediscovered in the 1970s. Early mathematical treatment of chaotic nonlinearity was brought to the attention of the general scientific community by May, using examples from population biology (May, 1974; 1976; May & Oster, 1976). Since then the study of chaos has become a scientific discipline in its own right and is used throughout the physical and biological sciences.

The most influential feature of chaotic dynamics is the *sensitivity to initial conditions* (SIC), popularly known as the *butterfly effect* (Markus, 1992). In a non-chaotic system, trajectories starting at nearby initial points will remain close together indefinitely. This underpins classical science, which assumes that small starting errors will remain small. However, chaotic trajectories that start close will rapidly diverge, so that perturbations are amplified (McGlade, 1994). The SIC of chaotic systems means that predictability is limited. Although chaos is deterministic, an initial condition can never be determined precisely, so the long term future of the system cannot be described.

This has produced two different reactions in ecologists: while some despair of predicting the future of any non-trivial ecological systems, others reject chaos as a natural phenomenon because they believe that prediction must be possible. There are, however, some clear compatibilities

between chaos and modern ecology. SIC shows that the past of a system fundamentally affects its future, which emphasises the importance of the history of an ecological system (chapter 7; Cohen & Stewart, 1991). Such ideas are also seen, for example, in community construction (Robinson & Edgemon, 1988; Facelli & Pickett, 1990) and succession (Clements, 1936; Horn, 1975; Clark, 1991). Chaos also has implications for the sampling of real systems: given a certain amount of data, the extra data needed to provide more information about the system increases exponentially.

It is, however, premature to abandon all hope of predicting behaviour and formulating general laws of a chaotic system (May, 1995). There needs to be a shift in the techniques used to analyse such systems (Stewart, 1995): rather than producing exact trajectories for given initial conditions, the *type* of behaviour should be investigated. Statistical and geometrical methods are suitable for producing information such as the range of possible dynamics, the structure of the underlying attractor and the probabilities of getting different outcomes. Judson (1994a) calls this the *texture* of a system. Although chaotic dynamics are locally unstable, characteristically there is a global stability. There are also different classes of chaos with different levels of stability, including *fully-developed spatiotemporal chaos*, which is robust to parametric perturbations (Kaneko, 1990).

2.2.2. Chaos and Ecology.

'The very simplest nonlinear difference equations can possess an extraordinarily rich spectrum of dynamical behaviour...' - May 1976

'Chaos gives us a very different picture of the world in which we live' - Yorke 1989

As stated in section 1.2, there are various situations which promote chaos and these are frequently applicable to ecological systems. High dimensionality is one such criterion, so that ecosystems with many species and interactions may easily be chaotic (May, 1976; Fielding, 1991; Ferrière & Gatto, 1994). Similarly, size, age or spatial structuring of populations have been shown to promote chaos (Hastings, 1992; Solé & Valls, 1992a; Lloyd, 1995; Ruxton, 1995).

Chaos is also more likely in the presence of *feedback*, either positive (raised growth rates) or negative (overcompensation, inducing time lags or delays), both of which are common in ecological community interactions[34]. There has recently been a demonstration that noise can cause transient chaos to become permanent (Rand & Wilson, 1991a); the ubiquity of noise in ecology thus further promotes chaos.

In spite of these points, there is limited direct evidence of chaos in the natural world. Ecologists have offered various explanations for this. Some consider that chaos is *maladaptive* and that natural selection will act against chaotic systems (Łomnicki, 1989; Mani, 1989). It is suggested that the large fluctuations seen in chaotic (and oscillatory) systems will result in susceptibility to stochastic extinctions (Thomas et al., 1980; Mueller & Ayala, 1981; Fielding, 1991). Dispersal has been cited as a mechanism to promote non-chaotic dynamics (Hastings, 1993). A more controversial idea is that natural selection has excluded chaos in nature, but that anthropogenic intervention has increased the tendency of systems to be chaotic (Berryman & Millstein, 1989a; Pool, 1989b).

The revolutionary articles of May (1974; 1975; 1976) introduced the concept of chaos in invertebrate population ecology using the logistic map and simple two-dimensional competition models. There has since been a deluge of ecological models which exhibit chaotic dynamics (Renshaw, 1994), including predator-prey models (Beddington et al., 1975; Hanski et al., 1993), resource-predator-prey models (Rand et al., 1994) and Leslie matrices (Guckenheimer et al., 1977). There has also been considerable interest about chaos in epidemiology (Bartlett, 1990), since the SEIR equations, which model the spread of diseases such as measles, were suggested to show chaotic dynamics [35].

Spatially-extended models have provided several cases of chaos, both in forced continuum systems (Tsonis et al., 1989) and discrete lattices of logistic and other one-dimensional maps

[34] Pimm & Hyman, 1987; Berryman & Millstein, 1989b; Allen, 1990; Hunter & Price, 1992; Power, 1992; McGlade et al., 1994.

[35] Schaffer & Kot, 1985; Pool, 1989a; Rand & Wilson, 1991a; Grenfell, 1992; Sidorowich, 1992; Bolker & Grenfell, 1993; Grenfell et al., 1995.

(Kaneko, 1985; 1986; 1989; Solé & Valls, 1992a; Bascompte & Solé, 1994), the Nicholson-Bailey equation for host-parasite equations (Hassell et al., 1991; 1994) and Lotka-Volterra systems (Solé & Valls, 1991; Solé et al., 1992b). Two-species CML have produced a new class of spatial dynamics, *chaotic Turing structures*, which consist of patches which have chaotic dynamics within them, but stable boundaries (Solé et al., 1992a; Solé & Bascompte, 1993).

There has been less conclusive identification of chaos in empirical data, because of methodological problems, caused by the tendency of ecological time series to be short and noisy (Lloyd, 1994). Phase space reconstruction produced some evidence of chaos in lynx populations (Schaffer, 1984; 1985a; Godfray & Blythe, 1990) and measles epidemics (Schaffer, 1985b). Forecasting techniques (Sugihara & May, 1991; Sugihara et al., 1990), fitting to the SEIR equation (Olsen & Schaffer, 1990; Grenfell, 1992) and spectral analysis (Olsen et al., 1988) have all claimed to prove that measles epidemics are chaotic. Some of these techniques have however been questioned, in particular the forecasting techniques (Rand & Wilson, 1991b). The dynamics of voles (Hanski et al., 1993) and ant trails (Cole, 1991) are also potentially chaotic, while little clear evidence of cycles or chaos in plant population data has been found (Thrall et al., 1989; Rees & Crawley, 1991; Tilman & Wedin, 1991b).

Many ecologists have focused on detecting chaos by fitting simple maps to experimental data. Frequently a one-dimensional map has its parameters estimated from a time series, then chaos is accepted or rejected for the natural or laboratory system depending on whether the map is chaotic for the estimated parameters. In the 1970s studies based on such techniques were used to suggest that insect populations rarely exhibited chaos or cycles. The key paper by Hassell et al. (1976) led most ecologists to reject any relevance of chaos to the natural world and to view it as a mathematical artefact of certain models (Pool, 1989b). More recent studies of two- and higher-dimensional maps have been much more suggestive of chaos (one-dimensional systems are inherently unlikely to be oscillatory or chaotic (Gatto, 1993)). This has produced various criticisms of the whole use of model fitting in the detection of chaos, as the procedure is too sensitive both to the dimension and form of the selected map and the method of parameter estimation used (Nisbet et al., 1989; Morris, 1990; Bascompte & Solé, 1994).

The key to identifying chaos in time series depends on distinguishing it from genuinely random noise. A natural system certainly has some noise - environmental stochasticity - to which some measurement error is inevitably added. At first it was thought that determinism and stochasticity were indistinguishable (May, 1976), but in recent years much effort has been put into their separation. In natural systems this is equivalent to identifying density-dependent (nonlinear) and density-independent (noise) effects (May, 1986; McGlade, 1994; Ellner & Turchin, 1995). In mathematical terms, the difference between noise and chaos is dimensional: deterministic dynamics can be reduced to a finite-, often low-dimensional attractor, whereas uncorrelated noise is of infinite dimension (chapter 7; Casdagli, 1991). In natural systems there will always be a balance between the two extremes of pure determinism and pure stochasticity.

2.2.3. Quantifying Chaotic Behaviour.

'Data indicating complicated population fluctuations do not necessarily testify to environmental stochasticity, nor to random experimental error, but can arise from simple and rigidly deterministic density-dependent mechanisms' - May & Oster 1976

'...order disguised as disorder...' - Pool 1989a

A fundamental character which varies between chaotic systems is the *degree of predictability*: sometimes a reasonably long term prediction is accurate, other times there is no predictability even on very short time scales. The most basic and useful measure of chaotic dynamics is the *Lyapunov exponent*, which gives the rate of exponential divergence of initially close trajectories (Zeng et al., 1991). The Lyapunov exponent has had various interpretations: a measure of long term unpredictability; the rate of growth of errors (Markus, 1992); the time scale over which dynamics become unpredictable; the rate of creation or destruction of information (Wolf et al., 1985). A recent observation is that exponents are not constant for a given system, but can vary substantially over the dynamical attractor (Palmer et al., 1994; Smith, 1994), in part explaining the variable success of forecasting.

A multi-dimensional system has several Lyapunov exponents, one for each degree of freedom.

The maximum exponent characterises the dynamics: if it is positive there is SIC and hence chaos. Thus determining the maximum exponent is the first step in analysing a nonlinear system that may be chaotic.

In a one-dimensional system, the exponent $\bar{\lambda}$ is easily approximated by evaluating the ratio in equation (13), where $\boldsymbol{x}^t$ represents the state of the system at time t. However, in a higher order system with several exponents, the stretching and folding involved in a chaotic regime will generally lead to converging orbits in at least one direction and diverging orbits in other directions. Hence equation (13) produces an exponent, $\bar{\lambda}$, averaged over the attractor. This provides preliminary information about the dynamics, as it indicates the average predictability of the system. If $\bar{\lambda} > 0$ then certainly the maximum positive exponent, λ_1, will be positive, which means that the system is chaotic. If $\bar{\lambda} < 0$ then λ_1 could be of either sign, so it is not possible to say whether or not there is chaos. However, in this case, it can be stated that the dynamics are, on average, predictable to some extent over the long term.

$$\bar{\lambda} \quad = \quad \log_2 \left(\frac{\left\| \boldsymbol{x}^{t+1} - \boldsymbol{x}^{u+1} \right\|}{\| \boldsymbol{x}^t - \boldsymbol{x}^u \|} \right) \tag{13}$$

For data where the average exponent is found to be negative, the sign of the maximum positive exponent must be found. This requires the rate of divergence of the trajectories to be evaluated in the direction of maximum divergence. This can be achieved by using a method of Wilson & Rand (1993), which is a development of Wolf et al. (1985).

The nearest trajectory point $\boldsymbol{x}^{u^0}$ to a given point $\boldsymbol{x}^t$ is found, with the separation of these points being denoted by δ. The divergence of the two points is followed for several steps, until the separation has increased (or decreased) by a given factor, denoted by k. Then the second point $\boldsymbol{x}^{u^0}$ is replaced by a point $\boldsymbol{x}^{u^1}$ in the same direction, but only a distance δ away. This procedure is repeated until all the available data points are used. The use of multiple iterations ensure that the maximally-expanding trajectory direction is used and the resetting of the points avoids nonlinearities affecting the results. The Lyapunov exponent λ_1^δ is then evaluated for a range of values of initial separation δ using equation (14), where τ^i is the number of steps used

between resettings i and $i+1$ and there are a total of I resettings.

$$\lambda_1^{\delta} \quad = \quad \frac{1}{I}\sum_{i=1}^{I} D_i \tag{14}$$

where:

$$D_i \quad = \quad \frac{1}{\tau^i}\log_2 \frac{\left\| \boldsymbol{x}_{t+\Sigma_{j=1}^{i}\tau^j} - \boldsymbol{x}_{u^i+\tau^i} \right\|}{\left\| \boldsymbol{x}_{t+\Sigma_{j=1}^{i-1}\tau^j} - \boldsymbol{x}_{u^i} \right\|}$$

A graph of λ_1^{δ} against δ can then be plotted. For small δ ($\delta < \delta_{noise}$) the dynamics are overwhelmed by noise and for large δ ($\delta > \delta_{nonlinear}$) nonlinearities dominate the dynamics. At intermediate values ($\delta_{noise} < \delta < \delta_{nonlinear}$) λ_1^{δ} is constant and provides the value for λ_1. This assumes that $\delta_{noise} < \delta_{nonlinear}$, which is not always true. This condition fails if the system is so noisy that nonlinearities set in at scales at which there is substantial noise (Wilson, 1994). The maximum exponent cannot be estimated in this situation, as there is no flat section of the curve.

Implementation of an extension to this method by Keeling (1995) does allow an estimate of λ_1 to be made. This relies on the fact that λ_1^{δ} will depend on k in the very noisy and nonlinear ranges of δ, but at intermediate values the same λ_1 should be predicted by all values of k. Therefore, the graphs of λ_1^{δ} against δ should be plotted for several values of k. Then λ_1 can be estimated by the point at which the different k-curves meet. The value obtained in this way is not particularly accurate, but it provides a good indication of the presence or absence of chaos in the underlying dynamics.

The main way of detecting chaos in real or artificial systems is through the estimation of Lyapunov exponents. Accurate estimation unfortunately requires very long time series: the number of data points needed rises exponentially with the system dimension (Eckmann & Ruelle, 1992; Rapp, 1993) and as described in chapter 7, unknown dimensionality of systems adds to the technical difficulties of exponent estimation. Another, rather crude, technique for

identifying chaos is phase space reconstruction. The dimension of the system underlying an empirical time series is estimated and the attractor is reconstructed by *embedding* techniques (Packard et al., 1980). The appearance of the 'typical' geometry of a strange attractor is taken to indicate of the presence of chaos.

2.3. Individual-Based Models in Ecology.

'The ultimate parts of the community are the individual plants, but a description of it in terms of the characters of these units and their spatial relations to each other is impracticable at the individual level' - Watt 1947.

'The individual organism is the logical basic unit for the modelling of ecological phenomena' - Huston et al. 1988

The new generation of individual-based ecological models that has recently appeared and become widespread (Judson, 1994a) is discussed in section 1.3.3. This revolution has been largely driven by the development of computing power over the past thirty years. In the early days of ecological modelling, the explicit representation of individual organisms was not feasible and therefore rarely considered. As computers have become more widely available and more powerful, it has become possible to track the fate of individual ecological entities. The rise of the IBM has demonstrated the dependence of scientific development of technology - the comments of Watt (1947) illustrate the fact that the desire to consider individuals has long existed.

Individual organisms have a unique role in ecological systems (Lomnicki, 1992). They are generally considered to be the unit of selection, as higher biological levels have different genotypes and lower levels have identical genes. Individuals are in many cases more easily defined than, for example, populations or communities, generally being seen as discrete units and although clonal species do highlight some problems, it is possible even in these cases to define basic units such as modules or ramets.

The key feature of individuals is that they are all different; such differences can only be explicitly dealt with by an IBM. Uniqueness of physical, behavioural and genetic characters can be

modelled, as well as the occupation by an individual of a unique spatial location.

Another fundamental but questionable assumption of many ecological models is that of perfect mixing. In population and community models it is necessarily assumed that all individuals interact with all other individuals, this assumption generally lies somewhere between inaccurate and totally false. This is particularly true of plants and sessile animals, for which a lot of experimental data show that the extent of interactions are limited[36]. Mixing is also limited in many motile species, such as territorial animals, where interactions are restricted to neighbouring territory holders and sparse populations where mixing is limited. Using an IBM embedded in space allows individuals to interact with neighbours within a defined region, thus overcoming the assumption of mixing (Caswell & John, 1992).

There are many other, mainly technical, advantages of IBM. They are simple to implement and are generally explicit and mechanistic rather than phenomenological (Murdoch et al., 1992; section 1.3.2), enabling greater insights to be gained and new ideas generated. Large stochasticities, discontinuities, dominance by a few particular individuals and important rare events can easily be incorporated. An IBM can be based in heterogeneous space, which is sometimes difficult to treat in classical models. The uniqueness of the history of an individual, such as the record of interactions with other individuals, can also be tracked. Small populations are particularly suitable for IBM treatment, as they are easy to handle and are particularly likely to break various assumptions of population level systems (DeAngelis & Rose, 1992).

Multiple spatiotemporal scales can also be incorporated more easily in IBM than in traditional models. Events can be modelled on two or more time scales, such as daily and annual (chapters 4 and 5) as well as sequentially or concurrently (McCauley et al., 1993) and a hierarchy of spatial scales can be studied, from local to global.

There are, however, various valid criticisms made of IBM. They are generally non-analytical and hence rely on the quality of the computational methodology, which is hard to judge as

[36] Mead, 1966; Mack & Harper, 1977; Ford & Diggle, 1981; Watkinson et al., 1983; Weiner, 1984; Silander & Pacala, 1985; Firbank & Watkinson, 1987; Goldberg, 1987.

publications rarely give either computer code or sufficiently-detailed descriptions. The macroscopic dynamics and patterns which emerge from an IBM are often very complicated and their interpretation can be challenging, although techniques are being developed to deal with these complexities. Intensive computation is often needed for modelling sufficient numbers of individuals, which restricts use to large computer systems or small ecological systems. This problem is decreasing as computer power is becoming rapidly cheaper and more widely available.

There is however one significant restriction in the applicability of IBM: the numbers of individuals cannot vary very much. Each individual organisms must be labelled and tracked, so that there cannot practically be variation in numbers over more than a couple of orders of magnitude. Thus situations where marked population explosions or declines are expected are less suitable for these techniques. Overall, an IBM provides an elegant and intuitive representation, which can be simple or complicated, specific or general, covering a range of temporal and spatial scales.

3. A Coupled Map Lattice Model for a Plant Monoculture.

Chapter Summary

An overview of plant population ecology is presented, which explores empirical and theoretical approaches to the role of neighbourhood effects, plasticity and the formation of size hierarchies in plant communities.

The terms absolute asymmetry, relative asymmetry, relative symmetry and absolute symmetry are introduced as representatives of the spectrum of possible pairwise competitive interactions of individual plants. Two hypotheses concerning the underlying mechanistic causes of size variation are summarised, attributed respectively to Bonan and Weiner:

- the increase in size variation at high stand densities is evidence solely for local neighbourhood effects;
- the increase in size variation at high stand densities occurs only when competition interactions are asymmetric.

An individual-based coupled map lattice model of a plant monoculture is introduced with local mappings based on a model of Aikman & Watkinson. Measures of size variation in the model population increase significantly with density under asymmetric competition, supporting the hypothesis of Weiner that variation provides evidence for distinguishing between symmetric and asymmetric competition.

The coupled map lattice is adapted to mimic a field experiment carried out on carrot plants. The presence of a significant degree of asymmetry within the stand is indicated by a comparison of empirical and model data; this has implications for crop management.

'What is a weed? A plant whose virtues have not been discovered.' - Ralph Waldo Emerson

3.1. Introduction.

Spatial models of single and multiple species plant communities are presented in the following three chapters. It is established that the derivation of quantitatively testable dynamic models of plant species is difficult and that empirical validation is problematic. The difficulties are compounded by the frequent sensitivity of communities to initial conditions of the biotic and physical environments, which are not easily controlled in experiments to a sufficiently high precision. It is therefore useful to construct artificial ecological systems to model dynamics of real systems under a range of assumptions and to assess whether qualitatively different behaviours arise.

It may then be possible to perform discriminatory experiments to identify the actual mechanisms operating in the real system. This approach is especially suitable for studying the spatiotemporal dynamics of plant communities, as the feasibility of conducting experiments on large spatial scales or over long time scales is limited, especially when an individual-based approach is taken. Different mechanisms and processes can be analysed and the role of spatial effects assessed. In some cases fair approximations of observed behaviour are provided by non-spatial or mean field models, but many important features arise directly from spatial processes. In this chapter the interdependence of competitive interactions between individuals and spatial processes in a single species is considered, before multiple species and extended time scales are considered in the subsequent chapters.

3.2. Overview of Plant Population Ecology.

Plant population modelling began in the 1950s in Japan, with mean field representations of yields and *self-thinning* (or progressive stand mortality). Various yield, allometric and density relationships were presented during the following years and compared to field and greenhouse data. The major breakthrough came in the late 1960s when data were first gathered on *spatial effects* in plant communities. Many studies followed, in which the extent to which plant size is

attributable to number, distance, size and angular dispersion of neighbours was investigated. Considerable importance was placed on the effect of neighbours in determining population structure of experimental plant communities[37]. A wide variety of species were used, including carrots (Mead, 1966; Benjamin & Sutherland, 1992), pine trees (Weiner, 1984) and grasses (Liddle et al., 1982). Experiments also studied the effects of neighbourhood interactions on other plant features, such as allocation (Goldberg, 1987) and growth form (Weiner et al., 1990a). However, a few experiments failed to support neighbourhood effects[38]. Apart from inadequate experimental and analytical methodology, these anomalous result may have arisen via dominance by factors such as variable germination time, interdependence of clonal modules and high seed dispersal levels.

A popular technique for quantifying neighbourhood effects has been *Dirichlet*, *Thiessen* or *Voronoi polygon analysis*[39]. The area controlled by an individual plant is determined by creating a polygon around it, using the perpendicular bisectors of lines to the nearest neighbours. Thus a plant with few neighbours occupies a large polygon and competitive interactions are represented by the polygon area. In other studies, spatial interactions have been represented by pseudospatial models, where plant weights are related to a combination of number, size and aggregation of plants in specified neighbourhoods[40]. Both techniques have been used to identify the extent to which population structure can be attributed to the distribution, and other features, of neighbouring plants.

A new generation of plant models followed the increase in data confirming the importance of local neighbourhood interactions in plant dynamics. The emphasis on local effects, in association

[37] Ford, 1975; Mack & Harper, 1977; Phillips & MacMahon, 1981; Gates, 1982b; Weiner, 1982; Wixley, 1983; Fowler, 1984; Mithen et al., 1984; Renshaw, 1984; Silander & Pacala, 1985; Penridge & Walker, 1986; Smith & Goodman, 1986; Mitchell-Olds, 1987; Pacala & Silander, 1987; Gurevitch et al., 1990; Weiner et al., 1990b; Bergelson, 1993; Sutherland & Benjamin, 1993.

[38] Waller, 1981; Watkinson et al., 1983; Weiner, 1985; Firbank & Watkinson, 1987; Pacala & Silander, 1990.

[39] Mead, 1966; Fischer & Miles, 1973; Liddle et al., 1982; Watkinson et al., 1983; Mithen et al., 1984; Kenkel et al., 1989a; 1989b; Miller & Weiner, 1989; Galitsky, 1990.

[40] Mack & Harper, 1977; Weiner, 1982; 1984; Silander & Pacala, 1985; Penridge & Walker, 1986; Weiner & Thomas, 1986; Firbank & Watkinson, 1987; Thomas & Weiner, 1989a.

with the *sessile* nature of plants, encouraged modelling using *spatially-explicit individual-based models* (sections 2.1and 2.3). These largely used *zone of influence* (ZOI) methods, where the area available for resource utilisation was represented by a region around each plant[41]. This was often a circle, although squares (Gates, 1978), ellipses (Wixley, 1983) and cones (Ford & Diggle, 1981) were also used, with the size of the ZOI related to sizes of plants and types of interactions. Models have been simulated on computers and treated analytically by mean field approximations. The earliest ZOI model, however, used pencil and paper, with circles of given radii being drawn with compasses (Pielou, 1960).

Plant ZOI interactions were treated in two different ways (Benjamin, 1993). Non-overlapping domain models allowed the ZOI to grow outwards through time until neighbouring zones touch, at which point the plants stopped growing or else died. Overlapping domain models offered greater flexibility in their representation of local interference, as the zones grew continually and many overlap. The intersecting regions corresponded to areas of contested resources, which were allocated to the competing plants according to the type of competition, perhaps by size.

The studies of spatial effects in plant populations focus on size distributions. A fundamental characteristic of plants is their *plasticity*, which means that genetically identical individuals can respond strongly through their phenotypes to differences in their physical and biotic environments, resulting in wide variation of size and growth forms (Levin, 1988). There also exist feedback loops where plants modify their environments (Raynal & Bazzaz, 1975; Silander & Pacala, 1990) and hence alter their phenotypes. Since most populations show great size variability, there has been much interest in the determinants of size variation[42]. With a few notable exceptions (Turner & Rabinowitz, 1983; Ellison, 1987), populations of plants grown at higher densities show greater size inequality than populations grown at lower densities[43]. Many

[41] Gates et al., 1979; Aikman & Watkinson, 1980; Gates, 1980a; 1980b; 1982a; Slatkin & Anderson, 1984; Firbank & Watkinson, 1985; Pacala & Silander, 1985; Pacala, 1986; Lepš & Kindlmann, 1987; Bonan, 1988; Ellison et al., 1994.

[42] Rabinowitz, 1979; Burdon & Harper, 1980; Mithen et al., 1984; Weiner & Solbrig, 1984; Benjamin & Hardwick, 1986; Weiner, 1986; Dixon et al., 1987; Hara, 1988; Weiner, 1988; Weiner & Whigham, 1988; Geber, 1989; Crawley & Weiner, 1991; Bonan, 1993; Weiner, 1993; Stoll et al., 1994.

[43] Watkinson, 1980b; Waller, 1985; Weiner, 1985; Schmitt et al., 1986; Weiner & Thomas, 1986; Schmitt et

factors have been suggested as being influential on the sizes of individuals, including microenvironmental heterogeneity, density, competition, morphology, herbivores, parasites, pathogens, genetics and germination characteristics (Weiner, 1985; Weiner, 1988). Focusing on a plant monoculture in a homogeneous environment, protected from herbivory and disease, the main influential factor remaining is intraspecific competition.

Two alternative views of how competition contributes to the generation of size distributions have been advanced. One view holds that competition among plants is usually *asymmetric* (Weiner, 1990). (Symmetry of competition is considered in detail below.) An opposing view emphasises the role of spatial effects. Plants do not grow in uniform patterns, so they experience variable degrees of crowding. The differences in local neighbourhood conditions lead to variation in growth rates and hence to size differences or *hierarchies* (Bonan, 1988; 1991).

The degree of symmetry of competition describes the outcome of the interaction between a smaller plant and a larger plant. There is a complete spectrum of possible behaviours, from purely symmetric, where both plants have equal resource uptake, through to total asymmetry where the large plant takes all of the contested resources. Some degree of asymmetry has been noted in large numbers of studies (Weiner & Thomas, 1986), where it has also been termed *dominance and suppression*. Populations often consist of a canopy of large dominant individuals with smaller suppressed individuals below (McMurtrie, 1981; Knox et al., 1989).

Suppression has implications beyond size: suppressed plants typically have different morphologies, with a tendency to have thinners stems and less branching (Thomas & Weiner, 1989b; Ballaré et al., 1994; Weiner & Fishman, 1994). This is a two way effect: different degrees of asymmetry arise from differences in morphologies between species[44]. While large plants clearly shade nearby small plants, smaller plants can affect larger ones by shading their lower branches. This observation firstly suggests that asymmetry may be moderate and secondly confirms the effect of morphology on asymmetry (Ford & Sorrensen, 1992).

---

al., 1987; Ellison & Rabinowitz, 1989; Knox et al., 1989; Firbank & Watkinson, 1990.

[44] Berntson & Weiner, 1990; Ellison & Rabinowitz, 1989; Geber, 1989; Holbrook & Putz, 1989; Weiner & Thomas, 1992

An important implication of asymmetry is *sensitivity to initial conditions* (Silvertown, 1988). Slight differences in sizes at the onset of competition, whether arising from germination, genetics or other factors, will be amplified through time, as those individuals with even a slight size advantage gain proportionately more resources.

Symmetry is critically dependent on which resource(s) are limiting in a given situation (Schmitt et al., 1986). It is generally agreed that competition for light is asymmetric, because of shading effects (Weiner, 1986; Lieffers & Titus, 1989). In contrast, soil nutrients are thought to be more evenly divided. For example, root competition with the artificial exclusion of light competition minimises the importance of initial size (Wilson, 1988). Light and soil competition have also been described as *one- and two-sided* competition respectively, also *contest* and *scramble* (Watkinson, 1980a). In an interesting experiment with morning glory vines, Weiner (1986) showed that higher size variation develops under shoot competition than under root competition. It has further been suggested that early interference is for nutrients, followed by one-sided competition for light after canopy closure (Huston, 1986; Kenkel, 1988). Various models have addressed one- and two-sided interactions[45]. In particular, overlapping ZOI models have investigated different methods of allocation of resources in the overlap[46]. These models have highlighted the effects of different interference mechanisms on resulting population structure.

The results are presented here of two different models, aimed at (i) examining the effects of space and competition on individual plant growth and (ii) generating testable results on the relationships between size variability, density dependence and self-thinning for further field studies. Both models use an individual approach and in particular test:

- Bonan's (1988; 1991) assertion that a positive relationship between density and size inequality is evidence for neighbourhood effects and does *not* indicate the presence of competitive asymmetry;
- Miller & Weiner's (1989) claim that neighbourhood effects without asymmetry can only

[45] Diggle, 1976; Britton, 1982b; Miller & Weiner, 1989; Thomas & Weiner, 1989a; Tollenaar, 1992.

[46] Gates, 1978; Gates et al., 1979; Ford & Diggle, 1981; Huston, 1986; Bonan, 1988; 1991.

give rise to a positive relationship between density and size inequality over a range of very low densities. In their models increasing inequality at higher densities occurred only when competition was asymmetric.

The main model is a CML (chapter 2). The second model comes directly from Bonan (1988; 1991; 1993) and uses circular ZOI about each plant; the only difference is that the boundaries are treated as continuous or wrap-round. In each case, overlaps between neighbouring plants are calculated and the growth modelled for four types of competition (absolute symmetry, relative symmetry, absolute asymmetry, relative asymmetry). Stochasticity is limited to the random distribution of seedlings in the stand, so that neighbourhood effects are isolated. Although previous models have considered uniform patterns of plants, these are not realistic for natural populations and they are not used here. Finally, because density-dependent mortality has been said to mask the effects of asymmetric competition, death has been suppressed by restricting growth to be non-negative.

3.3. A Coupled Map Lattice Model.

A toroidal CML is used as an IBM of a plant monoculture, with the value of each cell representing the mass of the plant present in that cell. Mass is given as a proportion of the maximum possible plant size attainable by the model, multiplied by a factor of 1.1. This factor allows for possible overshooting caused by the discrete nature of the mathematical model. Each cell has a fixed area equal to one fifth of the maximum area attainable by a plant grown under the conditions set by the model. This is justified as follows. The neighbourhood of a cell consists of its four nearest neighbours and itself - a total of five cells (figure 6). As this is a model of competition between plants, plant growth is restricted so that it is never larger than its neighbourhood (ZOI). If this rule were violated, the plant would grow into regions where the model could not treat the interactions. Hence a suitable cell size is one fifth of the maximum area occupied by a single plant. The following mathematical model controls the growth of the plants through time. It is an extension of the model of Aikman & Watkinson (1980) and includes explicit spatial effects.

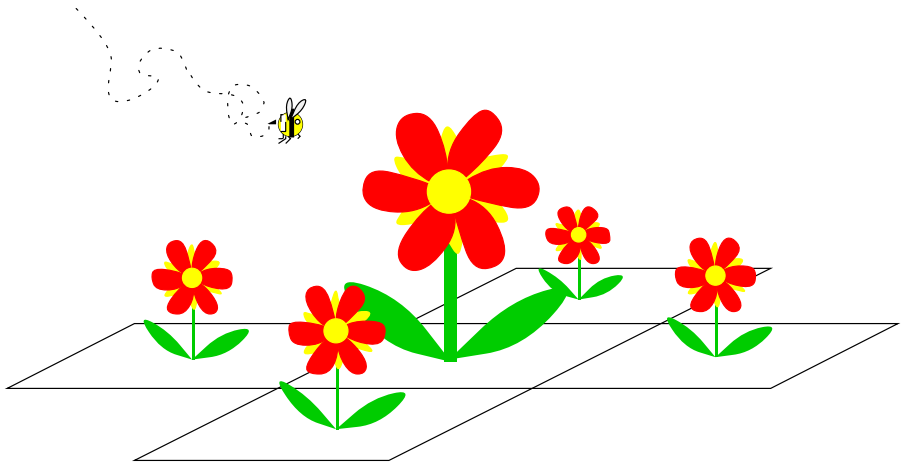

Figure 6: Representation of a Von Neumann cell neighbourhood.

Parameter	**Value**	
g	25	$gm^{-2}day^{-1}$
b	0.00147	$gday^{-1}$
c	0.00434	$m^{-2}g^{-\frac{2}{3}}$

Table 2: Parameter values for the plant growth equations in the single species CML model.

Symmetry option	**Competitive regime**
1	absolutely symmetric
2	relatively symmetric
3	relatively asymmetric
4	absolutely asymmetric

Table 3: Definitions of the competitive regimes in the single species CML model: 'symmetry 1' - 'symmetry 4'.

The change in mass ($\triangle m_i$) of plant i from one time step to the next is given by equation (15). a_i is the area covered by plant i and is given by the $\frac{3}{2}$ *self-thinning rule* of equation (41) (Moore, 1977; Westoby, 1977; Watkinson, 1980a; Hutchings & Budd, 1981; Westoby, 1984). ℓ_i is the growing area lost via competition, g is the intrinsic growth rate of the plant, b and c are constant parameters and $\triangle t$ is the time step.

$$\triangle m_i \quad = \quad \left(g\left(a_i - \ell_i\right) - b m_i^2\right) \triangle t \tag{15}$$

$$a_i \quad = \quad c m_i^{\frac{2}{3}} \tag{16}$$

It is necessary to establish the lost growing area for a plant in the lattice as a result of the competitive regime under consideration. This involves finding the areas by which neighbouring plants overlap each other. Firstly, the maximum size for a plant that is not experiencing competition (m_i^{max}) is obtained from equation (15) by taking $\ell_i = 0$ and $\triangle m_i = 0$:

$$g a_i \quad = \quad b m_i^2 \qquad \Rightarrow \qquad m_i^{max} \quad = \quad \left(\frac{gc}{b}\right)^{\frac{3}{4}}. \tag{17}$$

Hence, by equation (16), the area of each lattice cell, α, as the maximum mass divided over 5 sites, is:

$$\alpha \quad = \quad \frac{c}{5}\sqrt{\frac{gc}{b}}. \tag{18}$$

Assuming that a plant overflowing its own cell expands equally into the areas occupied by its four neighbours, the overlap into a neighbouring cell of plant i is:

$$\max\left(\frac{a_i - \alpha}{4}, 0\right)$$

and hence the total overlap between two neighbours i and j is:

$$\Omega_{i,j} \quad = \quad \max\left(\frac{a_i - \alpha}{4}, 0\right) + \max\left(\frac{a_j - \alpha}{4}, 0\right).$$

This leads to equation (19), which gives the total overlap of the area of the plant, Ω_i. *nhd* denotes the four-cell neighbourhood described above. (This is not a perfect model of the overlap of areas, but is a good approximation of the infinitely recursive series of overlaps that would have to be considered for an exact representation.)

$$\Omega_i \quad = \quad \sum_{i \in nhd} \max\left(\frac{a_i - \alpha}{4}, 0\right) + \max\left(\frac{a_j - \alpha}{4}, 0\right) \tag{19}$$

The area lost to competition, ℓ_i, depends on the type of competition used in the model. The four types of competition used here are representative of the spectrum of possibilities ranging from fully symmetric to completely asymmetric. For *absolute asymmetry*, the larger plant of two plants takes resources from the entire overlap area; equal-sized plants will share the area equally. For *absolute symmetry*, plants divide the area equally. For relative situations, the overlap is weighted by the relative masses, linearly for *relative symmetry* and quadratically for *relative asymmetry*. Hence the following equation can be derived to give the total area lost to competitors under the different competitive regimes:

$$\ell_i \quad = \quad \begin{cases} \sum_{j \in nhd} \frac{1}{2}\Omega_{i,j} & \text{absolute symmetry} \\ \sum_{j \in nhd} \frac{m_j}{m_i + m_j}\Omega_{i,j} & \text{relative symmetry} \\ \sum_{j \in nhd} \frac{m_j^2}{m_i^2 + m_j^2}\Omega_{i,j} & \text{relative asymmetry} \\ \sum_{j \in nhd} \phi(i,j)\Omega_{i,j} & \text{absolute asymmetry} \end{cases} \tag{20}$$

where:

$$\phi(i,j) \quad = \quad \begin{cases} 0 & m_i > m_j \\ 1 & m_i < m_j \\ \frac{1}{2} & m_i = m_j \,. \end{cases}$$

As self-thinning may mask the effects of local neighbourhood interactions and variation in competitive regime, density-dependent mortality is suppressed in this model. When $\triangle m_i < 0$, plant growth is prevented by setting this increment to zero. Thus the model can be expressed by:

$$m_i^{(t+1)} \quad = \quad m_i^{(t)} + \max\left\{ \left(g(a_i - \ell_i) - b m_i^2 \right), 0 \right\} ,$$

where the superscript t refers to the time step.

3.4. Analysis of the Basic Model.

The model of equations (15) and (16) is appropriate for annual plants. This section considers the density-dependent behaviour of the model when applied to a symmetric mean field scenario. If a certain number of plants is grown in a fixed area, then, under a symmetric competitive regime, each plant has a fixed maximum growing area, denoted by A. If the plants are able to reach the maximum mass, $m^{max} = \left(\frac{gc}{b}\right)^{\frac{3}{4}}$, before they suffer competition, then clearly the plants grow to this terminal size. If they fill their available area, no further growing space exists and their growth is restricted. This modifies the maximum size by changing the growing area a_i to A, so that $m^{max} = \sqrt{\frac{gA}{b}}$. There is thus a threshold value of density, above which the maximum plant mass is constrained. This threshold is determined by setting the area in equation (16) to A. Hence the density-dependence of the terminal mass is given by:

$$m^{max} \quad = \quad \begin{cases} \sqrt{\frac{gA}{b}} & A < \sqrt{\frac{gc^3}{b}} \\ \left(\frac{gc}{b}\right)^{\frac{3}{4}} & A \geq \sqrt{\frac{gc^3}{b}} \end{cases} \tag{21}$$

The maximum yield per unit area, Y, is then obtained in terms of the density, $\rho \equiv \frac{1}{A}$:

$$Y \quad = \quad \begin{cases} \rho\left(\frac{gc}{b}\right)^{\frac{3}{4}} & \rho < \sqrt{\frac{b}{gc^3}} \\ \sqrt{\frac{g\rho}{b}} & \rho \geq \sqrt{\frac{b}{gc^3}} \end{cases} .$$

Thus the yield increases indefinitely as the density rises. However, the growing time is restricted for annual plants, so the yield does not become infinite as growing space decline to zero. A suitable range of densities for the model must therefore be estimated.

3.5. The Circular Neighbourhood Model.

An alternative spatial model of plant monoculture development involves the construction of *circular neighbourhoods* (ZOI). The simulations allow plants to grow on a square plot and the plot edges are treated toroidally, as with the CML. Seedlings are randomly distributed over the plot and growth is simulated using the same model as before (equations (15) and (16)). The technique for allocation of seedlings ensures that the ZOI do not initially overlap, so that competition cannot occur immediately. The area of a plant (equation (15)) is translated into a circle of appropriate radius centred on the plant.

The spatial scheme is illustrated in figure 7, which represents a plot occupied by eight plants, labelled A to H. Plants A and B overlap the plot edge. In order that the plot may be treated as a torus, A* and B* are created as imaginary or *virtual* plants. These have 'real' effects on neighbours E and F (respectively). Thus G and H have no close neighbours; B, C and F have one neighbour; D and E have two neighbours; A has three neighbours (D, E and F). Plant C is entirely within the zone of influence of plant D and under asymmetric competition would not be able to grow.

The overlaps between neighbouring plants are needed to calculate the growing area lost to competition, ℓ_i. The overlap between two interfering neighbours, i and j, with zones of radius p and q respectively, which are a distance d apart, is:

$$\Omega_{i,j} \quad = \quad p^2 \cos^{-1}\left(\frac{p^2+d^2-q^2}{2pd}\right) + q^2 \cos^{-1}\left(\frac{q^2+d^2-p^2}{2qd}\right)$$

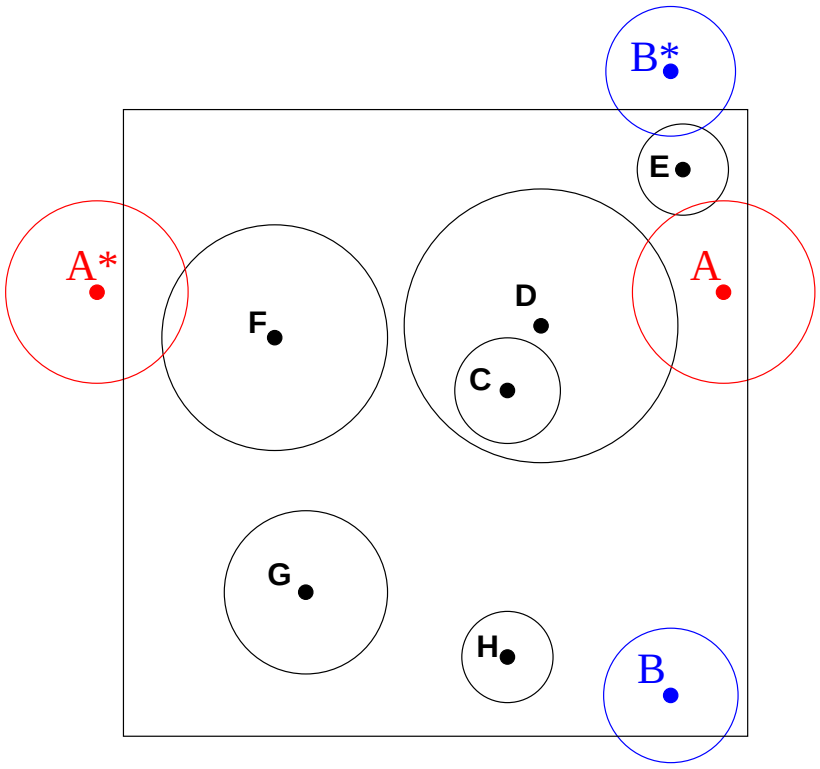

Figure 7: Schematic representation of eight plants in the circular neighbourhood model. A* and B* are *virtual* plants, generated to satisfy the toroidal boundary conditions.

$$- \quad qd \sin\left(\cos^{-1}\left(\frac{q^2+d^2-p^2}{2qd}\right)\right)$$

where:

$$p \quad = \quad \sqrt{\frac{cm_i^{\frac{2}{3}}}{\pi}} \quad \text{and} \quad q \quad = \quad \sqrt{\frac{cm_j^{\frac{2}{3}}}{\pi}}.$$

If one plant is entirely contained within the zone of influence of another, then the overlap is equal to the area of the smaller circle ($cm_i^{\frac{2}{3}}$). The lost growing area is then calculated according to the type of competition, as in equation (20). In this model the neighbourhood *nhd* of plant i consists of all plants whose ZOI overlap plant i. Again, mortality is avoided by constraining the mass increment to obey $\triangle m_i \geq 0$.

3.6. Population Statistics and Simulation Parameters.

3.6.1. Statistical Measures.

The following statistics were used to examine the plant population statistics of the two models. The mean mass, μ, (equation (22) is averaged over the lattice $\mathcal{L}$). The coefficient of variation (equation (23)) is the standard deviation adjusted for the mean mass. This provides a good measure of the variability within a population. Another indicator of variability is the Gini coefficient used in the plant ecology literature, which is related to the Lorenz curve of cumulative frequencies. Equation (24) gives a relatively unbiased estimator of the Gini coefficient for $||\mathcal{L}|| > 100$ (Weiner & Solbrig, 1984; Dixon et al., 1987, Bendel et al., 1989).

$$\mu \quad = \quad \frac{1}{||\mathcal{L}||}\sum_{i\in\mathcal{L}} m_i \tag{22}$$

$$\text{coefficient of variation} \quad = \quad \frac{1}{\mu}\sum_{i\in\mathcal{L}} \frac{(m_i-\mu)^2}{||\mathcal{L}||-1} \tag{23}$$

$$\text{Gini coefficient} \quad = \quad \frac{\sum_{i \in \mathcal{L}} \sum_{j \in \mathcal{L}} |m_i - m_j|}{2\|\mathcal{L}\|.\|\mathcal{L} - 1\|} \tag{24}$$

3.6.2. Computational details.

The parameters for equations (15) and (16), which are taken from Bonan (1991), are given in table table 2. A time step of $\triangle t = 1\ day$ was used, after comparative simulations showed negligible impact of smaller steps. Seedlings were sown with size $0.1g$, which was small enough (by several orders of magnitude) to ensure no competition in the first few times steps. Previous studies of spatial plant growth involved the variation of the initial mass and parameters g, c or b. These variations were usually taken to be *Gaussian* or *Normal*. Such distributions were used to represent genetical variation, micro-environmental heterogeneity and variation in seedling emergence times. The parameters were taken here to be constant so that neighbourhood effects and the influence of competitive regime could be studied. Runs with a uniform distribution of initial seedling mass between 0 and $0.1g$ produced very similar results to those with a constant seedling size of $0.1g$. The effect of Normal seedling size distribution on the population structure is investigated in section 3.8.

The CML model was run on grids of 20 by 20, 50 by 50 and 100 by 100 cells. Densities were expressed as the proportion of cells occupied by plants, ranging from 0.1 to 1.0. The circular neighbourhood model was run on a square plot with dimensions $0.1m$. Densities were given in terms of the number of plants randomly distributed on this plot; specifically the ten values are 7, 19, 37, 61, 91, 127, 181, 233, 291 and 355 plants, as used by Bonan (1991). This range extended to higher values than the CML; the latter was restricted by the ratio of neighbourhood size to cell size. Repeated simulations were run to produce smoother averaged results. The statistical variables considered were mean, coefficient of variation and Gini coefficient. The distribution of sizes and the patterns of suppressed thinning were also considered.

3.7. Results.

3.7.1. Coupled Map Lattice Model.

The growth of plants through time, for five different densities in the range 0.2 to 1.0, is illustrated in figure 8. The absolutely symmetric regime is illustrated here, but the form of growth is similar for all of the types of competition. The mass is seen to increase sigmoidally with time and to decrease as density rises. Equilibrium has been (approximately) attained within the 200 time steps. These results shown are those obtained from a 20 by 20 grid. The model has also been run for larger grid sizes, but as the growth did not differ in any way, a smaller grid size has been used for computational speed.

The model was then run for 200 time steps (= 200 days) on a 50 by 50 lattice, for ten different densities in the range 0.1 to 1.0. The results were averaged over 50 simulations. Figures 9a - c give the dependence on density of mean mass, coefficient of variation and Gini coefficient.

The distribution of plant sizes after 500 time steps is shown in figures 10a - d for density 0.5. These graphs were produced by a single run on a 50 by 50 lattice. The large time used ensured that the equilibrium was reached in all cases. At this density of 0.5, the distributions contained fewer peaks as the degree of asymmetry increases, but they become narrower. When the density was set at 1.0, a single very sharp peak was obtained for all competitive types, as all plant neighbourhoods and hence all growth rates were identical.

3.7.2. Circular Neighbourhood Model.

The model was run for 100 time steps at ten different densities (7 to 355 plants in the plot) and the results averaged over 100 simulations. Figures 9d - f give the dependence on density of the three statistics of mass: mean, coefficient of variation and Gini coefficient. The model was run for the higher densities of 400, 450, 500 and 550, but the results showed no different behaviour. It should be noted that these new results using Bonan's model are different from those reported in Bonan (1991) and the results here are smooth due to the number of replicated runs.

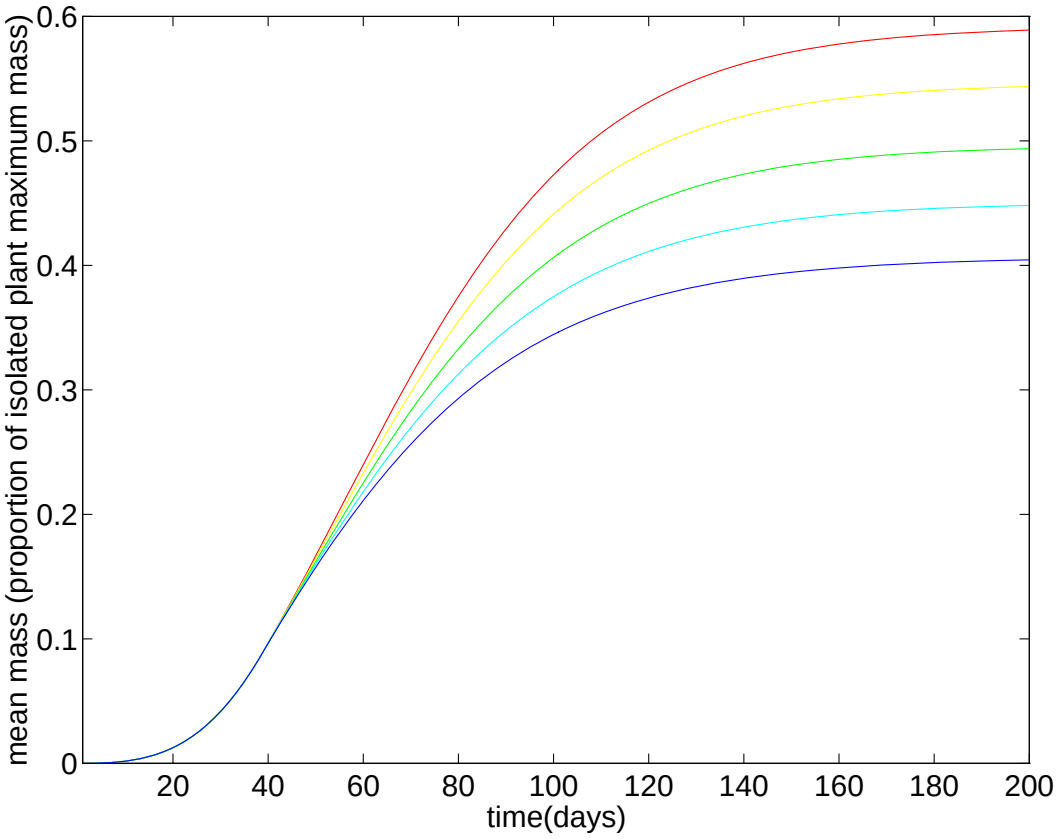

Figure 8: Mean mass of plants grown under the single species CML model: proportion of maximum isolated plant size as a function of time. The five curves show different densities, from 0.2 (red) to 1.0 (blue) rising in steps of 0.2. Competition is absolutely symmetric.

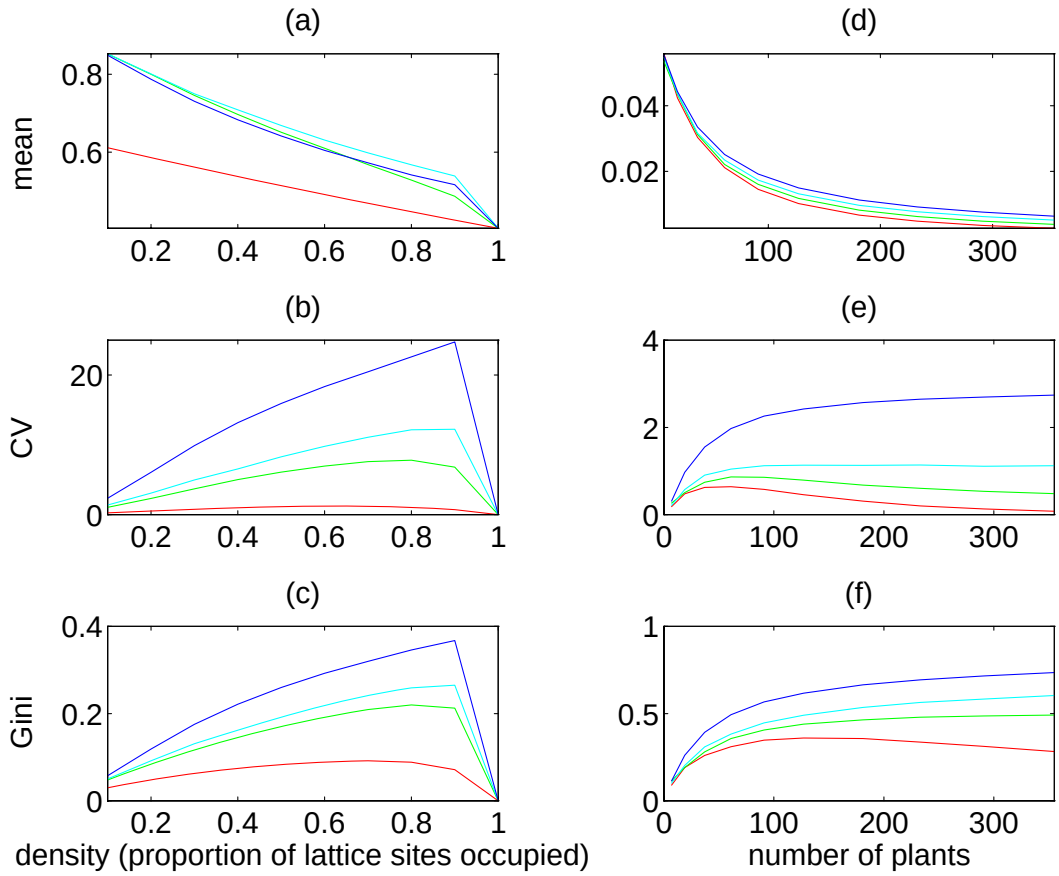

Figure 9: Population statistics for the single species CML model. (a) - (c) The CML model at time 200 days. (a) Mean mass (proportion of maximum isolated plant size) as a function of density. (b) Coefficient of variation of mass as a function of density. (c) Gini coefficient of mass as a function of density. (d) - (f) The circular neighbourhood model at time 100 days. (a) Mean mass (g) as a function of number of plants (equivalent to density). (e) Coefficient of variation of mass as a function of number of plants. (f) Gini coefficient of mass as a function of number of plants. In all cases the competitive types are absolute symmetry (red), relative symmetry (green), relative asymmetry (cyan) and absolute asymmetry (blue).

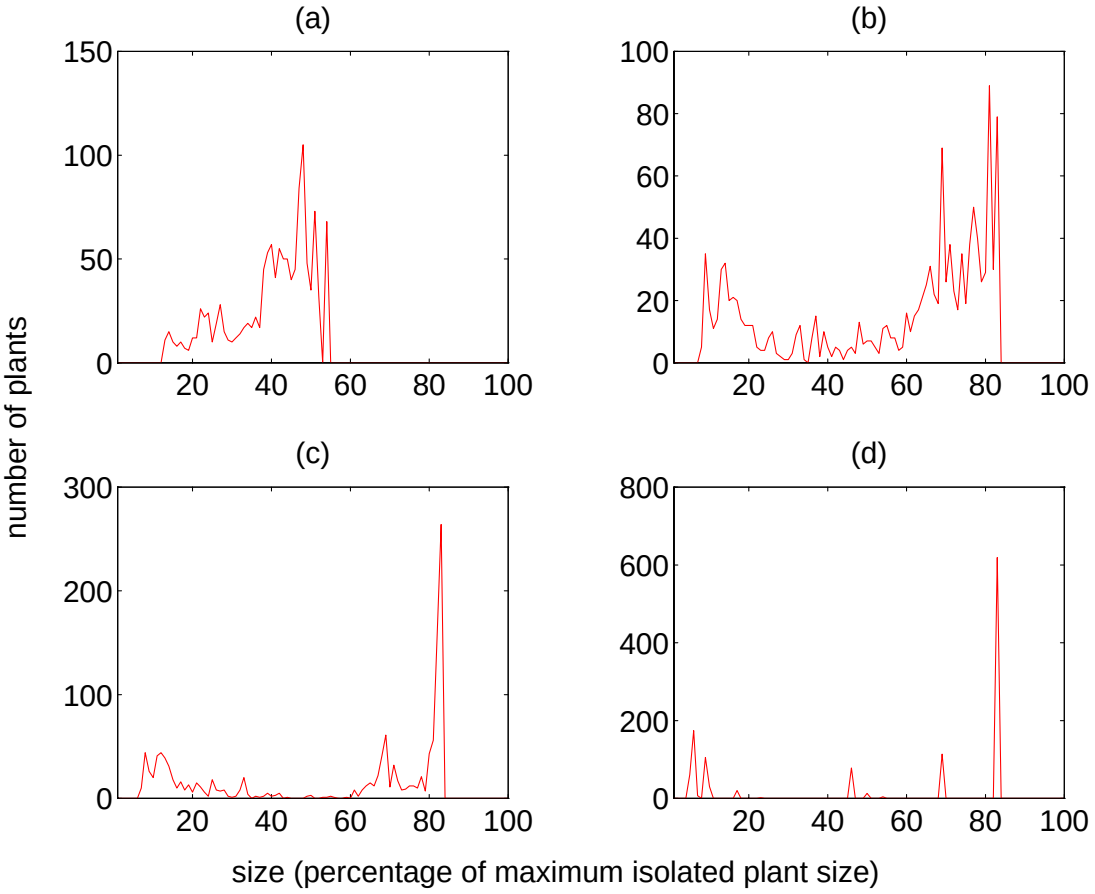

Figure 10: Distribution of plant sizes in the single species CML model at time 500 and density 0.5 for the CML model, as a percentage of the maximum size of an isolated plant. (a) Absolute symmetry. (b) Relative symmetry. (c) Relative asymmetry. (d) Absolute asymmetry.

3.7.3. Self-thinning.

Since the condition $\triangle m_i \geq 0$ prevented density-dependent mortality, it was of interest to find the extent to which this constraint was implemented. The two models were run for 100 time steps and the number of plants where the mass increment was reset to zero was found as a function of density. The circular neighbourhood model was run only once because of the highly intensive computation, whereas the CML was averaged over 50 simulations. Figures 11a - b illustrate the results: the degree of self-thinning that would occur, if permitted, increased with the level of asymmetry, particularly for the CML.

3.8. Discussion.

The results show that the mean mass decreases as density increases (figures 9a and d). Because mass in the CML is given as a proportion of maximum isolated plant size, it is clear that size has been constrained by competition (Mack & Harper, 1977; Ellison & Rabinowitz, 1989; Grace & Tilman, 1990). Competition can thus be considered a boundary constraint on plant size, as previously described by Goldberg (1987).

Growth of the plants is sigmoidal, so the early phase is exponential. Turner and Rabinowitz (1983) claim that variation in the early exponential phase of growth leads to the generation of size hierarchies. However, interference does not occur immediately, as mass is the same for all densities for the first 50 or so time steps (figure 8). As the initial plant masses are constant and no competition occurs during the early part of growth, there can be no size hierarchy formation at this stage. Variation in growth rates can thus only occur when competition sets in *after* the exponential stage of growth.

The mean mass of plants is similar for all the competitive schemes, except for the absolute symmetry in the CML (figure 9a). This may be attributed to the equal sharing of resources, that is, two neighbours of a similar size in adjacent cells prevent each other growing. If there is any asymmetry present, at least one of the plants is able to grow. Because of this, the even spacing of plants caused by the regularity of the lattice and interference by neighbours the total

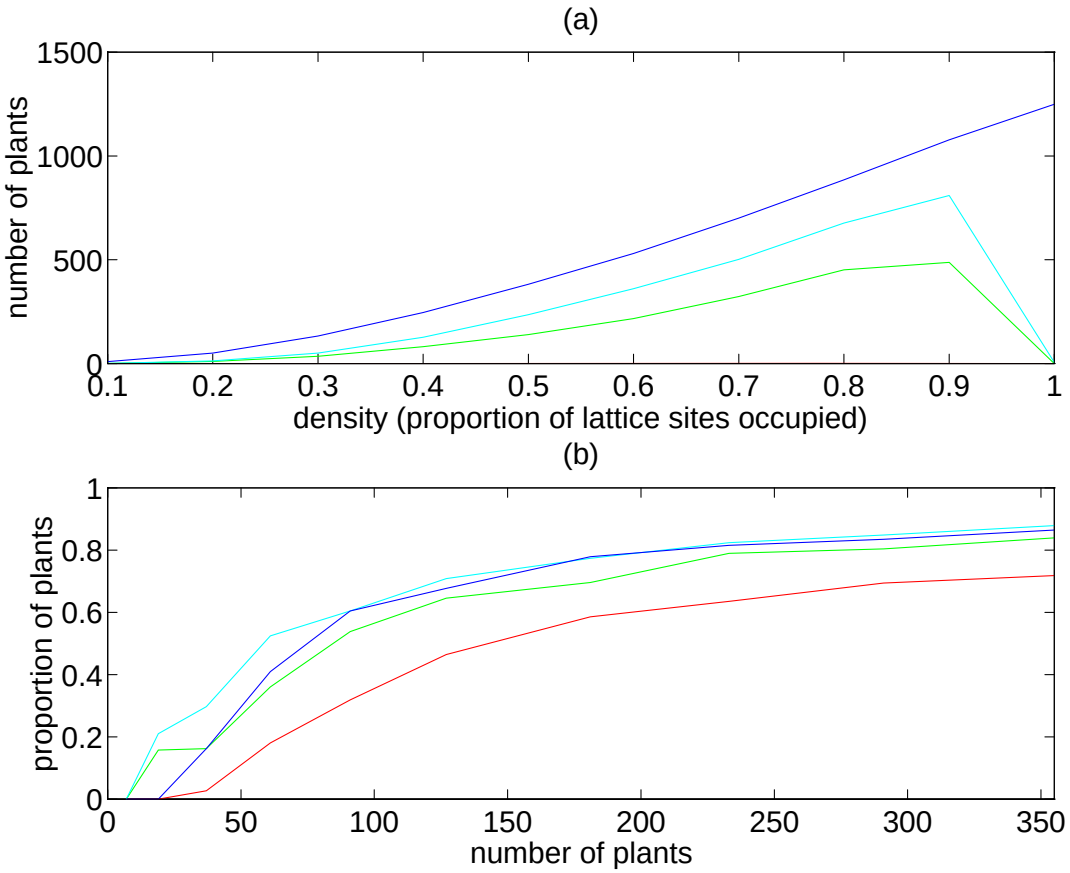

Figure 11: The proportion of plants which stop growing in the single species CML model by time 100 days. (a) CML model, shown as a function of density. (b) Circular neighbourhood model, shown as a function of initial number of plants. In both cases the competitive types are absolute symmetry (red), relative symmetry (green), relative asymmetry (cyan) and absolute asymmetry(blue). (The values are so low in the CML model for absolute symmetry (a) that the red curve is not easily distinguished from the horizontal axis.)

population yield is suppressed.

The coefficient of variation and Gini coefficient demonstrate the existence of variation in the population, allowing the formation of size hierarchies to be seen (figures 9b, c, e and f). The variation increases as the density rises, because higher densities lead to earlier and stronger interactions between plants. The variation is considerably greater with absolutely asymmetric competition. There is a clear difference between the coefficient of variation for relative symmetry and absolute asymmetry, which are the most commonly considered modes of competition (figures 9b and e). The difference is less marked with the Gini coefficient (figures 9c and f). Bendel et al. (1989) have noted that the coefficient of variation is more sensitive to hierarchy differences than the Gini coefficient.

It is therefore reasonable to state that the formation of hierarchies can distinguish between symmetric and asymmetric competition, as claimed by Miller and Weiner (1989) and Weiner (1985, 1986, 1990) but disputed by Bonan (1988, 1991). There is, however, some variation even in the symmetric case. This confirms that spatial/neighbourhood effects do play a significant role in the generation of size variability (Bonan 1988, 1991), but they are secondary to the competitive regime. The use of the four different symmetries illustrates the progressive nature of competition mechanisms. It is relevant to express the conclusion as follows: *higher variability at higher densities implies greater asymmetry in neighbourhood interactions.*

The sudden decrease in all the mass statistics at the highest density of the CML (figures 9a - c) is caused by the regularity of the lattice. This is because for low and intermediate densities, the plants are scattered through the grid, whereas when the lattice is full (density 1.0), the plants are necessarily regularly spaced, so the randomness of the spatial distribution is lost. The rate of increase in the coefficient of variation and Gini coefficient for both models falls off as density rises. This partially reflects a decrease in the effective randomness of the distribution as the initial density of plants is increased. There is less variation at higher densities in the overlapping of zones of influence and so the growth rates and hence the plant sizes are more similar.

The hierarchy is still able to remain strong in the asymmetric case and there is a large variation in plant sizes (figures 10c and d). Here the asymmetry dominates the plant growth and the distribution is of secondary importance in determining the final population structure. The size distribution plots (figures 10a - d) give an insight into the effects of the degree of asymmetry on the population structure. Symmetric competition results in a wide distribution, which is skewed to the right because of the suppression of mortality. Absolute asymmetry restricts the plants to a discrete set of sizes. These size classes are used in Appendix A to reduce the CML model to a CA, thus allowing long time scales to be used.

The levels of thinning (figures 11a and b) exhibit an appreciable difference between the two models. The coupled map lattice shows that greater asymmetry leads to more density-dependent mortality, as suggested by Bonan (1988). The self-thinning is less dependent on symmetry in the circular neighbourhood model. Greater asymmetry means that large plants cause the death of smaller plants, whereas with symmetry, similar neighbours will reduce each others' growth rather than bring about death. These discrepancies between the models demonstrate that the type of spatial distribution used is important.

The comparison of the two types of model (CML and circular neighbourhood model) highlights the issue of the aims of ecological modelling (Wissel, 1992b). The excessive computation of the latter type of model limits the extent of investigation of the system. The CML allows critical mechanisms to be quickly and thoroughly studied and general results extracted; it is ideal for use at low and intermediate densities. The current implementation of the CML does have the shortcoming of limiting the upper end of the density range. However, the model is suitable for extension to higher densities through development of the use of larger neighbourhoods.

In summary, the results of both models support the view that size hierarchies can be used as evidence to distinguish between asymmetric and symmetric competition (Weiner & Thomas, 1986) over the alternative view that size hierarchies are evidence for neighbourhood effects (Bonan 1988; 1991). Asymmetric competition is a key factor in determining size variation in plant populations and communities.

3.9. The Effect of Variation of Initial Seedling Weight.

The effect of a Normal distribution of initial seedling sizes on the mean and coefficient of variation of plant mass is considered in this section. The initial conditions of the CML were altered so that the plants were independent normally-distributed random variables of mean $0.1g$ and standard deviation σ, where σ is expressed as a percentage of the mean. The parameters of table 2 were again used and the full range of symmetry types (table 3) were run on a 50×50 grid for 200 time steps. Firstly σ was varied between 1% and 50% for a full grid (density 1), then the response of non-zero σ to a range of densities was studied.

The final mean mass of plants was very little affected by σ, whereas the coefficient of variation of mass was strongly affected by the value of σ (figure 12a). The impact of seedling variation was particularly strong for the more symmetric competitive types, with the coefficient of variation for absolute symmetry rising by five orders of magnitude as σ increases from 1% to 50%. There was little effect of σ on absolute asymmetry, because even small plant-to-plant variation was greatly amplified by one-sided competition. On the other hand, symmetric interactions did not appreciably affect the population structure, reflecting the initial distribution much more closely in this case.

Figure 12b shows the coefficient of variation of mass as a function of density for $\sigma = 10\%$ initial seedling weight variation. By comparison with figure 9b, it can be seen that σ played no significant part in the response of the population structure to density effects. The only exception was for the full grid (density 1), where $\sigma = 0\%$ did not allow any variation because all neighbourhoods were necessary identical, as discussed in section 3.7. For $\sigma > 0\%$, initial variation was able to develop with the stand; in particular the coefficient of variation increased monotonically under absolute asymmetry. Thus the conclusions of section 3.7 hold for populations with varied seedling sizes: increased variation at higher density implies asymmetry of interactions.

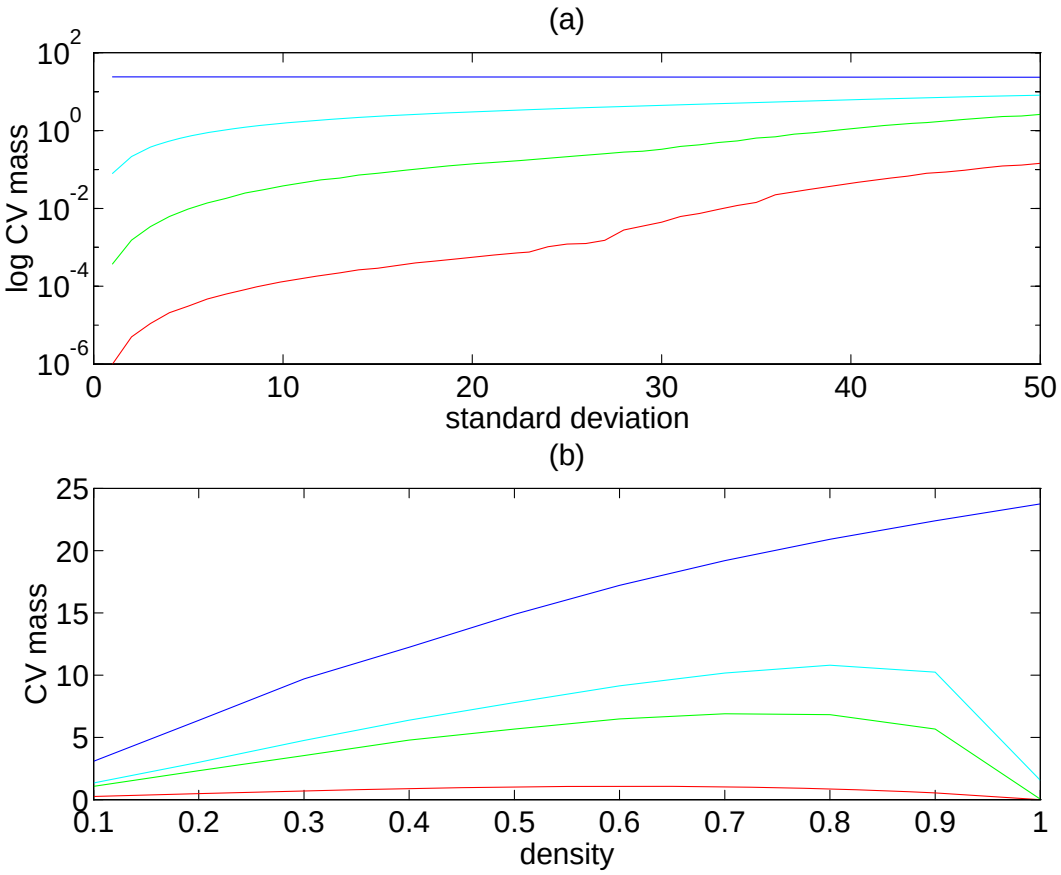

Figure 12: Results of the single species CML model assuming initial seedling variation. (a) Coefficient of variation of mass as a function of initial variation σ (% of mean initial seedling size) assuming a Gaussian distribution. (b) Coefficient of variation of mass as a function of density for $\sigma = 10\%$. In all cases the competitive types are absolute symmetry (red), relative symmetry (green), relative asymmetry (cyan) and absolute asymmetry (blue).

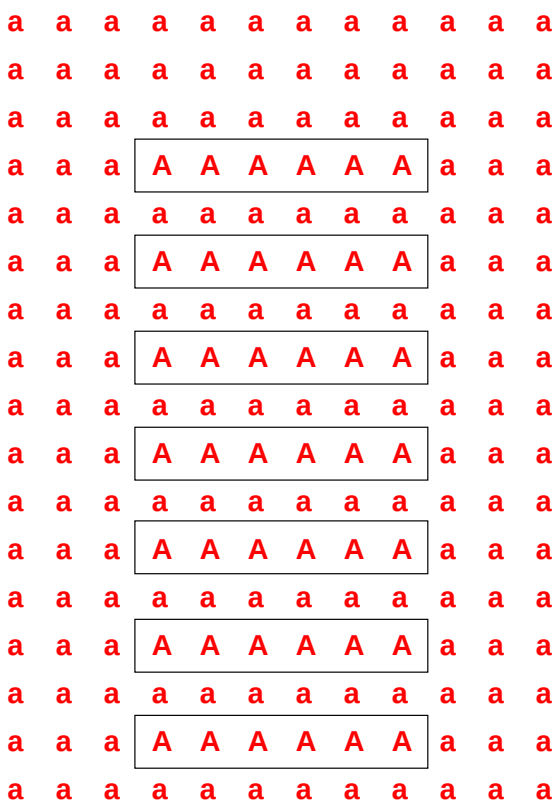

Figure 13: Arrangement of carrot seedlings in the single sowing experiment. Upper case letters give harvested plants.

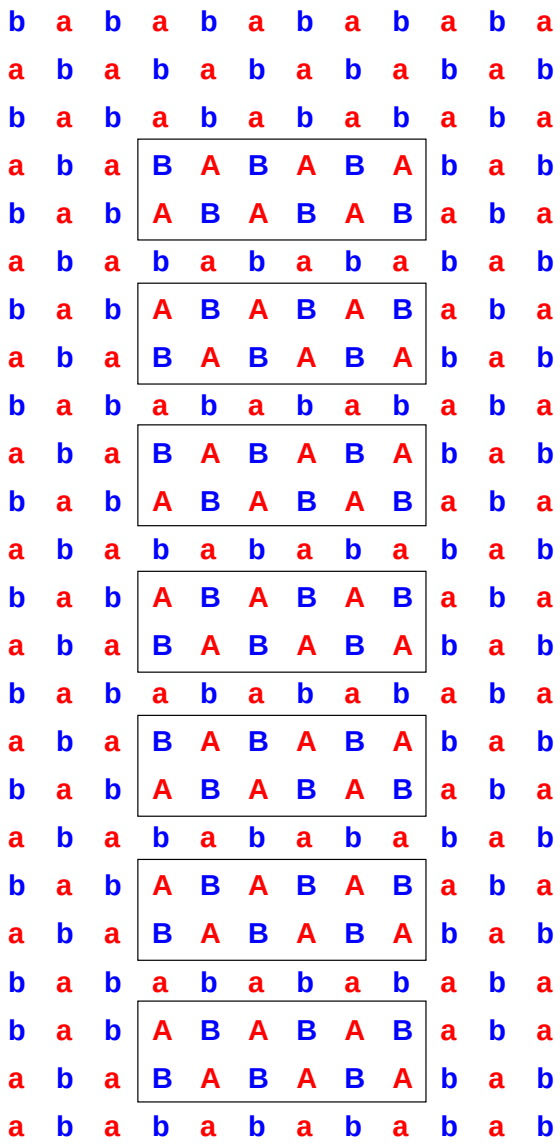

Figure 14: Arrangement of carrot seedlings in the double sowing experiment. Upper case letters give harvested plants. **a** is sown on day 1; **b** is sown on day 14.

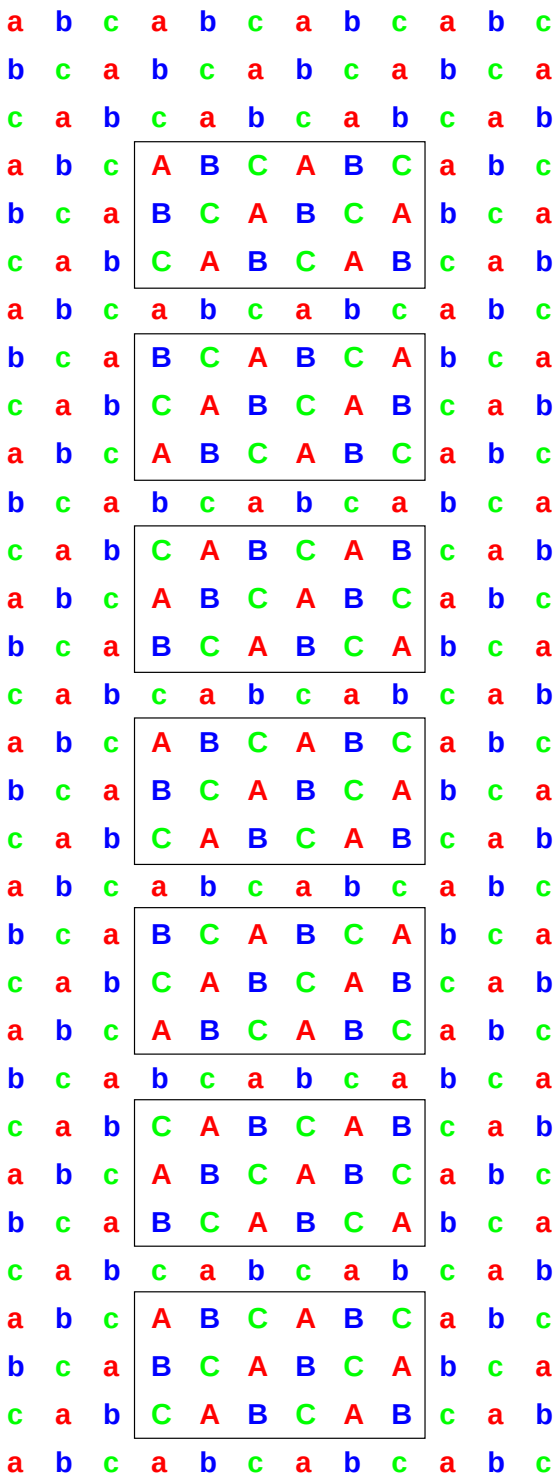

Figure 15: Arrangement of carrot seedlings in the triple sowing experiment. Upper case letters give harvested plants. **a** is sown on day 1; **b** is sown on day 14; **c** is sown on day 21.

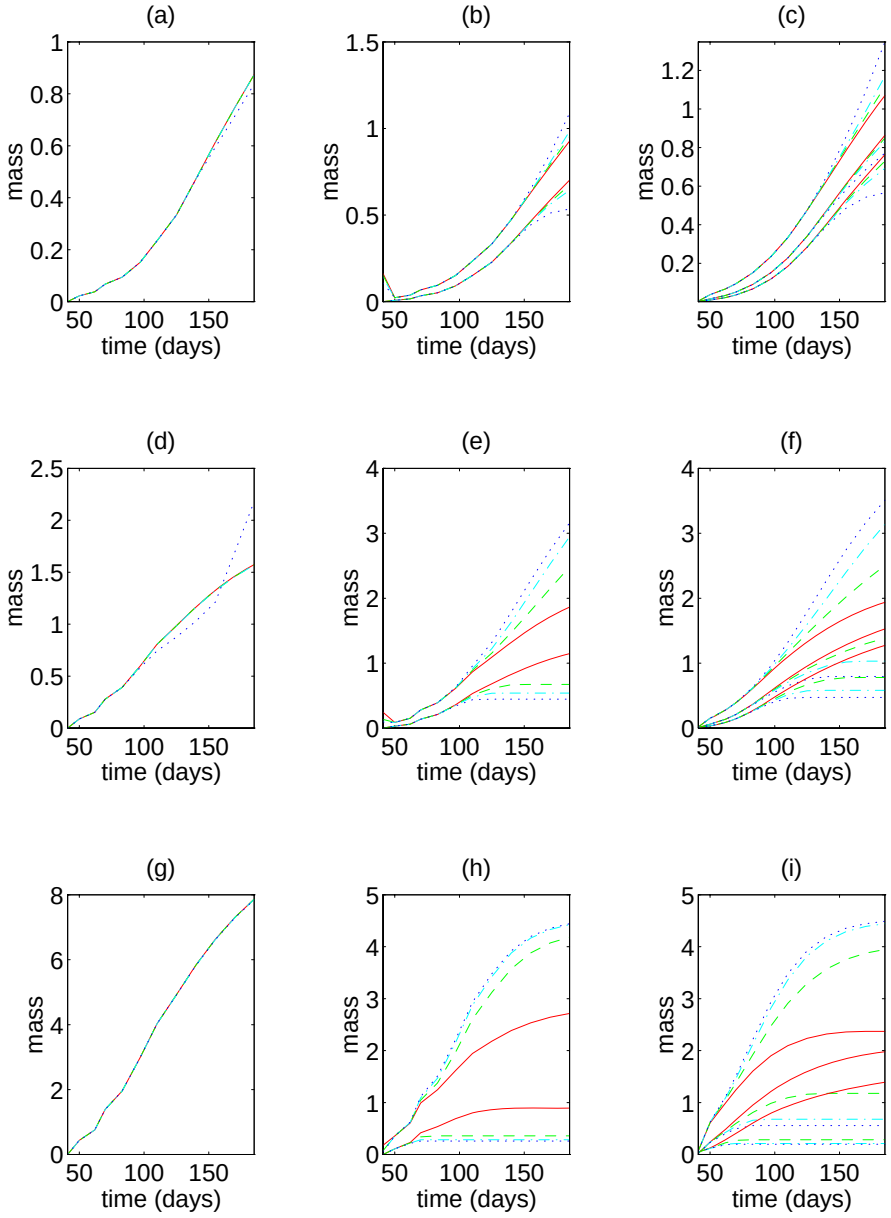

Figure 16: Results of the carrot CML model: mean masses for the 6 harvested plants at each harvest date. Intrinsic growth rates are $g = 5$ (a - c), 10 (d - f) and 20 (g - i). The columns are respectively the single, double and triple sowing simulations. The competition types are absolute symmetry (red), relative symmetry (green), relative asymmetry (cyan) and absolute asymmetry (blue).

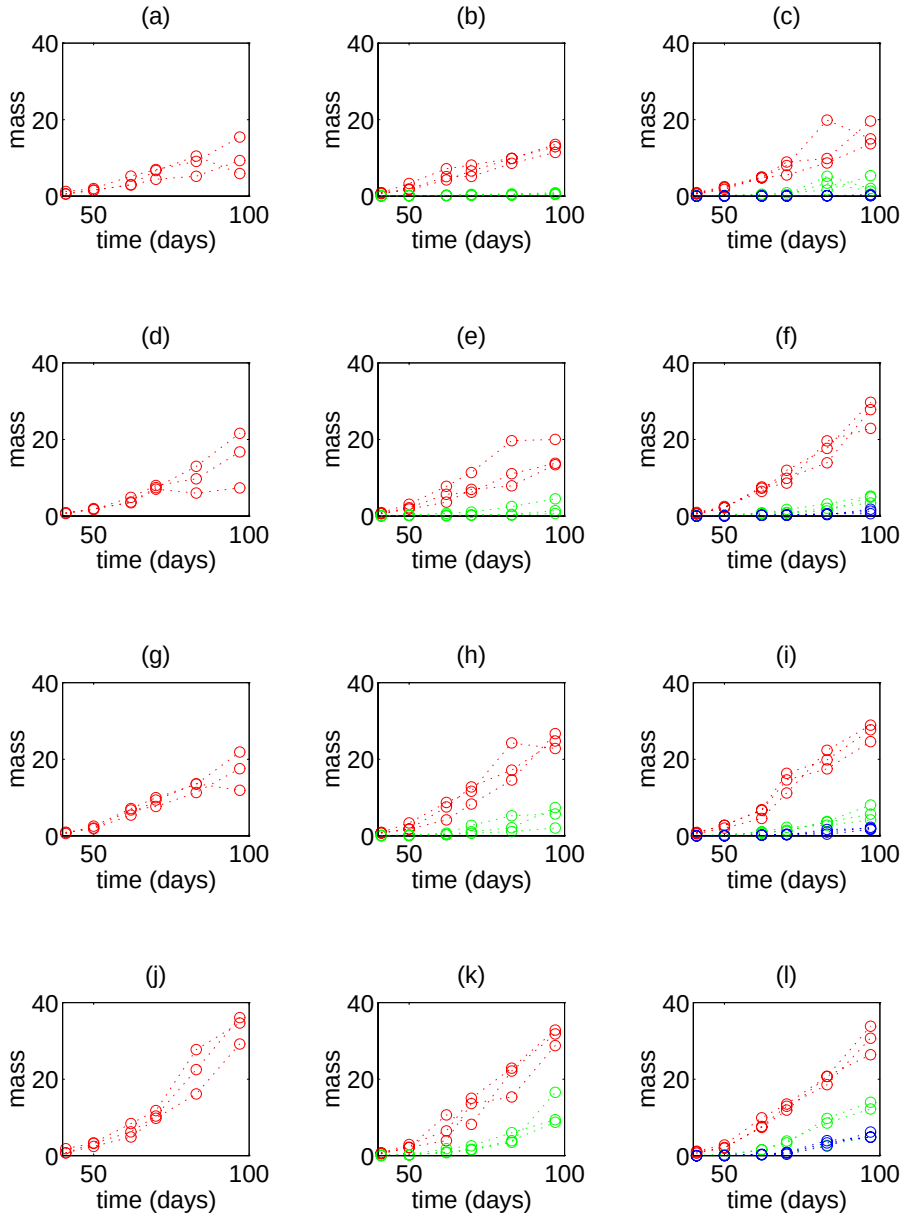

Figure 17: Experimental data for the carrot experiments: mean masses for the 6 harvested plants at each harvest date. Inter-plant spacings are $5.0cm$ (a - c), $7.5cm$ (d - f) $10.0cm$ (g - i) and $15.0cm$ (j - l). The columns are respectively the single, double and triple sowing simulations. Three replicates are shown for each experiment.

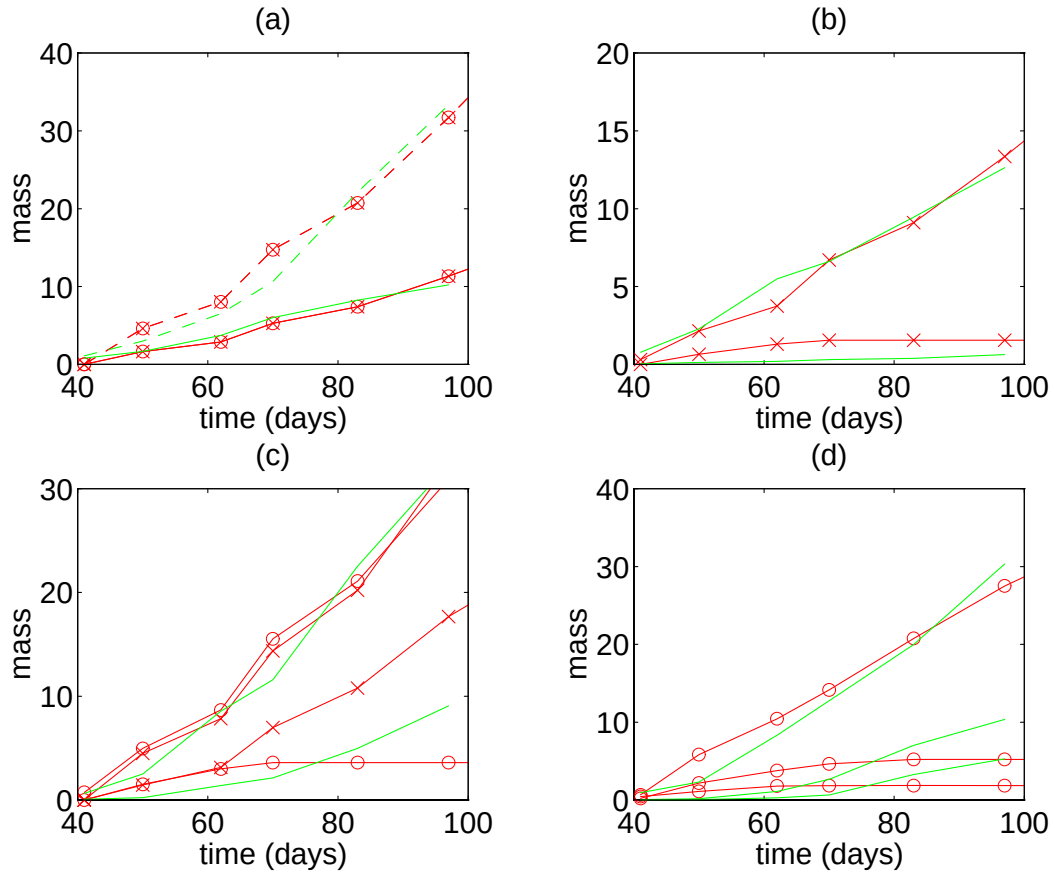

Figure 18: Sample fits of CML output to empirical carrot data: mean masses for the 6 harvested plants at each harvest date. (a) Single sowing, data (green) for spacing $5cm$ (—) and $15cm$ (- - -) with fitted models (red): absolutely symmetric (- o -) and absolutely asymmetric (- × -) with $g = 20$. (b) Double sowing, data for spacing $5cm$ (green) with fitted model absolutely asymmetric and $g = 20$ (red). (c) Double sowing, data for spacing $15cm$ (green) with fitted model absolutely asymmetric (red): $g = 20$ (- o -) and $g = 10$ (- × -). (d) Triple sowing, data for spacing $5cm$ (green) with fitted model absolutely asymmetric and $g = 20$ (red).

3.10. Application of the Coupled Map Lattice to Crop Data.

3.10.1. Introduction.

In this section the CML model is adjusted to model a field experiment on carrot plants (Daucus carota) carried out at Horticulture Research International at Wellesbourne in Warwickshire in the summer of 1985. Seedlings were planted on three sowing dates in a grid and harvested over the subsequent 100 days. Three of the sowing patterns were examined: *single*, *double* and *triple* sowing dates. In the first case all plants were sown on day 1. In the second case alternate plants were sown on day 1 and the remainder on day 14. The final experiment planted every third plant on day 1, half of the gaps were filled on day 14 and the rest on day 21. Plants of each cohort were harvested on days 41, 50, 62, 70, 83 and 97. Four different inter-plant spacings were used: 5, $7\frac{1}{2}$, 10 and $15cm$; there were three replicates of each sowing treatment.

The sowing and harvesting patterns are shown in figures 13 - 15. The letters **a**, **b** and **c** refer respectively to the sowings on days 1, 14 and 21. Upper case letters indicate harvested plants and lower case letters give 'guard plants'. The blocks of harvested plants were removed and weighed, starting from one end of the grid. Further experimental details are given in Benjamin (1988) as experiment 2.

3.10.2. Extension of the Basic Model.

The carrot experiment is ideal for simulation by a CML because of the rectilinear pattern of the plants. The width of the CML model was changed to 12, as in the experiments. The length was changed to 29, 42 and 55 for the single, double and triple sowings, to allow 12 harvestings to be simulated. This was twice as many as the experiment, to allow further development of the stand to be studied.

Seedlings were 'sown' on the CML at the three sowing dates in the patterns given by figures 13 - 15, with mean initial mass 10^{-5} (relative to the maximum mass described in section 3.2 and equation (17)) and with a standard deviation of σ. At the appropriate iterations, 6 plants were removed of each type (**a**, **b** or **c**) by resetting their masses to zero and the mean masses

attained were recorded. The model was run for the single, double and triple sowings and for all four competitive symmetries (table 3). Standard deviations of $\sigma = 0\%$, 1% and 10% of the initial plant size were used. A range of intrinsic growth rates were used: $g = 5$, 10 and 20 ($gm^{-2}day^{-1}$). The results were averaged over 25 runs to produce smooth curves.

3.10.3. Results and Discussion.

Figure 16 shows the mean mass for the single, double and triple sowings for the three growth rates. These curves are for the 0% standard deviation, but the other cases resulted in values differing by less than 0.1%. Variation of symmetry type has significantly different effects only for the multiple sowings and for sufficiently higher growth rates (comparing firstly figures 16a, d, g with c, f, i and secondly a, b, c, with g, h, i). Since there is a plant in every CML cell (density 1.0) in the single-sowing even-aged stand, there is no significant difference between the plants to be enhanced by greater asymmetry of competition. In the multiple-aged stands, the first-sown plants have an advantage over later cohorts. This is magnified by asymmetric interference as is particularly clear in figures 16h - i.

The intrinsic growth rate g (equation (15)) also significantly affects the resulting population structure. If the growth rate is low, the first cohort does not gain such an advantage over later plants and there is less effect of asymmetric competition. If the growth rate is high, the first plants gain such a size advantage that even slight asymmetry leads to great size differences between the cohorts. Hence there is the most difference between the symmetry types at intermediate growth rates (figures 16d - f).

Figure 17 shows the experimental data for the 12 combinations of plant spacings and sowing treatments, each with three replicates. The double and triple sowing experiments show significant differences between the first and subsequent cohorts, which indicates considerable asymmetry of interaction. These differences arise at a fairly early stage, indicating a relatively high intrinsic growth rate. As the spacing between plants rises, the second and third sowings produce relatively larger plants. The larger growing space delays interactions, so there is less opportunity for size differences to arise. Wider spacing is thus equivalent to a lower growth

rate at a fixed spacing, which is a constraint of the CML model.

Although this model is intended only to study the type of interactions, data not being available for parameter estimation, a basic comparison can be made by fitting a constant multiple of the model output to the empirical data by a least squares technique. Figure 18 shows fittings for sample single, double and triple sowings. Figure 18a shows the results for a single sowing at the maximum and minimum spacings, with a good fit to the data by the absolutely asymmetry model with $g = 20$. Figure 18b shows the $5cm$ spacing for the double sowing, with a reasonable fit for absolutely asymmetry and $g = 20$. The largest spacing, figure 18c, is apparently mid-way between the $g = 10$ and $g = 20$ model results. Thus as expected, the wider spacing is equivalent to a lower growth rate. The triple sowing data provide a less good fit, as the later cohorts of carrots carried on growing larger for slightly longer than the model predicted (figure 18d).

In conclusion, the plant CML model was able to show that carrot plants grown on a rectangular lattice experienced predominantly asymmetric competition, resulting in high levels of suppression in later cohorts of plants.

4. A Model for Annual and Perennial Plant Communities.

Chapter Summary

The plant coupled map lattice of chapter 3 is extended to two species and multiple years. The two species are described as short-lived annuals and long-lived clonal perennials. Growth is represented deterministically, as in chapter 3, whereas reproduction is modelled stochastically. Perennials propagate via localised ramet production and annuals produce seeds that are dispersed via a random walk.

Annuals in monoculture persist for a wide range of demographic parameters. In contrast, perennial survival depends on a threshold function of the birth:death ratio. A mean field approximation highlights the importance of space by presenting discrepancies between the spatial and non-spatial systems at high and at low perennial reproduction rates.

Patterns form in the lattice system: the clumping index is used to quantify the deviation of the pattern from random. Perennials are clumped both in monoculture and in competition, whereas the annuals are very nearly random in monoculture, but are constrained to patches in competition with the perennials. The imposition of a range of scaling relations on the annuals population by the presence of perennials is demonstrated by multifractal analysis, which further illustrates the asymmetrical relationship of the two species and provides an indication of underlying complex interactive mechanisms.

The coherence length scale is shown to be of order 10^2, which means that a large grid size is essential to the dynamics. The length scale analysis identifies negative spatial coherence of annuals over small scales, corresponding to the dispersal process, while the perennials always show positive spatial coherence.

'If one way be better than another, that you may be sure is Nature's way' - Aristotle

4.1. Introduction.

The CML model of chapter 3, which examined the interaction of individual plants, competitive mechanisms and population structure in a single species plant community over a short time scale is expanded in this chapter. The model is extended both to multiple years and to two species and is used to investigate the effect of individual plant performance on the size and spatial structure of a bispecific community. The impact of long-lived clonal species on the persistence and spatial structure of short-lived localised species is investigated and illustrated using selected numerical techniques, including a *clumping index* and *multifractal analysis*.

The long-lived *perennial* species is assumed to rely on propagation by vegetative growth, in a manner motivated by the CA type model of Crawley & May (1987), in which the dynamics of an annual-perennial community are simulated by simply recording the presence/absence of each plant. The short-lived *annual* species, in contrast, reproduces by scattering seeds over its immediate locality. The use of a CML rather than a CA allows the plasticity of individuals to be incorporated in the system and the distribution of mass to be studied in addition to the distribution of individual plants.

4.2. Extension of the Coupled Map Lattice to Competing Plant Populations.

In each growing season, the individual annual and perennial plants both follow the same growth patterns as in chapter 3, as summarised by equations (15) and (16). Thus the species difference is limited to the propagation mechanism (Hegazy, 1994) and species longevity (Symonides, 1988). At the end of each year, all of the annual plants produce seeds and die. The number of seeds per annual plant depends on the size of the plant at the end of the year (Dolan & Sharitz, 1984; Thompson et al., 1991; Klinkhamer et al., 1992). A full size annual (whose growth has not been limited by competition) is assumed to produce 100 seeds; smaller plants produce proportionately fewer seeds. Each seed is scattered in turn from the cell occupied by

the parent plant. A scattering probability P_s controls the level of dispersion via a random walk. At each step, the seed moves in a north-south direction with probability P_s and in an east-west direction with probability P_s. The seed moves north *or* south with equal probability and similarly for east *or* west. Assuming that the lattice is sufficiently large to neglect the possibility of seeds looping round the lattice and returning to a position near the parent plant, the expected distance that a seed travels in each direction is:

$$\frac{P_s}{(P_s - 1)^2},$$

so that the expected final displacement from the parent plant is:

$$\frac{\sqrt{2}P_s}{(P_s - 1)^2}. \tag{25}$$

This is an increasing function of P_s on $[0, 1]$, which rises very sharply after $P_s = 0.9$. For example, a scattering of $P_s > 0.85$ will give a more or less randomly-distributed seed bath covering a 100 by 100 grid. It should be noted that a large scattering parameter leads to excessive computation.

At the end of each year, the perennials generally survive, but a small proportion are assumed to die during the winter period. If p_i is taken to be the *relative mass* of plant i:

$$p_i \quad = \quad \frac{m_i}{m^{max}},$$

where m_{max} is the maximum mass of an isolated plant (equation (17)), then the probability that a perennial with relative mass p_i will die is given by equation (26). d_{min} is the probability that a plant of maximum size ($p_i = 1$) will die during a winter and thus is the minimum probability of death.

$$\begin{array}{l}\text{probability of}\\ \text{perennial death}\end{array} = \frac{d_{min}}{d_{min} + p_i(1 - d_{min})} \tag{26}$$

The perennials are assumed to propagate vegetatively by ramets. An empty cell will receive a perennial's ramet with probabilities according to the total mass of perennials in the four neighbouring cells. The probability of a new perennial growing in a cell is given by equation (27), where P_{max} is the probability that a cell surrounded by four maximum size plants will receive a new ramet and nhd represents the four cell von Neumann neighbourhood.

$$\begin{array}{l}\text{probability of}\\ \text{new ramet}\end{array} = \frac{1}{4} P_{max} \sum_{j \in nhd} p_j \tag{27}$$

A surviving perennial ramet will severely suppress the growth of an annual seed that falls into a neighbouring cell under all but absolutely symmetric competition, because of its initial size advantage. Thus perennials are assumed to have a competitive advantage over annuals at the reproduction stage: annual seeds do not germinate in the immediate neighbourhood of a perennial ramet. The ramets are spread first, then seeds are able to grow in any cells that remain empty. Each individual seed grows with probability P_g so that the probability a new annual grows in a given cell is given by equation (28), where n_s is the number of seeds which have fallen into the cell. Thus the surviving perennials, new perennial ramets and the new annual seedlings together contribute to the initial conditions for the next year's growth, controlled by equations (15) and (16).

In general the results presented here correspond to absolutely asymmetric competition; in many cases the competitive type does not affect the results; occasionally the computation is too intensive to allow all of the types to be used. It should be noted that the growth phase is modelled deterministically, whereas the reproductive phase incorporates stochastic elements.

$$\begin{matrix}\text{probability of} \\ \text{new annual}\end{matrix} \quad = \quad 1-(1-P_g)^{n_s} \tag{28}$$

4.3. Parameter Testing.

The model was tested under absolutely asymmetric competition for a full range of parameters. Simulations were for 50 years with a 200 day growing season on a 96×96 grid. The annual parameters, P_g (seed growth probability) and P_s (seed scattering probability) were tested for 110 parameter combinations, while the perennial parameters, d_{min} (winter death probability) and P_{max} (ramet production probability) were tested for 121 parameter pairs.

The parameter ranges are given in table 4. The total biomass after the fifty year period is shown for the annuals in figure a and for the perennials in figure b. The results for the annuals (consisting of $\sim 10^6$ time steps) took approximately one week to run on a SPARC10 workstation, so none of the results were replicated and only one competitive type was used. Thus the irregularity of the plot is due to stochastic noise, which would be expected to be removed if it were feasible to make repeated runs.

The behaviour of the annual plants is relatively uniform for most of the parameter range. A total biomass $\sim 10^3$ mass units is produced after 50 years for $P_g > 0.1$ and $P_s > 0.1$. (The units of mass are grams relative to the maximum mass of an isolated plant as described in chapter 3.) The perennials are unlikely to survive under all but the smallest death probabilities, that is, $d_{min} < 0.3$ is needed. The functional forms for the critical parameter values for survival are considered later.

4.4. Results.

Figures 19a - d show examples of the spatial patterns reached by the model after 100 years. Figure 19a (absolute asymmetry) illustrates the restricting effect of the high density of perennials on the dispersion of the annuals. The annuals are unable to scatter seeds extensively and appear clumped in certain regions of the grid. By comparison, the pure annual population covers the

(a)

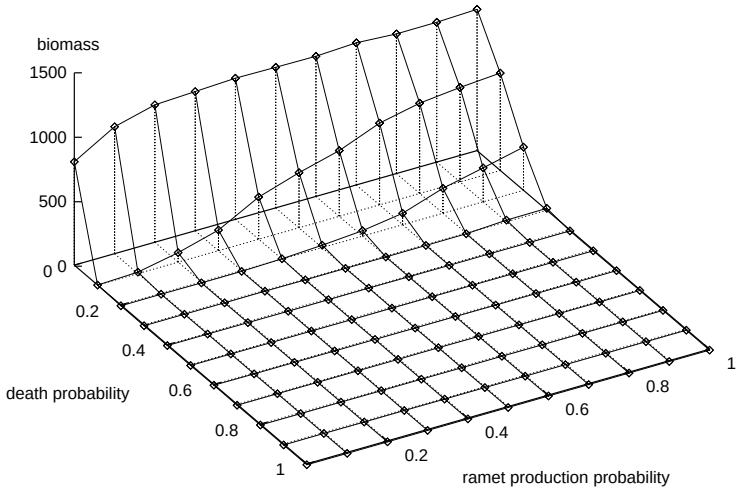
biomass
1500
1000
500
0
0
0.2
0.4
0.6
0.8
1
death probability
0.2
0.4
0.6
0.8
1
ramet production probability

(b)

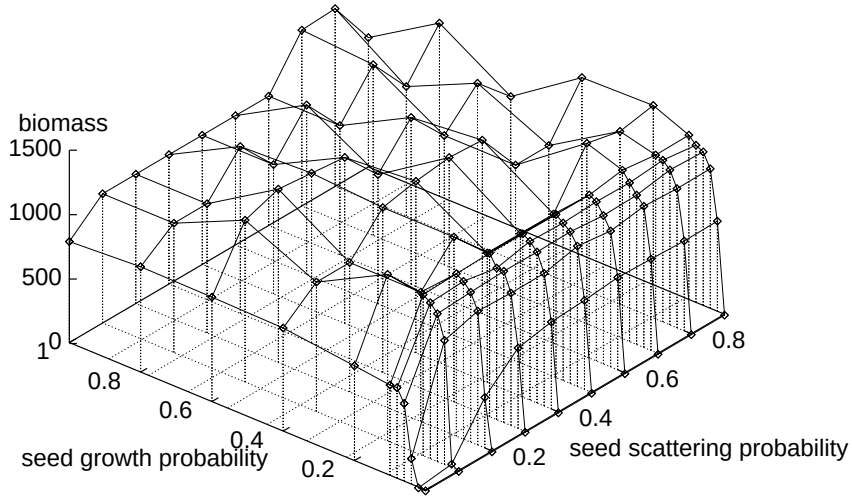
biomass
1500
1000
500
0
0.8
0.6
0.4
0.2
seed growth probability
0.2
0.4
0.6
0.8
seed scattering probability

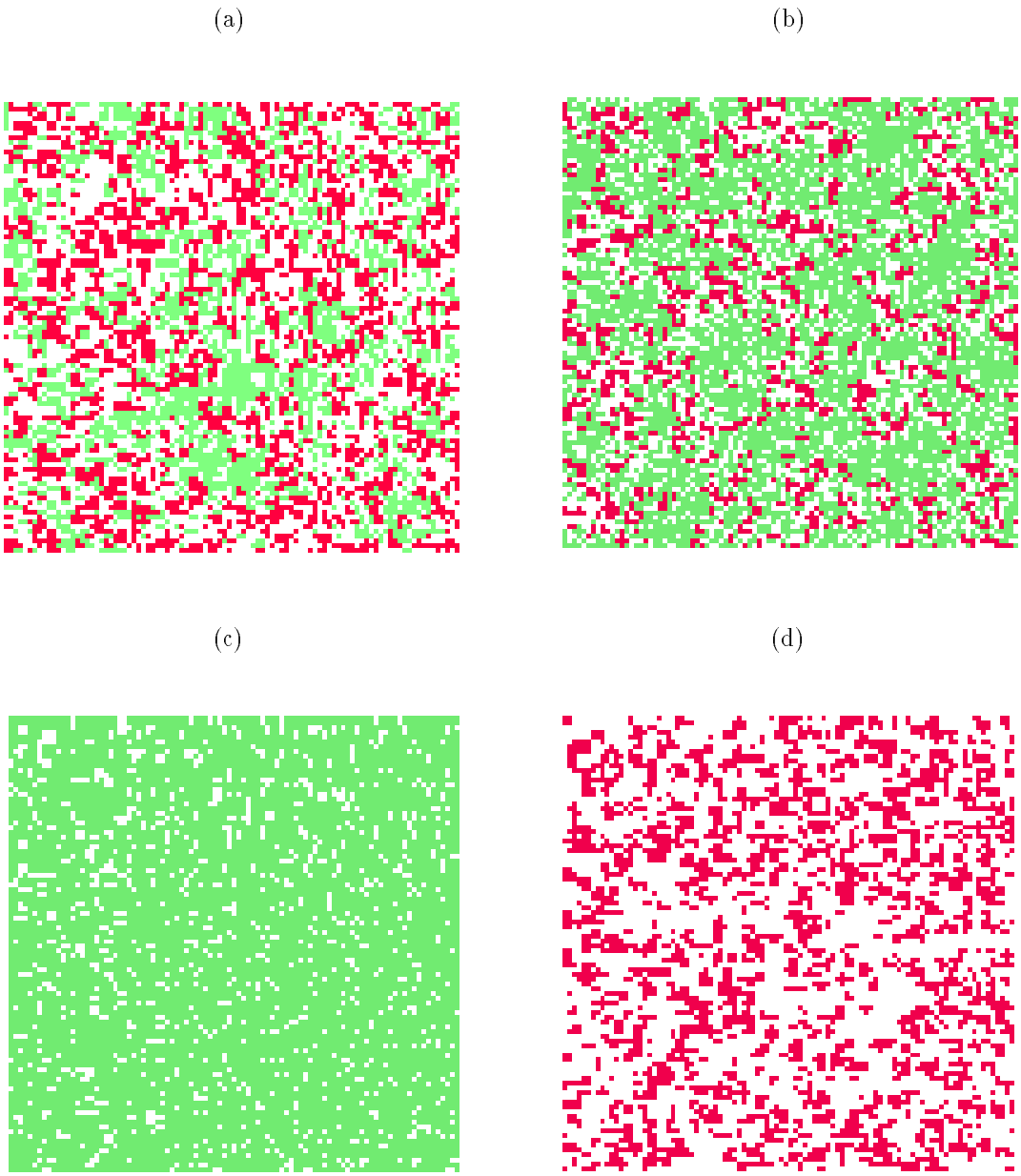

Figure 19: Spatial pattern in the annual-perennial CML model after 100 years. Red cells are perennials, green cells are annuals and white cells are empty. (a) Mixed population: absolute asymmetry (b) Mixed population: absolute asymmetry with higher perennial mortality. (c) Pure annual population: absolute asymmetry. (d) Pure perennial population: absolute asymmetry.

lattice (figure 19c). Figure 19b, with higher perennial mortality has a much smaller perennial population, which allows the annuals to be more widely and evenly spread. Figure 19d shows a typical perennial distribution, which is relatively unaffected by the presence of annuals. Hence the pattern of annuals is affected by coexisting perennials, but not appreciably vice versa. The manifestation of this relationship is examined numerically in section 4.7.

4.5. Using Singular Value Decomposition to Test Robustness.

The robustness of the values at each lattice point cannot be considered here because the model is too large. Indeed, it is of more interest whether the structure is statistically consistent rather than identical at every cell and at every time step. The presence or absence of a plant in any one cell after 100 years cannot be expected to be predictable because the plants are randomly distributed nad reproduction and death are stochastic. It is, however, relevant whether the characteristics of the spatial patterns are robust. Thus the sizes of *clumps* of plants produced are suitable for consideration. A simple measure of these is obtained by counting the number of adjacent cells with plants in, across each row of the grid. The lengths of these blocks are recorded and the frequency of each block length found. These are divided into the classes 1, 2, $\cdots$, 9 and '10 and over'. The decision to use ten classes is somewhat arbitrary, but based on the heuristic observation that there are few blocks greater that ten cells in length.

The model was run ten times, to produce a 10×10 replication matrix $\boldsymbol{X}$, given in table 5. Table 6 shows the singular values $e_1, \ldots, e_{10}$ obtained for matrix $\boldsymbol{X}$, using the SVD technique described in chapter 2. The ratio of the first two singular values is 0.018, which for $n = 10$ corresponds to Gaussian noise of about 2.5% of the maximum data value. The spatial structure is clearly substantially robust to repeated simulations of the CML.

4.6. A Mean Field Approximation for the CML Model.

4.6.1. Mathematical Analysis.

The role of the spatial dimension can be highlighted and the parameter ranges for which the spatial model is essential can be determined by analysing a mean field version of the system.

Plant type	Parameter	Values
Annual	P_g	{0, 0.02, 0.04, 0.06, 0.08, 0.1, 0.2, 0.4, 0.6, 0.8, 1.0 }
	P_s	{0, 0.1, 0.2, 0.3, 0.4, 0.5, 0.6, 0.7, 0.8, 0.9}
Perennial	d_{min}	{0, 0.1, 0.2, 0.3, 0.4, 0.5, 0.6, 0.7, 0.8, 0.9, 1.0}
	P_s	{0, 0.1, 0.2, 0.3, 0.4, 0.5, 0.6, 0.7, 0.8, 0.9, 1.0}

Table 4: Parameter values used for parameter-testing runs of the annual-perennial model.

Class	Run number									
1	778	803	752	794	820	769	731	789	811	825
2	235	226	239	278	270	233	225	231	244	265
3	117	113	107	134	124	117	90	136	113	101
4	61	39	62	63	51	61	46	70	53	46
5	25	22	34	30	33	30	29	27	23	22
6	17	13	17	15	18	12	8	14	15	18
7	6	6	11	8	14	12	12	13	14	5
8	6	3	7	3	6	4	1	6	3	2
9	4	3	2	3	5	4	0	3	2	2
10+	0	1	7	7	1	4	7	1	3	2

Table 5: Replication matrix for the annual-perennial system.

Singular value	
e_1	2641.8
e_2	48.8
e_3	42.7
e_4	20.9
e_5	12.9
e_6	9.4
e_7	7.3
e_8	3.6
e_9	1.6
e_{10}	0.3

Table 6: Singular values of the replication matrix for the annual-perennial system.

Parameter	Value
d_{min}	0.18
P_{max}	1.0
P_s	0.7
P_g	0.05
competition type	4

Table 7: Parameter values used for error analysis runs for the annual-perennial CML.

Such a model is constructed in this section, by extending the basic method of Crawley & May (1987) and Durrett & Levin (1994b). This is compared with the full CML model, allowing the impact of spatial processes to be assessed.

The perennials are dealt with first, as the model assumptions limit the influence of the annuals on them. Annuals do not affect the yearly spread of ramets, as it is assumed that they have died at the end of the previous growing season and the seeds have not yet germinated. Annuals also have little impact on the growth of perennials as seeds falling near existing clumps of perennials will have their growth suppressed. As observed by Crawley & May, it is simplest to model the proportion of cells not occupied by perennials, denoted here by E_t at time step t, where the time steps are years. If the probability that any one perennial dies at each time step is given by a parameter γ and the probability an empty cell receives a ramet is proportional to the number of neighbouring ramets and a parameter λ, then the following difference equation models the dynamics of the empty cells:

$$E_{t+1} \quad = \quad (\gamma + (1-\gamma)E_t)\,(1-(1-E_t)(1-\gamma)\lambda)\,.$$

Expressions are now needed for the parameters γ and λ. Substituting for average plant size $\bar{p}$ provides an expression for the probability of death (equation (29)), where $\bar{p}$ is relative to the maximum plant size m^{max}. Similarly equation (30) gives a mean field approximation for the probability of a new ramet being produced.

$$\gamma(\bar{p}) \quad = \quad \frac{\bar{p}d_{min}}{\bar{p}(1-d_{min})+d_{min}} \tag{29}$$

$$\lambda(\bar{p}) \quad = \quad \bar{p}P_{max} \tag{30}$$

It is clear that as the population develops the density and average mass will vary, so that $\bar{p} = \bar{p}(t)$. However, an expression can be obtained for the equilibrium value of $\lim_{t\to\infty} \bar{p}(t) = \bar{p}_\infty$.

It has been shown in chapter 3 that the maximum (and hence non-trivial equilibrium) plant mass under a mean field approximation is given by equation (21), the area per cell by equation (18), so that the area per plant is:

$$\frac{1}{5\rho}\sqrt{\frac{gc^3}{b}},$$

where ρ is the proportion of cells occupied at equilibrium, that is:

$$\rho \quad = \quad 1 - E_\infty .$$

Hence the average plant size at equilibrium will be $\bar{p}_\infty$ (equation (31)). Equilibria can be sought by solving $E_{t+1} = E_t$ with $\bar{p} = \bar{p}_\infty$, which is equivalent to roots of equation (32).

$$\bar{p}_\infty \quad = \quad \min\left(1, \frac{1}{\sqrt{5\,(1 - E_\infty)}}\right) \tag{31}$$

$$\begin{aligned} E_\infty \quad = \quad & \left(\tfrac{\bar{p}_\infty d_{min}}{\bar{p}_\infty (1-d_{min})+d_{min}} + \left(1 - \tfrac{\bar{p}_\infty d_{min}}{\bar{p}_\infty (1-d_{min})+d_{min}}\right) E_\infty\right) \\ & \cdot \left(1 - (1 - E_\infty)\left(1 - \tfrac{\bar{p}_\infty d_{min}}{\bar{p}_\infty (1-d_{min})+d_{min}}\right) \bar{p}_\infty P_{max}\right) \end{aligned} \tag{32}$$

Conditions for the existence of a non-trivial solution to (32) in $[0, 1]$ can be obtained in terms of the mean mass, $\bar{p}$, but it is more informative to obtain an approximation to equation (32) in terms of powers of E_∞. Figure 20a shows a plot of $\phi(E)$ against E. $\phi(E)$ is the right hand side of (32) and the '∞' subscripts have been dropped for brevity. The discontinuity in $\phi'(E)$ at $E = 0.8$ is caused by the *min* function in equation (31). Since ϕ is nearly linear in $[0, 0.8]$ and in $[0.8, 1]$, ϕ' is positive and approximately constant in each interval. Therefore, there clearly exists a critical value of d_{min}, $d_c = d_c(P_{max})$, below which there exists an internal equilibrium in $[0, 0.8]$ and above which there are only boundary equilibria. Since $\phi(1) \equiv 1$ for all values of d_{min} and P_{max}, $E = 1$ (no perennials) is always a stable equilibrium, as would be expected. The critical death rate, d_c can be determined by solving $\phi(0.8) = 0.8$. Using a

quadratic approximation to ϕ, the following estimate is obtained, with the negative root falling in the required interval $[0,1]$:

$$d_c = -\frac{5}{2}\left(\frac{\frac{3}{5}P_{max}+1 \pm \sqrt{\frac{6}{5}P_{max}+P_{max}^2+1}}{P_{max}}\right). \tag{33}$$

The proportion of cells occupied by annuals, A_t, can now be found, in terms of the empty cells, E_t. The number of annuals depends on the number of seeds sown, which in turn depends linearly on the mean mass $\bar{p}$. The expected number of seeds per plant is $100\bar{p}A_t$, so the number of seeds per empty cell is $100\bar{p}A_tE_t$. This leads to the difference equation (34). Again $\bar{p}=\bar{p}(t)$, but the equilibrium value of $\bar{p}(t)$ can be found (equation (35)). Then the equilibrium proportion of annuals, A_∞, is determined by solving $A_{t+1}=A_t$ (equation (36)).

$$A_{t+1} = \left(1-(1-\sigma)^{100\bar{p}A_tE_t}\right) \tag{34}$$

$$\bar{p}_\infty = \min\left(\frac{1}{\sqrt{5A_\infty}},1\right) \tag{35}$$

$$A_\infty = \left(1-(1-\sigma)^{20\sqrt{5A_\infty}E_\infty}\right) \tag{36}$$

Denoting the left hand side of equation (36) by $\psi(A)$ and again dropping the subscripts '∞', third order polynomial approximations to ψ can be found for $A>0.2$ and $A<0.2$. (These ranges represent the two terms of the *min* function.) The third order solution to $\psi(A)=A$, $\zeta(E,\sigma)$, is given in equations (37) and (38) for the intervals $[0,0.2]$ and $[0.2,1]$ respectively, where $\tilde{\sigma}=\log(1-\sigma)$. These two expressions combine to produce a continuous function with a discontinuous derivative (figure 20b).

$$\zeta(E,\sigma) = \frac{-15\left(1000\tilde{\sigma}^2E^3+1-\frac{1}{\sqrt{3}}\sqrt{-5000000\tilde{\sigma}^4E^6+6000\tilde{\sigma}^2E^3+3}\right)}{200000\sqrt{5}\tilde{\sigma}^3E^4} \tag{37}$$

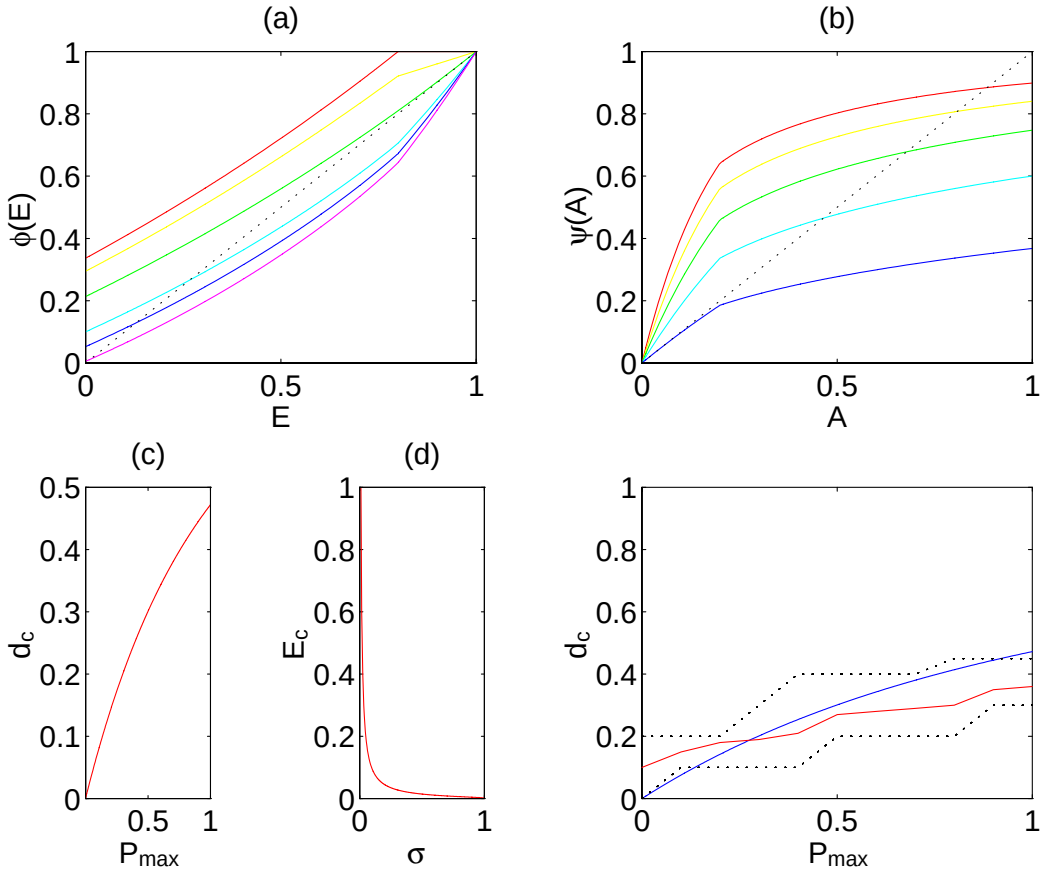

Figure 20: Mean field analysis of the annual-perennial system. (a) Graph of $\phi(E)$ for different values of d_{min}, the probability of perennial death. d_{min} increases from 0.01 (magenta) to 1 (red) as ϕ increases. Intersection of the curve with $\phi = E$ gives the position of equilibria of the mean field perennial model. (b) Graph of $\psi(A)$ for different values of E, the proportion of cells free of perennials and for $\sigma = 0.05$, where σ is the probability of seed germination. E increases from 0.2 (blue) to 1 (red) in steps of 0.2 as ψ increases. Intersection of the curve with $\psi = A$ gives the position of equilibria of the mean field annual model. (c) The critical value, d_c, of the perennial death rate, d_{min}, above which the perennials become extinct. (d) The critical value, E_c, of the equilibrium proportion of cells free of perennials, E_∞, below which the annuals become extinct. (e) Comparison of numerical values for the critical perennial death rate, d_c, with the mean field values: value of d_c from the simulation (red); theoretical value of d_c (blue).

$$\zeta(E,\sigma) = \frac{-3\left(5000\tilde{\sigma}^2E^3+1-\frac{1}{\sqrt{3}}\sqrt{-1000000\tilde{\sigma}^3E^4\left(125\tilde{\sigma}E^2+2\right)}\right)}{1000000\tilde{\sigma}^3E^4} \quad (38)$$

It is clear that there exists a critical value of the proportion of cells without perennials, E_c. This is the solution to $\zeta(E,\sigma)=0$, which for the third order approximation is given by equation (39). Hence the value of σ controls the lower limit of the gap frequency E which a population of annuals can tolerate.

$$E_c = \frac{1}{100|\log(1-\sigma)|} \quad (39)$$

Figures 20c - d illustrate the two critical value expressions derived respectively for d_c and E_c.

4.6.2. Comparison with Computational Results.

Since the annuals have minimal effect on the perennials, parameter testing for the perennials (figure b) can be compared to the mean field critical value expression (equation (33) and figure 20c). Approximate dependence of d_c on P_{max} can be extracted from the surface plot by nonlinear interpolation (figure b). The critical value, d_c is the point at which the subset of parameter pairs under which extinction occurs meets the subset where the population survives. Upper and lower limits for the value of d_c are given by the parameter values in figure a, which correspond to zero and non-zero values of stand biomass. This is necessarily a rough approximation because the model contains stochastic fluctuations and is subject to demographic extinction and the results are not replicated for reasons of computational infeasibility.

Figure 20e shows that the mean field approximation is a fair predictor of the survival of the perennial species for intermediate values of reproduction (P_{max}). However, at low reproductive rates, perennials survive better in a spatial system than in the mean field, so that space provides a refuge effect. In contrast, at high perennial reproductive rates - aggressive expansion - spatial extensiveness is detrimental to survival; propagation restricted by the clonal spatial structures. It is thus clear that spatial dimensions are essential in the model for most of the range of this parameter.

The parameter testing for the annuals (figure a) shows that the population survives for all parameter combinations when $P_g > 0$. Since the population is pure, $E = 1$, so the population should survive as long as $E_c \leq 1$. The value of E_c depends only on σ ($\equiv P_g$), as infinite scattering (or a seed bath) is assumed in the mean field derivations. Hence extinction is expected if:

$$E_c \quad = \quad \frac{1}{100 \| \log(1-\sigma) \|} \quad > \quad 1,$$

that is, if:

$$\sigma \quad < \quad 1 - e^{-\frac{1}{100}} \quad \simeq \quad 0.01.$$

The numerical simulation has no values of P_g in the open set $(0, 0.01)$, so the only parameter values which should exhibit extinction are those with $P_g = 0$, as seen in figure a.

4.7. Analysis of Spatial Structure.

The evolution of the spatial structure of the annual-perennial model can be examined by following the variation of the clumping index of section 2.1.6 through time. Figures 21a - c give various paths of the index for different compositions of populations. All results shown are for absolutely symmetric competition, but the type of competition has negligible effect on the form of the clumping index path. Effects are mostly limited to the variation of density. Figure 21a (mixed population, absolute symmetry) shows that both plant types quickly reach a level of clumping somewhat larger that for a random distribution. Thereafter the density changes but the clumping index remains about the same distance from the random C_ρ line. The clumping appears to be slightly higher for the perennials.

Figure 21b shows the path of the index for a pure annual population. The annuals remain close to the C_ρ curve at all times, so the plants are approximately randomly distributed, despite limited seed dispersal. Hence competition considerably increases the clumping of the annuals. The path for pure perennial populations is shown in figure 21c: the level of clumping increases

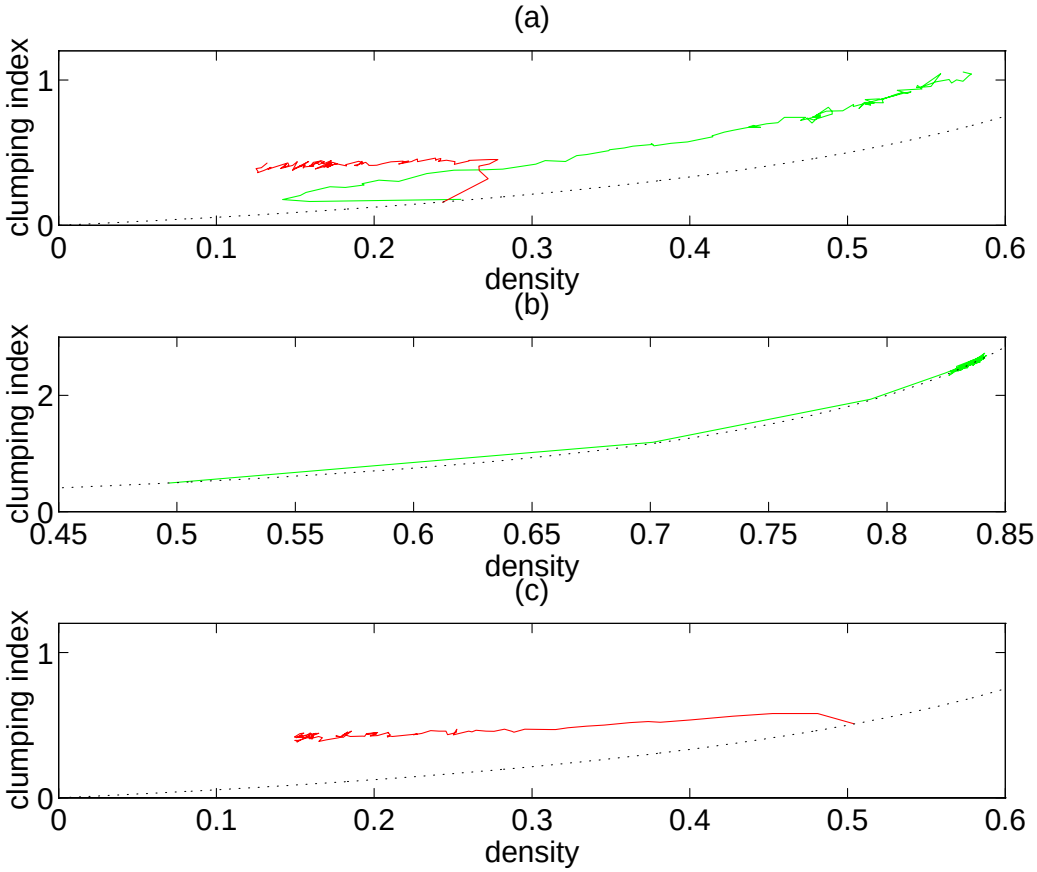

Figure 21: Paths of clumping indices through time in the annual-perennial system as a function of density ρ. Paths always start on the curve C_ρ $(\cdots)$, which is the clumping index for random distributions. (a) Mixed population: annuals (green) and perennials (red) for absolute symmetry. (b) Pure annual population. (c) Pure perennial population.

more gradually than in the mixed population.

4.8. Multifractal Analysis.

Data from several runs of the model were used with the techniques of section 2.1.6 to analyse the multifractal scales of the plant distributions resulting at the end of the 100 years. Different combinations of plant and competition types were studied (figures 22a - d). The mass exponents (or fractal pressures) $\tau(q)$ were calculated for $-8 \leq q \leq 16$ using equations (7) and (8). The exponents were then used to find the Lipschitz-Hölder exponents, $\alpha(q)$ (equation (12)) and the spectrum $f(\alpha(q))$ (equation (11)).

The mass exponents for mixed populations under absolutely asymmetric competition are shown in figure 22a. There is a large variation in the slope of the curve for the annuals. This is clearly equivalent to a large range of the scaling (α). The multifractal spectrum corresponding to these mass exponents is given in figure 22b, where a large range ($0 < \alpha < 2.5$) can be seen for the annuals. There is a much smaller range for the results obtained for the distribution arising from symmetric competition.

Figures 22c - d show the spectra for pure annual and perennial populations respectively. It is clearly demonstrated for the pure populations (figures 22c - d) that the range of scaling parameters, α, increases as the competition becomes less symmetric. For example, the annuals have a scaling range of 0.4 under asymmetric competition, but only a range of 0.1 for the absolutely symmetric case. A shift of the scale is sometimes seen as well as a widening of the range. The same observations also apply to the mixed populations (not illustrated). The perennials are never seen to exhibit a large range of scales. The annuals only show a significant range of α in mixed population. As expected the perennials are relatively unaffected by the annuals; similar spectra are seen in figure 22b as in figure 22d. In contrast, the distribution of annuals is substantially altered by the perennials: the range of α increases from 0.5 to 2.5. Thus competition induces a multifractal character in the pattern of annual plants.

The graphical representation, clumping index and multifractal spectrum all combine to under-

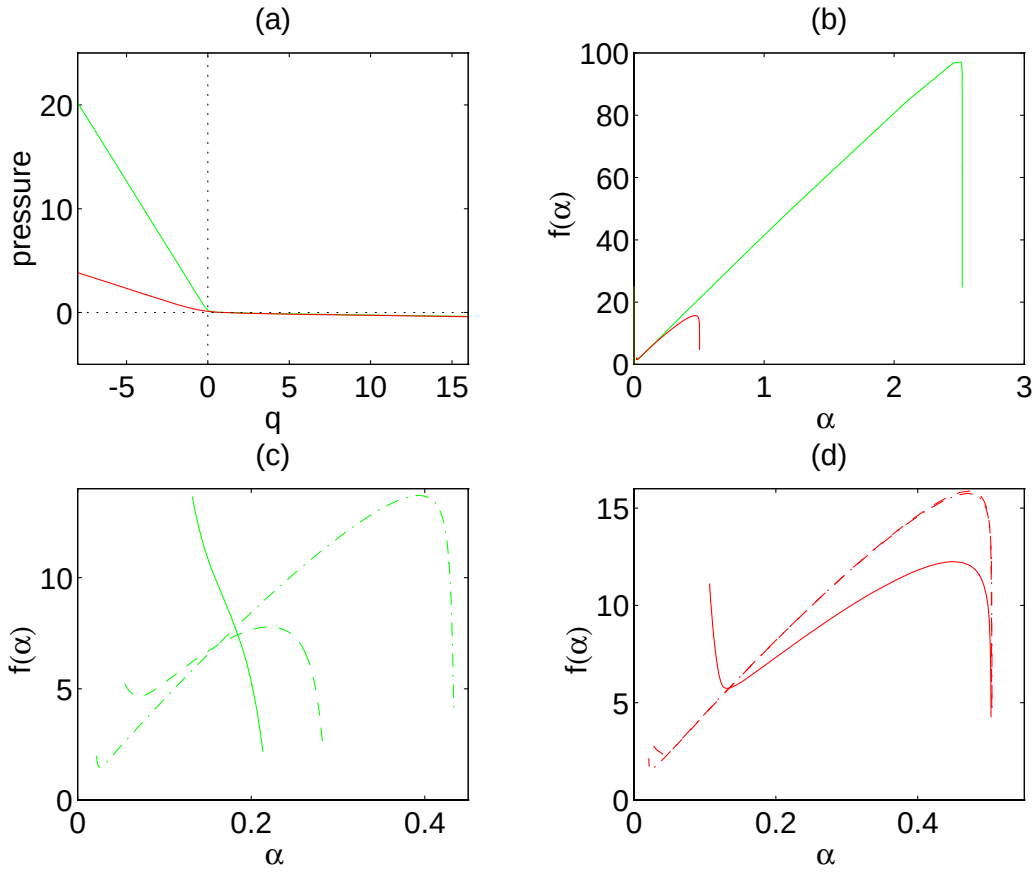

Figure 22: Multifractal analysis of the annual-perennial system. (a) Graph of fractal pressure $\tau(q)$ against moment index q for mixed population with absolute asymmetry: annuals (green) and perennials (red). (b) - (d) Multifractal spectrum $f(\alpha)$ as a function of scaling exponent α. (b) Mixed population with absolute asymmetry: annuals (red) and perennials (green); (c) pure annual population with absolute symmetry (—), relative symmetry (- - -) and absolute asymmetry (- · -); (d) pure perennial population with absolute symmetry (—), relative symmetry (- - -) and absolute asymmetry (- · -).

line the asymmetrical relationship (Crawley, 1990b) between the annual and perennial species; this is discussed further in chapter 9.

4.9. Length Scale Analysis.

For investigating the coherence length scale, the model was run on a 300×300 grid with a mixed population. $N = 300$ was, however, extremely computationally intensive, so the error analysis was only performed for one competition type (absolute asymmetry). The period over which the error analysis was carried out is $T = 50$ years, starting after $t_0 = 50$ years. A constant k was fitted to $n\mathcal{E}_n$ (section 2.1.5) for four cases: a mixed population of annuals and perennials, monocultures of annuals and perennials and a mixed population with reduced annual seed dispersal (figure 23).

The coherence length scale is around $n_c \simeq 125$ for the mixed population (figure 23a). There is, however, very little error above $n_c \simeq 100$, so that the grid size of $N = 96$ used in this chapter is acceptable, particularly in view of the great computation involved in this model.

The mixed population shows slight negative spatial coherence at small scales ($0 < n < 10$) as $\mathcal{E}_n < \mathcal{E}'_n$. Since $\frac{\partial}{\partial n}(n\mathcal{E}_n) > 0$, an aggregating tendency is exhibited as n increases over a wide range of scales ($0 < n < 80$), resulting in positive spatial coherence at intermediate scales ($10 < n < n_c$). Disaggregation necessarily occurs at larger scales ($75 < n < n_c$), as the mass tends towards a random distribution above the coherence length scale ($\frac{\partial}{\partial n}(n\mathcal{E}_n) < 0$).

The annual monoculture (figure 23b) has a slightly lower coherence length ($n_c \simeq 105$) and starts with slightly more negative coherence than the mixture ($0 < n < 10$), with a stronger aggregating force as n increases for $0 < n < 80$. The perennial monoculture (figure 23c) is, in contrast, always shows significant positive coherence below $n_c \simeq 140$ ($\mathcal{E}_n > \mathcal{E}'_n$) with a very slight aggregating tendency as n rises at smaller scales ($0 < n < 50$) and disaggregation at larger scales ($50 < n < n_c$). Thus there is a clear difference between the annuals, which have the dispersing effect of seed scattering, and the perennials, whose clumping mechanisms are always dominant.

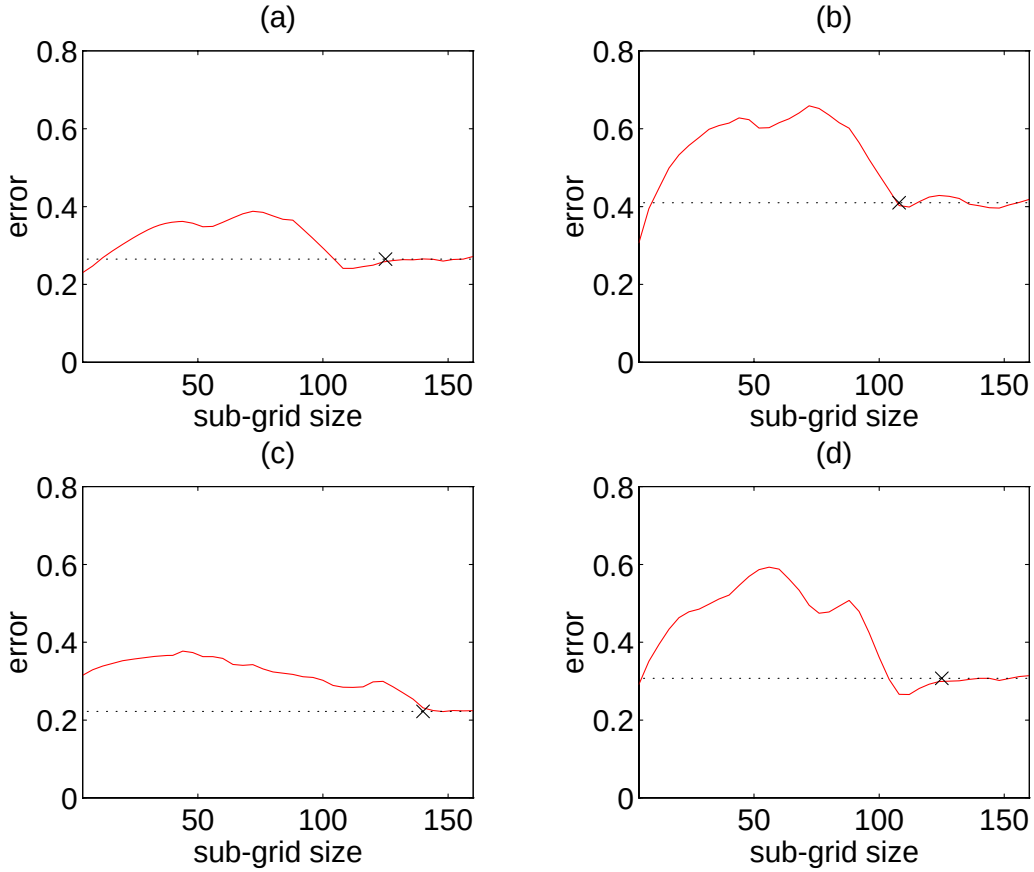

Figure 23: Error analysis for the annual-perennial system: numerical error $n\mathcal{E}_n$ for the model (—) and theoretical error $n\mathcal{E}'_n$ $(\cdots)$. (a) Total mixed population ($P_s = 0.7$). (b) Annual plants only. (c) Perennial plants only. (d) Total mixed population for reduced seed dispersal ($P_s = 0.3$).

The length scale analysis is not valid above half of the total grid size ($n = 150$), because of the toroidal boundary conditions, so the results are only shown up to this value. However, the error values for $n > 150$ do in fact support the results by giving a constant value of $n\mathcal{E}_n$.

A lower annual seed scattering distance leads to a weaker negative coherence and to a stronger aggregating tendency as n increases ($\left\| \frac{\partial}{\partial n}(n\mathcal{E}_n) \right\|$ is greater in figure 23d than in figure 23a), but the coherence length scale is the same ($n_c \simeq 125$). Thus the error analysis identifies this change to a mechanism with greater aggregation.

By examination of the coherence length scale of the model, it is clear that a large lattice is needed: doubt is cast on the many lattice models which have used small grids of sizes as small a 5×5 (Auld & Coote, 1980; Karlson & Jackson, 1981; Bard, 1981). Each model naturally requires individual analysis as the coherence length scale can be a low as 15 (section 7.6.1), but this is likely to correspond to near random patterns where a spatial model is probably not needed.

5. A Resource-Based Coupled Map Lattice Model for Plant Populations.

Chapter Summary

The plant coupled map lattice of chapters 3 and 4 is extended to incorporate an explicit resource base, through the introduction of a second lattice variable. Resource depletion and crowding suppress plant growth and both positive and negative feedback processes mediate the formation of size hierarchies.

Environmental or resource heterogeneity is introduced using an algorithm for generating different sizes of patches; a necessary balance of computational speed and accuracy is identified. Patchy resources are shown to lead to suppressed stand yields and increased size variation.

The result of chapter 3, asserting that hierarchy development can be used to discriminate between symmetric and asymmetric competition, is seen to hold with a homogeneous or moderately heterogeneous resource distribution. The model is extended to multiple years, allowing the coherence length scale to be found, demonstrating that a moderately-sized lattice is sufficient.

An overview of the ecology of seed sizes is presented, focusing on the opposing selective forces on large seeds, which are sometimes adapted to tolerate adverse conditions, but are also suited to the intense competition of rich habitats. In a homogeneous environment, higher resource levels favour large-seeded species, which exclude the small-seeded species; the opposite happens with lower resources. Coexistence of the two species is seen in intermediate environments. Small- and large-seeded species are seen to coexist in a heterogeneous environment with sufficiently large high and low resource patches.

'And nature must obey necessity' - William Shakespeare - Julius Caesar IV, iii

5.1. Introduction.

Resources - soil nutrients, light and physical space - naturally play a central role in plant ecosystems. The effect of resource availability and heterogeneity on both plant and animal systems have been studied for many years, in natural and agricultural systems[47] and via patch, reaction-diffusion and lattice models[48]. Resource patterns have been shown to have fundamental implications for community structure, species diversity and evolution of physiological and behavioural characters. Spatial and temporal resource heterogeneities challenge the survival of plant species (Fowler, 1988) and consequently different ecological types of plants have evolved various mechanisms to overcome unreliability of nutrient supply. Examples are *dispersal* of propagules to overcome spatial fluctuations, *dormancy* as a response to temporal heterogeneity and *physiological integration* in clonal species to exploit spatial patchiness (Hutchings & Slade, 1988; Caraco & Kelly, 1991; Fahrig et al., 1994).

In chapters 3 and 4 the CML models of plant populations adopt the common assumption that occupation of space is representative of the acquisition of nutrients and light as well as physical space. In this chapter an explicit resource distribution is added to the CML, which affects growth rates and is depleted as individual plants grow. Using a separate variable for a generalised representative nutrient allows different environments, both homogeneous and heterogeneous, to be applied to the CML plant populations. Thus the CML can be used to assess the impact of nutrient levels on the structure of plant monocultures during a growing season. An algorithm is added to the CML to deal with heterogeneous resource distributions, in the form of patches of high and low resources. The consequences of such heterogeneities

[47] Cohen, 1971; Hartnett & Bazzaz, 1983; 1985; Ferrara & Quinn, 1987; Inouye & Tilman, 1988; Hocking & Steer, 1989; Naeem, 1990; Grieve & François, 1992; Jackson & Caldwell, 1992; Kelly & Canham, 1992; Jackson & Caldwell, 1993; Robertson et al., 1993; Birch & Hutchings, 1994; Mian & Nafziger, 1994; Gross et al., 1995; Kadmon, 1995.

[48] Horn & McArthur, 1972; Comins & Blatt, 1974; Ludwig et al., 1979; Shigesada et al., 1979; Chesson, 1981; Elderkin, 1982; Pacala & Roughgarden, 1982; Pacala, 1987; Abrams, 1988; Armesto et al., 1991; Colasanti & Grime, 1993; Vail, 1993; Lavorel et al., 1994; Oborny, 1994a; 1994b.

are investigated in monospecific stands for single growing seasons and for competing species over several years and the role of dispersal in providing spatiotemporal integration of resource supplies is examined.

The CML is applied to the specific issue of the ecology of seed sizes. After a detailed study of the growth over a single season of species with different sizes of seeds, the controversial subject of the adaptation of seed sizes to high or low resource habitats is investigated.

5.2. A Resource Base for the Coupled Map Lattice Plant Model.

5.2.1. The Model.

The CML of chapter 3 is extended here to include an *explicit resource base*. The resource is assumed to affect the growth rate of individual plants, by a factor r_i in the growth term (equation (40)); variables are defined as in chapter 3. The resource is 'used up' according to equation (41). Resource consumption is taken to be of two forms: a *growth cost* proportional to the change in mass and a *maintenance cost* proportional to the mass. It has been shown that different species differ in their patterns of depletion of soil nutrients (Tilman & Wedin, 1991a), so the resource dynamics can be varied, via the controlling parameters k_g and k_m, which correspond respectively to the growth and maintenance costs. A similar functional form is used in a resource-based mechanistic model by Tilman (Grace, 1990).

Initially a single growing season is modelled, so a resource distribution is imposed at the start of the season and is depleted as the stand develops. A constant or temporally-varying resource flow could potentially be added to the model.

$$\frac{dm_i}{dt} = r_i g(a_i - l_i) - b m_i^2 \tag{40}$$

$$a_i = c m_i^{\frac{2}{3}}$$

$$\frac{dr_i}{dt} = -k_g \frac{dm_i}{dt} - k_m m_i \tag{41}$$

5.2.2. Local Stability Analysis in the Mean Field.

The basic two-dimensional mean field system can be analysed for stability by considering the growth of a stand of identical plants of density ρ on a plot of area A. After competition has set in the equations reduce to:

$$\frac{dm}{dt} = \alpha m^2 + \beta r$$

$$\frac{dr}{dt} = \gamma m^2 + \delta m + \varepsilon r$$

where:

$$\begin{aligned} \alpha &= -b & \delta &= -k_m \\ \beta &= gA\rho & \varepsilon &= -k_g\beta \\ \gamma &= k_g b \end{aligned} \quad .$$

Hence the eigenvalues of the Jacobian matrix are given by:

$$\lambda = \frac{\varepsilon + 2\alpha m \pm \sqrt{(\varepsilon + 2\alpha m)^2 + 4\delta\beta}}{2}.$$

The eigenvalues are real if $m > 0$ or if $k_g > \sqrt{\frac{k_m}{\beta}}$ for $m = 0$. Both eigenvalues are negative (or have negative real parts) for $m \geq 0$. Hence a non-zero equilibrium is a stable node and a stable node or focus is seen at $m = 0$ depending on the values of k_g and k_m. There only exists an equilibrium value for r if $m = 0$ or $k_m = 0$, so if there is a maintenance cost then there is a sole attracting fixed point at the origin. If, however, there is only a growth cost ($k_g > 0$, $k_m = 0$) then there is a degenerate line of stable nodes given by:

$$r \quad = \quad \frac{bm^2}{gA\rho}.$$

The mean field equilibrium therefore depends on the initial conditions, which here strictly are the values at the onset of competition. As the path of competition is highly dependent on spatial effects, the following section investigates the behaviour of the CML as various parameters are varied.

5.2.3. Computational Methods.

The resource CML was run on a 50×50 grid (section 5.4 gives a length scale analysis) for 200 iterations and the mean and coefficient of variation of mass were calculated at each time step (equations (29) and (30)). A range of parameters were investigated for their impact on the dynamics: growth cost (k_g), maintenance cost (k_m), plant density (ρ), initial resource level (r_I) and symmetry (table 5). The same values were used for the constants b, c and g as in chapter 3 (table 4).

Also investigated was the form of *mortality*. In chapter 3, plants were assumed to stop growing if the mass increment ($\triangle m_i$) fell below zero. This was called mortality option 0 here and two further possibilities were considered. Option 1 assumed that a plant with negative growth dies and the mass is reset to zero. Option 2 allowed negative growth, so that a negative increment simply subtracts from the current mass, subject to the obvious constraint that mass is non-negative. The mortality options are summarised in table 8.

5.2.4. Results and Discussion.

(a) Variation of Growth Cost.

As the cost of incremental growth rises, the mean mass of fully-grown plants falls, as would be expected with a fixed supply of resources (figure 24a). This is accompanied by a fall in mean resource level, as greater growth leads to greater resource uptake (figure 24b). Higher growth costs reduce the mass variation in the population by a negative feedback process (figure 24c).

Mortality option	**Regime**	**Treatment of plants with $\triangle m_i < 0$**
0	plants stop growing	set $\triangle m_i = 0$
1	plants stop die	set $\triangle m_i = 0$
2	plants decrease in size	set $m_i^{(t)} = max(m_i^{(t+1)} + \triangle m_i, 0)$

Table 8: Definitions of the mortality options in the resource-based CML model.

Clumping level	**low**	**medium**	**high**
First factor φ	0.0005	0.001	0.005
Aggregation factor ϑ	0.5	0.01	0.001
Approximate number of iterations	300	1200	900
Accuracy of density	99.9 %	99.95%	99.9%
Range of clumping indices	3.3 - 3.4	16 - 17	39 - 52

Table 9: The three clumping levels used in the patchy resource-based CML model.

Larger plants arise from faster growth rates in less crowded areas, but they incur higher costs as resources are depleted faster and growth is restricted. There is an opposite effect on the variation of resource levels, as higher growth costs amplify differential resource use (figure 24d).

(b) Variation of Maintenance Cost.

As with the growth cost, higher maintenance costs push down the mean mass and the mean resource remaining (figures 24e - f). The effect is much more severe, particularly on the resource depletion, as an increased maintenance cost is compounded over time, whereas the growth cost acts on each unit of mass only once. There is a very similar relationship between mass variation and both types of costs (figures 24c and g), as both suppress growth of large plants and promote growth of small plants, as already described. Maintenance cost has a significantly different impact on resource variation across the stand (figure 24h). Initially an increase in maintenance cost amplifies resource variation, but at higher levels the complete depletion of resources (as seen in figure 24f) leads to decreased and eventually zero resource variation. As the two types of costs have similar effects on population structure, only k_g is given positive values in the rest of this chapter, which also allows non-zero mean field equilibria.

(c) Variation of Density.

Decreased plant mass at higher population densities (figure 25a) shows that competition intensifies as growing space is reduced. Mean resource levels rise with density, indicating that crowding is restricting resource uptake (figure 25b). Both mean mass and mean resource show greater variation at higher density, arising primarily by one-sided interactions as in chapter 3 and secondarily through neighbourhood effects (figures 25c - d). As previously noted, there is a sharp drop in the coefficients of variation as density approaches 1.0 (a full grid), because of reduced randomness of plant distribution (section 3.7).

(d) Variation of Initial Resource Level.

Raising the total amount of resources available to the plant population allows higher mean masses to be attained (figure 25c) while more resources are still left at the end of the growing

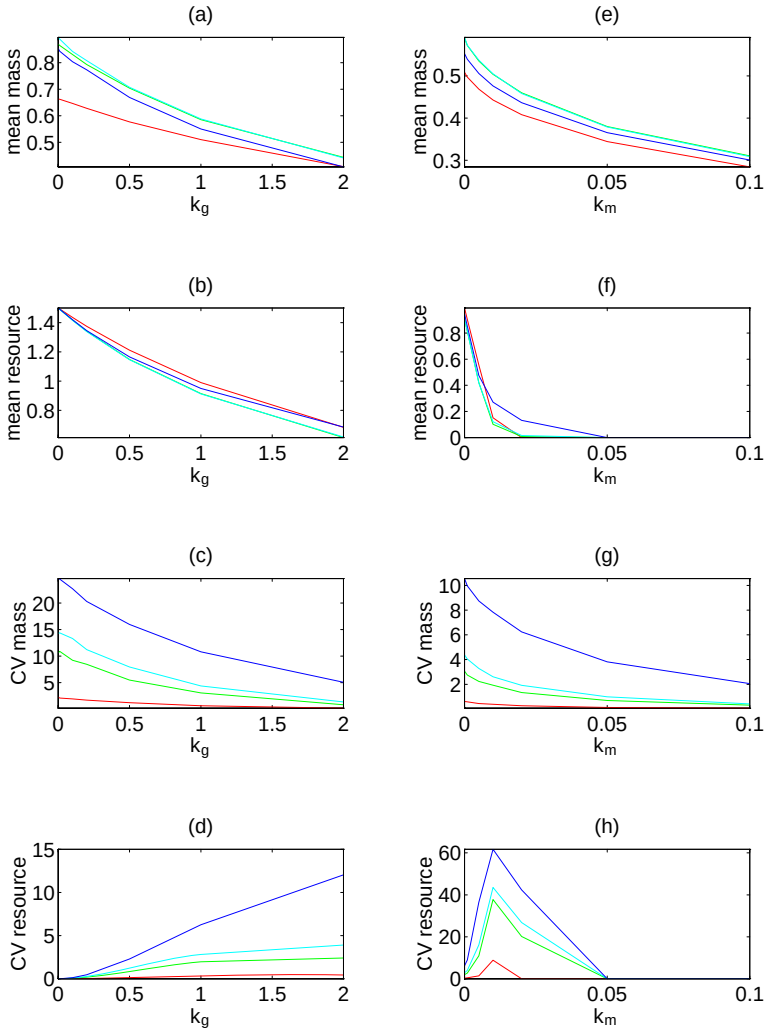

Figure 24: Population statistics for the single species resource-based CML model as growth and maintenance costs vary at time 250 days with mortality option 0. (a) - (d) Variation of population parameters with growth cost k_g. Parameters are $k_m = 0$, $r_I = 1.5$ and $\rho = 0.5$. (e) - (h) Variation of population parameters with maintenance cost k_m. Parameters are $k_g = 1$, $r_I = 1.5$ and $\rho = 0.5$. (a), (e) Mean mass (proportion of maximum isolated plant size). (b), (f) Mean remaining resource. (c), (g) Coefficient of variation of mass. (d), (h) Coefficient of variation of remaining resource. In all cases the competitive types are absolute symmetry (red), relative symmetry (green), relative asymmetry (cyan) and absolute asymmetry (blue).

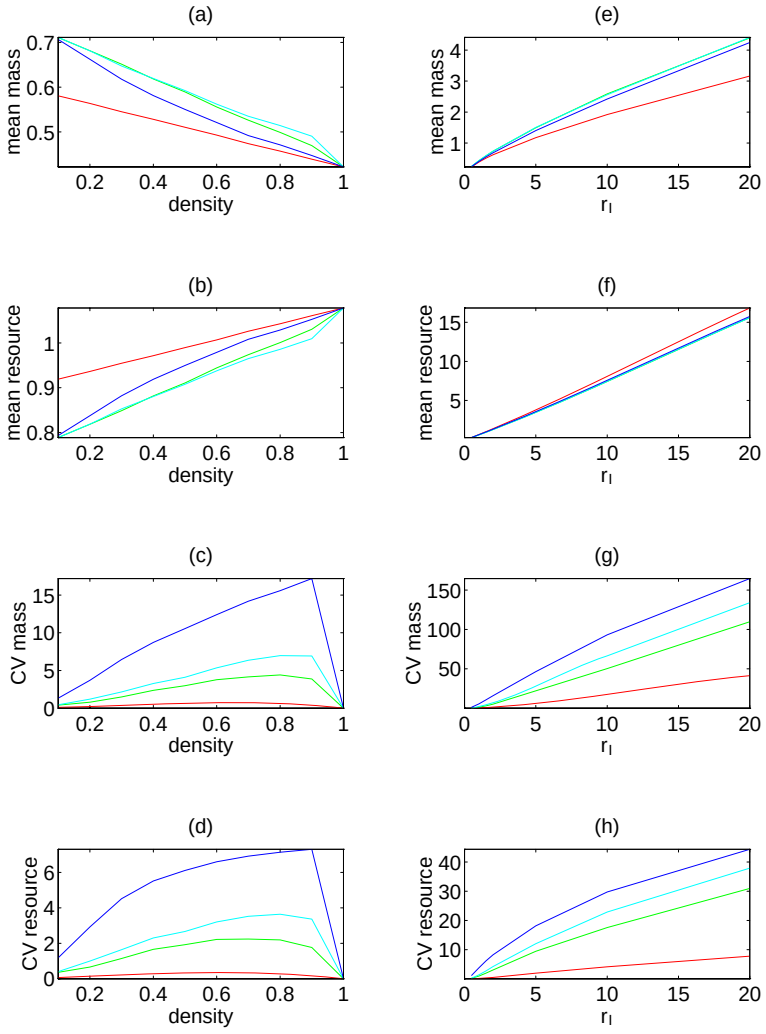

Figure 25: Population statistics for the single species resource-based CML model as density and initial resource levels vary at time 250 days with mortality option 0. (a) - (d) Variation of population parameters with density ρ. Parameters are $k_g = 1$, $k_m = 0$ and $r_I = 1.5$. (e) - (h) Variation of population parameters with initial resource level r_I. Parameters are $k_g = 1$, $k_m = 0$ and $\rho = 0.5$. (a), (e) Mean mass (proportion of maximum isolated plant size). (b), (f) Mean remaining resource. (c), (g) Coefficient of variation of mass. (d), (h) Coefficient of variation of remaining resource. In all cases the competitive types are absolute symmetry (red), relative symmetry (green), relative asymmetry (cyan) and absolute asymmetry (blue).

season (figure 25f). Increased initial resources also allow greater variation of masses and resources to arise in the stand, as a less restricted resource supply allows hierarchies to develop fully (figures 25g - h).

(e) Variation of Symmetry.

Symmetry generally has little effect on mean resource levels or mass levels (figures 24a - b, e - f and 25e - f). There is however a slightly higher usage of resources in the absolutely symmetric case; with correspondingly lower mean masses this indicates lower of efficiency of this mechanism, in terms of resource used per unit mass accumulated. There is a more noticeable impact at lower densities, where absolute symmetry leads to appreciably greater depletion of resources (figures 24a - b).

In contrast, symmetry has a profound effect on the coefficients of variation of both mass and resource, as variation always increases substantially with asymmetry (figures 24c - d, g - h and 25c - d, g - h). Higher growth and maintenance costs lead to especially strong size hierarchies under absolutely asymmetric competition (figure 24c and g). Greater initial resource levels lead to higher coefficients of variation, but there is a much smaller rise under absolutely symmetric competition (figure 25g - h). The rise in mass variation with density observed in chapter 3 is still present in the resource-based CML (figure 25c).

These results affirm that higher variation at higher density implies asymmetry of interactions, as stated in section 3.7. This conclusion can equally well be drawn from the variation of resource (figure 25d).

(f) Variation of Mortality Regime.

Implementation of mortality option 0, where plants stop growing, generally results in smooth sigmoidal growth. Figure 26a is a sample of such and illustrates the increase with time and decrease with growth cost of mass variation. Similar curves are produced for all competitive symmetries.

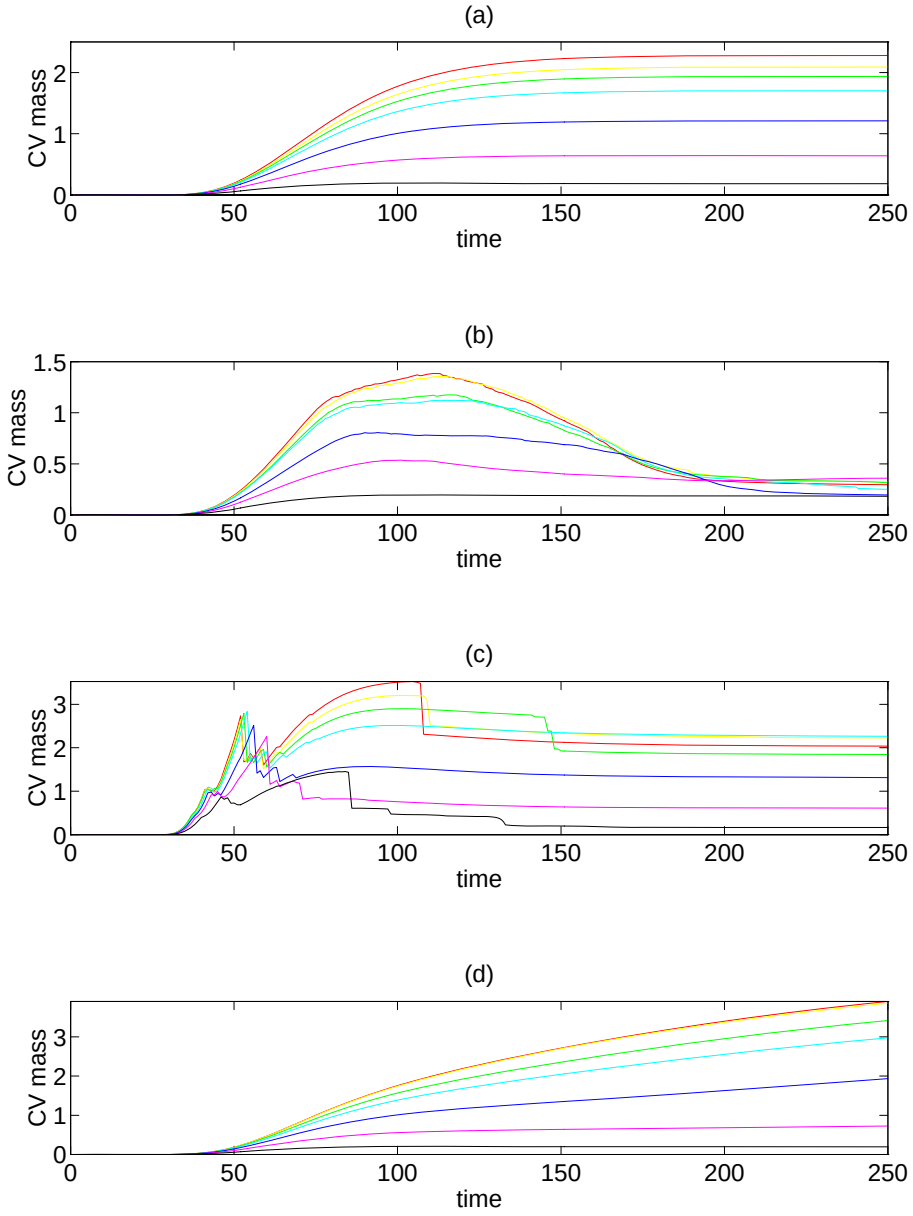

Figure 26: Time series for the single species resource-based CML model over 250 days: variation of coefficient of variation of mass with time. (a) Symmetry 1 and mortality option 0. (b) Symmetry 1 and mortality option 1. (c) Symmetry 4 and mortality option 1. (d) Symmetry 1 and mortality option 2. Results are for a range of values of growth cost k_g, varying from 0 (red) to 2 (black).

The inclusion of plant death in mortality option 1 has two main effects. Firstly the coefficient of variation of mass rises to a peak then falls off as self-thinning progresses (figure 26b). This shows the importance of the suppression of thinning as in chapter 3, to avoid masking the dynamics of competitive interference. Secondly, mortality 1 leads to erratic dynamics, as shown in figure 26c, particularly for more asymmetric competition. Extensive self-thinning removes the characteristic decrease in mean mass as density rises (figure 27a); likewise mean resource uptake is fairly constant as density varies (figure 27b). The coefficients of variation of mass and resource increase as density rises from low to moderate, but decrease again at the highest levels of crowding as more thinning takes place (figures 27c - d), confirming the confounding effects of self-thinning.

Allowing plants to decrease in size in the absence of adequate resources and growing space (mortality option 2) has relatively low impact on the dynamics, which remain smooth as with option 0, but the population hierarchies continue to develop over a longer time period (figure 26d). In general there is much more effect of symmetry on resource variation than mass variation (figures 26e - h).

5.3. The Impact of Resource Heterogeneity.

5.3.1. Normal Distribution of Resources.

A simple method of introducing spatial variation of the resource base into the CML is to treat the resource in each cell as a *normally-distributed random variable* with standard deviation σ, so that $r_i \sim N(r_I, \sigma)$. The effect of a normal distribution on the resource CML was studied on a 50×50 grid for a range of standard deviations $\sigma \in [0, 1]$ for parameters $r_I = 1.5$, $k_g = 1$, $k_m = 0$ and $\rho = 0.5$ and for the full range of symmetries and mortality option 0.

Figure 28 shows the population statistics after a growing season of 200 days. The mass is virtually independent of the initial resource distribution, whereas the resource remaining at $t = 200$ does vary with σ. The constancy of the yield can be attributed to the independence of the normal random variables.

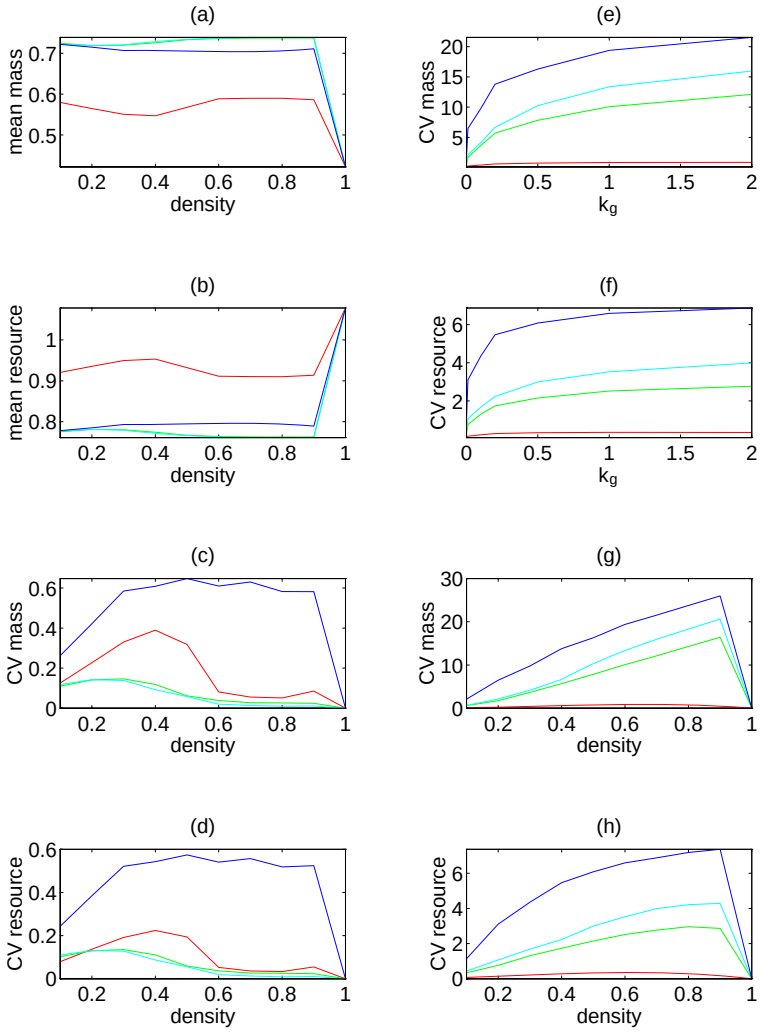

Figure 27: Population statistics for the single species resource-based CML model as mortality varies at time 250 days. (a) - (d) Variation of population parameters with density ρ for mortality option 1. (e) - (f) Variation of population parameters with growth cost k_g for mortality option 2. (g) - (h) Variation of population parameters with density ρ for mortality option 2. (a) Mean mass (proportion of maximum isolated plant size). (b) Mean remaining resource. (c), (e), (g) Coefficient of variation of mass. (d), (f), (h) Coefficient of variation of remaining resource. In all cases the competitive types are absolute symmetry (red), relative symmetry (green), relative asymmetry (cyan) and absolute asymmetry (blue).

Heterogeneity of resource supply imposes a range of growth rates and hence plant sizes on a local population. However, a distribution of sizes also arises under a uniform resource distribution, through a combination of competitive and neighbourhood effects. Thus in any locality, interference mechanisms 'buffer' the resource heterogeneity and allows the same yield to be maintained over a range of standard deviations (figure 28a).

There is, however, less resource depletion under greater heterogeneity of resource supply (figure 28c) which means that the exploitation of limited resources is more thorough. Since some plants will remain small because of competitive suppression, their resource supplies remain mostly unused. If all plants have the same initial resources, large dominant plants will experience more severe resource limitation that small suppressed individuals. If the resource base is heterogeneous, then small plants are generally found on low resource sites and large plants on high resource sites, clearly resulting in greater efficiency of resource utilisation. Absolutely symmetric competition leads to significantly greater resource exploitation (figure 28c), because the plant interactions are more equal and small plants will require a large resource supply than under more asymmetric conditions. The variation in resource uptake is not, however, particularly significant as the resource remaining here is no more than 10% of the initial level.

The variation of masses attained in the stand is strongly dependent on the resource heterogeneity. This shows that the initial resource distribution largely imposes the size hierarchy on the population. Absolute symmetry of interference, however, acts as an equalising force and reduces the size variation by around 50% (figure 28b). The coefficient of variation of remaining resource also reflects the initial resource, but it is misleading simply to consider the final ($t = 200$) values (figure 28d), as is highlighted by a sample path of the resource variation through time (figure 28e). The high variation of the imposed initial resource distribution is rapidly destroyed as the stand grows and large plants deplete the richest sites. Competition then leads to the re-establishment of high levels of variation as existing size differences and hence resource uptakes are amplified. The early phase of stand growth does not completely remove the resource variation, as even absolutely symmetric competition leads to high final resource variation (figure 28d).

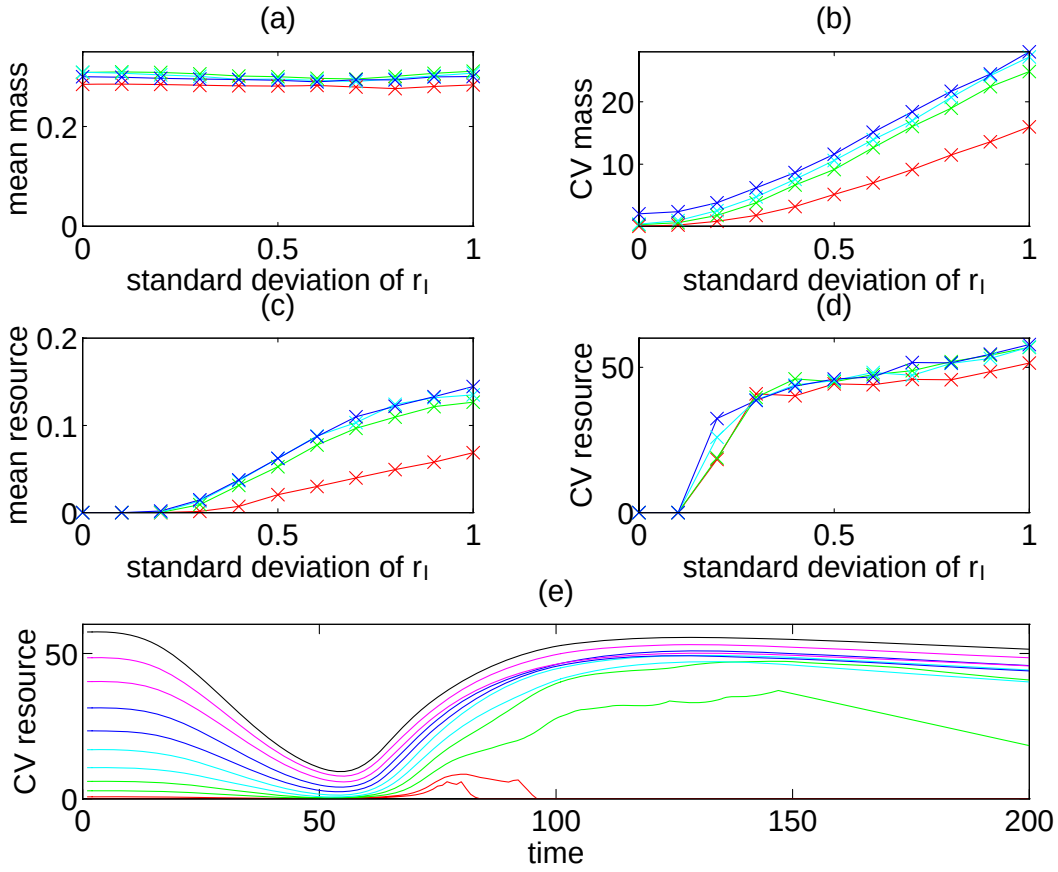

Figure 28: (a) - (d) Population statistics for the single species resource-based CML model as the standard deviation of initial resource levels varies at time 200 days with mortality option 0. Parameters are $k_g = 1$, $k_m = 0$, $r_I = 1.5$ and $\rho = 0.5$. (a) Mean mass (proportion of maximum isolated plant size). (b) Coefficient of variation of mass. (c) Mean remaining resource. (d) Coefficient of variation of remaining resource. In all cases the competitive types are absolute symmetry (red), relative symmetry (green), relative asymmetry (cyan) and absolute asymmetry (blue). (e) Variation of the coefficient of variation of remaining resource with time for symmetry 1 and mortality option 0. Parameters are $k_g = 1$, $k_m = 0$, $r_I = 1.5$ and $\rho = 0.5$.

5.3.2. Generation of Patchy Distributions of Resources.

The normal distribution of initial resources in the previous section only provides local *(microsite)* variation, whereas resources are often variable over a larger *(regional)* scale. An algorithm for generating patchy distributions at any required level of aggregation is described in this section.

A square grid is partitioned into two states - high and low resources - using a technique which sweeps the grid many times, setting a few cells at each sweep. Such a concept was used by Deutschman et al. (1993) for studying grid resolution, but the details of the sweeping algorithm are different here and more appropriate to the generation of a patchy distribution.

Initially the grid cells are all set to a default state (the low resource level or *'off'*). The grid is then 'seeded' by a number of cells, which are reset to a second state (the high resource level or *'on'*); these cells are a fixed proportion φ (the *'first factor'*) of the total grid. The distribution of *on* cells is random, achieved by switching each cell *on* with probability φ. Then the algorithm sweeps through the grid and resets each cell to *on* with probability ϑn, where n is the number of neighbours in an 8 cell neighbourhood that are *on*. ϑ is the *'aggregation factor'* and controls the degree of clumping of the final distribution of *on* states. The algorithm continues to sweep the grid until the required number of cells are switched *on*. The level of aggregation is dependent on φ as well as ϑ, as a greater number of initial points leads to many small clusters of *on* cells while lower φ leads to a few large clumps.

There are three considerations which influence the choice of the first factor and the aggregation factor. Firstly φ and ϑ combine to produce a certain level of aggregation or patchiness. Secondly, the amount of computation is highly dependent on ϑ, as a very low value will require a lot of sweeps and hence is likely to be unacceptably slow to produce the distribution. The final point to note is that a large value of ϑ may lead to quantitative inaccuracy: if a lot of cells are switched *on* the intended density of *on* cells may be overshot considerably. Thus computation times and numerical accuracy must both be monitored.

The algorithm was used to generate sample patchy distributions on a 100×100 grid using a range of the factors φ and ϑ with a target density of 50% of each cell type. The clumping index (chapter 2) was used to quantify the patchiness of the *on* and *off* states. The clumping index, number of iterations required to attain the target density and the density actually attained were recorded for values of φ and ϑ ranging over several orders of magnitude.

Figure 29 illustrates a variety of distributions with a range of clumping indices (6.3, 9.0, 16.7, 25.2, 35.6 and 67.7). Figure 30 shows the results of a detailed investigation of the first factor φ and clumping factor ϑ. The clumping index rises with both φ and ϑ (figure 30a), attaining peak values where both φ and ϑ are largest. The accuracy is only severely affected by large values of the aggregation factor ϑ, where the density of the *off* cell is nearer 0 than the target density of 0.5 (figure 30d). There is a substantial increase in the number of iterations needed for small values of φ and ϑ (figure 30c). Thus a balance must be found between accuracy and computational feasibility. Figure 30d shows the ratio of computational intensity to accuracy of density and indicates that it is best to have one of the factors φ and ϑ small and one large. These results are used to choose suitable values of φ and ϑ to provide a range of clumping indices for the resource-based CML.

5.3.3. Patchy Resources in the Coupled Map Lattice.

(a) Introduction.

The algorithm described in the previous section was used to investigate the effects of patchy distributions of rich and poor resources on the growth of a monoculture over a single season. The CML was run on a 50×50 grid for a range of clumping levels, densities and growth costs.

A further variable of interest in the model was the *resource differentiation*. As described by Kotliar & Wiens (1990), there are two aspects of heterogeneity: *aggregation* and *contrast*, that is, the level of clumping and the difference between clumps. The model was run for a range of resource differentiations from total homogeneity to maximum contrast. The average resource level was kept constant at 1.25, but 50% of the grid cells were given a higher resource

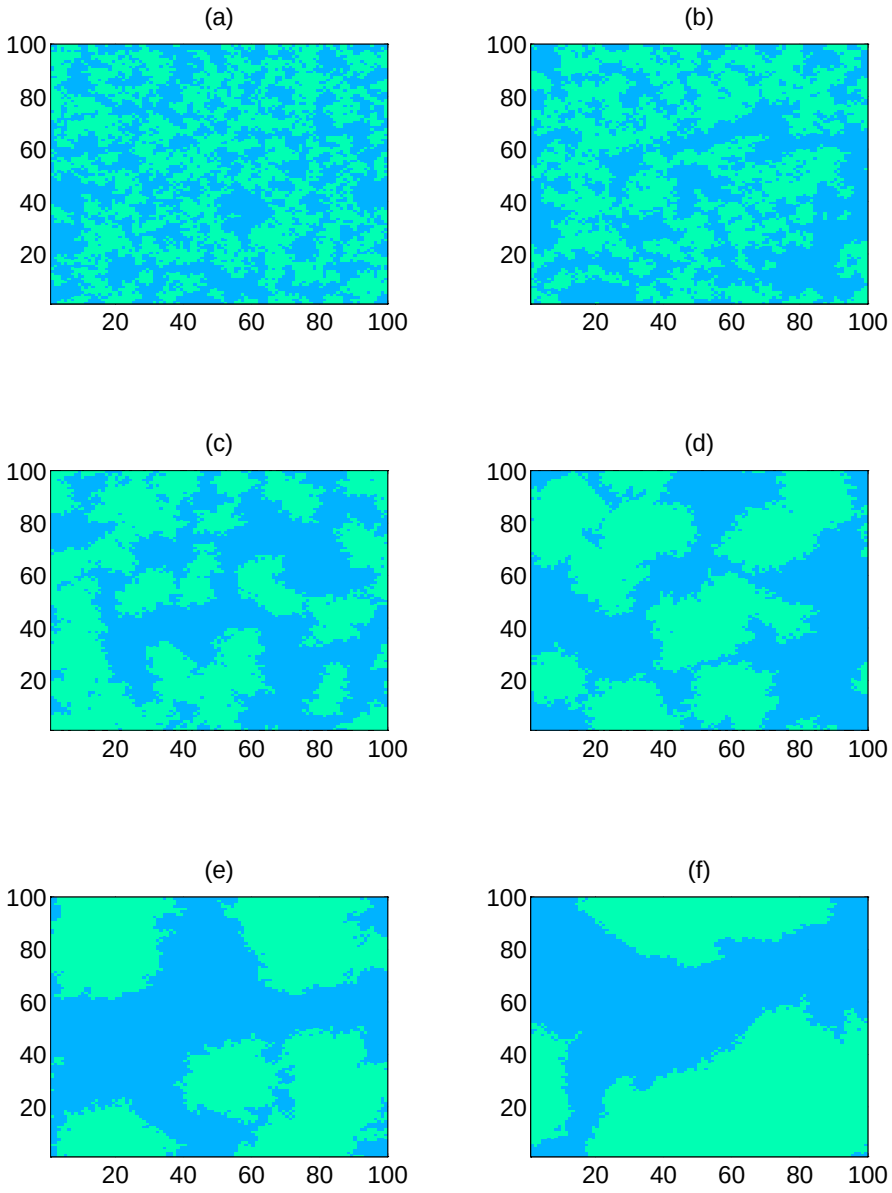

Figure 29: Patterns generated by the patch algorithm. The clumping indices are (a) 6.3 (b) 9.0 (c) 16.7 (d) 25.2 (e) 35.6 and (f) 67.7.

level and 50% a correspondingly lower level. Six sample pairs of resource values were used: (1.25, 1.25) (homogeneous), (1.5, 1.0), (1.75, 0.75), (2.0, 0.5), (2.25, 0.25) and (2.5, 0.0) (fully heterogeneous). The resource differentiation is denoted by r_H, the higher resource level, so that $1.25 \leq r_H \leq 2.5$.

Three clumping levels were taken - high, medium and low - generated by the factors φ and ϑ given in table 9, which were chosen to provide the required aggregation with sufficient accuracy and speed. The clumping indices were not identical for every run but provide reasonable consistency, as shown in table 9.

(b) Variation of Contrast and Aggregation.

Figure 31 shows the effect of varied resource differentiation r_H on the plant population dynamics. There is a small effect of r_H on final mean mass and resource. At high levels of clumping the mass decreases as the contrast rises, so that homogeneous distributions provide optimal yields. Maximum differentiation ($r_H = 2.5$) leads to an approximately 20% lower yield than the uniform case. Interesting behaviour occurs with the finest aggregation: the yield falls off at first as r_H increases, before rising again at the highest r_H values. Thus the (2.5, 0.0) case, where half of the plot has zero resources and is therefore totally hostile to growth, is not the worst pattern for stand yield. This minimum yield at intermediate r_H is a robust feature of fine-scale heterogeneity, seen for a wide range of densities ρ, growth costs k_g and for all symmetries.

The growth process can be better understood by studying the development of mass and resource levels over time (figure 32a - b). These time series show a reversal of the ordering of yield as a function of differentiation r_H. At first plants on the richest patches grow rapidly and use up resources. These plants dominate the population, so at times $0 \leq t \leq 80$ the mean mass rises with r_H and the mean remaining resource falls. By the end of this time, the largest plants are near to their maximum asymptotic sizes and growth focuses on the poorest patches. Later dynamics ($t \geq 80$) are dominated by the smaller plants, so that situations of lower contrast fare relatively better and mean mass now falls with r_H. Thus higher differentiation scenarios see earlier resource depletion. It is therefore apparent that, in general, particularly low resources

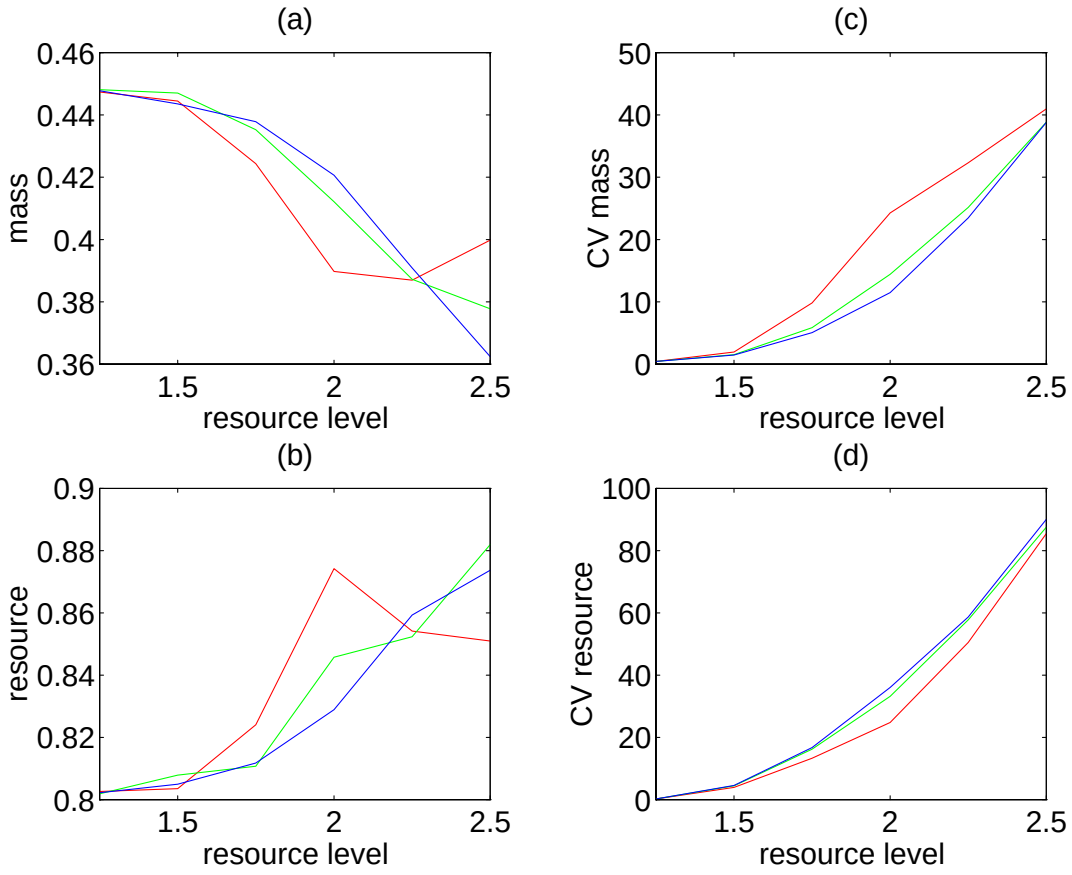

Figure 31: Population statistics for the patchy single species resource-based CML as resource differentiation varies at time 200 days with mortality option 0 and symmetry 1: variation of population parameters with resource differentiation r_H. (a) Mean mass. (b) Mean resource. (c) Coefficient of variation of mass. (d) Coefficient of variation of resource. In all cases three clumping levels are shown: low (red), medium (green) and high (blue).

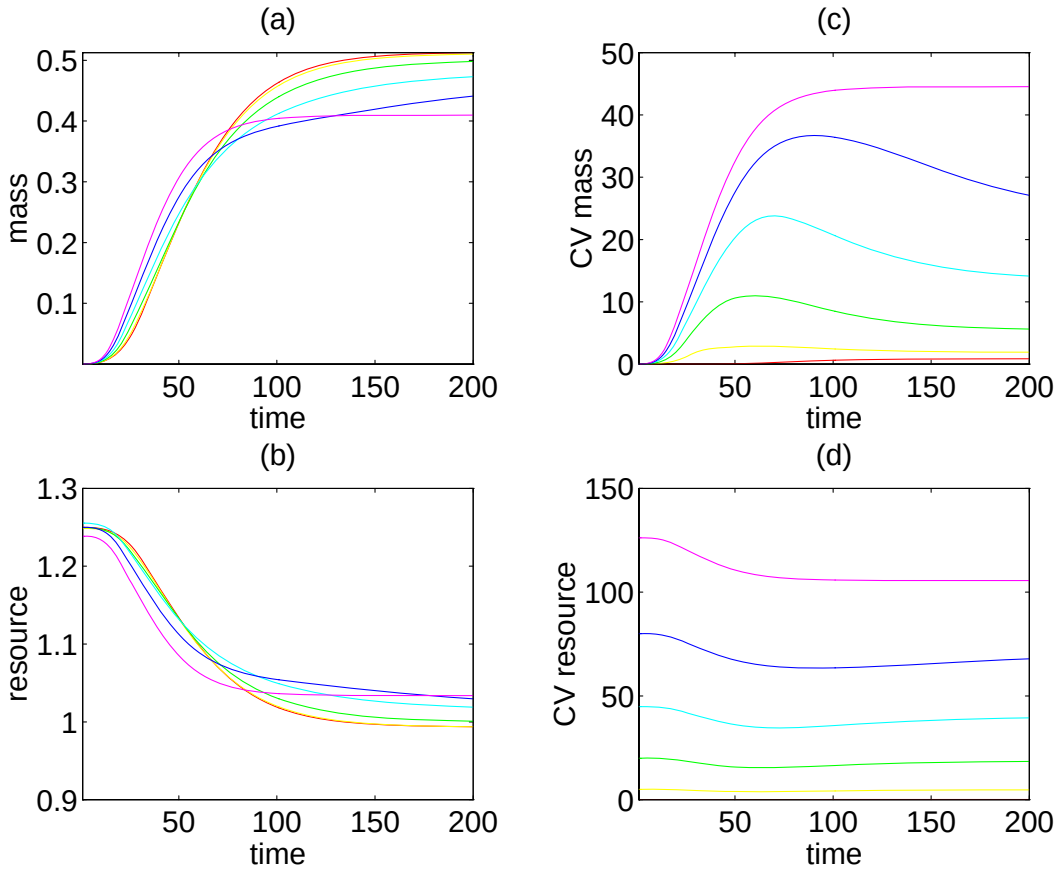

Figure 32: Time series for the patchy single species resource-based CML with mortality option 0 and symmetry 4: variation of population parameters with time for a range of resource differentiation r_H. (a) Mean mass. (b) Mean resource. (c) Coefficient of variation of mass. (d) Coefficient of variation of resource. Values of r_H vary between 1.25 (red) and 2.5 (magenta).

are more disadvantageous to growth than high resources are beneficial.

The low level clumping promotes a different relationship between mass and r_H because of local competitive effects. If there is a fine scale to the heterogeneity, then large plants on high resource patches will be direct neighbours to small plants on low resource patches. This means that the small plants are much more suppressed when intermingled with the large plants, than if they were in clumps of smaller plants. Hence the maximum resource differentiation, which puts all resources into the larger plants, is able to do better than intermediate differentiation, which 'wastes' resource on small plants that are doomed to suppression.

The formation of hierarchies is not greatly affected by the level of clumping but mass and resource coefficients of variation rise rapidly with r_H (figures 31c - d). Figure 32d shows that the high variation predominantly arises from the initial bimodal resource distribution, which imposes variation on the mass distribution (figure 32c).

(c) Variation of Density and Symmetry.

It is now of interest to examine the effect of patchy resources on the mass variation-density relationship discussed in chapter 3, with particular emphasis on the effect of competitive symmetry. Figure 33 shows the impact of different degrees of contrast on the coefficients of variation of mass, for the high clumping level, as density varies between 0.1 and 1.0 for all four symmetry types and for the six values of r_H.

The homogeneous resource base (figure 33a) shows the familiar sharp rise of variation with density, particular under asymmetric competition (equivalent to figure 9b). Although the mass variation clearly rises with asymmetry for all contrasts r_H, there is not the same rise with density at very high differentiation; there is actually a decrease in mass variation at higher r_H (figures 33e - f). There is also less difference here between symmetry 4 and symmetries 1 - 3 (seen in figure 33a); the most noticeable difference at high r_H is that absolute symmetry shows significantly lower mass variation than the other symmetry types (figures 33c - f). The more symmetric plant interactions damp initial resource variations, so that higher densities, having

stronger interactions, allow more damping of initial variation. Mean mass decreases with rising density, as seen previously in chapter 3 (figure 20a), because of greater competition.

5.4. Long Term Dynamics of the Resource-Based Coupled Map Lattice.

5.4.1. Introduction.

The long term impact of resource heterogeneity on plant communities can be studied by extending the resource-based CML to multiple years in a similar way to chapter 4. At the end of each growing season, all plants produce seeds in proportion to their sizes, which are scattered across the grid and then die. The new season begins with the growth of the seeds into seedlings.

The random walk algorithm used in chapter 4 for seed dispersal was found to be highly computationally intensive, so an alternative algorithm is presented here. Seeds are scattered with a uniform distribution with maximum distance M_s in both north-south and east-west directions on the grid. As in chapter 4, the seed moves north or south with equal probability, likewise east or west. Although the binomial distribution generated by the random walk of chapter 4 is an appropriate representation of seed dispersal shadows (Okubo & Levin, 1989; Willson, 1992), the uniform distribution allows a comparison of different scattering distances and corresponding population dynamics. The benefit of the uniform scattering is substantially reduced computation time, with all values of M_s requiring similar computation, unlike the random walk which is very slow for high values of the scattering parameter P_s. In summary, a seed moves $(x, y) \rightarrow (x \pm \Delta x, y \pm \Delta y)$ where $\Delta x \sim U(0, M_s)$ and $\Delta y \sim U(0, M_s)$.

When a heterogeneous environment is used, a scheme for deriving the next year's resource distribution from the current year's pattern must be chosen. The simplest option is to have a fixed distribution of patches that remains invariant over many years, representing persistent topographical features such as rock outcrops or long-lived vegetational patches. An alternative is to have completely random patches each year, where only the degree of aggregation remains the same from year to year. This represents, for example, ephemeral nutrients or annually changing patches.

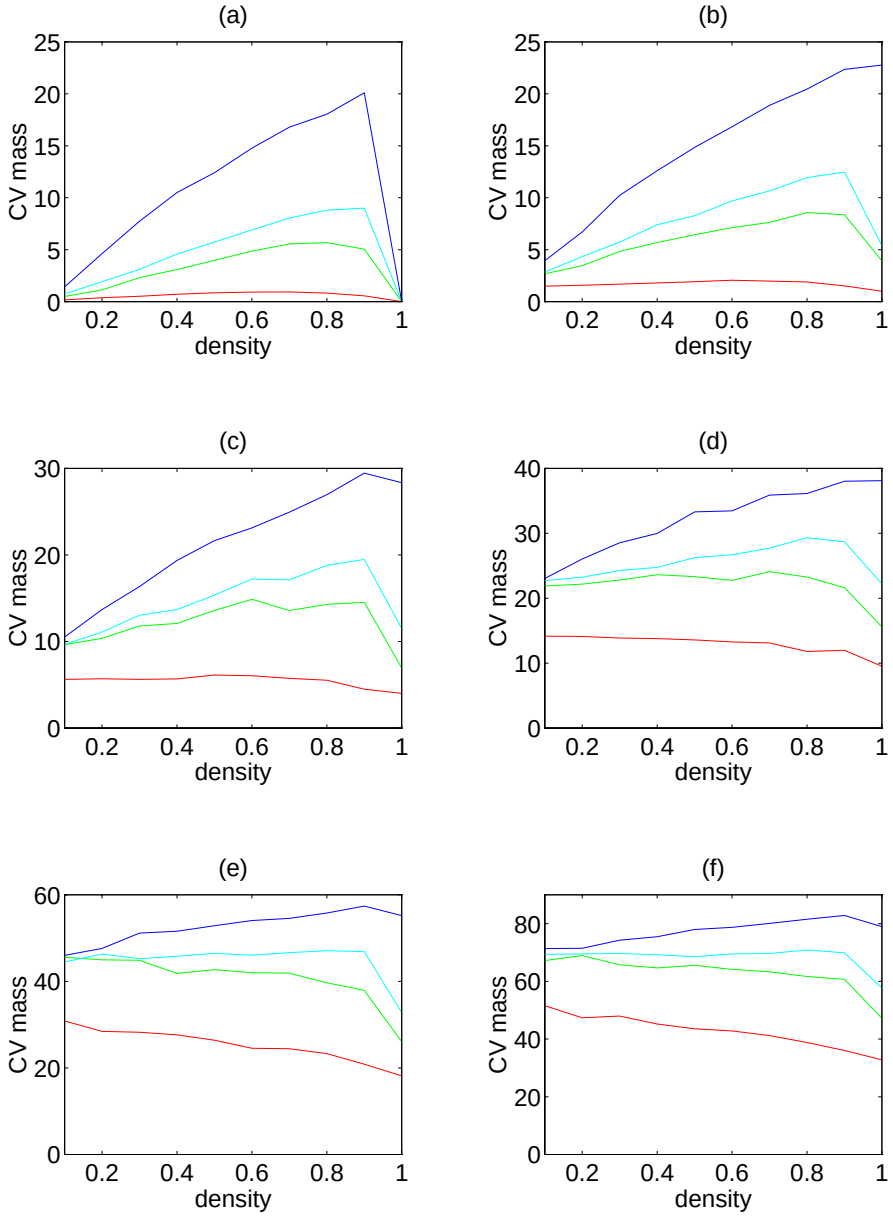

Figure 33: Population statistics for the patchy single species resource-based CMLas density varies: coefficient of variation of mass as a function of density ρ for a range of resource differentiation r_H. (a) $r_H = 1.25$. (b) $r_H = 1.5$. (c) $r_H = 1.75$. (d) $r_H = 2.0$. (e) $r_H = 2.25$. (f) $r_H = 2.5$. In all cases the competitive types are absolute symmetry (red), relative symmetry (green), relative asymmetry (cyan) and absolute asymmetry (blue).

An intermediate scenario occurs when the resource patches are a mutation or shift of the previous year, which covers a wide range of naturally occurring resource distributions. This idea can be incorporated in the patch-generating algorithm of section 5.3.2 as follows. The algorithm may be stopped prematurely when a fraction ϖ of the desired final number of cells have been switched *on*. This intermediate stage is recorded and used as the initial distribution for all of the patch distributions. Thus the resource patterns vary in a limited way from year to year. The amount of correlation between the patches generated by this *shifting algorithm* is controlled by parameter ϖ. The proportion of cells that are identical in two typical shifted patterns varies approximately linearly from around 70% for $\varpi = 0.1$ to around 90% for $\varpi = 0.9$.

Thus three resource allocation regimes are considered here and termed respectively *fixed*, *random* and *shifting patches*. After a consideration of the spatial scales of the CML, the long term dynamics of one and two species systems are investigated for these three cases.

5.4.2. Characteristic Spatial Scales.

Figure 34 shows the error analysis of the resource-based CML for four combinations of parameters on a 200×200 grid. In each case the coherence length scale is between $n_c \simeq 25$ and $n_c \simeq 45$ cells. Therefore the 50×50 grid used throughout this chapter is adequate to avoid distortion of the dynamics by spatial correlations.

The relative constancy of n_c for different degrees of resource clumping and different mean dispersal distances indicates relative insensitivity of the spatial scales of the dynamics to the imposed distributions. However, there are marginally shorter length scales of $n_c \simeq 35$ and $n_c \simeq 25$ for the lower clumping cases (figure 34b, d) than the higher clumping cases (figures 34a, c; $n_c \simeq 45$ and $n_c \simeq 30$). Restricted seed scattering has more effect on the scale, with a decrease in the coherence length scale by 10 or 15 cells compared with the more widely-scattered species. The error is below the theoretical curve in each case, so the distribution on small subgrids is more evenly dispersed than on an infinite lattice and so it exhibits positive coherence for $0 < n < n_c$. The cases of lower scattering deviate less from $\mathcal{E}'_n$, consistent with a lower dispersing tendency.

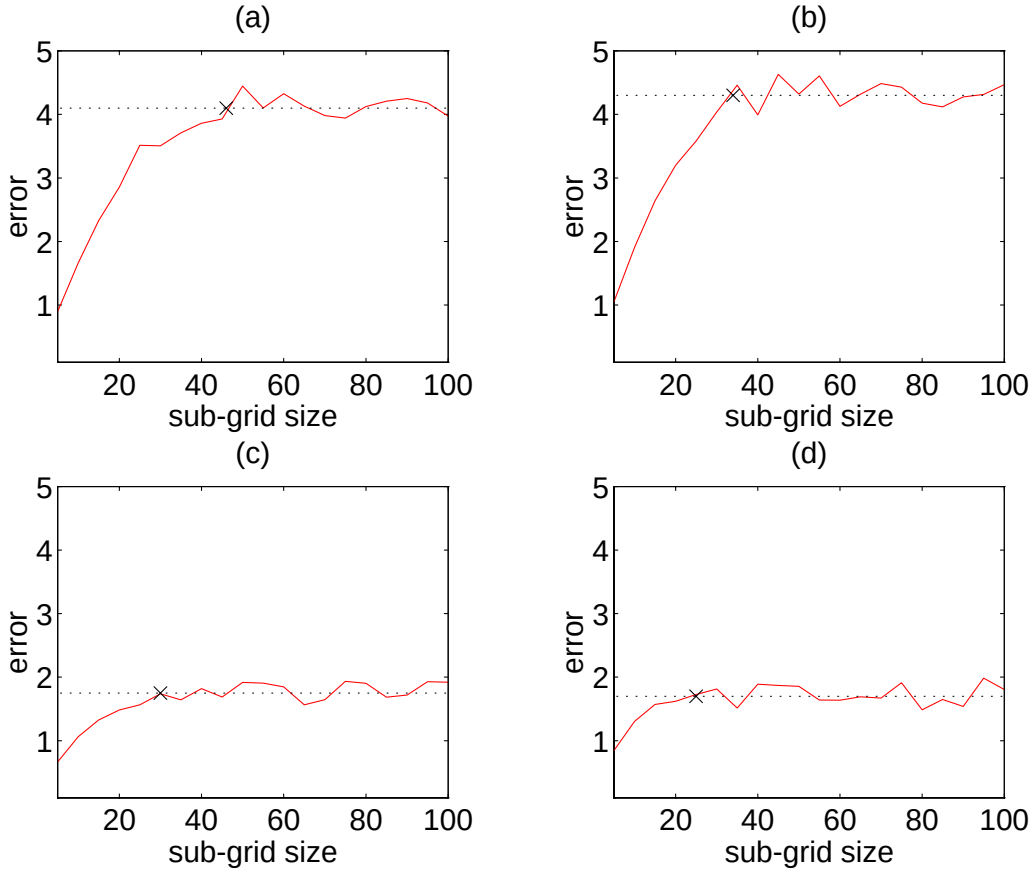

Figure 34: Error analysis for the resource-based CML: numerical error $n\mathcal{E}_n$ for the model (—) and theoretical error $n\mathcal{E}'_n$ $(\cdots)$. (a) High resource aggregation, high scattering ($M_s = 16$); (b) low resource aggregation, high scattering ($M_s = 16$); (c) high resource aggregation, low scattering ($M_s = 2$) ; (a) low resource aggregation, low scattering ($M_s = 2$).

5.4.3. Single Species Dynamics.

The effect of varying mean dispersal distance was studied using the CML over a period of 50 years, by which time single populations consistently settle to equilibria. Figures 35a - c show mean masses after 50 years as a function of dispersal (M_s) for a homogeneous resource environment and for fixed, random and shifting patches. The homogeneous case is naturally independent of the allocation regime and M_s has little effect, except that $M_s = 1$ is slightly preferable, as the offspring of a large plant can use the space immediately around the parent plant, previously occupied by poorly-reproducing suppressed plants.

When there are fixed resource patches, low scattering is optimal in the long term (figure 35a), in agreement with Lavorel et al. (1994). Plants that have reached favourable regions produce their offspring nearby, so they can use the rich resources in the locality. In contrast, random patches lead to the extinction of species with limited dispersal ($M_s < 4$), as a certain level of dispersal is needed to allow plants to follow resources as they move randomly from year to year. The changing resources do not allow the plants to grow as well as fixed resources, as a proportion of seeds will always be lost in poor resource patches each year. Thus the average mass of a plant population which manages to survive on a patchy landscape is similar to the homogeneous case (figure 35b). Shifting patches are similar to fixed patches, with low dispersal being favoured by plants in those high resource areas which do not change to low resources at any particular time (figure 35c).

In addition to dispersal distance, the number of seeds produced by an adult plant of maximum size may be varied. Figure 35d illustrates the combined effect of dispersal and seed number on the number of plants present after 50 years in a stand with fixed resource patches. For any number of seeds, lower scattering produces fewer plants. The seed number does, however, provide a trade-off against dispersal distance, so that more locally-scattered seeds and fewer widely-scattered seeds produce similar numbers of adult plants. Figure 35d also shows that the number of plants reaches saturation as the seed number rises, so that there is no benefit to the production of excessive numbers of propagules.

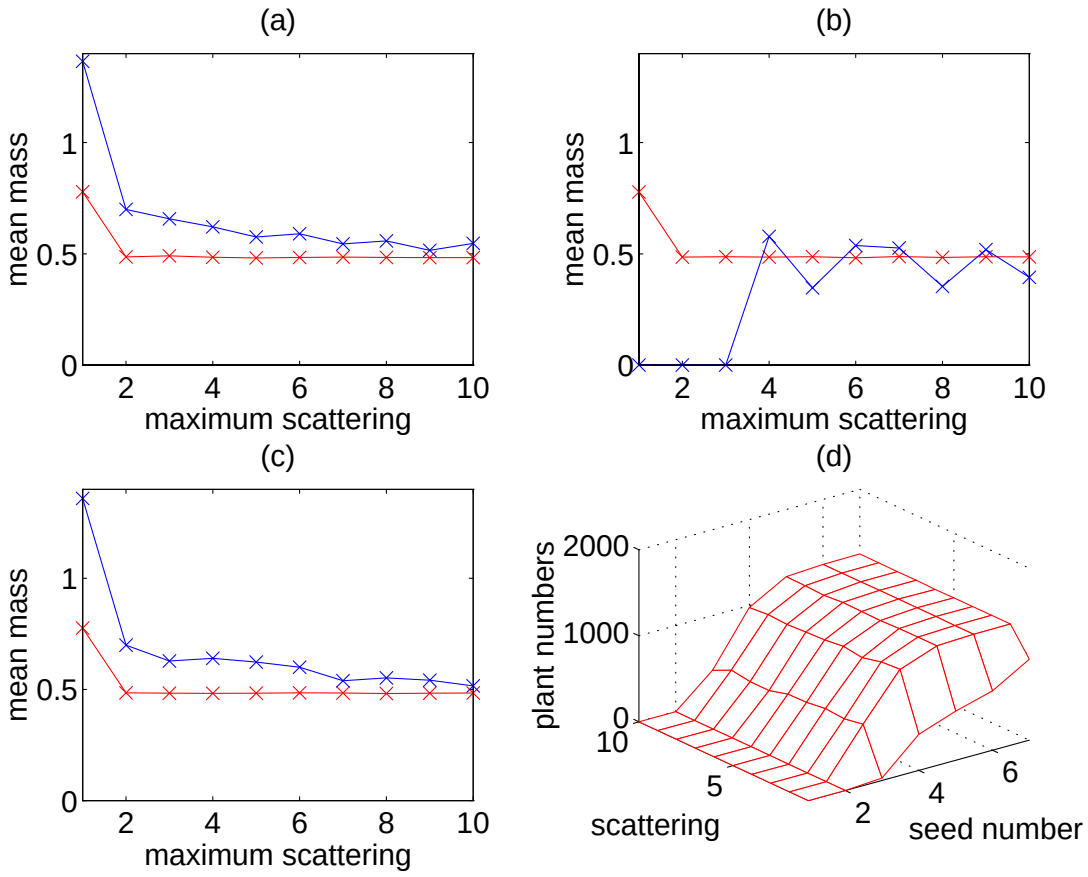

Figure 35: Results for the basic and patchy multiple year single species resource-based CML with asymmetric competition. (a) - (c) Mean mass in year 50 as a function of maximum scattering distance (M_s): (a) fixed resource patches; (b) random resource patches; (c) shifting resource patches ($\varpi = 0.5$). In each case results are shown for homogeneous (red) and heterogeneous resources with large clumping and high resource differentiation (blue). (d) Number of plants in year 50 as a function of maximum scattering distance (M_s) and the number of seeds per plant for fixed resource patches.

5.4.4. Two Species Dynamics.

The effect of patchy resources and varied dispersal distances on pairwise interspecific competition was studied using the CML. Figure 36 shows time series for the number of plants of each species over a 50 year period. Where the resource are homogeneously distributed, the species with higher dispersal excludes the other species (figures 36a - c). The inferior species does better in the short term when it has a higher dispersal distance, as the number of plants with $M_s = 2$ increases at first before slowly going to extinction (figure 36c), whereas $M_s = 1$ immediately declines (figures 36a - b). Thus the *absolute* dispersal distance of a species is important in determining its response to a more widely-dispersing species.

Heterogeneous environments also consistently favour the more widely dispersed of two competing species, although the successful species does less well than in the homogeneous case. In particular, neither $M_S = 2$ nor $M_s = 1$ survive on random patches (figure 36d), although $M_s = 2$ goes to extinction more slowly than $M_s = 1$. $M_s = 4$ is able to survive (figures 36e - f), but with fewer plants than on fixed patches. As in section 5.4.3, the shifting patch regime exhibits similar dynamics to the fixed patch case (figures 36g - i).

5.5. Introduction to the Ecology of Seed Sizes.

The evolution and ecology of *seed sizes* has received much attention in the literature, with an overwhelming volume of agricultural research into the relationship of seed size and crop yield of biomass, grain or oil. The experimental data is conflicting, with evidence presented for positive[49] and negative[50] correlations of seed weight with stand yield as well as many examples of no correlation of the variables[51]. Aspects of germination have been focused upon in agricultural

[49] Pet & Garretsen, 1983; Murray et al., 1984; Tekrony et al., 1987; Spilde, 1989; Reddy et al., 1989; Tinius et al., 1991; Heather & Sieczka, 1991; Grieve & François, 1992; Pearson & Miklas, 1992; Tinius et al., 1992; Tinius et al., 1993; Leishman & Westoby, 1994b.

[50] White & Gonzales, 1990; Bebawi et al., 1991; Acquaah, 1992; Singh, 1992; White et al., 1992; Mehlman, 1993; Sexton et al., 1994.

[51] Pyke & Hedley, 1983; Murray et al., 1984; Stanton, 1984; Tekrony et al., 1987; Reddy et al., 1989; Graven & Carter, 1990; Nafziger, 1992.

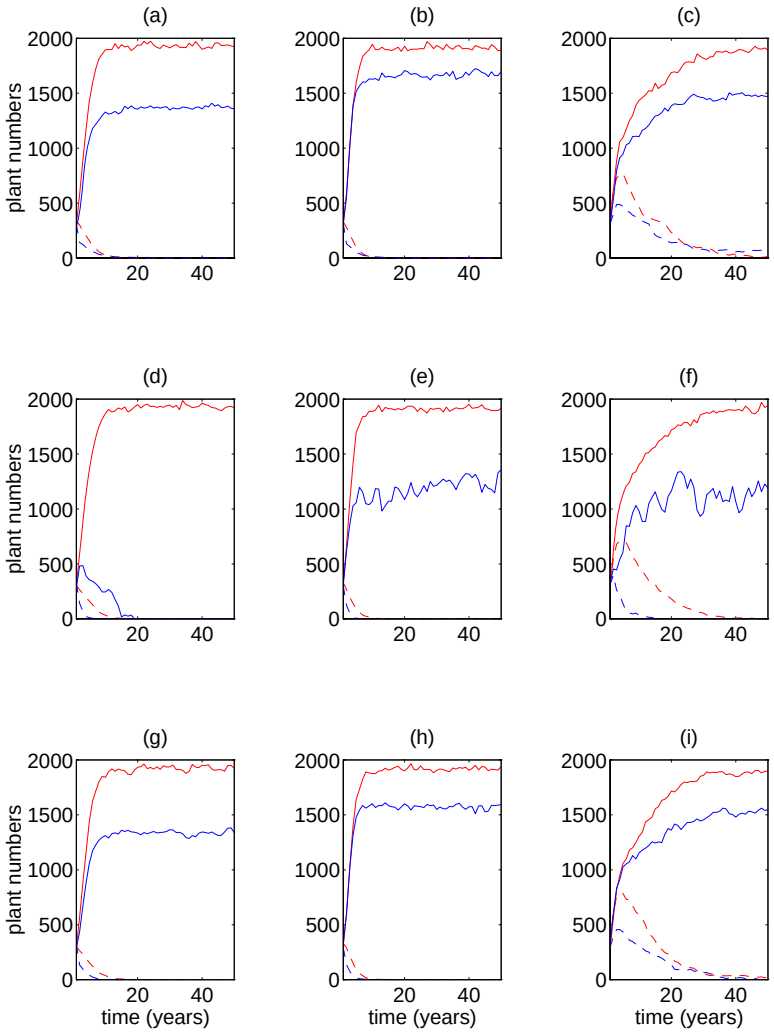

Figure 36: Results for the basic and patchy multiple year two species resource-based CML with asymmetric competition between pairs of species with different seed dispersal distances. In each case the number of plants surviving is shown in a homogeneous environment (red) and in a highly clumped heterogeneous environment (blue) for the highest dispersal (—) and lowest dispersal (- - -) species. The resource allocation regimes are: (a) - (c) fixed patches; (d) - (f) random patches; (g) - (i) shifting patches. The pairs of species are: (a), (d), (g) $M_s = 1$ and 2; (b), (e), (h) $M_s = 1$ and 4; (c), (f), (i) $M_s = 2$ and 4.

studies, with proportions of emergence generally rising with seed weight[52] or staying constant[53], but speed of germination or emergence showing both positive[54] and negative[55] correlation with seed weight. The species for these studies have ranged from herbaceous annuals and perennials through to shrubs and trees in a wide range of geographical locations and habitats. The empirical background for the determination of the ecological significance of seed size is thus very complex and requires a wide range of factors to be taken into consideration.

Many advantages of large seeds have been suggested and in some cases demonstrated. A large seed provides a nutrient reserve and a moisture supply which can give a seedling a better chance of establishment under circumstances of depleted nutrients or drought[56]. Similarly an intrinsic nutrient store reduces the reliance of seedlings on photosynthesis, so growth is possible in shaded areas[57]. Thus large-seeded species can be expected to dominate in mesic environments, arid regions and understoreys of dense canopy vegetation.

Nutrient deprivation also occurs in the opposite circumstances of intense competition, which will tend to correspond to rich habitats[58]. Reserves within a large seed give the seedling a competitive advantage, as the seed will generally produce a large vigorous seedling, well-equipped to compete for space and nutrients. There is thus a tendency for late successional species to have relatively large seeds[59]. There is also some evidence that larger seeds can remain

[52] Stanton, 1984; Singh & Makne, 1985; Winn, 1988; Chandra-Babu et al., 1990; Milosevic et al., 1992; Naylor, 1993; Leishman & Westoby, 1994a.

[53] Tekrony et al., 1987; Zhang & Maun, 1990; Shipley & Parent, 1991; Gonzales, 1993; Sung, 1992; Douglas et al., 1993.

[54] Pet & Garretsen, 1983; Marshall, 1986; Winn, 1988; Zhang & Maun, 1990; Heather & Sieczka, 1991; Grieve & François, 1992; Kelly & Purvis, 1993; Naylor, 1993.

[55] Lafond & Baker, 1986; Marshall, 1986; Stamp, 1990; Giles, 1990; Seiwa & Kikuzawa, 1991; Sung, 1992; Milosevic et al., 1992.

[56] Baker, 1972; Murray et al., 1984; Stanton, 1984; Gross, 1986; Venable, 1986; Zammit & Zedler, 1990; Grieve & François, 1992; Jurado & Westoby, 1992; Huyghe, 1993; Krannitz et al., 1991; Mian & Nafziger, 1994.

[57] Salisbury, 1942; Baker, 1972; Foster & Janson, 1985; Seiwa & Kikuzawa, 1991; Leishman & Westoby, 1994a; 1994c.

[58] Baker, 1972; Harper, 1977; Stanton, 1984; McConnaughay & Bazzaz, 1987; Marañon & Grubb, 1993; Armstrong & Westoby, 1993.

[59] Salisbury, 1942; 1974; Stanton, 1984; Foster & Janson, 1985; Gross, 1986; McConnaughay & Bazzaz, 1987; Houssard & Escarre, 1991; Seiwa & Kikuzawa, 1991.

dormant in a seed bank for longer, providing a temporal integration of resource heterogeneity (Venable, 1987; Silvertown, 1988; Thompson et al., 1993).

The suitability of large-seeded species for both rich and poor habitats suggests that there should be strong selection towards increasingly large seeds or fruit. There are, however, benefits of small seeds in many circumstances. The most obvious factor is the ease of dispersal (Westoby et al., 1990). The widest scattering of seeds usually occurs via the mechanism of wind, which clearly is biased towards small propagules, often with wings or other similar adaptations for flight[60]. Thus small seeds can be advantageous in environments with patchy or ephemeral resources. Likewise, greater dispersive mechanisms allow species to invade uncolonised regions, so small seeds species often dominate early successional vegetation (McConnaughay & Bazzaz, 1987) and larger canopy gaps (Winn, 1988).

A second, less immediately apparent feature of smaller seeds concerns the growth rate of the resultant seedlings. There have been repeated observations of a negative correlation of *relative growth rate* (RGR) with seed weight[61]. Thus a small-seeded species can grow rapidly and catch up with seedlings from larger seeds after a certain time. There is, however, some empirical data showing a positive correlation of RGR and seed weight[62], so the growth rate advantage of small seeds is not necessarily universal.

Alternative hypotheses have been put forward for the superior growth rates of smaller seeds. Small seeds have less DNA per cell which permits faster cell division, although Marañon & Grubb (1993) suggest this effect is secondary. They demonstrated that small seeds produce seedlings with higher *specific leaf areas* (SLA) but lower *unit leaf rates* (ULR). This means that they have a greater area of leaf per unit mass, but the leaves are thin and photosynthetically less efficient. The balance of SLA and ULR determines the correlation of seed size with RGR

[60] Stanton, 1984; McConnaughay & Bazzaz, 1987; Ganeshaiah & Uma-Shaanker, 1991; Pons, 1992; Willson, 1992.

[61] McConnaughay & Bazzaz, 1987; Houssard & Escarre, 1991; Nafziger, 1992; White et al., 1992; Marañon & Grubb, 1993.

[62] Stanton, 1984; Elrahman & Bourdu, 1986; Tekrony et al., 1987; Zhang & Maun, 1990; Huyghe, 1993.

and explains the conflicting data.

There are thus opposing selective forces for seed size. Long range dispersal and high RGR favour small seeds and nutrient reserves and initial competitive advantage favours large seeds (Allsopp & Stock, 1995; Leishman et al., 1995). There are therefore arguments why large seeds should be found in either rich or poor habitats and different authors usually have their preferred theory, which will often be dependent on their study area (Moore, 1993).

The resource CML is used here to investigate the growth of pairs of species with different seed sizes as their RGRs vary, in a range of homogeneous and heterogeneous environments.

5.6. Short Term Dynamics of Different Seed Sizes.

5.6.1. Introduction.

Given the substantial body of evidence that large seeds initially produce large seedlings[63], the CML model may be used to investigate the interaction of seed sizes and growing conditions in the determination of stand yields. Throughout this section, it is assumed that the initial masses on the CML represent initial seedling sizes and hence pre-germination seed sizes. The CML was used to determine the response of different seed sizes growing in competition to resource availability and density. The balance of seed size and growth rate was assessed by varying the parameter g, the intrinsic growth rate, which directly influences the relative growth rate.

5.6.2. Computational Methods.

The resource-based CML was run on a 50×50 grid for 200 iterations with mortality 0 (section 5.2.3) under a range of conditions. Symmetries 1 and 4 (absolute symmetry and asymmetry) were used throughout to represent the range of possible competitive interactions, where a limitation to the computational intensity was necessary.

[63] Ferrara & Quinn, 1987; Hocking & Steer, 1989; Giles, 1990; Stock et al., 1990; Shanmuganathan & Benjamin, 1992; Douglas et al., 1993; Gonzales, 1993.

(a) Variation of Seed Sizes.

Firstly, pairs of seed sizes were investigated: one species (small-seeded) was given a fixed seed size of 0.00001 mass units. The large-seeded species was given a size ranging between 0.000011 and 0.01, so that the large seeds were 10% to 1000% greater than the small seeds. These initial sizes reflect a realistic range of seed sizes (Marañon & Grubb, 1993) given the model parameters of chapter 3 (table 2). The relative yields of the two species were found for the two extreme symmetries and assuming a constant resource base of value 1.0 ($k_m = k_g = 0$).

(b) Variation of Growth Rate.

The effects of a negative correlation between seed size and relative growth rate was studied using a range of intrinsic growth rates. Two fixed seed sizes were used, of 0.00001 and 0.0001, with the growth rate of the small seed fixed at $g = 25$ and the growth rate of the large seed varied between $g = 25$ and $g = 5$. A change in g was balanced by a change in b, to maintain a constant maximum plant size (equation (17)).

(c) Variation of Initial Resource Level.

The two fixed seed sizes were also used to investigate the effect of different resource availabilities or habitat qualities assuming a growth cost of $k_g = 0.5$ and a range of symmetries, but fixed growth rate $g = 25$.

(d) Variation of Density.

Sections (a) - (c) used a full grid of plants (density $\rho = 1.0$), but density is also an important determinant of stand yield. Sample pairs of seedlings with sizes of (0.00001, 0.0001) and (0.00001, 0.01) were used, as well as four densities ($\rho = 0.25, 0.5, 0.75$ and 1.0) and five growth rates ($g = 5, 10, 15, 20$ and 25).

(e) Variation of Growth Cost.

The growth cost was varied between $k_g = 0.5$ and $k_g = 2.0$ for the five growth rates given in (d)

and seed sizes 0.00001 and 0.0001. Again only two symmetries were used to limit computation.

5.6.3. Results and Discussion.

(a) Variation of Seed Sizes.

Figures 37a - b show sample growth curves for absolutely symmetric competition between small- and large-seeded species. Growth is typically sigmoidal and competition shows a greater impact on the smaller seedling as the difference in size increases. Figures 37c - d show the final yield of each species for a range of sizes of the larger seedling. A larger seedling has a strong competitive effect on a smaller seedling but is little affected by the other's presence: this is more apparent under asymmetric competition. The competitive response of the smaller seedling weakens as the larger seedling increases in size, with its yield exhibiting a roughly linear decline. The total stand yield (figure 37e) demonstrates a marked decrease as the size gap widens, showing that similarity of initial size allows a more efficient use of limited growing space.

(b) Variation of Growth Rate.

A large-seeded species produces a greater yield than a small-seeded species assuming equal growth rates, but a negative correlation of growth rate and seed size easily confers an advantage on the smaller seedling (figure 38a - b). As the growth rate of the large seedling is reduced, there is a crossing-over point ('o') where the small seed starts to gain ground. The total yield shows that the stand as a whole grows more efficiently if the difference of growth rates is less. If competition is asymmetric, a mixed stand is able to produce a higher total output than a monoculture (figure 38c), since the available space may be more efficiently used by mixing small and large plants.

(c) Variation of Initial Resource Level.

As the supply of resources rises, both small and large seedlings do better and attain their full size more quickly. Yields typically increase exponentially, as shown for absolutely symmetric competition (figure 39a). Small seedlings do relatively better at lower resource levels

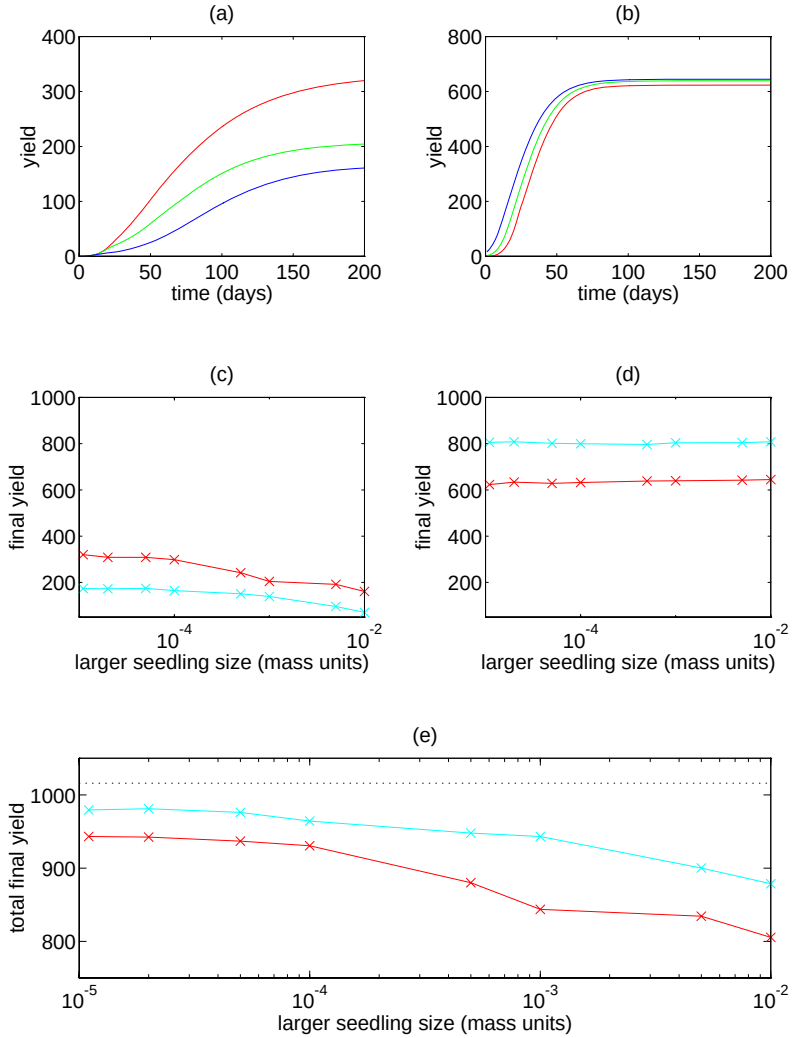

Figure 37: Yields for the resource-based seed size CML model. (a) - (b) Yield as a function of time with absolute symmetry for small seeds of size 0.00001 and large seeds of sizes 0.000011 (red), 0.001 (green) and 0.01 (blue): (a) yield of small-seeded species; (b) yield of large-seeded species. (c) - (d) Relationship of final yield and size of large seeds: final yield of (c) small-seeded species; (d) large-seeded species. (e) Total yield of stand as a function of size of large seeds and theoretical yield for an equivalent monoculture ($\cdots$). For (c) - (e) the competitive types are absolute symmetry (red) and absolute asymmetry (cyan).

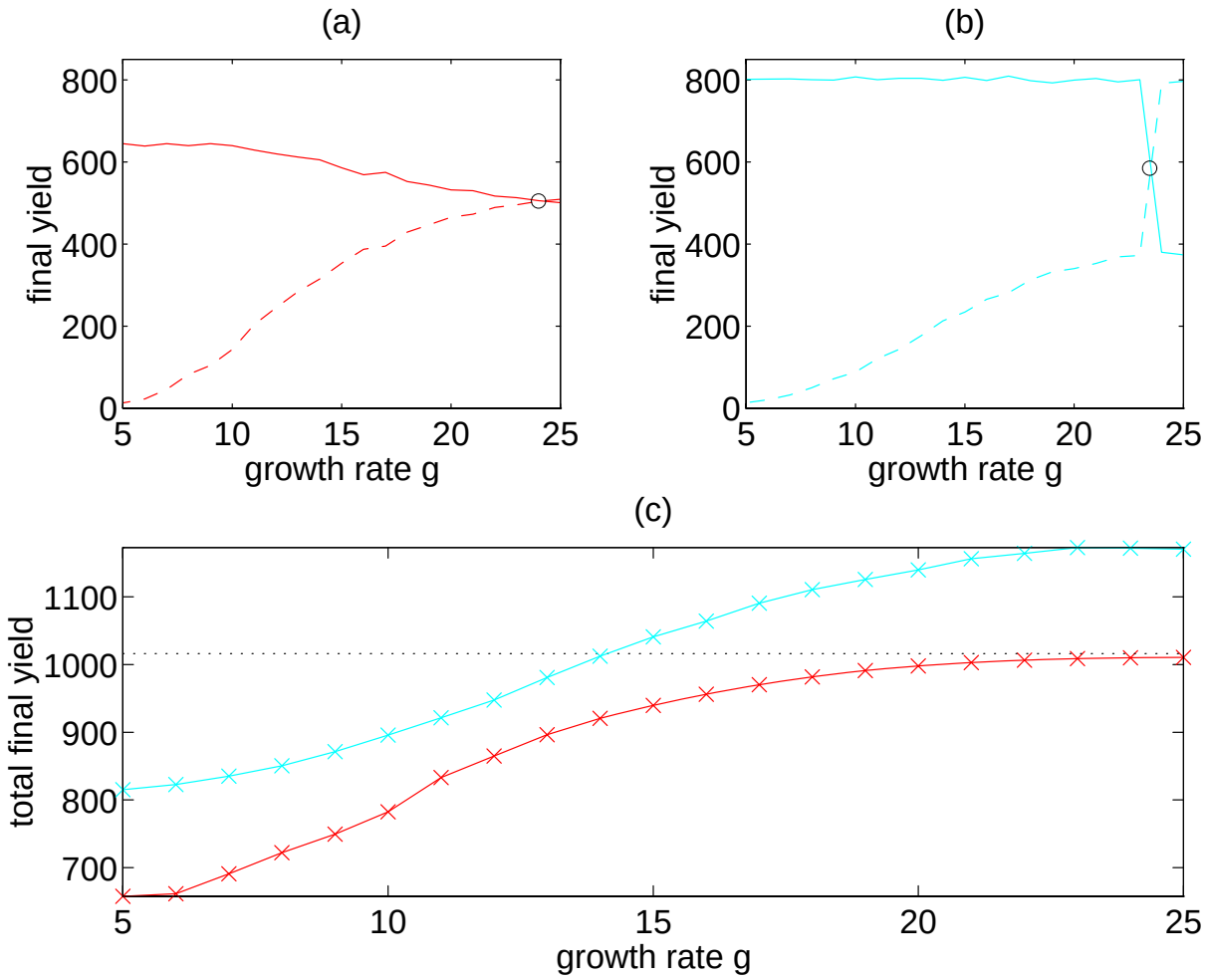

Figure 38: Yields for the resource-based seed size CML model as growth rates vary. Competition between species with seed sizes 0.00001 and 0.0001 as the growth rate of the large-seeded species varies. Yield of small- (—) and large- (- - -) seeded species for (a) absolute symmetry and (b) absolute asymmetry. (c) Total stand yield for absolute symmetry (red) and absolute asymmetry (cyan) and theoretical yield for a monoculture ($\cdots$).

(figure 39b); high resource levels promote rapid growth, so that small seedlings are less able to catch up with big seedlings before competition sets in. Asymmetric competition puts small seedlings at more of a disadvantage, so that the yield relative to the large seedlings is less than under symmetric competition for all resource levels.

(d) Variation of Density.

Lower density always favours the inferior competitor (figure 39c - f). Where large seedlings have low growth rates, low density delays the onset of competition and reduces the loss of space to the smaller-seeded species. Similarly, where large seedlings have growth rates nearer to those of the small seedlings, low density reduces the detrimental impact of competition on the small seedlings. There is therefore a cross-over point ('o') where all densities lead to similar yield ratios. Greater seed size difference and greater asymmetry both lead to the cross-over point occurring at small growth rates (g).

(e) Variation of Growth Cost.

As growth costs rise, plant growth has greater impact on the resource base, so yields of large-seeded species rise at the expense of small-seeded species. In cases with high growth cost, maximum growth will occur at the start of the growing season, before the resource level has decreased; larger seedlings are better able to derive benefit from the early resources. Figures 40a - j show the balance of the advantage to small seedlings of higher growth rates against the disadvantage of high growth costs. A cross-over point therefore exists for each growth rate g where higher costs lead to dominance by the large-seeded species and lower costs lead to higher yields by small-seeded species. The cross-over points ('o') are shown in figure 40 if they lie in the range $0.6 \leq k_g \leq 2.0$; otherwise they may be estimated from the slope of the yield curves. Under asymmetric competition the initial advantage is more influential in determining final yields, so the cross-over points take more extreme values of k_g (figures 40b, d, f, h, j).

5.6.4. Theory of Monoculture Growth.

Given the basic equations of growth for unit resource level (equations (15) and (16)) the area of

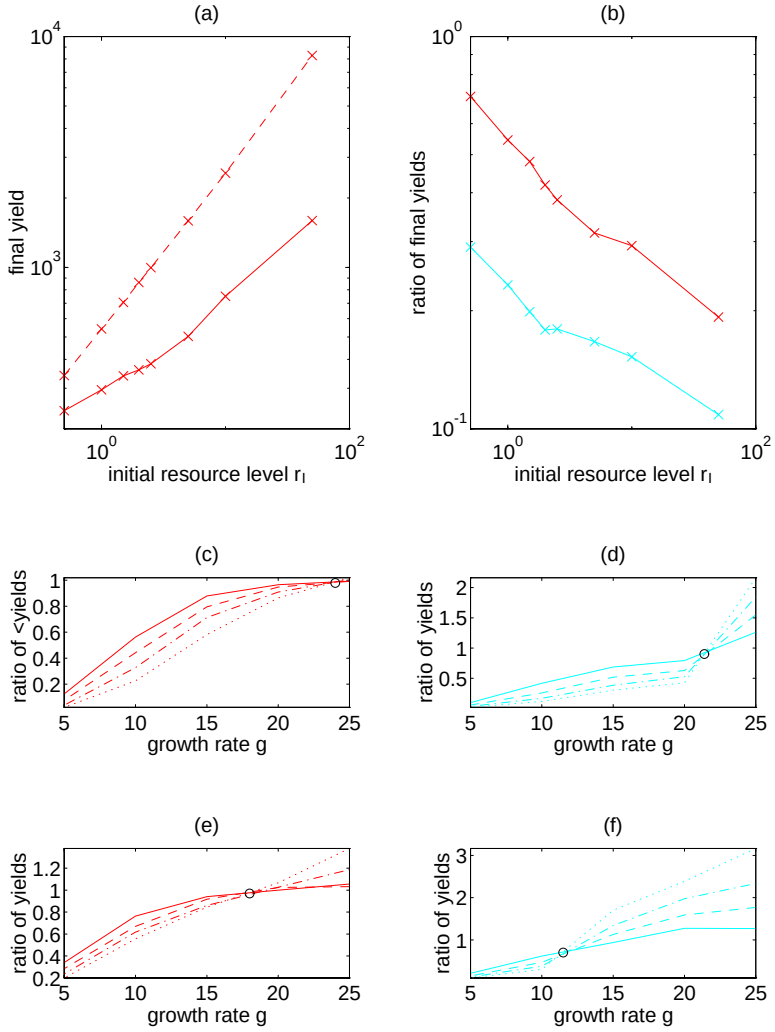

Figure 39: Yields for the resource-based seed size CML model as initial resource levels and densities vary. (a) - (b) Varying the initial resource level (r_I): (a) yield of small-seeded species of size 0.00001 (—) and large-seeded species of size 0.0001(- - -); (b) ratio of yields of small- to large-seeded species for absolute symmetry (red) and absolute asymmetry (cyan). (c) - (f) Ratio of yields of large- to small-seeded species as density varies from 0.25 (—) to 0.5(- - -), 0.75 (- · -) and 1.0 (· · ·): (c), (e) absolute symmetry (red); (d), (f) absolute asymmetry (cyan). Seed sizes are: (c) - (d) 0.00001 and 0.0001; (e) - (f) 0.00001 and 0.01.

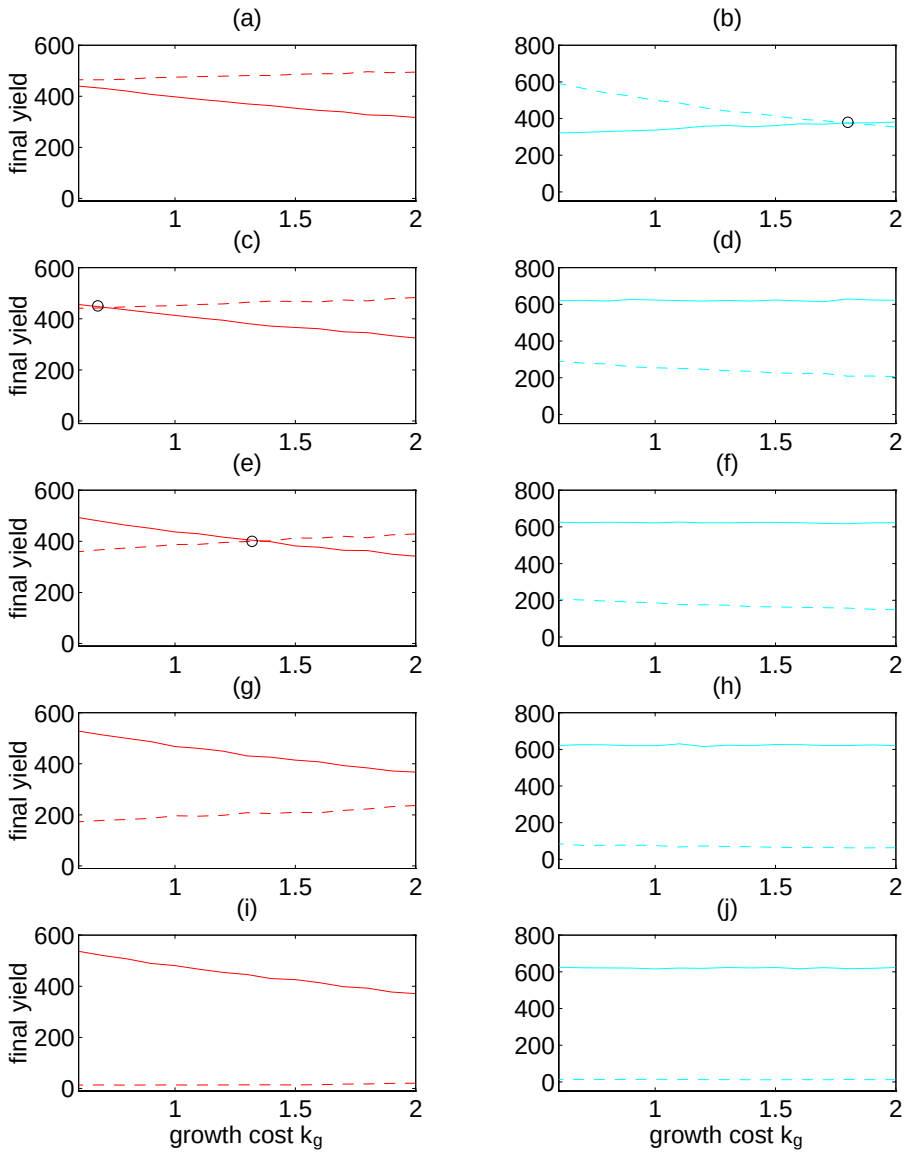

Figure 40: Yields for the resource-based seed size CML model as growth costs vary with seed sizes 0.00001 and 0.0001: yield of small- (—) and large- (- - -) seeded species for (a), (c), (e), (g), (i) absolute symmetry (red) and (b), (d), (f), (h), (j) absolute asymmetry (cyan). Growth rates of the large-seeded species are: (a) - (b) $g = 25$; (c) - (d) $g = 20$; (e) - (f) $g = 15$; (g) - (h) $g = 10$; (i) - (j) $g = 5$.

a cell is given as α (equation (19)) or one-fifth of the maximum possible individual plant area. Thus for a grid of maximum density, allowing for the discretisation constant 1.1 of chapter 3, the expected mean field yield of a monoculture, Y, is given by:

$$Y = \frac{1}{\sqrt{5}} N^2 \left(\frac{1}{1.1} \right),$$

which means that $Y \simeq 1016$ for a 50×50 grid, or $Y \simeq 508$ for a species present in exactly half of the grid cells. Figure 37e shows that the total yield of the CML varies roughly between 800 and 1020, that is, 79% and 100% of the mean field yield in monoculture.

Consideration of the individual species (figure 37c - d) shows that the small-seeded species attains between 14% and 63% of the monoculture yield, while the large-seeded species exceeds the monoculture with a yield of 122% to 160%. The total yield is in general depressed by the presence of a variety of seed sizes: while large seeds gain in competition relative to monocultures, small seeds lose out to a greater extent.

The situation is different when a negative correlation of seed size and growth rate g is assumed (figure 38): the maintenance of a constant ratio $\frac{g}{b}$ ensures the same maximum plant size is attained for all values of g. Total yield varies between 65% and 115%, small seed yields between 75% and 157% and large seed yields between 4% and 157%. Thus a difference in growth rates allows a higher total yield to be attained in mixture than in monoculture, although for a wide range of parameter values yield is depressed.

5.6.5. Response to Resource Heterogeneity.

The algorithm described in section 5.3.2 was used to examine the response of different sizes of seedlings to patchy distributions of resources over the course of a single growing season. As in section 5.3.3(b), three levels of resource clumping were used (table 9). Three pairs of resource levels were used: (1.25, 1.25), (1.875, 0.625) and (2.5, 0.0), which respectively represent low, medium and high resource differentiation (r_H).

Figure 41 shows the yields attained on the CML grid for plants undergoing symmetric competition with a large seedling growth rate $g = 10$; similar results were obtained for asymmetric competition and a range of growth rates. Figure 41a shows the yield of two species of seed sizes 0.00001 and 0.0001. The yield of both species on the poorer patches falls to zero with the resource level, that is, as the differentiation r_H rises. In contrast, the high resource patches support greater yields of both species at either low or high levels of r_H, but the yield is depressed at intermediate r_H. This observation echoes the results of section 5.3.3(b), but the reduced yields for intermediate r_H are observed for a range of clumping levels, whereas the single species case of 5.3.3(b) only behaves in this way under fine scale aggregation. In the single species case, fine scale high and low resource patches lead to the emergence of larger and smaller plants in close proximity and hence to economy of resource utilisation. In the two species case, the species naturally lead to cohorts of smaller and larger plants, which are emphasised by resource heterogeneity.

Figure 41b shows that aggregation slightly restricts the growth of both species on the richer resource patches and promotes growth in poor areas. In large patches of high resources, any cell of the lattice can theoretically support a large plant, but limited space means that large plants cannot grow in all the cells of a neighbourhood, so some growth is restricted. In contrast, plants in large clumps of low resources are able to grow freely, unaffected by the large neighbouring plants they would experience in a more homogeneous environment.

The total yields of each species and of the whole stand all decrease as both clumping level and resource differentiation increase (figures 41c - d), except under fine resource aggregation (figure 41e as described in 5.3.3(b)). Thus homogeneous resource distributions promote optimal yields of the stand and both species. When competition is asymmetric, the dominant faster-growing small-seeded species gains less of an advantage in large clumps, where space is limited; asymmetry of competition highlights this effect.

5.7. Long Term Dynamics of Different Seed Sizes.

The CML was extended to multiple years, so that the long term effects of different seed sizes

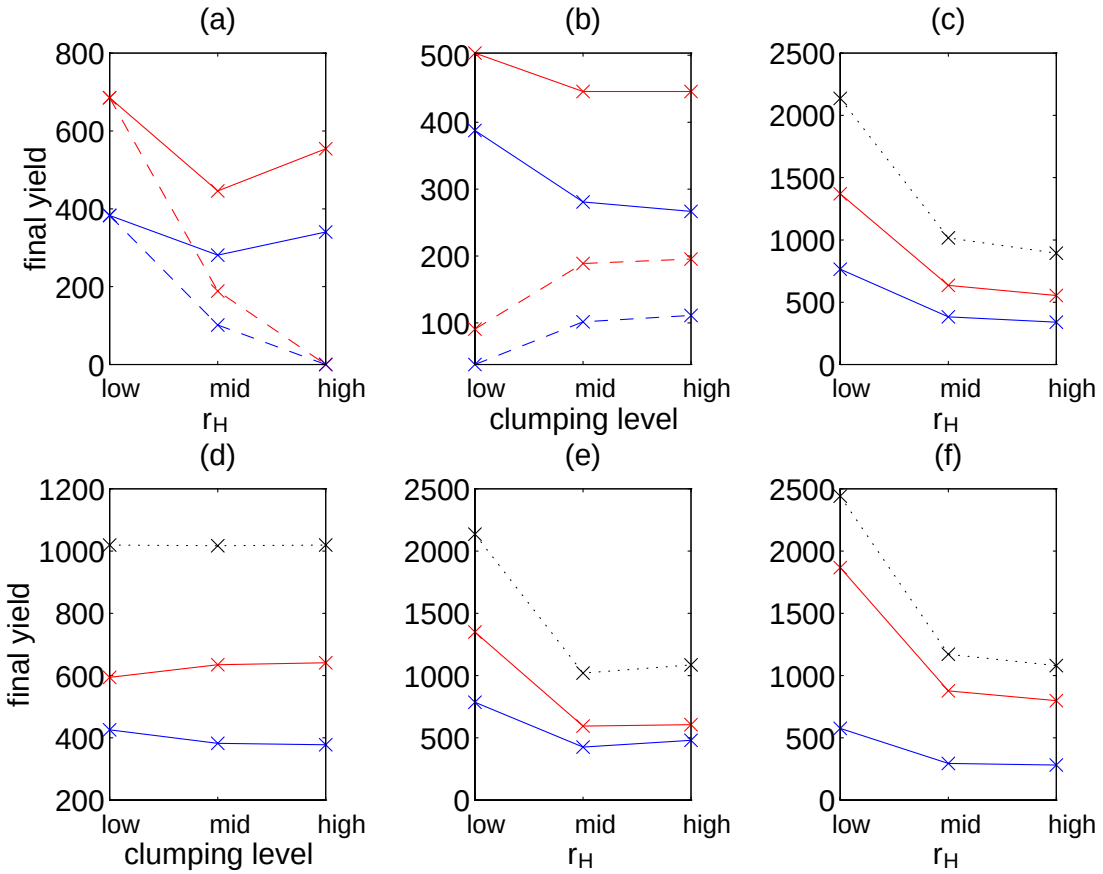

Figure 41: Yields for the patchy resource-based seed size CML model as resource differentiation and clumping levels vary with seed sizes 0.00001 and 0.0001 and growth rates $g = 25$ and $g = 10$ with absolute symmetry. (a), (c), (e) Final yield for (a), (c) medium clumping and (e) low clumping. (b), (d) Final yield as a function of clumping level for medium resource differentiation. (a) - (b) Yield on the two patch types: small-seeded species (red) and large-seeded species (blue) on high (—) and low (- - -) patches. (c) - (e) Total yield for small- (red) and large- (blue) seeded species and total stand yield ($\cdots$). (f) Total yields for absolute asymmetry.

could be assessed and the interaction of seed size and resource distribution examined. Both species were assumed to reproduce according to the method of section 5.4. As discussed in section 5.5, there is a complex relationship between seed size, seed number, seed survival and dispersal distance, so for simplicity a constant dispersal distance and seed number is assumed here for all sizes of seeds.

5.7.1. Competition in a Homogeneous Environment.

Two species with different sizes of seeds were placed in equal quantities on a 50×50 grid. The small-seeded species was given a size of 0.00001 and a growth rate $g = 25$ and the large-seeded species was permitted a range of sizes and growth rates. A range of initial resource levels was used, with the resource homogeneously distributed across the grid at the start of each year.

Figure 42 illustrates typical behaviour of the system as the resource level is varied. Here the large seeds are of size 0.001 and growth rate $g = 20$. At low resource levels (figure 42a) the small-seeded species drives the other to extinction within 50 years. At high resource levels (figure 42c) selection favours the large-seeded species and the small-seeded species disappears before 50 years have passed. At intermediate resource levels (figure 42b) both species are able to persist over many years at roughly equal levels. Thus high resource levels are able to promote the survival of large seeds which otherwise lose ground to smaller seeds under poorer conditions.

The transition from a small-seeded monoculture to a large-seeded monoculture is illustrated in figure 42d by the yields in year 100. A mixed community is supported by the intermediate range of resources ($6 \leq r_I \leq 8$), while outside these values a monoculture results. The total stand yield naturally increases - approximately linearly with r_I - as more resources support more growth of either species.

The change in stand composition may also be seen by evaluating the rates of exponential increase and decrease of the annual yields over the first part of the study period. Exponents were estimated by a weighted linear least-squares method. Exponents are positive for the dominant species at each resource level and approach zero for each seed type near $r_I = 7$ where

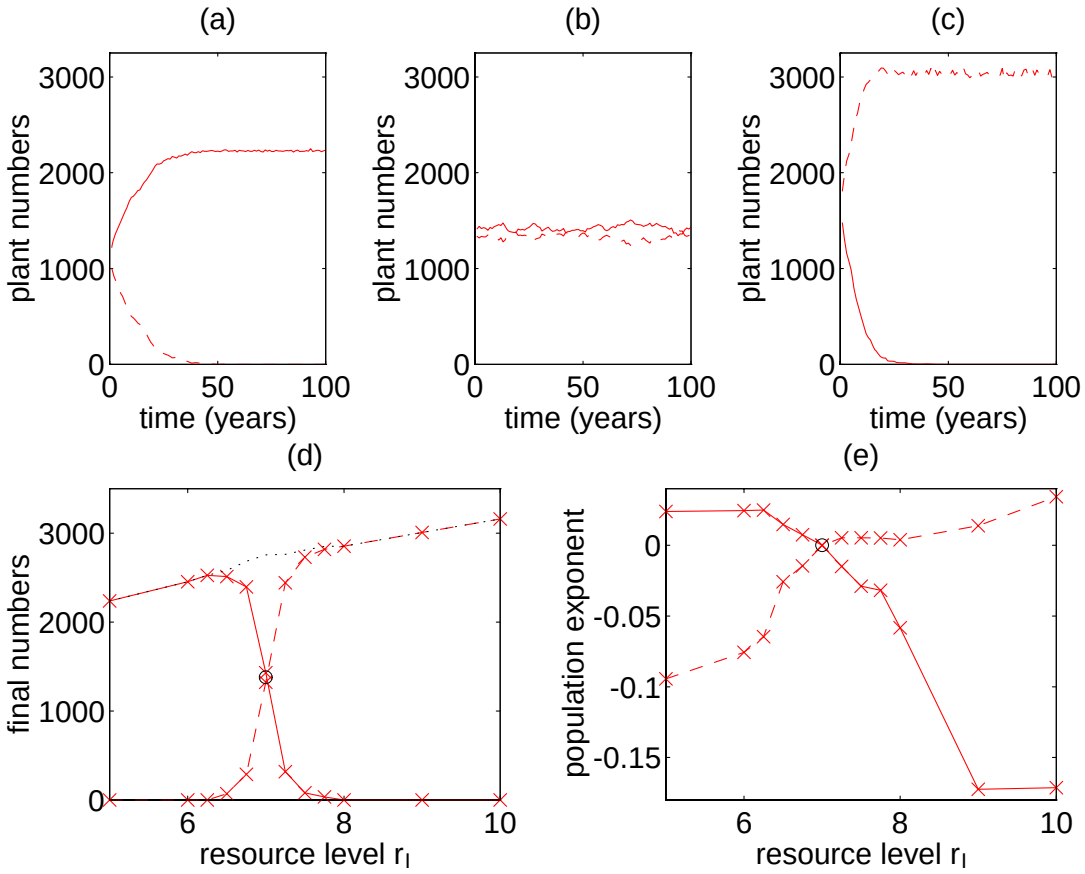

Figure 42: Results for the multiple year resource-based seed size CML model: two species with seed sizes 0.00001 and 0.001 and growth rates $g = 25$ and $g = 20$ under symmetric competition. (a) - (c) Evolution of community composition over 100 years for initial resource levels (a) $r_I = 5$; (b) $r_I = 7$; (c) $r_I = 9$: annual yield of small- (—) and large- (- - -) seeded species. (d) Yield after 100 years of small- (—) and large- (- - -) seeded species as a function of initial resource level (r_I). (e) Mean rate of exponential increase or decrease of annual yields of small- (—) and large- (- - -) seeded species over the early years of competition.

(a)

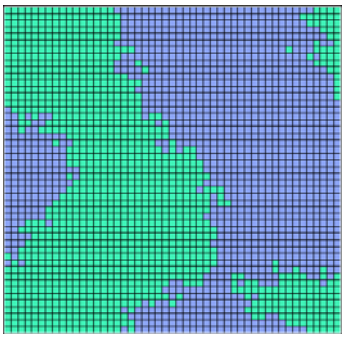

(b)

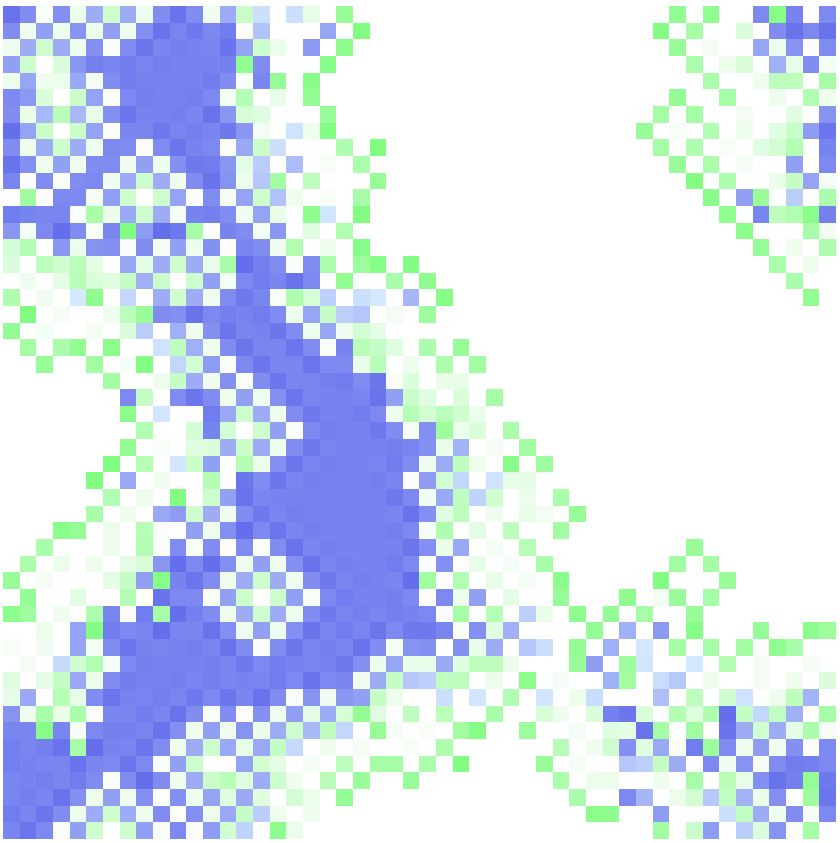

Figure 43: Spatial pattern in the multiple year resource-based seed size CML model. (a) Distribution of high and low resources: $r_I = 5$ (blue) and $r_I = 10$ (green). (b) Distribution of plants after 50 years: seed sizes 0.00001 (green) and 0.001 (blue) with growth rates $g = 25$ and $g = 20$ respectively under symmetric competition. Darker shades indicate larger plants.

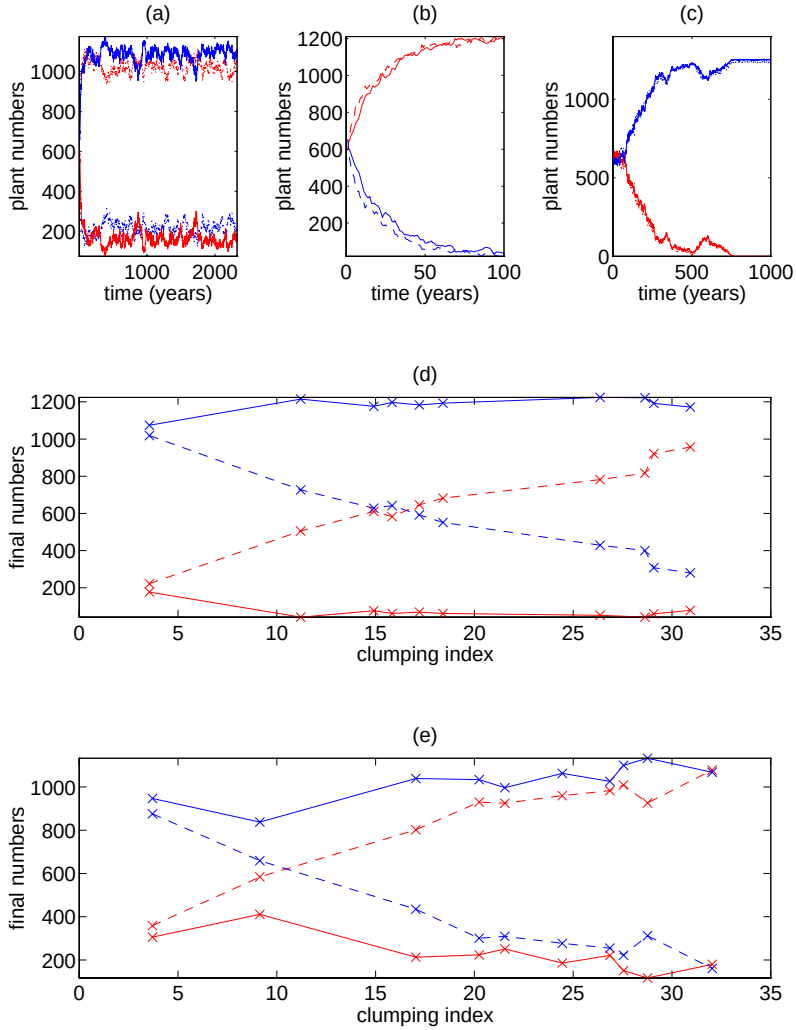

Figure 44: Results for the patchy multiple year resource-based seed size CML model: two species with seed sizes 0.00001 and 0.001 and growth rates $g = 25$ and $g = 20$ under symmetric competition with a heterogeneous resource distribution. (a) - (c) Number of small-seeded (red) and large-seeded (blue) on high (—) and low (- - -) resource patches. (a) High resource aggregation and resource levels $r_I = 6, 8$; (b) high aggregation and $r_I = 4, 6$; (c) low aggregation and $r_I = 6, 8$. (d) - (e) Number of small-seeded (red) and large-seeded (blue) on high (—) and low (- - -) resource patches as a function of clumping index: (d) $r_I = 5, 10$; (e) $r_I = 6, 8$.

the mixture is stable. Thus the initial rates of population change are indicative of the final community structure.

5.7.2. Response to Resource Heterogeneity.

The CML model was run with patchy resource distributions over multiple years for different degrees of aggregation and various pairs of resource levels. Figures 43 shows a typical distribution of small- and large-seeded plants for large patches of resource levels 5 and 10. These resource levels in a homogeneous distribution correspond respectively to monocultures of small- and large-seeded species. The patchy distribution, however, allows both species to coexist over a long time scale: figure 44a shows that both species persist for at least two and a half millennia on resource patches of levels $r_I = 6$ and 8.

The spatial distribution in figure 43 shows that the large-seeded species dominates the higher resources patches with the small-seeded plants clustered around the edges of these patches. There are similar numbers of small-seeded plants on low resources and large-seeded plants on high resources (figure 44a). Likewise there are roughly equal, and significantly lower, numbers of small-seeded plants on high resources and large-seeded plants on low resources. Thus the species are mainly found on the patch type where they exists in monoculture under homogeneous conditions. These do not, however, indicate the preferred resource level for each species, as all plants will naturally perform better in isolation with more resources.

A heterogeneous environment also affects the rates of exclusion of inferior species. If patches with $r_I = 4$ and 6 are used, both of which favour small-seeded plants, then the large-seeded species is indeed driven to extinction (figure 44b) but at a much slower rate than under homogeneous conditions (around 150 years rather than 50 years).

The dynamics are significantly affected by the degree of resource aggregation. When the patches are very small the small-seeded species is eventually driven out of the system (figure 44c). This is because there is enough dispersal of seeds from the large-seeded species to allow it to colonise both patch types.

A range of parameters for the patch-generating algorithm were used and the final yields of the different species and patches were recorded together with the resulting clumping indices. Figures 44d - e illustrate a further investigation of the effect of clumping level an community structure. The large-seeded species always exploits the resource rich patches and maintains a constantly high yield. The small-seeded species is consistently unsuccessful on these rich patches. The clumping level has a strong effect on the poorer patches: in low resource grid cells, fine scale patchiness favours big seeds and coarse patches favour small seeds. Thus the yield curves of the small- and large-seeded species on the poor resources cross over at an intermediate scale. The cross-over point represents a balance between the ability of the poor resource patches to act as refuges and the dominance of the large-seeded species on the rich patches.

6. A Grouse Model.

Chapter Summary

The population and behavioural ecology of the red grouse *Lagopus lagopus scoticus* is described and the idea of kin tolerance is discussed in relation to the observed cyclic population dynamics of red grouse.

A brief overview of previous modelling approaches to the population dynamics of red grouse is given. The algorithm for a two-dimensional spatial artificial ecology is described in detail and typical graphical output is presented.

Simple selection between kin tolerant and kin intolerant grouse types is shown to be an inadequate mechanism for the production of cyclic dynamics. However, it is demonstrated that direct density responses of either individual or social behaviours, in terms of kin tolerance, are feasible underlying processes for the population cycling.

'The fascination of shooting as a sport depends almost wholly on whether you are at the right or wrong end of the gun.' - P.G. Wodehouse

6.1. Introduction.

The population dynamics of the red grouse (*Lagopus lagopus scoticus*) are particularly noteworthy among natural populations, since there is long term data exhibiting relatively regular cyclic fluctuations in population numbers. The red grouse also has anthropocentric interest as it is economically important, with shooting on approximately 10^6 hectares of grouse moors producing an income in excess of £10m annually (Lance & Lawton, 1989). There is thus a need to understand the population biology of the grouse, so that appropriate management techniques can be implemented to guarantee the persistence of the species and shooting interests.

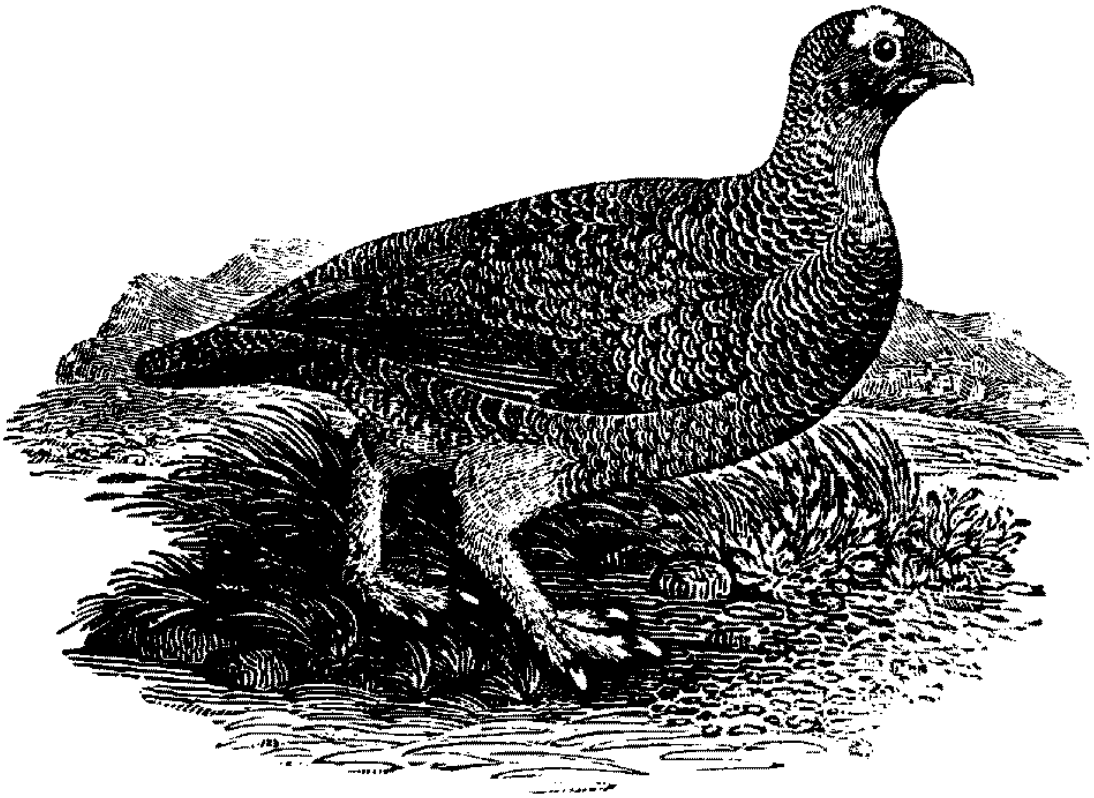

Figure 45: The red grouse *Lagopus lagopus* (after Thomas Bewick (1826)).

This chapter discusses the possible phenomena underlying observed dynamics and formulates an individual-based spatially explicit model to investigate key mechanisms in the red grouse system.

6.2. Overview of the Behavioural and Population Ecology of the Red Grouse.

The red grouse is a territorial game bird found in several parts of the British Isles and Europe, notably Northern England and North East Scotland. The extent of the species is limited by suitable habitat, namely the moorland dominated by swards of the common heather *Calluna vulgaris*.

6.2.1. Population Dynamics.

The red grouse is almost unique in having continuous sets of population data going back to 1834. This is in the form of 'bag data' and keepers' records, which provide the annual numbers of grouse shot on dozens of moors around England and Scotland, as well as information on weather and other extrinsic factors (MacKenzie, 1952). Figure 46a shows a typical set of bag data accumulated from moors in Central England over the course of nearly a century. Although the bag data provides an accurate record only of birds shot, it is considered to provide a good indication of the size of the population in any given year (Williams, 1985). However, the bag data, which provides an autumn population count, will fluctuate with greater amplitudes than a spring count, because rapid population increases are buffered by autumn and winter mortality through natural causes or shooting. Figure 46b gives a sample set of field data giving actual counts for a study site at Rickarton in North East Scotland.

Many time series of bag data from around the British Isles have been analysed and have demonstrated widespread cycling of population sizes, with more regularity than would be expected for random fluctuations (Moran, 1952; Williams, 1985), with cycles often being synchronised over extensive areas of moors (Moss & Watson, 1989c) and evidence of correlation with other Tetraonids (MacKenzie, 1952; Moran, 1952). In North East Scotland cyclic fluctuations are

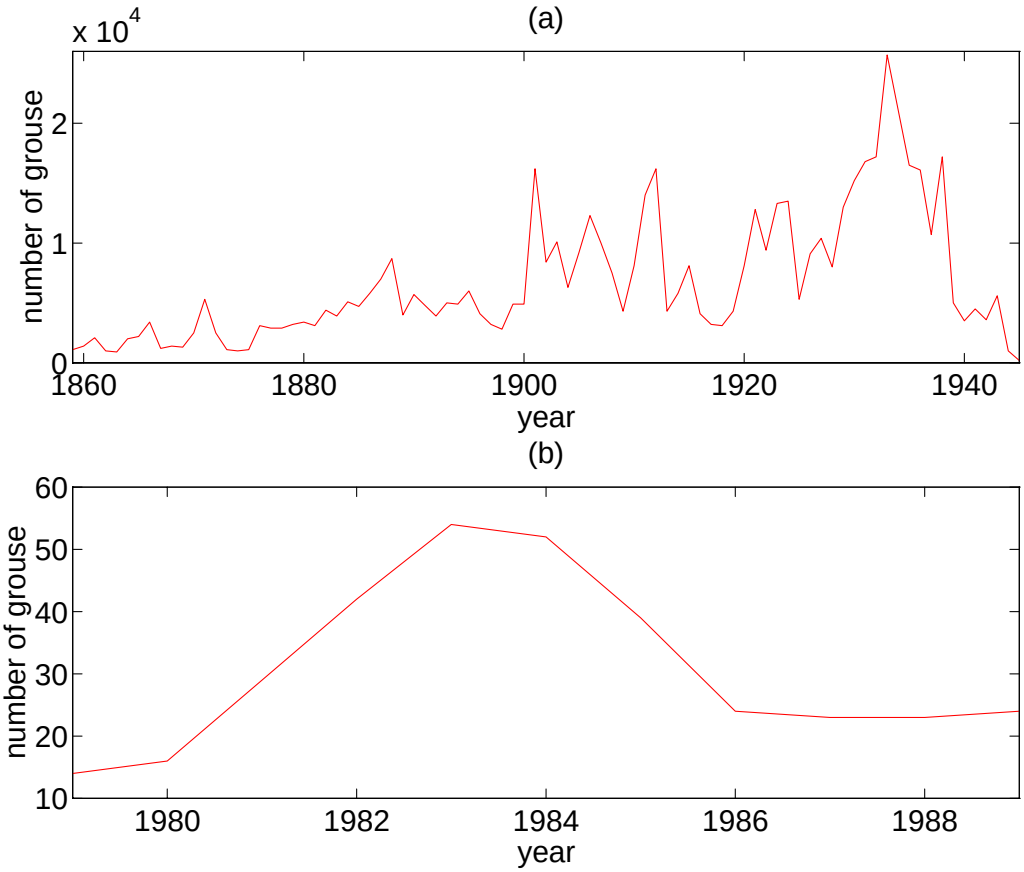

Figure 46: Bag data and field data for red grouse. (a) Bag data from moors in Central Scotland from 1859 to 1945, from data in MacKenzie (1952). (b) Population count data from the study site at Rickarton in North East Scotland, from Moss (personal communication).

seen of lengths 6 to 9 years, with shorter cycles around 4 years in length found in some English estates (Moss et al., 1993). The amplitude of the cycles varies, with increases from trough to peak typically being between two- and five-fold, as seen at Kerloch (south west of Aberdeen) respectively in 1963 - 1969 and 1969 - 1977 (Watson et al., 1994).

A second feature of the bag records is a marked long term decline in red grouse numbers throughout the British Isles over the last century (Moss & Watson, 1989b). This is attributed largely to habitat destruction - for example as moorland is reforested - and to reduction in habitat quality by poor management and overgrazing by sheep (*Ovis* spp.), deer (*Cervus* spp.), rabbits (*Oryctolagus cuniculus*) and hares (*Lepus* spp.); there is also evidence of a climatic effect. Inevitable short term erratic fluctuations attributable to environmental noise are also seen, which may be caused by complex interactions of such features as weather, resources and predator dynamics.

6.2.2. Food and Cover.

Red grouse feed primarily on the heather *Calluna vulgaris*, which also acts as cover (Watson & Moss, 1972). The heather is a short evergreen shrub which has particularly low nutritional content, being low in protein and high in fibre (Moss & Watson, 1989b). The quantity of heather available is not considered to be a limiting factor for population density, with the quality and distribution being of greater significance. Grouse feed selectively on a mere 2 - 3% of the available heather, preferring younger more nutritious shoots. Higher levels of nitrogen in the heather leads to correspondingly smaller territories as a higher density of birds can be supported (Moss & Watson, 1989a).

Grouse do, however, generally choose to remain close to taller old heather, which provides safe cover from predators, as well as being the location of most nesting sites. There is good indication that a fine scale mosaic of old and young heather is more suitable for grouse and such an environment is able to support a greater density of birds. For this reason it is standard management practice, on keepered moors, to maintain the local heterogeneity by burning the heather in small patches in rotation.

Although over 90% of a grouse's diet consists of heather, other plants including bilberry *(Vaccinium myrtillus)* and cotton grass *(Eriophorum vaginatum)* contribute nutrients to the birds. In particular, alternative species are consumed preferentially in early spring before the new shoots of the heather appear. In addition, arthropods form an important source of extra protein in the early weeks of chick growth.

Reduced food supply at peak density does not, however, appear to have a significant role in the cyclic dynamics, as resources have been observed to remain relatively constant while population size varies significantly (Moss & Watson, 1994). Food supply is more likely simply to set the peak density of birds. Likewise, an experimental fertilisation of heather has been demonstrated to have negligible effect on the cycling of grouse numbers (Moss & Watson, 1985).

6.2.3. Shooting.

The prevalence of shooting on the grouse moors certainly means that the moorland ecosystem is unnatural, but it is generally believed that shooting has limited effect on the population dynamics of the grouse. The shooting season opens on 12th August, when the chicks are almost fully grown, so that the effect is simply a reduction in the adult population. This is assumed by some to be balanced by a correspondingly lower winter mortality and thus the total population size is unaffected by the shooting. However, it is argued by some workers that the shooting will remove birds at random, whereas the winter mortality will generally affect the weaker individuals of the species; it has been observed by others that in practice shooting primarily removes slower birds at the rear of a flock. There may thus be a decrease in the average fitness of the population where shooting takes place. Some authors dispute this, producing evidence that predation, a major cause of winter death, is not selective of weaker individuals (Hudson, 1989).

A second implication of shooting is that it could cause territory configurations to be broken up. Under the hypothesis that territorial behaviour and territory configuration is a key process in determining red grouse dynamics (see section 6.2.6), shooting could have a significant impact on the population numbers, for example by reducing the magnitude of cyclic fluctuations (Moss

& Watson, 1985).

Many recent study sites are located on unshot moors, so that the shooting factor is not of great significance, except in terms of movement between shot and unshot moors. There is a further consideration in this situation: a lack of shooting is generally accompanied by lower levels of management and in particular the absence of keepers means that natural predation is much higher. Some sites - such as Kerloch and Rickarton - have, however, continued to be keepered whilst shooting has not taken place. There has been a widespread increase in the numbers of predators of grouse of the past few decades, so the extrinsic environment of current study areas cannot be assumed to be representative of the conditions which produced the early bag data.

6.2.4. Disease and Predation.

The primary disease of red grouse is, appropriately, *grouse disease* or *trichostrongylosis*, which is caused by the caecal nematode *Trichostrongylus tenuis*. Most red grouse have some of these worms, but low concentrations have little apparent effect on fitness. There are, however, repeated observations of outbreaks of grouse disease dating back to the last century, when heavy worm burdens and subsequent fatalities are seen. The effect of the parasite is chiefly seen in spring and early summer (Moss et al., 1989), when both direct mortality and reproductive effects are seen (Hudson & Dobson, 1989). High parasite intensities have been positively correlated with the production of smaller later clutches and chicks with lower hatching weights. There is a much weaker relation between worm burden and individual adult condition (Moss et al., 1989; 1990).

Some authors consider *T. tenuis* to be a key factor in the regulation of grouse population densities and assert that cyclic populations correspond to higher prevalence of the parasite. However, there is a relatively low intensity of *T. tenuis* on the East Scottish moors, where cycles have been frequently recorded.

A second disease found in the red grouse species is *Louping ill*, which is a virus transmitted by the sheep tick *Idoxes ricinus*. The condition is usually fatal and particularly affects chicks

(Lawton, 1989), but its occurrence is patchy and is generally a problem only in areas of intensive sheep grazing. There are also two tapeworms, *Hymenolepsis microps* and *Davainen urigalli*, but their role in grouse population ecology dynamics has yet to be ascertained.

As stated in section 6.2.3, predation was not a significant factor on the traditional shot moors, where keepers were able to keep predator numbers at a low level. At the present time, there are many areas of moorland where predators are now present in substantial numbers, including the red fox *(Vulpes vulpes)*, stoat *(Mustela erminea)*, carrion crow *(Corvus corone)*, golden eagle *(Aquila chrysaëtus)*, peregrine falcon *(Falco peregrinus)* and the hen harrier *(Circus cyaneus)*. Predators will take adult birds throughout the year, with foxes, stoats and crows also robbing nests of entire clutches of eggs in the spring, although females are sometimes able to lay a replacement clutch if this happens.

6.2.5. Reproduction.

The red grouse is typically monogamous (Moss & Watson, 1991), with mating being restricted to territorial males, most of which are paired with a single hen, although there is a low incidence of bigamy (Watson et al., 1994). Some territorial males do not have hens, especially in poorer habitats, where the sex ratio tends to be biased towards more males; it is generally more uniform in richer environments, where bigamy may occur. Experimental fertilisation of heather has been shown to shift the sex ratio away from the males and hence breeding is more successful (Moss & Watson, 1994).

Hens lay clutches of approximately seven eggs in mid April, which hatch in late May or early June; males tend to stay near the nest during this time. There is high mortality in the first couple of weeks after hatching (Jenkins et al., 1967), but chicks which survive this first phase experience minimal further mortality. The pairs tends to move around the moor during the summer, taking their families with them, but they usually return to the natal site in time for the autumn territorial disputes (Lance, 1978). The young grouse are fully grown after about three months and young males compete with older birds on roughly equal terms in the autumn (Watson & Moss, 1972). While young males will attempt to gain territory near their fathers'

territories, young females will often disperse over distances of several kilometers (Lawton, 1989; Moss & Watson, 1991).

6.2.6. Territorial Behaviour.

Many authors assert that a key stage in the life history of the red grouse is the recruitment of young males to the adult territory-holding population in the autumn[64]. The autumn territory distribution is then assumed largely to determine the spring distribution and hence control the breeding density (Watson, 1968). Thus the density and distribution of the male population is assumed to be fundamental and to limit the breeding density of females (Moss & Watson, 1991). This agrees with the observation that population declines can occur despite successful breeding seasons and increases can occur when the reproductive rate is low (Watson & Moss, 1989). This is disputed by other authors (Hudson, 1989), who claim that most winter mortality occurs when there is snow cover, which is accompanied by the temporary breakdown of the territorial structure. However, it has also been stated that the flocks which form during periods of snow cover also exhibit patterns of spacing associated with dominance behaviour (Watson & Moss, 1989).

Young and old male grouse start to attempt to take their own territories in early autumn. On the whole, old birds will stay close to their original territory and young birds will attempt to recruit fairly near their fathers' territories *('natal philopatry')* (Moss & Watson, 1994). Aggressive behaviour during the autumn includes *song flights*, which end with a characteristic call known as *becking*, and patrolling of territory boundaries accompanied by calling and aggressive posturing (Jenkins et al., 1963). These behaviours mostly occur at dawn and dusk, although territory is defended throughout the day just before the breeding season (Watson & Jenkins, 1968) and most encounters are observed to be pairwise, as neighbouring birds try to maintain or expand their territories.

When the population is at high density, more of the weaker individuals will fail to capture

[64] Jenkins et al., 1963; 1967; Watson & Jenkins, 1968; Watson & Miller, 1971; Watson & Moss, 1980; Moss et al., 1984; Watson, 1985; Watson et al. 1994.

or hold a territory. Thus a pool of non-territorial males is established by the winter time. Territorial birds which die tend to be replaced by non-territorial birds (Watson & Jenkins, 1968; Watson & Miller, 1971), but those individuals which do not gain a territory always die or emigrate from the area before breeding[65]. Thus territory acquisition is crucial to a bird's survival and hence to the species' population dynamics.

The size of territories held by males has various implications. It appears that hens select males that have larger territories, with the important aspect being the relative rather than absolute territory size in any one year. Quality of the territorial habitat is also a relevant factor in their selection. Larger territories will usually encompass a greater quantity of food resources and are more likely to include regions of higher quality food and well as better cover. There must, of course, be a upper bound on territory size, given the necessary energy and time cost of maintaining territory and repelling intrusions by neighbours, although this bound may often not be limiting.

There have been several studies on the causes and consequences of *aggression* in male grouse. Aggression is measured by the tendency of an individual to threaten or attack in pairwise encounters. Breeding and implantation experiments have provided good evidence that the level of aggression in an individual is partly heritable and partly controlled by hormones. Implants of testosterone in male grouse have been made in both captive and wild grouse (Moss et al., 1994). In natural populations, implanted territorial males executed more song flights, took part in more aggressive encounters and chased more females. This resulted in substantial increases in the territory sizes of experimental males at the expense of unimplanted individuals which died or emigrated. Likewise, implanted non-territorial birds were able to capture territories. Hens paired with implanted birds were seen to produce marginally larger broods.

A slightly different aspect of territorial behaviour is *dominance*. Male grouse can be attributed a *social dominance rank* which defines their positions in a pecking order within a group of males. Dominance has shown to be heritable from both parents and is partially correlated with

[65] Jenkins et al., 1963; 1967; Watson & Miller, 1971; Watson & Moss, 1972; Moss & Watson, 1985.

aggression and physiological condition (Watson, 1968).

The mean dominance within the population may provide clues to the mechanisms underlying the observed density cycles. It has been established that mean population dominance falls during the increase phase of the cycles and rises during the decline phase (Watson & Moss, 1980; Moss et al., 1984). The mechanisms generating the cyclic phenomenon must therefore correspond to selection for subordinate types during density increases and selection for dominant types during declines (Moss et al., 1985). In contrast, displays of aggression are seen to increase in frequency as density rises. The cycling is initiated by events at, or just after, the peak density: an annual experimental removal of birds, which kept the density below the maximum value, was shown to stop the decline phase (Watson et al., 1988; Moss & Watson, 1989c; 1991).

6.2.7. Kin Selection.

Red grouse are observed to recognise their close relatives and hence are able to identify their family (Mountford et al., 1989). Males tend to recruit in family clusters of territories, with most young males dispersing a limited distance from their natal sites. A lower rate of boundary disputes is seen between close kin (by a factor of four) and fathers have been observed assisting their sons in establishing territories (Watson et al., 1994). Thus a father may accept a territory that is smaller than its personal optimum, to facilitate the establishment of territories by its sons. Thus groups of related individuals may allow recruitment to take place at a higher density. This behaviour may be described as *kin tolerance*.

Kin tolerance appears to have a dynamical nature, as the mean degree of family association varies with the phase of the population cycle. The level of aggregation of family groups falls during the decline phase, with sons dispersing further from their natal sites (Watson et al., 1994). Thus cycles either cause, or perhaps are caused by, the break up of the family territory structure. The cycles are therefore accompanied by switches between tolerant and intolerant social environments, which correspond to higher and lower equilibrium densities respectively. The decline sees increased aggression, with higher rates of territorial disputes relative to density, as well as selection for greater dominance. In contrast, the increase phase sees selection for

subordinate types, as kin tolerance allows less dominant individuals to gain territories with passive or active assistance of their families.

There are two slightly different mechanisms that can be proposed to explain the observed change in behaviour. Firstly, some event around the peak of the cycle may cause the grouse to become intolerant to their kin. This makes it more difficult for young chicks to recruit near their fathers, promoting dispersal and breaking up family structures, as well as increasing the mean territory size, which causes the population density to fall. Secondly, some event may trigger dispersal at or after the peak of the cycles, which breaks up the philopatric distribution. Each grouse is then adjacent to fewer or no kin, so that intolerance is prevalent in the population. This may reduce the tendency to accept smaller territories, so the population density falls. Under both scenarios, the population will continue to fall in size until the situation becomes favourable for kin tolerance and family clustering.

6.3 Modelling the Red Grouse.

6.3.1. Overview of Previous Models.

Several models have been developed to address the issue of the red grouse population cycles. One approach assumes that the key mechanism involves the parasite *T. tenuis* and constructs a system based on the standard host-parasite equations of Anderson & May (1992). Hudson & Dobson (1989) show that simple host-parasite interactions can lead to cycling of both host and parasite, especially given some conditions which the grouse-nematode system appear to satisfy. These are firstly that the parasite affects the host reproduction to a greater extent than its survival, secondly that the parasite displays a weakly-aggregated distribution within the host population and finally that the life cycle of *T. tenuis* involves developmental delay or *hypobiosis*. Density-dependence of the host population is needed to stabilise the resultant oscillations, which are roughly of the correct period. Workers on the East Scottish moors dispute the assertion that this model demonstrates that parasites are essential for cycling and claim that the parasite prevalence in Scotland is too low to support the assumptions of the model. It is, however, possible that the host-parasite explanation of the population cycles applies in the

English habitats and an alternative mechanism holds in Scotland, so that *T. tenuis* is sufficient but not necessary to cause cycling.

Empirical models with linear difference equations have been suggested which use a *chick production ratio* (ratio of young grouse in autumn to adults in spring) with a two year lag and winter survival rates with a one year lag to find adult population densities in the following spring (Rothery et al., 1984; Watson et al., 1984; Moss & Watson, 1989a; Watson & Moss, 1989). The model has been shown to have predictive value, producing damped oscillations which may be sustained by stochastic factors (Watson et al., 1984), but it yields little insight into the functioning of the system. The model has been extended to include details of resource levels and emigration, but the equations are hypothetical and based on intuitive reasoning.

The *Mountford model* uses the ratio of young to old grouse as the key variable, which represents the recruitment rate (Moss & Watson, 1991). This is taken to increase as family clustering rises and to decrease as density rises. High recruitment leads to a rise in density, which leads to small territories and a decline in the recruitment rate. This causes density to fall and the subsequent large territories allow recruitment to rise. This argument clearly predicts cycling, which is indeed shown by the model.

The above models operate in the mean field: no spatially explicit models of the red grouse ecosystem exist in the literature. One-dimensional models addressing kin selection are currently being developed (P.J. Bacon (personal communication); S. Palmer (personal communication)) which assign locations on a line segment to each individual grouse. Grouse interact with a given number of neighbours - which they can recognise if they are kin - and disperse along the line at the appropriate stage of the life cycle. These models do not yet, however, exhibit cyclic dynamics.

6.3.2. A Two-dimensional Spatial Model for Red Grouse.

A model is presented here which examines the dynamics of reproductive and territorial behaviour in two dimensions. The aim is to study the form of the population dynamics which

arise naturally from the assumptions of the model which, in turn, are based on a combination of qualitative and quantitative observations of grouse behaviour and demography. The main question that is to be asked is whether tolerance of kin can result in cyclic behaviour, so that the cycling is an intrinsic dynamic, or whether extrinsic factors are essential.

The grouse model is both individual-based and spatially explicit and has an essential difference from the plant models of chapters 3 to 5: grouse can move around. This requires an extension from a conventional lattice model to an *artificial ecology* (AE). In this case, the AE is more like a CA than a CML, as each cell will give information on the presence or absence of an individual grouse via a discrete variable on a finite set. The model follows the observation that population dynamics are usually driven by the male grouse and hence only records the males. As in previous chapters, boundaries are treated toroidally.

Each live grouse is allocated an index number $n \in \{1, \ldots, N\}$ and each grid cell i of the AE has two discrete variables associated with it, namely X_i and T_i, which both take values between 0 and N. $X_i = n$ gives the central point of the territory of grouse n, which will be assumed to be the natal site for any offspring of grouse n; all other cells will take value 0. $T_i = n$ represents all other cells which belong to the territory of grouse n. All values of T_i will be between 1 and N, except when a grouse has just died or emigrated, when $T_i = 0$ until the space is occupied by remaining birds.

At the beginning of each year, the birds are moved to the centres of their territories, using an algorithm which locates the centroid of a region of grid cells, with an adjustment if the centroid falls outside of the region, which may occur in the very rare case of a significantly concave territory. The grouse are assumed to be paired with a female, which then produces a clutch of offspring. Clutches are assumed to be normally distributed, with mean μ_{brood} and standard deviation σ_{brood}; an even sex ratio is assumed. In addition, there is a probability p_{fail} that an entire brood will fail, because of late snowfall, heavy rain or predation. These three parameters are taken from empirical observations and μ_{brood} and σ_{brood} are calculated to include summer mortality of chicks which successfully hatched but later died.

At this stage, the surviving chicks are noted as individuals in their own right and allocated an index number n, so that the total population size N increases. Details of lineage and phenotype are recorded by variables K_{mn}, F_n, Tol_n and FRS_n. K_{mn} takes the value 1 if birds m and n are related ($m < n$) and 0 otherwise. 'Related' in this situation refers to fathers, brothers (full- and half-), uncles and grandfathers. Chicks are assumed to recognise their more distant relatives by the behaviour of their fathers. $F_n \in \{1, \ldots, N\}$ records the index number of the birds' fathers, so certainly $K_{F_n n} = 1$. $Tol_n = 1$ if the grouse can display tolerant behaviour towards its kin and is 0 otherwise; this characteristic is assumed to be heritable.

Each bird is also allocated a *fighting rank strength* (FRS) (P.J. Bacon, personal communication) which determines its relative dominance status in the population. This is a suggested realistic mechanism which allows the outcome of pairwise contests to be determined non-randomly. The chicks disperse a small distance from their natal sites, which is determined by a uniform random variable based on the current mean territory size.

During the summer, the model simply records the survival or death of each adult, with each being killed by a predator or shot with probability p_{die}. The cells in the grid are then allocated to the nearest surviving grouse, using a searching algorithm based on a pre-determined matrix of search paths. This procedure sets up the initial configurations for the autumn territorial disputes, at which point young and old grouse fight on equal terms. It should also be noted that the life expectancy is similar for existing adults and the new generation of young males, so that age structure is not required in the model.

The algorithm for territory allocation is constructed around the concept of *pressure*. Each individual bird will effectively exert a force on the boundaries of its territory. If this force produces a pressure P_n greater than that exerted by an adjacent bird, then the former will expand its holding of territory; conversely it may lose ground to a neighbour. Since defending a larger territory will require a greater expenditure of energy, the pressure exerted is assumed to be inversely proportional to the current territory area (TS_n). Likewise, the fighting ability will depend on dominance status, represented by the FRS. The pressure can therefore be given

as follows:

$$P_n = \frac{FRS_n}{TS_n}.$$

The algorithm proceeds by considering each grid cell that has a neighbouring cell in the eight cell Moore neighbourhood which belongs to a different grouse. This cell is then reallocated to whichever grouse has a territorial cell in that neighbourhood and has the highest pressure value. The algorithm requires various refinements to ensure that it is robust and produces realistic distributions. For example, all the territory cells of each bird must be connected; this can be ensured by restricting the changes that are made to the distribution at each iteration. After a fixed maximum number of iterations, or when the distribution has converged to equilibrium, the procedure stops, and the territories are fixed for the new breeding season in the following spring, subject to the minimum critical territory size criterion discussed below.

One problem that arises is fluctuation of territory boundaries. When the pressures of adjacent territories are very similar, it is common for the boundary to fluctuate backwards and forwards by a single grid cell, which will prevent convergence of the algorithm. This is overcome by defining a minimum pressure difference, ΔP. If the difference between the pressures of two competing birds is below this value, that is: $P_n - P_m < \Delta P$, then the boundary will not move. The value of ΔP is set by experiment to avoid the majority of trivial binary oscillations.

It is observed that grouse will not attract a mate if their territory is below some *critical minimum territory size*, CTS_n. This cut-off is implemented by the model, which removes all birds with $TS_n < CTS_n$, where $CTS_n = \overline{CTS}$ is a fixed parameter. The territory map is then re-adjusted for the remaining birds until convergence is obtained. Removal of all subordinate individuals below CTS_n is not carried out instantaneously, as this would be too much of a shock in the system, but rather a few birds are removed at a time, starting with the smallest territories. This does allow some birds which are marginally below the critical size to gain a little extra space and thus survive.

Failed recruiters go into a surplus pool, which may be used for a *dispersal phase*, which is optional within the model. A proportion of the birds in the pool are assumed to die, then the survivors disperse over distances significantly greater than the dispersal at the start of the autumn. The dispersing birds then attempt to recruit at the new location, which is taken to be on an existing territory boundary, where the chances of success are greatest. Several (N_{disp}) dispersal attempts may be made, each of which sees iteration until equilibrium is reached, removal of birds with territories that are too small and subsequent iteration to equilibrium. At the end of the year, after the dispersal phase if one is implemented, all non-territorial birds are removed from the area, corresponding either to death or emigration.

The phenomenon of kin tolerance is included by three separate mechanisms. Firstly, a grouse is assumed to exert less pressure on its neighbours if it is surrounded by kin. The pressure function is therefore amended to:

$$P_n \quad = \quad \frac{FRS_n}{TS_n(1+NN_n)},$$

where NN_n is the number of kin neighbours of the kin tolerant individual n. If there are no kin adjacent to a bird it is effectively intolerant and a breakdown of family structure generates a socially intolerant regime. Tolerant birds are also assumed to put up with more pressure from kin before they respond and move territory boundaries, so that the minimum pressure difference ΔP is increased. Finally, it has been observed that grouse will tolerate a smaller territory so that a family member can be recruited nearby. Therefore the critical minimum territory size expression is modified to:

$$CTS_n \quad = \quad \max\left(0, \overline{CTS}\left(1-\Delta Tol\ NN_n\right)\right),$$

where ΔTol is a parameter representing the benefit of having a kin neighbour. It is thus possible to have a smaller mean territory size in a socially tolerant environment than in an intolerant situation. The parameter ΔTol provides the required mechanism for differentiating between kin

tolerant and kin intolerant behaviour and effectively sets the upper bound on the amplitude of any cycles that may arise. The one-dimensional models referred to in section 6.3.1 incorporate the same assumption via different parameters.

There has been a recent breakthrough in the genetic identification of individual grouse, so that it is now possible to determine the relatedness of any two grouse on a study site (P.J. Bacon, personal communication). Thus both the assumptions and results of models such as the one presented here are, in principle, testable, although the significance of any results will be harder to assess.

The structure of the program is detailed in the flow chart given in Appendix B; examples of the parameter values taken and variables used are also tabled in Appendix B. The following section describes the development of the model and discusses the results obtained for variants of the basic algorithm.

6.4. Details and Results of the Grouse Model.

6.4.1. Model 0.

(a) Introduction.

The basic two-dimensional grouse model as described above was investigated in a range of situations. Model 0 covers the development phase of the model, where the behaviour of the core algorithm was checked to see that it is robust and intuitively reasonable. An immediate conclusion drawn from the development concerned computing constraints. The algorithm is sufficiently complex to require considerable computational effort, in particular where repeated dispersal phases are incorporated in the system. There is thus an unfortunate but inevitable restriction on the length of simulations and the feasible number of replicates. Future access to supercomputing facilities is therefore very desirable and would open up the opportunity to carry out more rigorous sensitivity analyses as well as investigations of different modelling assumptions and techniques.

The cell size is defined by the maximum and minimum territory sizes held, or equivalently the population densities. On the assumption that a typical intermediate territory size is 2 hectares, then each lattice cell is taken to represent around 0.1 hectares of moorland. Thus the lattice corresponds to an area of around $10km^2$, which is much larger than any of the intensive study sites used.

Two types of grouse are potentially able to exist within these populations: *kin tolerants* and *kin intolerants*. The former display tolerant behaviour towards any neighbours that are kin, as described in the algorithm of section 6.3.2, whereas the latter are consistently intolerant to all other individuals.

(b) Spatial Pattern.

Figure 47 shows typical territorial configurations generated by the models at an intermediate population density. Territory boundaries are shown in black and family groups are indicated by territories of the same shade, clearly indicating natal philopatry. It was noted that the distribution of territory sizes (mean and variance) is reasonable. The same observations apply to the models that follow (I - II).

(c) Numerical Results.

Figure 48 displays typical dynamics generated by Model 0. In a purely intolerant population a relatively low and noise-free equilibrium results (figure 48a). In contrast, a population of non-dispersing tolerant grouse allows a higher density to be attained, but the dynamics are much more erratic. Including a dispersal phase causes the density to perform a two point oscillation, with the intolerant population and non-dispersing tolerant population densities respectively forming approximate lower and upper bounds to the oscillations. The dynamics are illustrated for $N_{disp} = 4$ dispersal attempts; for lower N_{disp} the amplitude of oscillations tends to be less, whereas higher N_{disp} still exhibits oscillations between the two bounds described above, but with increased stochastic noise. However, the dynamics are still 2-cycles for any N_{disp} between 1 and 8.

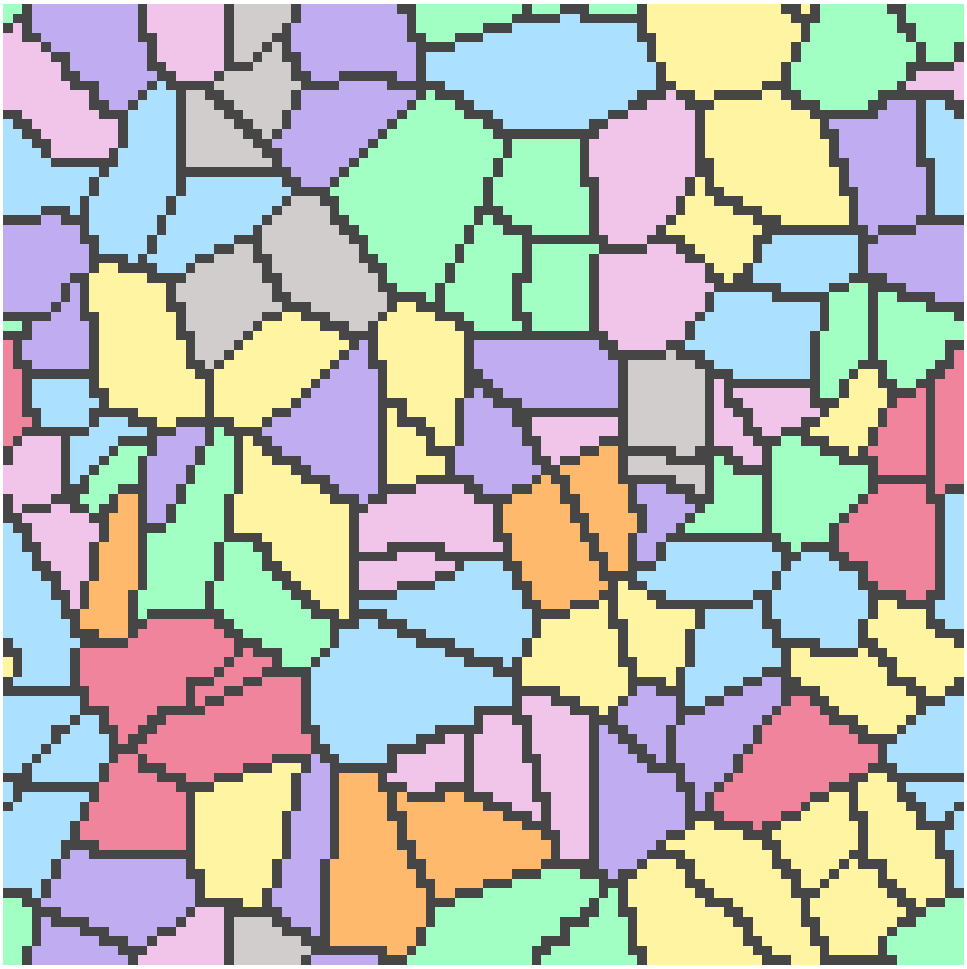

Figure 47: Typical territory distribution from the grouse AE.

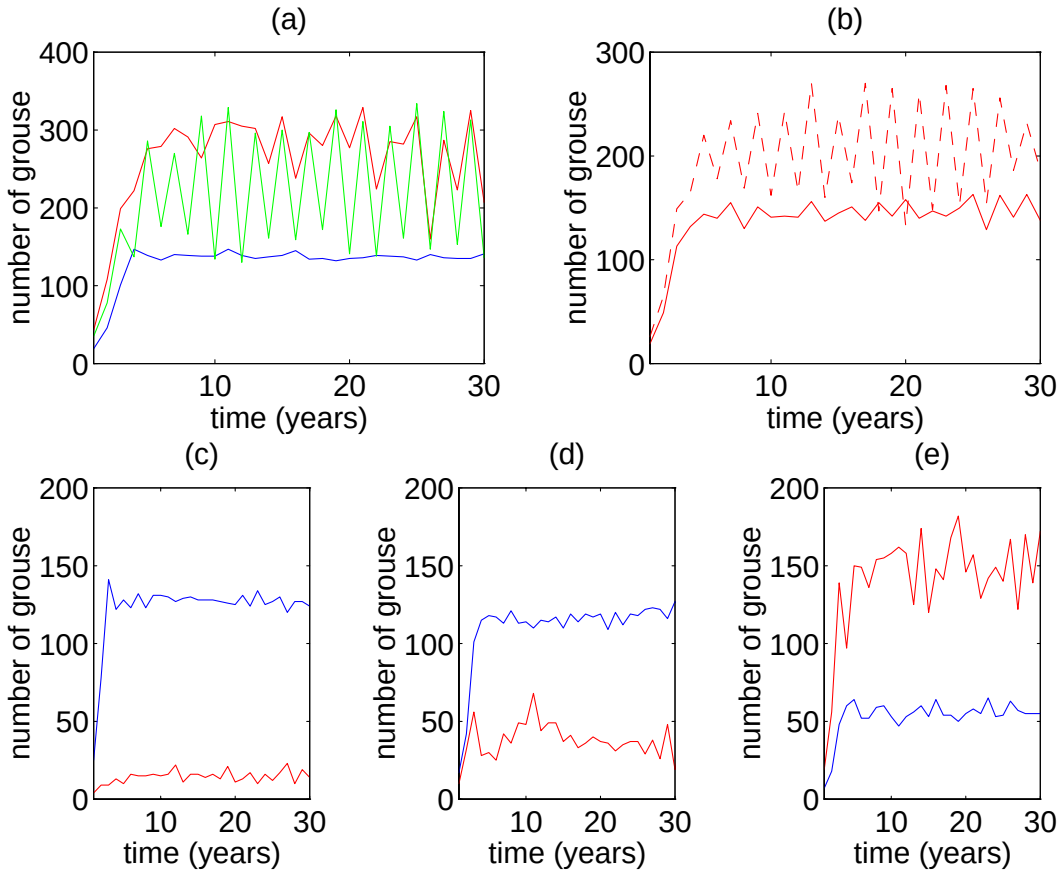

Figure 48: Population dynamics from red grouse Model 0. (a) Numbers of grouse in a 100×100 AE grid over a thirty year period for kin intolerant (blue), kin tolerant non-dispersing (red) and kin tolerant dispersing (four dispersal attempts) (green) types. (b) Numbers of kin tolerant grouse for parameters $\Delta Tol = 0.1$ (—) and $\Delta Tol = 0.2$ (- - -). (c) - (e) Numbers of grouse in competing populations of kin tolerant (red) and intolerant (blue) types. The initial proportion of tolerants is (c) 0.2, (d) 0.4 and (e) 0.6.

Various parameters in the model were tested for their effects on the model output. The brood size was seen to have no effect on the dynamics of an intolerant population, but larger broods induced greater stochasticity in the tolerant case. The population size was unaffected in all cases, but the dynamics oscillated with greater amplitude, predominantly with period 2, in a tolerant population with large broods; similarly smaller broods decreased the noise level. The parameter ΔTol was varied in the kin tolerant scenario and, as expected from its definition as the controlling parameter of the kin tolerant response to territory size, higher population densities resulted from larger values of ΔTol. Greater stochasticity was also noted as ΔTol increased (figure 48b), but the dynamics essentially remained in the form of a smooth increase towards a noisy equilibrium population density.

The simulation of mixed tolerant/intolerant populations is illustrated in figures 48c - e. There does not appear to be significant selection for or against kin tolerance, as the results are largely dependent on the initial conditions. If the initial proportion of kin tolerants in the population is below 0.2 or above 0.8, then they are respectively eliminated from or fixed in the population, but in intermediate cases the types coexist, as shown in figures 48c - e. This suggests that a stronger mechanism will be required to produce the desired oscillatory dynamics and relying on automatic selection between the two types is not sufficient.

It thus appears that introduction of the concept of kin tolerance to the grouse model is a destabilising factor. The non-dispersing populations have much noisier dynamics, when tolerance is present, with a considerable degree of fluctuation. The introduction of dispersal further destabilises the dynamics and generates two year oscillations. Although these are definitely not the extended four to ten year cycles observed in real populations of red grouse, Model 0 clearly provides a good basis for extension, since it possesses the capacity for the equilibrium to bifurcate to a cycle. It is now of interest to see whether a reasonable set of additional assumptions may lead to a model that cycles in a realistic manner. Variations on Model 0 are presented below which suggest some different mechanisms that may potentially lead to cycling.

6.4.2. Model I.

(a) Introduction.

In Model I - following the first hypothesis of section 6.2.7 - a decline is assumed to trigger a change in behaviour. As in Model 0, there are assumed to be two types of grouse: kin tolerants and kin intolerants. It is this tolerance or intolerance that provides the basis of the behavioural change. Since a total instantaneous change is unlikely, a proportion δ_{Tol} of the kin tolerant type change to intolerant for each year of decline and an increase in density is accompanied by the reverse change. It is a reasonable assumption that grouse can alter their behaviour according to their numbers, as it is believed that old grouse could perceive a change in local density from the previous year, while young grouse respond to their fathers' behaviours.

This process is predisposed to cycling, as the kin tolerant and intolerant types correspond independently to different equilibrium population densities, as shown in 6.4.1. It is not, however, immediately obvious what form of fluctuations will arise - two point oscillations, as seen in Model 0, may occur, which are not the required type of cycles. An investigation of the $(\Delta Tol, \delta_{Tol})$ parameter space is needed to assess the possibility of this type of behavioural adaptation underlying the red grouse population cycles.

(b) Numerical Results.

As shown in figure 49, cycles of length greater than two occur in Model I for a wide range of values of ΔTol and δ_{Tol}. As ΔTol increases, the pure tolerant and intolerant equilibria move apart, so the amplitudes of cycles increase. The system is far less sensitive to the parameter δ_{Tol}, with less noise arising from more sudden changes in social environment. Cycles of period between 6 and 7 years arise naturally for moderate values of ΔTol (around $\Delta Tol \sim 0.2$), with cycles nearer 9 or 10 years for larger ΔTol ($\Delta Tol \sim 0.3$). This mechanism of tolerance/intolerance adaptation thus naturally generates cycles of appropriate length.

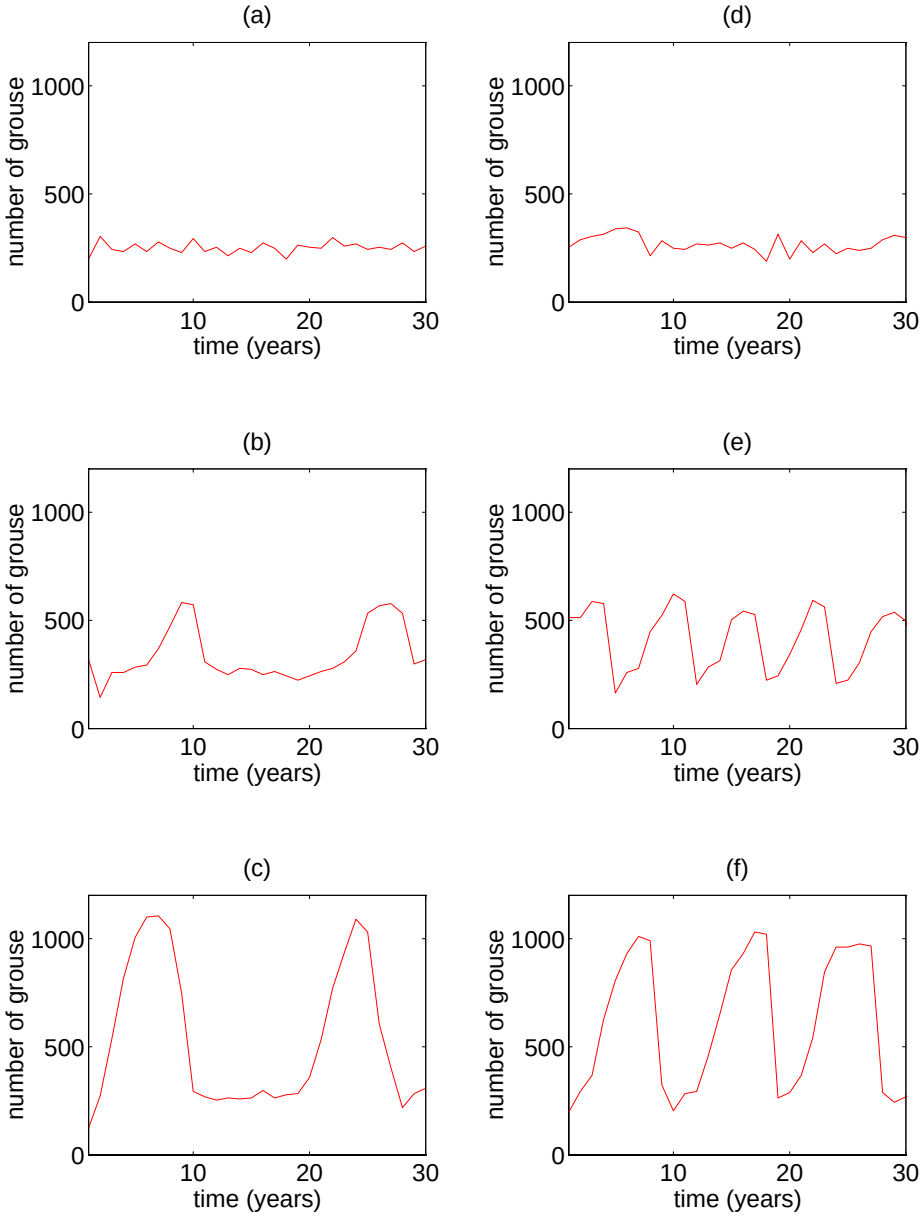

Figure 49: Population dynamics from red grouse Model I. Numbers of grouse in a 100×100 AE grid over a thirty year period as the benefit of having a kin neighbour (ΔTol) and the rate of change of tolerance level (δ_{Tol}) vary. (a) - (c) $\delta_{Tol} = 0.2$; (d) - (f) $\delta_{Tol} = 0.6$. (a), (d) $\Delta Tol = 0.1$; (b), (e) $\Delta Tol = 0.2$; (c), (f) $\Delta Tol = 0.3$.

6.4.3. Model II.

(a) Introduction.

The second mechanism suggested in section 6.2.7 does not assume an explicit change in tolerance of individual grouse towards their kin, but rather suggests that changes in movements of individuals may alter the social environment to more or less tolerant. In Model II, a decline in density triggers an increase (by δ_{Disp}) in the number of attempts to disperse (N_{disp}) that are made by birds that initially fail to be recruited to the territorial population. If the decline persists, then the number of dispersal attempts continues to rise. Likewise, any population rise is accompanied by a decrease in dispersal attempts, down to a minimum of zero.

As in Model I, there is an intrinsic tendency of the model to cycle, but it is not clear whether the dynamics will be limited to 2-cycles. It is possible that the first dispersal from a tolerant philopatric community will break up the family structure to such an extent that the grouse are all effectively intolerant, having no kin neighbours. This would cause the density to plummet immediately to a minimum, at which point numbers could only rise again, stopping dispersal leading to a large amplitude 2-cycle. Alternatively, the first dispersal may have a very minor effect, just allowing the population to recover at the next time step, leading to a small amplitude 2-cycle. However, a gradual break down of the philopatric social structure may allow extended decline and increase phases, leading to cycles of longer periods.

(b) Numerical Results.

Figure 50 gives the population dynamics for $\delta_{Disp} = 2$ and shows clear cycling with periods of nine to fifteen years. Although the cycles produced here are longer (15 years) than those typically quoted in the literature, long cycles such as these are observed: for example the ten year cycle at Rickarton (figure 46b) and cycles of up to sixteen years in Ireland.

6.4.4. Conclusions.

It has been shown that simple selection between kin tolerant and kin intolerant types of red

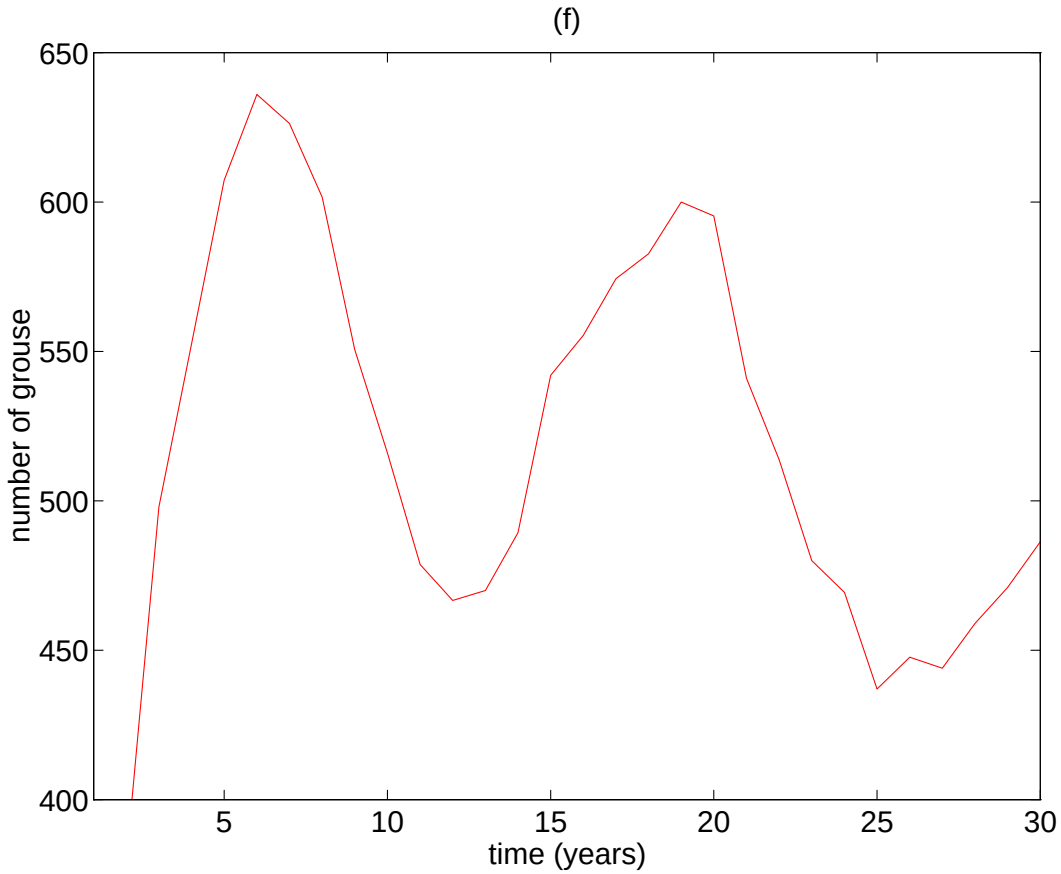

Figure 50: Population dynamics from red grouse Model II. Numbers of kin tolerant grouse in a 100×100 AE grid over a thirty year period, assuming dispersal attempts increase and decrease in steps of two in response to density.

grouse (Model 0) is insufficient to generate the observed long term cyclic behaviour of the population dynamics. However, further reasonable assumptions of density-related changes in behaviour, within this kin tolerance framework, can robustly produce model cycles of appropriate lengths to those observed. Two alternative behavioural patterns have been suggested and shown to be possible. These are, respectively, a change in individual tolerance and a change in social tolerance environment by a modification of dispersal behaviour.

It should now be possible to extend this modelling work, in association with appropriate field work (particularly incorporating the latest genetic techniques) to further probe the underlying processes operating within the red grouse ecosystem.

7. Memory in Ecological Systems.

Chapter Summary

A brief overview of the theory of mosaic cycles is presented and a non-individual-based cellular automaton model by Wissel is reconstructed to simulate a mid-European beech forest cycle.

The concept of 'memory' in an ecological system is introduced, which incorporates ideas of age, size and susceptibility to disease and mortality. Visual inspection and the clumping index demonstrate the evolution of a patchy structure in the presence of memory, independent of the presence of the mechanism of radiation death, showing that memory is fundamental to the system. A mean field analysis supports this result. Chaos is promoted by memory and the dimension of the system, analysed by an embedding technique, is lower in the presence of memory.

The memory concept is extended to a Susceptible - Infected - Recovered epidemic model, where memory is shown to be essential to the formation of a patchy spatial structure. A Markov approximation is again presented in support of this assertion.

'πάντα χωρεῖ ὁδὲν μὲνει. (Everything flows and nothing stays.)' - Plato after Heraclitus

7.1. Introduction.

The spatial structure and species composition of multispecies systems promote questions concerning mechanistic processes leading to the construction and maintenance of complex communities. Such systems involve large scales in time and space and hence demand an alternative modelling approach to the CML used in chapters 3 to 5 (figure 1). The processes underlying the coarse scale patchy structures observed over many centuries in large forest ecosystems are investigated using a discrete state CA model.

7.2. Mosaic Cycles.

7.2.1. Overview of Mosaic Cycles.

The theory of *mosaic cycles* arose in the 1930s. In contrast to classical ecology, which sought to describe a constant climax state for any given ecosystem (Clements, 1936), advocates of mosaic cycle theory asserted that an ecological system would never reach a fixed equilibrium, but rather would remain in constant flux (Watt, 1947). A mosaic landscape consisted of patches or *mosaic stones*, which cycled continually through a set of states, with adjacent patches cycling asynchronously. Over a large region, statistically stationary averages were attained, but local cycles persisted. The concept was largely abandoned, with the exception of Whittaker & Levin (1977), until its revival by Remmert in 1985 for temperate forests (Remmert, 1985). Mosaic cycles were subsequently suggested for temperate, tropical and subalpine forests (Müller-Dombois, 1991; Wissel, 1991; 1992a; Thiéry et al., 1995) and marine systems (Reise, 1991).

A model of a temperate forest mosaic cycle, originally developed by Wissel (1991; 1992a) is presented and re-examined here. This study focuses on the fundamental mechanisms in the mosaic cycle, in particular the concept of *memory* and its role in the evolution of local and global patterns. Techniques are introduced to characterise more fully the patterns and dynamics generated by the model. The mosaic cycle is modelled by a CA (section 2); dynamics are studied here in depth and the model is used to provide deeper mechanistic understanding of the mosaic system.

7.2.2. The Mid-European Beech Forest Mosaic Cycle.

(a) Description of the Forest Cycle.

The model is based on a cycle seen in a mid-European forest (Wissel, 1991; 1992a) where the dominant long-lived species is *beech*. *Gaps* caused by fallen beech are invaded by two early-successional communities. The first pioneers are *birch*, which survive for about 50 years. This monoculture is followed by a *mixed forest*, with species such as oak, cherry, ash and maple, which live for up to 150 years. This intermediate community is eventually succeeded by beech,

initially as a young thicket, followed by thinning and growth of survivors into mature trees over three centuries or longer. This cycle is represented in figure 51. It is generally accepted that life history traits play an important part in the successional patterning of forests. Those traits favoured early in succession, such as tolerance to full sunlight, rapid growth and efficient seed dispersal are often the opposite of the traits favoured later on: tolerance to shade and production of few seeds with large energy reserves.

The cycle can be interrupted at times through local interactions. One simple effect is early colonisation: if a gap has mixed forest nearby, rather than birch, then the birch phase is skipped and the mixed community invades the gap. A beech tree is not immediately succeeded by a beech sapling *(autosuccession)*, as the soil needs to recover an adequate supply of nutrients specific to beech.

A second process, *radiation death*, acts to induce premature death in the beech stand. A beech tree has smooth bark, which splits under exposure to solar radiation, often leading eventually to death. The nature of the physiological and biochemical effects of shock are not directly known, but are thought to involve photo-inhibition and the failure of stress proteins to repair heat-damaged molecules (Nagao et al., 1986; Welch, 1993). Thus, in the Northern Hemisphere, a gap to the south of a beech tree may lead to its death. The other species are not affected in this way: birch have paler bark and the mixed community species have rougher bark which is not particularly susceptible to splitting (Remmert, 1991). It will be shown that this is an important mechanism in the dynamics of the forest cycle, although not the dominant mechanism.

Although this mechanism is restricted to this particular system, similar dynamical effects are seen in other ecological situations, for example, Iwasa et al. (1991) have studied formation of intricate spatiotemporal patterns in models of fir forests, where a dominant mechanism is death by exposure to wind. As with the radiation death, this is a directional process, where the trees are only susceptible to damage in the direction of the wind and where they are not sheltered by other trees.

(b) A Model for the Mosaic Cycle.

The CA is based on Wissel's papers and consists of 55 states, each of which corresponds to a ten year period. The first two states are *gap*, the next five states are *birch*, the next fifteen are *mixed* and the final thirty three states are *beech*; each set of states represents communities of increasing age (table 10). In general, at each iteration, the states progress by 1, except state 55 (the oldest beech) which moves to state 1 as it dies. Early colonisation is modelled by either of the gap states (1 and 2) moving immediately to young birch (state 3) if any neighbouring states are birch (states 3 to 8). If no neighbours are birch but at least one neighbour is mixed (states 9 to 22), then the gap moves immediately to young mixed forest (state 9). The neighbourhood used here is the nine cell Moore neighbourhood (figure 52). Increased likelihood of death in old beech *(die-back)* is incorporated, by allowing states 51 to 54 to die with probability $P_0 < 1$.

Radiation death is modelled by considering separately the cells to the southwest, south and southeast of a beech cell (states 23 to 54). This requires the imposition of a direction on the CA. If a beech has a gap (state 1 or 2) in the southwest, south and southeast cell (marked SW, S and SE in figure 52), then it dies at the next iteration with probabilities p_W, p_S and p_E respectively.

(c) Summary of the Results of Wissel.

Wissel showed that the model produces a pattern of patches, demonstrating that the cyclic nature of the CA rules, combined with the local neighbourhood effects, are sufficient to produce a mosaic. The pattern was shown to be insensitive to the parameter values used, provided they are in the open set $(0, 1)$. Wissel also claimed that no patches are produced if there are no local radiation effects; this claim is reassessed here. Consideration of the rate of radiation death from empirical data allowed Wissel to define the cell size as approximately 30 metres by 30 metres. The patch sizes in the model were shown to be compatible with data from forests in the former Yugoslavia.

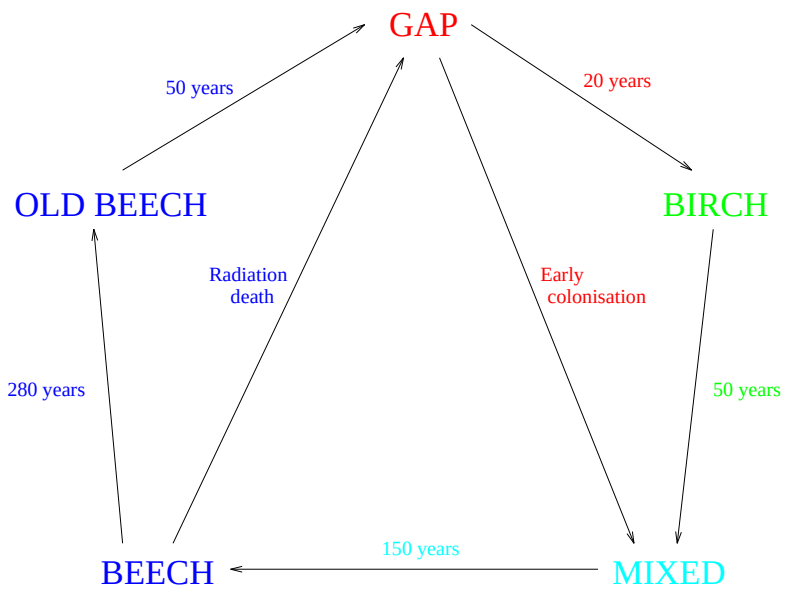

Figure 51: Representation of the mid-European beech forest mosaic cycle.

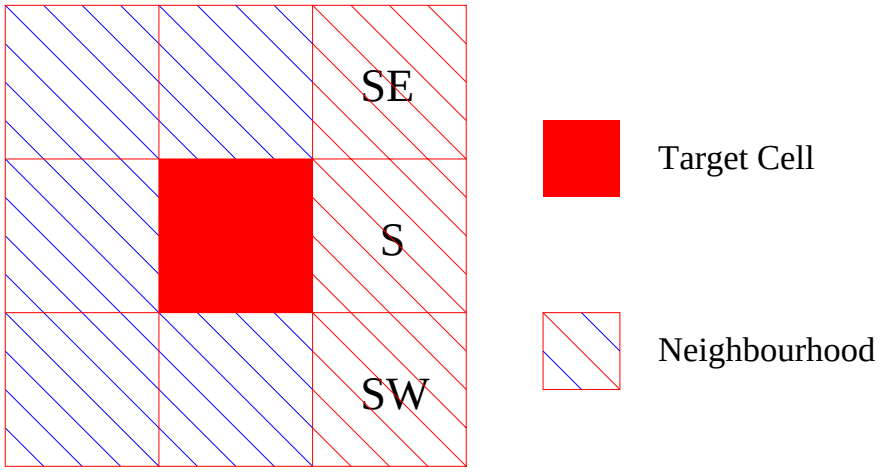

Figure 52: Representation of the nine cell Moore neighbourhood.

7.3. Memory in the Mosaic Cycle.

7.3.1. Introduction.

Wissel stated that the local neighbourhood effect, radiation death, is the critical mechanism in the cycle. Here a second mechanism - *memory* - is shown to be vital.

Memory in this context refers to the way the past history of a system affects its current structure and behaviour. History is a relatively simple concept in sessile organisms, where it is sufficient to consider fixed spatial locations. At the simplest level, the history of an individual tree is largely contained in its present age, which is equivalent to the time for which the tree has occupied that position in space.

In modular organisms, age is significant in several ways: susceptibility to physiological shock, native diseases and native parasites generally rises with age. Size usually increases with age (although a counter example is given by Thomas & Weiner (1989b)) and biomass allocation changes. When communities are examined on the level of individuals, size is strongly related to effects on neighbours (chapter 3). On a population or community level, growth may be considered to be controlled, to a first approximation, by density. This model is constructed on the level of spatially-defined communities, as the lattice cells correspond to subsections of the forest ecosystem. The use of an IBM is not feasible at these large scales of time and space, as seen on the diagram of scales in figure 1. Therefore the size of individuals is not recorded explicitly, but represented as an average stand age. The tendency to die in response to biotic or abiotic pressures is modelled by the probability of accelerated death, P_0, in the elderly beech stands.

The history of each spatial position goes back further than the lifetime of the plant currently sited there. The state of the soil, in terms of the previous depletion or addition of essential nutrients, has an important effect on the growth of current organisms. Similarly, the level of the water table has an effect on the forest growth: after a dominant species has been in a region of the forest for a few centuries, the water table is substantially lowered and essential nutrients

may be completely absent. Such factors are not explicit in this model, but exhaustion of the soil following long-lived beech stands is implied by the enforced absence of autosuccession.

It is asserted in Remmert (1991) that the driving force in any mosaic cycle is the *longevity* of the species involved. In this model, longevity is equivalent to the age of the individuals in the beech stands and hence, in basic terms, is equivalent to *memory*. This is represented in the CA in the form of the 33 different states of cells containing beech; these states represent beech of ages 10, 20, ..., 320, 330 years. Hence longevity or memory is explicit in this model and it is of interest to consider the impact of this mechanism on the behaviour of the model and the structure of the emergent mosaic patterns.

7.3.2. Removal of Memory from the Model.

The absence of memory from the cycle essentially means that the trees do not 'know' how old they are. This means that death and succession must be entirely independent of age. The range of states for each species is removed (the multispecies mixed forest is included as a 'species') and the whole cycle is represented by four amalgamated states: gap, birch, mixed and beech. The probabilities of transition between these four states are set so that the expectation of the duration of each successional stage is the same in both the *memory* and the *no memory* cases.

Wissel claimed that the production of clumped areas of beech forest depends critically on the local synchronising effect of the radiation death. The radiation effect is independent of age, so it is not necessarily expected that the removal of the age structure will affect the formation of patches. The *memory* and *no memory* models are compared here to see if the presence of memory in the system affects the formation and character of the mosaic patches. This involves characterising the spatial patterning and the dynamics of the system.

The *no memory* model is constructed as follows. The gap, birch and mixed states are simply transferred into single states, with transition probabilities equal to the reciprocal of the expected lifetimes. *Gap* is originally represented by two states, so that the expected lifetime, E_{gap}, is 2. Thus the transition probability in the new model, p_{gap}, is equal to $\frac{1}{2}$. This also gives an

expected lifetime of 2. Similarly the new *birch* and *mixed* states have transition probabilities $p_{birch} = \frac{1}{5}$ and $p_{mixed} = \frac{1}{15}$, respectively.

The transition probability for the *beech* state is more complicated, as the early death probabilities (P_0) for states 51 to 54 must be considered. The expected lifetime of beech trees, E_{beech}, is given by equation 42. Thus the transition probability for beech in the *no memory* model is given by the reciprocal of E_{beech}. The transitions are summarised in table 11. The early colonisation and radiation death mechanisms are implemented in the new model as before. It is therefore possible to consider four combinations of mechanisms: memory/radiation, memory/no radiation, no memory/radiation and no memory/no radiation. *No radiation* is simply implemented by setting $p_W = p_S = p_E = 0$.

$$\begin{aligned} E_{beech} &= 28 + P_0 + 2(1-P_0)P_0 + 3(1-P_0)^2P_0 + 4(1-P_0)^3P_0 \\ &\quad +5\left(1 - P_0 - (1-P_0)P_0 - (1-P_0)^2P_0 - (1-P_0)^3P_0\right) \\ &= 33 - 10P_0 + 10P_0^2 - 5P_0^3 + P_0^4 \end{aligned} \tag{42}$$

7.3.3. Preliminary Results.

Figure 53 shows typical CA configurations for the four combinations of mechanisms. These patterns are shown at iteration 1000, which has allowed transients to pass. It is clear that the memory mechanism plays a fundamental role: the top two patterns (memory/radiation and memory/no radiation) show patches, while the lower two patterns (no memory/radiation and no memory/no radiation) appear to be randomly distributed. This directly contradicts Wissel's claim that removal of radiation death prevents patches forming. In the following two sections firstly a basic analytical investigation of memory is presented and secondly various numerical techniques for analysing the structure of the spatial pattern are given for considering scale and for characterising the dynamics.

CA states	Description	Duration
1 - 2	forest gap	20 years
3 - 7	birch stand (monospecific)	50 years
8 - 22	mixed forest communities	150 years
23 - 50	beech stand (monospecific)	280 years
51 - 55	elderly beech stand (monospecific)	50 years
	TOTAL	550 years

Table 10: Description of the states of the mosaic cycle CA model

State	Transition probability
Gap	$\frac{1}{2}$
Birch	$\frac{1}{3}$
Mixed	$\frac{1}{15}$
Beech	$\frac{1}{33-10P_0+10P_0^2-5P_0^3+P_0^4}$

Table 11: Transition probabilities for the mosaic cycle CA model in the *no memory* case.

Mechanisms	**Mean field frequency** $(\pi_{gap}, \pi_{birch}, \pi_{mixed}, \pi_{beech})$	**Spatial frequencies** $(\pi_{gap}, \pi_{birch}, \pi_{mixed}, \pi_{beech})$	**Error**
memory/ radiation	(0.059, 0.147, 0.442, 0.352)	(0.075, 0.175, 0.55, 0.225)	0.1551
no memory/ radiation	(0.066, 0.164, 0.491, 0.230)	(0.065, 0.150, 0.465, 0.320)	0.0498
no memory/ no radiation	(0.038, 0.094, 0.281, 0.588)	(0.035, 0.095, 0.280, 0.590)	0.0038

Table 12: Comparison of the mean field Markovian model and the spatial CA model.

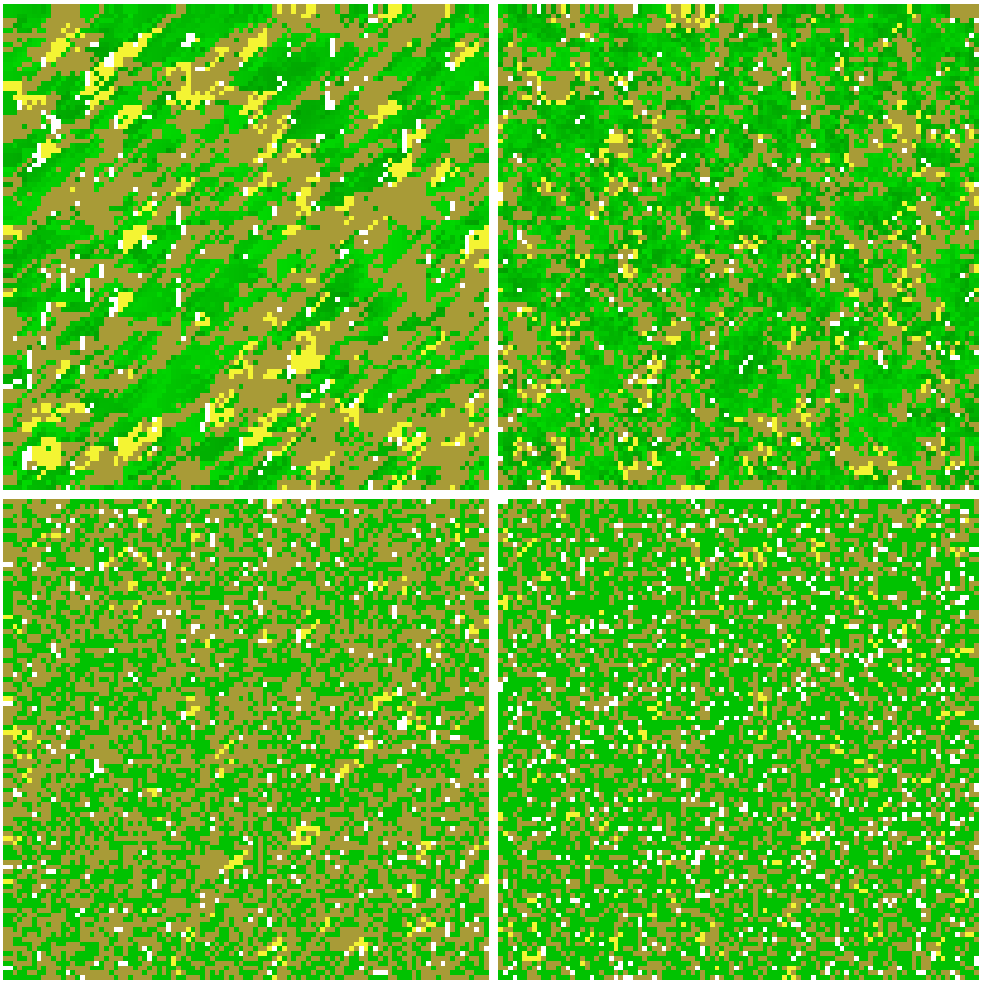

Figure 53: Spatial pattern in the mosaic cycle CA model at iteration 1000. Top left: memory/radiation; top right: memory/no radiation; bottom left: no memory/radiation; bottom right: no memory/no radiation. White - gap; yellow - birch; brown - mixed forest; darkening shades of green - beech of increasing age.

7.4. Analytical Investigation of the Memory Mechanism.

7.4.1. Introduction.

A mean field approximation to the mosaic cycle model is presented here as a *Markov process* (Rosanov, 1977). Analytical solutions are presented for three combinations of mechanisms and compared to numerical results of the spatial model. The local colonisation feature, whereby birch and mixed forest near to a gap may invade it, is omitted here as it causes the mean field model to be analytically intractable. This means that the radiation death is now the only local coupling mechanism, so the no memory/no radiation and memory/no radiation systems are identical.

7.4.2. Mean Field Models.

(a) No memory/no radiation.

In this simplest case there are the four basic states: gap, birch, mixed and beech. The transition matrix for the Markov chain, $\mathbf{P}$, is given by equation (43). The expected lifetime of beech (equation (42)) is denoted by $\mathcal{E}$.

$$\boldsymbol{P} = \begin{pmatrix} \frac{1}{2} & \frac{1}{2} & 0 & 0 \\ 0 & \frac{4}{5} & \frac{1}{5} & 0 \\ 0 & 0 & \frac{14}{15} & \frac{1}{15} \\ \frac{1}{\mathcal{E}} & 0 & 0 & 1-\frac{1}{\mathcal{E}} \end{pmatrix} \tag{43}$$

Using basic Markovian analysis, the mean occupancy rate of state i is given by π_i, where $\boldsymbol{\pi}$ is the solution to the equation $\boldsymbol{\pi P} = \boldsymbol{\pi}$. Thus, for this model, the relative frequencies of the four states are given (in the order gap, birch, mixed, beech) by:

$$\boldsymbol{\pi} = \left(\frac{2}{22+\mathcal{E}}, \frac{5}{22+\mathcal{E}}, \frac{15}{22+\mathcal{E}}, \frac{\mathcal{E}}{22+\mathcal{E}} \right).$$

(b) No memory/radiation.

The first step in developing the full model is to add the effect of radiation death to the fourth state in the Markov chain. Since the elements of $\boldsymbol{\pi}$ necessarily sum to unity, $\boldsymbol{\pi}$ may be denoted by $(\gamma, \beta, \mu, 1-\gamma-\beta-\mu)$ so that γ = frequency of gaps, β = frequency of beech cells and μ = frequency of mixed forest cells. The probability of radiation death depends on the frequency of gaps, γ, and the average probability of death, $p_R = p_W + p_S + p_E$:

$$\boldsymbol{P} = \begin{pmatrix} \frac{1}{2} & \frac{1}{2} & 0 & 0 \\ 0 & \frac{4}{5} & \frac{1}{5} & 0 \\ 0 & 0 & \frac{14}{15} & \frac{14}{15} \\ \frac{1}{\mathcal{E}} + \gamma p_R & 0 & 0 & 1 - \frac{1}{\mathcal{E}} - \gamma p_R \end{pmatrix}.$$

The solution of $\boldsymbol{\pi P} = \boldsymbol{\pi}$ may be found by solving simultaneous equations to obtain:

$$\gamma = \frac{2\beta}{5},$$

$$\mu = 3\beta$$

and

$$\beta = \frac{\frac{2}{5}p_R - \frac{1}{5} - \frac{22}{5\mathcal{E}} \pm \sqrt{\left(\frac{1}{5} + \frac{22}{5\mathcal{E}} - \frac{2}{5}p_R\right)^2 + \frac{176}{\mathcal{E}}p_R}}{\frac{88}{25}p_R}$$

where the positive square root ensures that $0 \leq \beta \leq 1$.

(c) Memory/radiation.

Memory is added to the basic Markov process by increasing the number of states from 4 to 55. The form of the matrix is given by equation (44). The solution (equation 45) is obtained, in

terms of a normalisation constant, $\bar{\pi}$. This constant can be found numerically to any required precision by solving:

$$\|\boldsymbol{\pi}\| \quad = \quad \sum_{i=1}^{55} \pi_i = 1.$$

$$\boldsymbol{P} \quad = \quad \begin{pmatrix}
0 & 1 & 0 & \cdots & 0 & 0 & 0 & \cdots & 0 & 0 & 0 & 0 & 0 \\
0 & 0 & 1 & \cdots & 0 & 0 & 0 & \cdots & 0 & 0 & 0 & 0 & 0 \\
\vdots & \vdots & \vdots & \ddots & \vdots & \vdots & \vdots & \ddots & \vdots & \vdots & \vdots & \vdots & \vdots \\
0 & 0 & 0 & \cdots & 1 & 0 & 0 & \cdots & 0 & 0 & 0 & 0 & 0 \\
R_1 & 0 & 0 & \cdots & 0 & 1-R_1 & 0 & \cdots & 0 & 0 & 0 & 0 & 0 \\
R_1 & 0 & 0 & \cdots & 0 & 0 & 1-R_1 & \cdots & 0 & 0 & 0 & 0 & 0 \\
\vdots & \vdots & \vdots & \ddots & \vdots & \vdots & \vdots & \ddots & \vdots & \vdots & \vdots & \vdots & \vdots \\
R_1 & 0 & 0 & \cdots & 0 & 0 & 0 & \cdots & 1-R_1 & 0 & 0 & 0 & 0 \\
R_2 & 0 & 0 & \cdots & 0 & 0 & 0 & \cdots & 0 & 1-R_2 & 0 & 0 & 0 \\
R_2 & 0 & 0 & \cdots & 0 & 0 & 0 & \cdots & 0 & 0 & 1-R_2 & 0 & 0 \\
R_2 & 0 & 0 & \cdots & 0 & 0 & 0 & \cdots & 0 & 0 & 0 & 1-R_2 & 0 \\
R_2 & 0 & 0 & \cdots & 0 & 0 & 0 & \cdots & 0 & 0 & 0 & 0 & 1-R_2 \\
1 & 0 & 0 & \cdots & 0 & 0 & 0 & \cdots & 0 & 0 & 0 & 0 & 0
\end{pmatrix} \tag{44}$$

where:

$$R_1 \quad = \quad (\pi_1 + \pi_2)p_R$$

and

$$R_2 \quad = \quad (\pi_1 + \pi_2)p_R + P_0,$$

$$\boldsymbol{\pi} = \frac{1}{\bar{\pi}}\left(1,1,\ldots,1,1-2p_R,(1-2p_R)^2,\ldots,(1-2p_R)^{28},\right. \tag{45}$$
$$\left.(1-2p_R)^{28}(1-2p_R-P_0),\ldots,(1-2p_R)^{28}(1-2p_R-P_0)^4\right)$$

7.4.3. Comparison with Spatial Models.

The full spatial model was run (with early colonisation omitted) and time series (figure 54) for the four 'species' used to estimate average values of $\boldsymbol{\pi}$. The parameters used were $P_0 = 0.2$, $p_W = 0.7$, $p_S = 0.5$ and $p_E = 0.1$. The frequencies obtained are given in table 12 for the numerical results and the mean field model, with $p_R = 1.3$ and $\mathcal{E} = 31.3616$. The normalising factor, $\bar{\pi}$, in the memory/radiation model was evaluated using the software package MAPLE (Char et al., 1985).

The 'error' in table 12 is the root mean square error of the mean field values relative to the spatial model. The spatial effects are only significant where the local radiation effects are present, as this provides the only coupling in the absence of early colonisation. Generically, any local process will considerably affect the frequency distributions in a spatially explicit model. The important feature to notice in the results is the magnification of the error by the memory of the system. Therefore, memory appears to play a substantial modifying role in the model, as an *amplifier* of local effects.

7.5. Description of Numerical Techniques.

7.5.1. Characteristic Spatial Scales.

As with the models of previous chapters, the mosaic model is explicitly spatial, so spatial scales need to be carefully considered. One important emergent scale is the coherence length scale of section 2.1.5, which is related to the optimisation of information from the system and is the minimum lattice size that should be used. At very small scales, below the coherence length scales, the deterministic dynamics are overwhelmed by stochastic fluctuations caused by the probabilistic nature of the local interactions. At large scales (above the *averaging length*

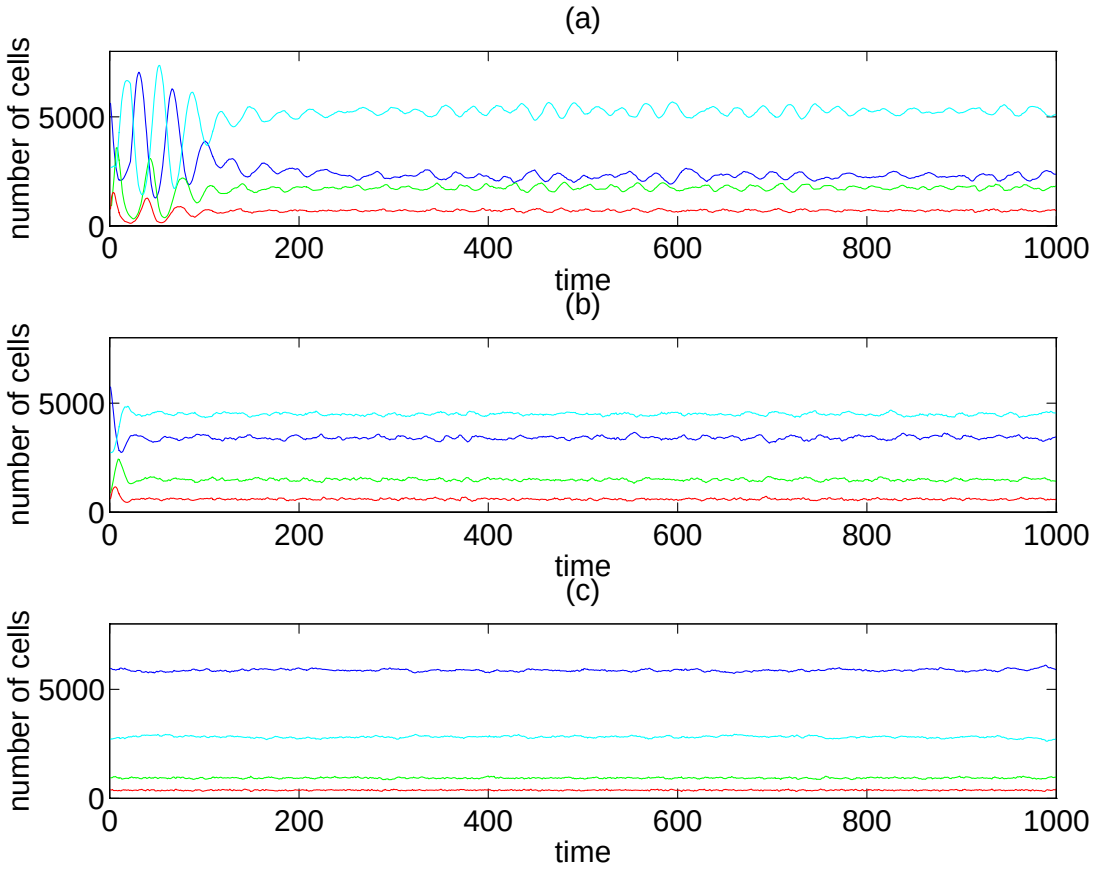

Figure 54: Time series from the mosaic cycle CA model with local colonisation effects omitted: (a) memory/radiation; (b) no memory/radiation; (c) no memory/no radiation. 'Species' are gap (red); birch (green); mixed (cyan); beech (blue).

scale) the dynamics are averaged out and therefore also provide minimal information about the dynamics. Hence there is clearly an intermediate spatial scale, at which the information about the deterministic dynamics is maximised while noise is minimised. The coherence length scale identifies the scale at which the 'error' in the system is simply that arising necessarily from the discrete two-dimensional spatial representation. Hence the coherence length scale usually provides an optimal scale for viewing the deterministic dynamics with a minimal level of stochastic noise.

The second emergent length scale mentioned above is the averaging length scale. An important feature that arises in the system is the decoupling of sufficiently remote parts of the lattice. While every cell directly influences all of its nearest neighbours, there is a separation distance above which cells do not influence each other, they are *decoupled*. Therefore, over sufficiently long spatial and temporal scales, the dynamics will be smoothed out to constant averages, regardless of the nature of the local dynamics, which may be periodic or even chaotic. Thus a grid size may be defined, which is the minimum scale for which the dynamics averaged over the whole grid are constant.

This minimum grid size can be estimated by using standard deviations. The standard deviation, σ_n, for all the cells in a subgrid of size $n \times n$, is found relative to a mean calculated over a large grid of size $N \times N$. The dynamical variation (and hence the standard deviation) decreases as the subgrid size rises. The averaging length scale, n_a, is the subgrid size at which the standard deviation has fallen to zero, which corresponds to fully-smoothed dynamics.

7.5.2. Characterising the Spatial Pattern and Dynamics.

(a) The Clumping Index.

The mosaic cycle model clearly produces clumped patterns, so that a statistical test to prove the presence of aggregation will not provide significant new information. The dynamical approach of the clumping indices to the variation in the level of clumping is ideal for this model (section 2.1.6), as the effect of different mechanisms on the spatial structure can be observed using

either the clumping index or the relative clumping index. A second use of the indices is in the identification of transience (section (c)).

(b) Lyapunov exponents.

Superficial examination of any time series from the model reveals erratic dynamics. It is of interest to determine whether the model is dominated by stochastic noise or by deterministic chaos. This is attempted by estimating the average and maximum *Lyapunov exponents* of the dynamics, as described in section 2.2.3. The average exponent characterises the global predictability of the system while the maximum exponent determines whether the dynamics are in fact chaotic.

(c) Transience.

It has recently been noted that transience is an important feature in ecological systems (Hastings & Higgins, 1994). Transient dynamics can persist for extremely long times, as has been demonstrated in simple coupled maps, where the length of transience increases exponentially with level of coupling (Kaneko, 1990; Solé & Valls, 1992a). It is possible for the transience to persist sufficiently long that it is the only relevant behaviour in the system. This disputes the traditional approach to biological modelling, which focuses on equilibrium or long term dynamics.

Distinguishing of transient and post-transient dynamics in ecological systems is now a central issue, along with the identification of the transience time. The apparently simple approach of studying time series is unsatisfactory for two reasons. Firstly, transience may persist beyond the time series data available. Although it may be possible to tell that the data displays transience (simple damped oscillations would be a straightforward example), it has been shown theoretically that a certain type of transience cannot be determined as such until it has passed (Crutchfield & Kaneko, 1988). Secondly, if the time series is produced on an unsuitable spatial scale, transient and post-transient behaviour may be indistinguishable. The first problem is minimised by modelling for as long a period as possible, while the second problem requires

identification of an optimal spatial scale.

The clumping index provides a new approach to analysing transience in a system, by focusing on the temporal evolution of a system's structure. Although the density or absolute number of a given species may be constant, or may be oscillating periodically or aperiodically with roughly constant cycle amplitude, the structure may be evolving. Thus a plot of the clumping index may demonstrate the evolution of the level of aggregation, in spite of fluctuating densities. A plot of relative clumping index may be used to illustrate contrasting transience properties of different systems.

7.5.3. Robustness and Stability of the Model.

(a) Singular Value Decomposition.

It is useful to determine the robustness of the model, which refers to the constancy of the global features of the results over replicated simulations. This is investigated using the SVD technique of section 2.1.7. The number of each of the 55 states of the CA is recorded for each of 55 replicates and a 55×55 replication matrix $\mathbf{X}$ is formed.

(b) Stability of the Model.

Stability covers a wide-range of concepts in ecology. Amongst the most important ideas are resistance and resilience (Grimm et al. 1992). A system is *resistant* if it is not changed by disturbances and is *resilient* if it returns to its original state after disturbances. Resistance and resilience of the structure of the mosaic patches are central stability concepts in this model.

It is important to define the type of disturbance, in terms of its spatiotemporal structure and amplitude. Wissel performs a basic stability analysis of the full model, but limits the perturbation to the removal of particular species and ages of trees. This corresponds to human interference in the communities. Here resistance and resilience of the system to catastrophic (natural) disturbances are considered. Whole subregions of the mosaic system are removed for various durations and over various spatial scales. Time series and the clumping index are used

to study the impact of disturbances.

(c) Dimensionality of the Model.

The technique of SVD is combined with that of *embedding* to provide a preliminary insight into the dimensionality of the dynamical system (Broomhead & King, 1986; Rand & Wilson, 1995). The system has four species and hence three degrees of freedom, but the age structure, spatial structure and stochastic noise potentially raise the dimension to a very high number. SVD of an embedded matrix allows the actual dimension to be estimated.

An embedded or time-delayed matrix $\mathbf{X}$ (equation (46)) is constructed from the time-delayed vectors $\boldsymbol{x}_t$ (equation (47)), which are based on a time series $\{x_1, x_2, \cdots\}$. For example, the series $\{x_t\}$ may be the total number of a particular species. E is the *embedding dimension* and should be taken sufficiently large; N, the number of vectors, should be of the same order as E.

$$\boldsymbol{X} = \frac{1}{\sqrt{N}} \begin{pmatrix} \boldsymbol{x}_1 - \overline{\boldsymbol{x}} \\ \boldsymbol{x}_2 - \overline{\boldsymbol{x}} \\ \vdots \\ \boldsymbol{x}_N - \overline{\boldsymbol{x}} \end{pmatrix} \tag{46}$$

where:

$$\overline{\boldsymbol{x}} = \frac{1}{N} \sum_{i=1}^{N} \boldsymbol{x}_i$$

$$\boldsymbol{x}_t = (x_t, x_{t+1}, \cdots, x_{t+E-1}) \tag{47}$$

The SVD of $\mathbf{X}$ is carried out, as in section 2.1.7. The singular values, $\{e_i\}$, are the diagonal entries of $\mathbf{S}$ and in the canonical SVD form are in decreasing order of magnitude. If a subset of the singular values $\{e_1, \cdots, e_d\}$ ($d \ll E$) are substantially larger than the remainder $\{e_{d+1}, \cdots, e_E\}$ then the dynamics are approximately of dimension d. The time series may be projected onto

the first d singular vectors and this projection provides a good approximation to the series. The higher singular values $\{e_{d+1}, \cdots, e_E\}$ correspond to noise in the system.

7.6. Results and Discussion.

7.6.1. Characteristic Spatial Scales.

The coherence length scale n_c, below which the lattice size interacts with the dynamics, is found from figures 55a - d. The simple no memory/no radiation model has a coherence length scale of around 15 (figure 55d); the spatial effects are clearly minimal in this case (in agreement with the mean field Markovian model). The coherent grid size for the full model is around 30×30 (figure 55a), which is still small compared with many discrete spatial models (Keeling et al., 1995). This means that it is not usually necessary, nor desirable, to run the model on a larger grid. However, later consideration of transience shows the importance of larger grids for some applications.

The memory/no radiation model (figure 55b) has a much larger value of $n_c \simeq 100$; in general both memory cases have a longer coherence scale than the no memory cases. The full model displays negative spatial coherence for $0 < n < 30$ and shows aggregation with increasing n ($\frac{\partial \mathcal{E}_n}{\partial n} > -1$), as does the no memory/radiation case (figure 55c). The memory/no radiation model is significantly different, showing positive coherence at all scales below n_c and a disaggregating tendency as n rises to n_c. Thus substantially different mechanisms are present in the memory case with and without radiation.

Figures 56a - d show the variation of standard deviation with grid size. The intersections of the curves with the horizontal axes give the averaging length scales. This scale is about 150 for the full model, but is significantly less (around 50) for the *no memory* models. The memory mechanism therefore causes the spatial coupling to extend over a larger distance; a larger grid is needed to see the dynamics as statistically stationary.

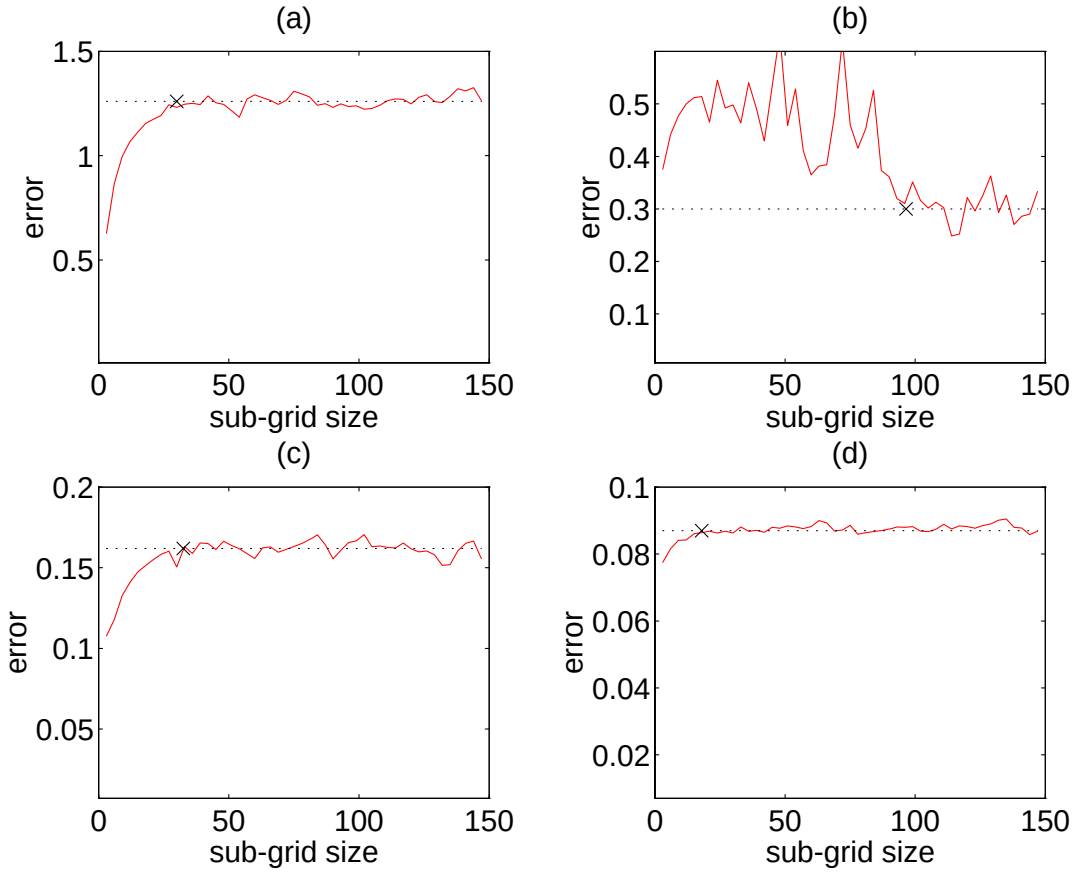

Figure 55: Error analysis for the mosaic cycle CA modelfor the four mechanisms: numerical error $n\mathcal{E}_n$ for the model (—) and theoretical error $n\mathcal{E}'_n$ $(\cdots)$. (a) Memory/radiation; (b) memory/no radiation; (c) no memory/radiation; (d) no memory/no radiation.

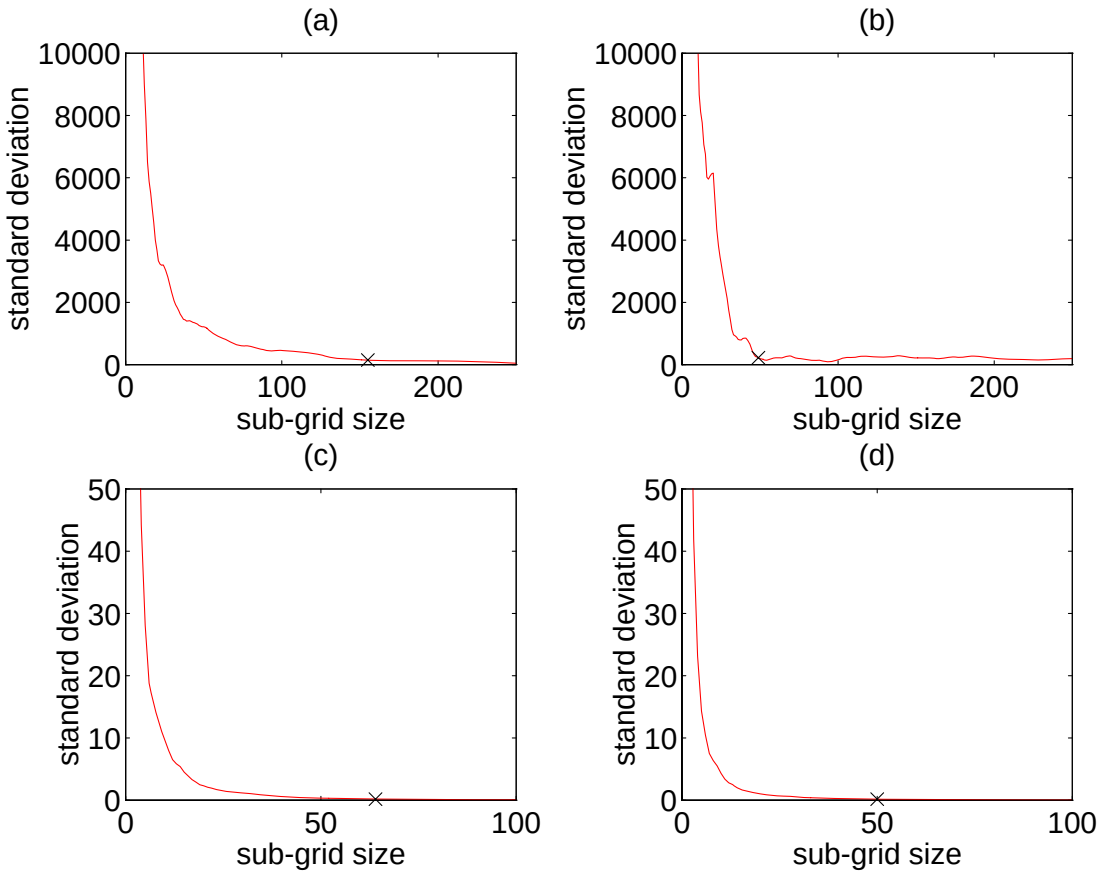

Figure 56: Standard deviation of the mosaic cycle CA model as a function of grid size. (a) Memory/radiation; (b) memory/no radiation; (c) no memory/radiation; (d) no memory/no radiation.

7.6.2. Spatial Pattern and Dynamics.

(a) The Clumping Index.

Figures 57a - d show the paths of the clumping indices as functions of density for the four mechanisms and each of the four 'species'. As the initial conditions are random, the paths always start on the dotted line, which is the clumping curve, C_ρ, for a random distribution of density ρ. The spatial structures can be seen evolving to clumped patterns, given that a greater distance normal to the dotted line represents greater aggregation. In the memory/no radiation case, the density is fluctuating, but the clumping index indicates substantial transience. Thus this method clearly demonstrates the form of the transient dynamics: in particular, the memory/no radiation model evolves slowly throughout a long transience from a random to a clumped structure.

Figure 58 shows the average post-transient clumping index for each mechanism and each species. This graph exhibits the effect of mechanism on the spatial structure of the models. The memory mechanism is clearly fundamental to the production of aggregated mosaic patches. The two memory models are away from the the random C_ρ curves, whereas the no memory models are very close to the C_ρ curves (especially the basic no memory/no radiation model).

(b) Lyapunov Exponents.

Figures 59a - d show the average Lyapunov exponents for the four mechanisms. The exponent (the horizontal part of the curve) is very close to zero, but just negative, in all four cases. It is therefore not possible to state from these results whether the dynamics are chaotic or not. It is, however, possible to state that the system is firstly very noisy and secondly predictable (to some limited extent) on average. Figure 59d demonstrates the effects of nonlinearities for large initial orbit separations ($\delta > 0.07$).

Figures 60a - b show the maximum Lyapunov exponents for the memory/radiation and no memory/radiation models (which are similar to the graphs for the respective *no radiation* models). The curves for the three values of k appear to meet at around 0.4 for the full model,

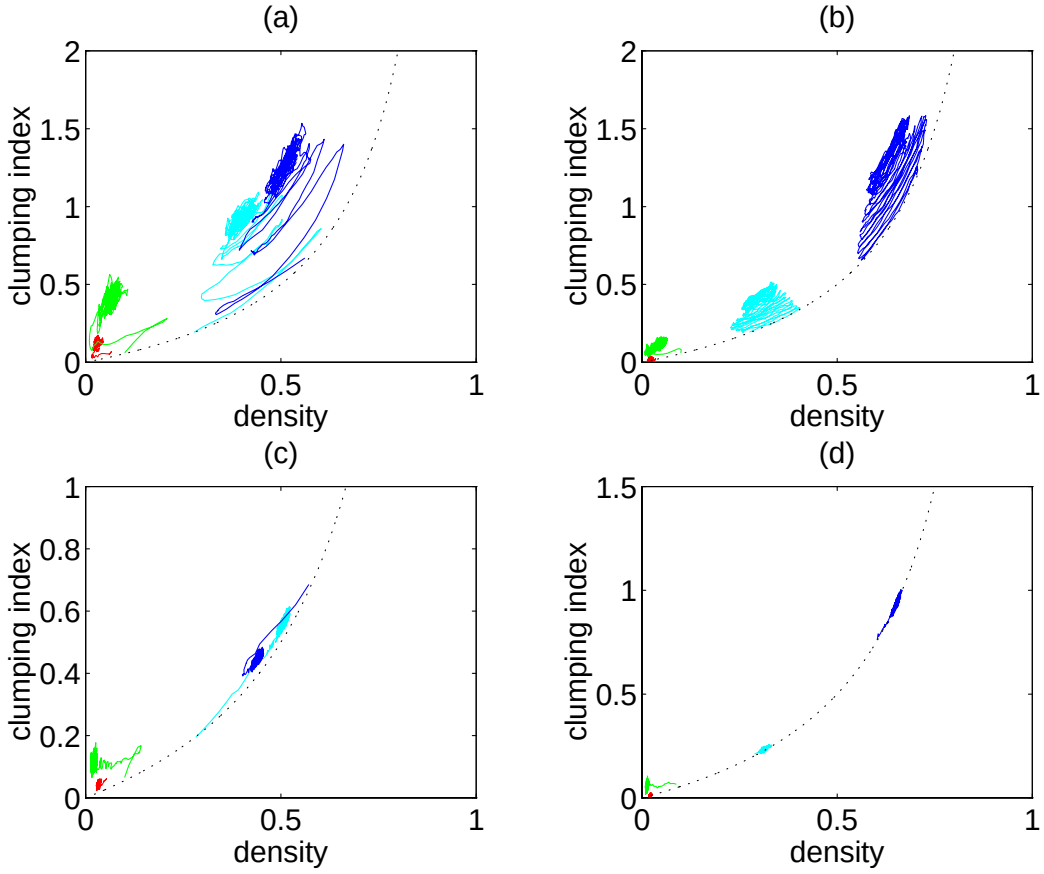

Figure 57: Clumping index paths for the mosaic cycle CA modelfor 1000 iterations for the four 'species' (gap, birch, mixed, beech). Clumping index C_i (—) and random distribution clumping curve C_ρ $(\cdots)$. (a) Memory/radiation; (b) memory/no radiation; (c) no memory/radiation; (d) no memory/no radiation. 'Species' are gap (red); birch (green); mixed (cyan); beech (blue).

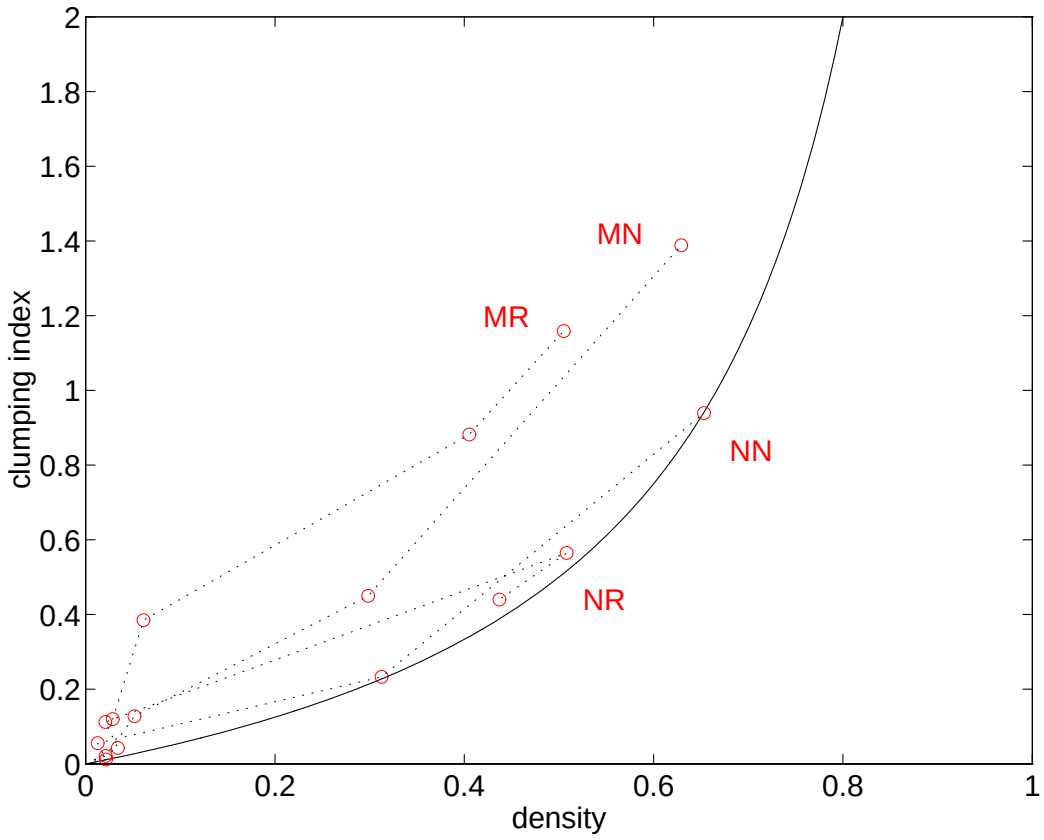

Figure 58: Mean post-transient clumping indices for the mosaic cycle CA model for iterations 1000 to 2000 ; random distribution clumping curve C_ρ (—). The four mechanisms are denoted: MR memory/radiation; MN memory/no radiation; NR no memory/radiation; NN no memory/no radiation The four 'species' are connected $(\cdots)$ in the order: gap (nearest the origin) - birch - mixed - beech.

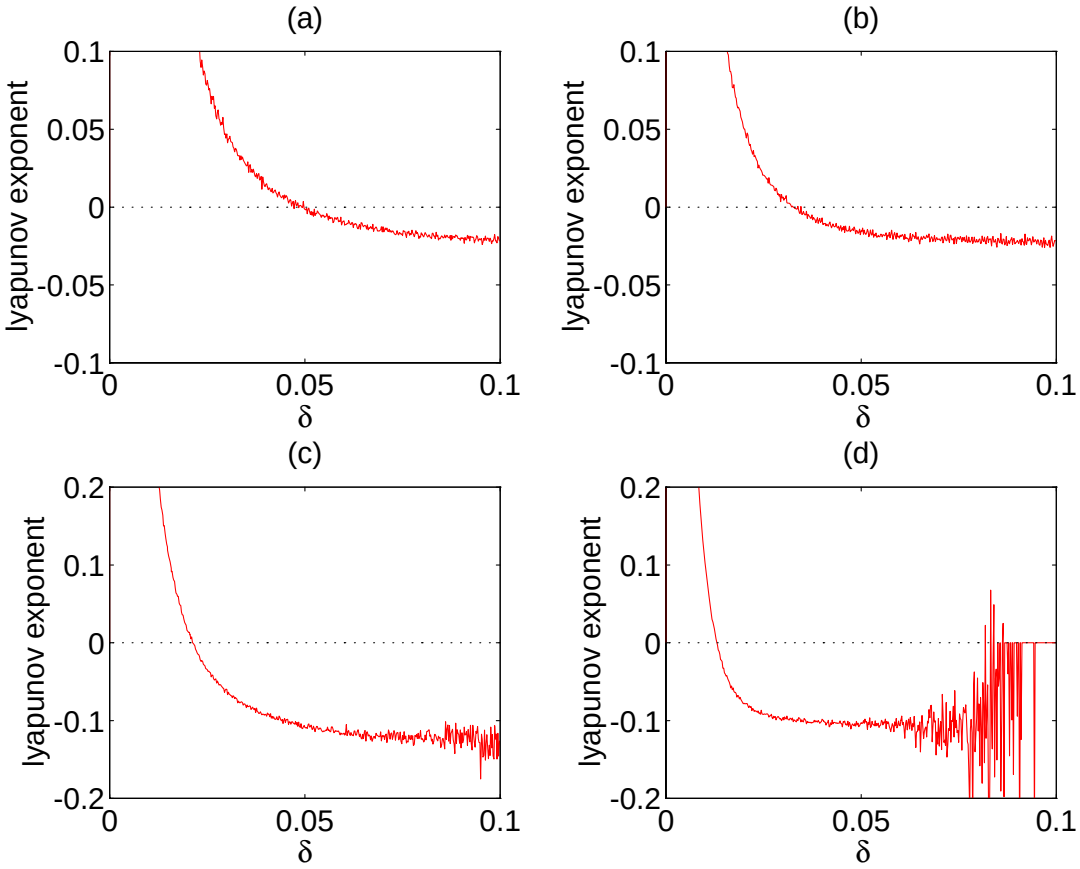

Figure 59: Average Lyapunov exponents for the mosaic cycle CA model as a function of initial orbit separation δ. (a) Memory/radiation; (b) memory/no radiation; (c) no memory/radiation; (d) no memory/no radiation.

so this is a strong indication that the model is chaotic. However, the no memory model has all exponents negative, so there is definitely no chaos here.

(c) Transience.

The time series for the beech states in the full model are shown in figures 61a - c for grid sizes 300×300, 100×100 and 30×30. The smallest grid, which is near the coherence length scale, has oscillations which are aperiodic but of relatively constant amplitude. There is no apparent difference between the early and later stages of the dynamics. The large grids, of the order of the averaging length scale, clearly show initial quasi-regular damped oscillations. The coherence length scale is therefore inadequate for determining the duration and character of transience. The full model has a transience time of around 400 iterations. During this time, the coupling in the system is extended and the whole lattice oscillates wildly in phase. The oscillations are damped out as the coupling decreases in extent.

The clumping index can be used to demonstrate structural transience. Figures 62a - b plot the relative clumping index for the beech states in the memory/radiation and memory/no radiation models. The transience persists considerably longer in the *no radiation* case, for almost 1000 iterations. The graphs also show that the full model varies more in its spatial structure, displaying erratic fluctuations about the mean index value.

7.6.3. Robustness and Stability.

(a) Singular Value Decomposition.

Figure 62c shows the singular values of a replication matrix for the full mosaic model. The ratio of the first singular values is 0.0066, which corresponds to 1.59% Gaussian noise for n = 55. This shows that the cell state structure is considerably robust to repeated simulations.

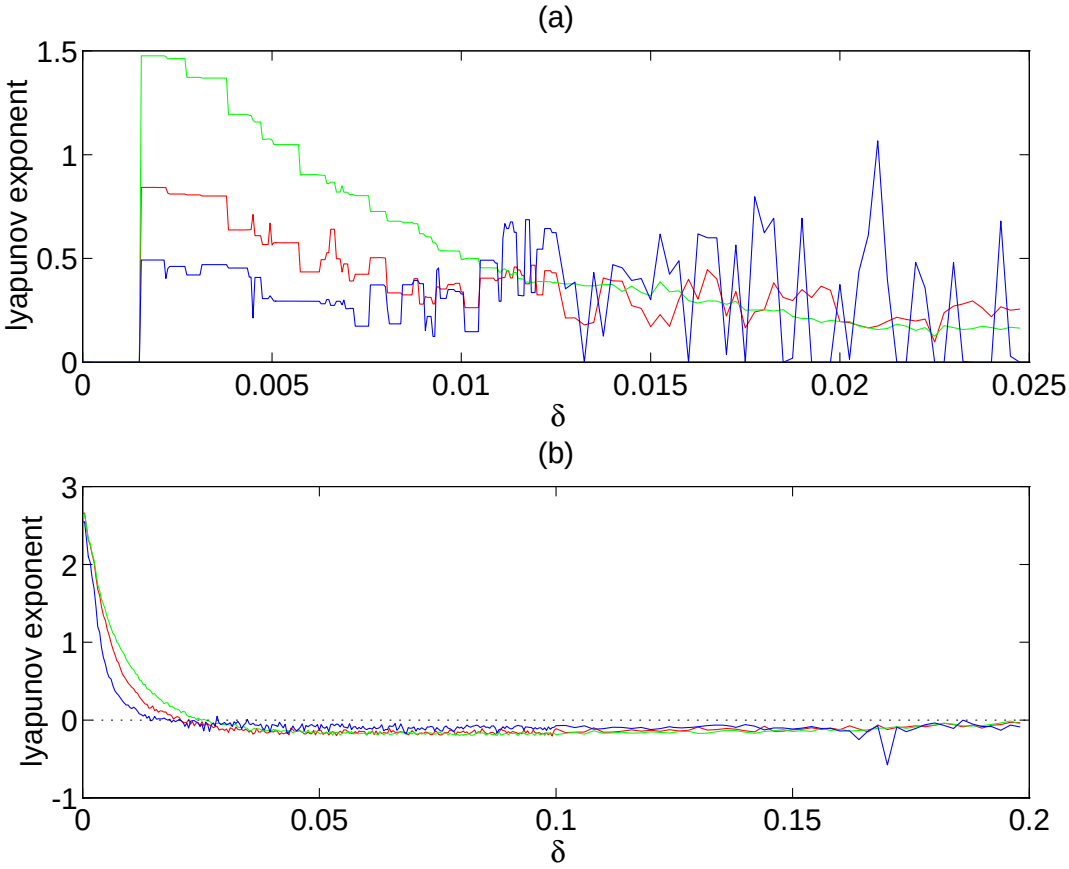

Figure 60: Maximum Lyapunov exponent for the mosaic cycle CA model as a function of initial orbit separation δ for three different values of maximum orbit separation ratio k. (a) Memory/radiation (k = 8 (blue), k = 17 (red), k = 33 (green)); (b) no memory/radiation (k = 2 (blue), k = 4 (red), k = 8 (green)).

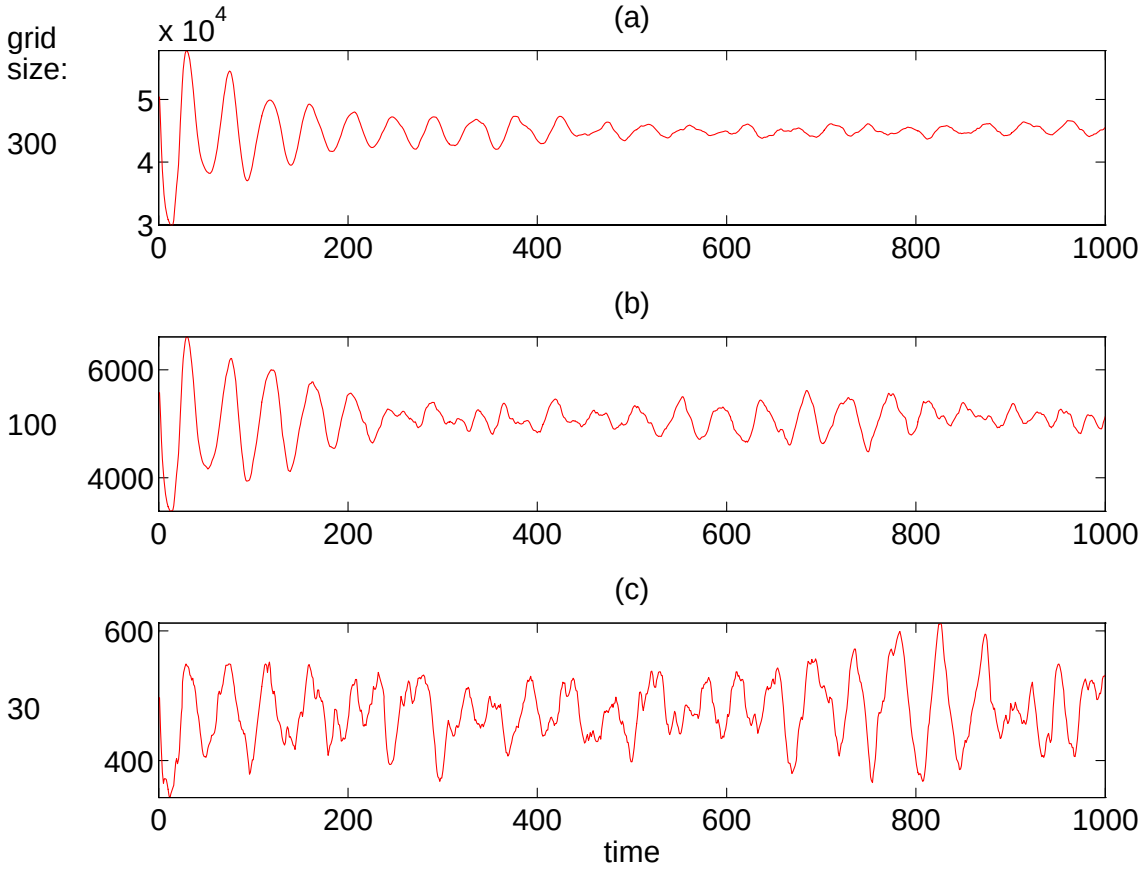

Figure 61: Number of beech cells in the mosaic cycle CA model as a function of time for various lattice sizes: (a) 300×300; (b) 100×100; (c) 30×30.

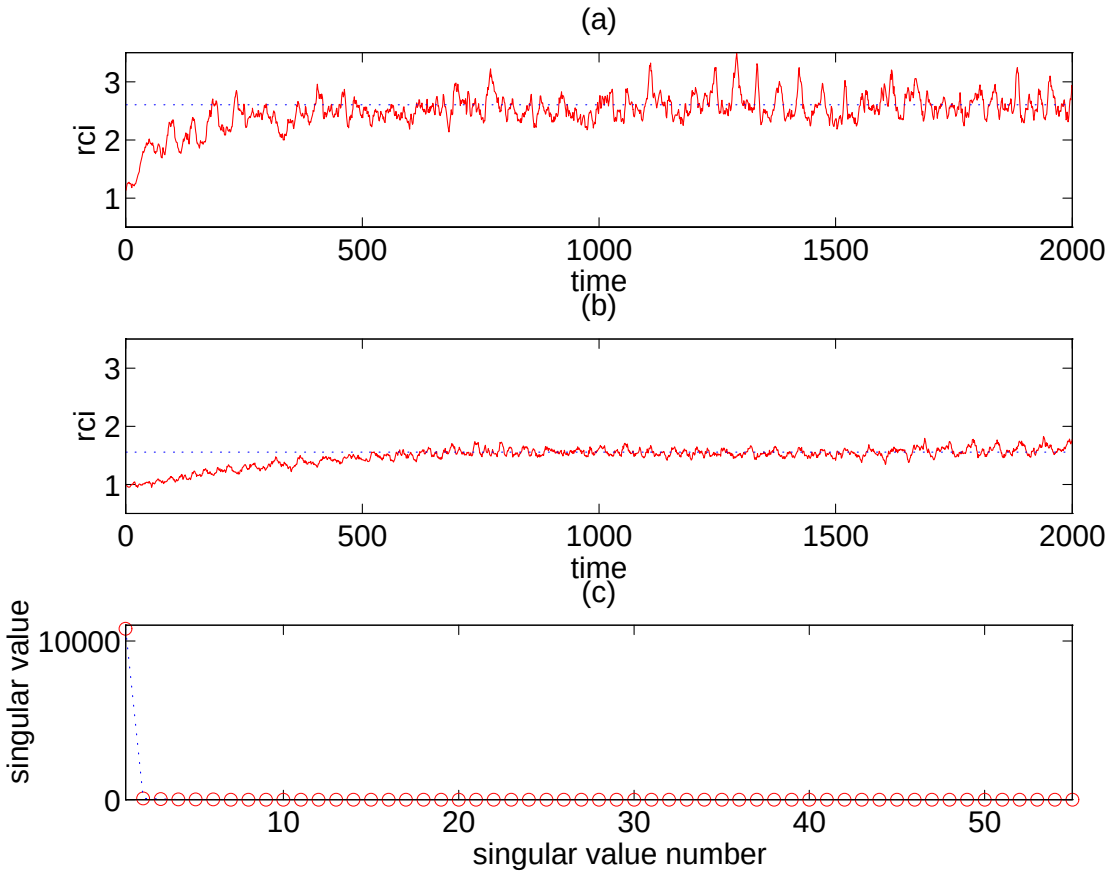

Figure 62: Relative clumping indices for the beech states in the mosaic cycle CA model for 2000 iterations: (a) memory/radiation; (b) memory/no radiation. (c) Singular values obtained by standard value decomposition of the replication matrix for the full mosaic cycle model.

(b) Resistance and Resilience to Catastrophic Disturbance.

All trees in areas of sizes from 10×10 to 90×90 were removed from a 100×100 lattice at time 2000 (well after transients had passed). The areas were constrained to remain empty for a range of times, from 1 iteration up to 2000 iterations. In all cases the system recovered its original (dynamic) equilibrium, as illustrated by figure 63 for a 500 iteration disturbance.

Perturbations of great spatial extent show wild but relatively even oscillations which are damped out over a period of about 500 iterations. The components of the system are therefore not at all resistant to perturbations but are extremely resilient. (These results are shown for the full model, but qualitatively similar results were obtained for all the types of mechanism.)

The relative clumping index is a useful measure of the reaction to a disturbance. Figure 64 shows (on logarithmic axes) the relative clumping index for beech averaged over various phases of the system's existence. The level of clumping increases greatly during large disturbances and remains at a raised level as the post-disturbance transients pass. The structure returns to the original level when the system has settled down after the perturbation. Thus the structure also demonstrates substantial resilience but no resistance to catastrophic disturbance.

(c) Dimensionality.

Figure 65a illustrates the time-delayed matrix for the number of beech cells at each iteration in the full model, with $E = 60$ and $N = 120$. Figure 65b shows the singular values for this matrix. Figure 66 shows the first 20 singular vectors and clearly demonstrates that the first few singular vectors are fairly smooth and simple, but that later ones are simply noise. The system is therefore predominantly low-dimensional but there is some noise in addition to the dynamics. Figures 67a - c show the projection of the time series onto the first 2, 4 and 6 singular vectors respectively. The four-dimensional projection is clearly a better fit than the two-dimensional projection, but the six-dimensional projection provides little improvement: a four-dimensional representation of the system captures all of the essential features of the dynamics.

Figure 65c shows the singular values for the *no memory* model. There are clearly at least eight

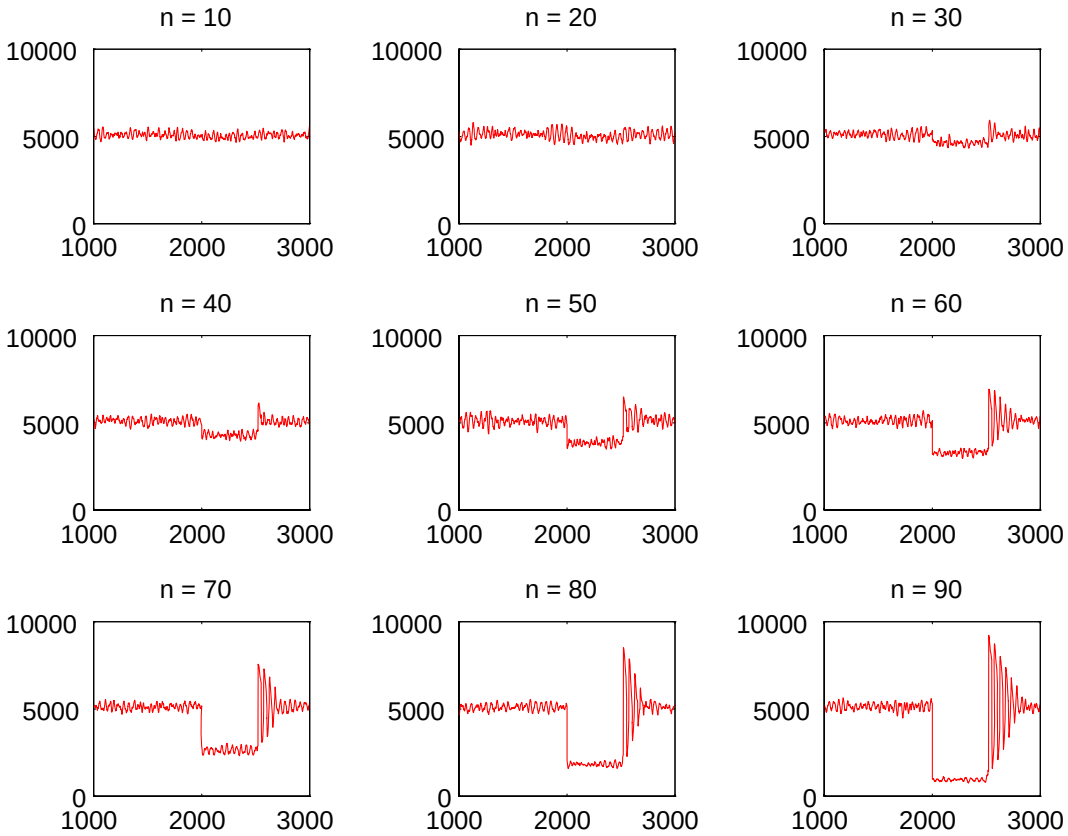

Figure 63: Number of beech cells in the mosaic cycle CA model with disturbance events in a 100×100 lattice. The disturbance of duration 500 iterations is of size $n \times n$ for $n = 10, \ldots, 90$.

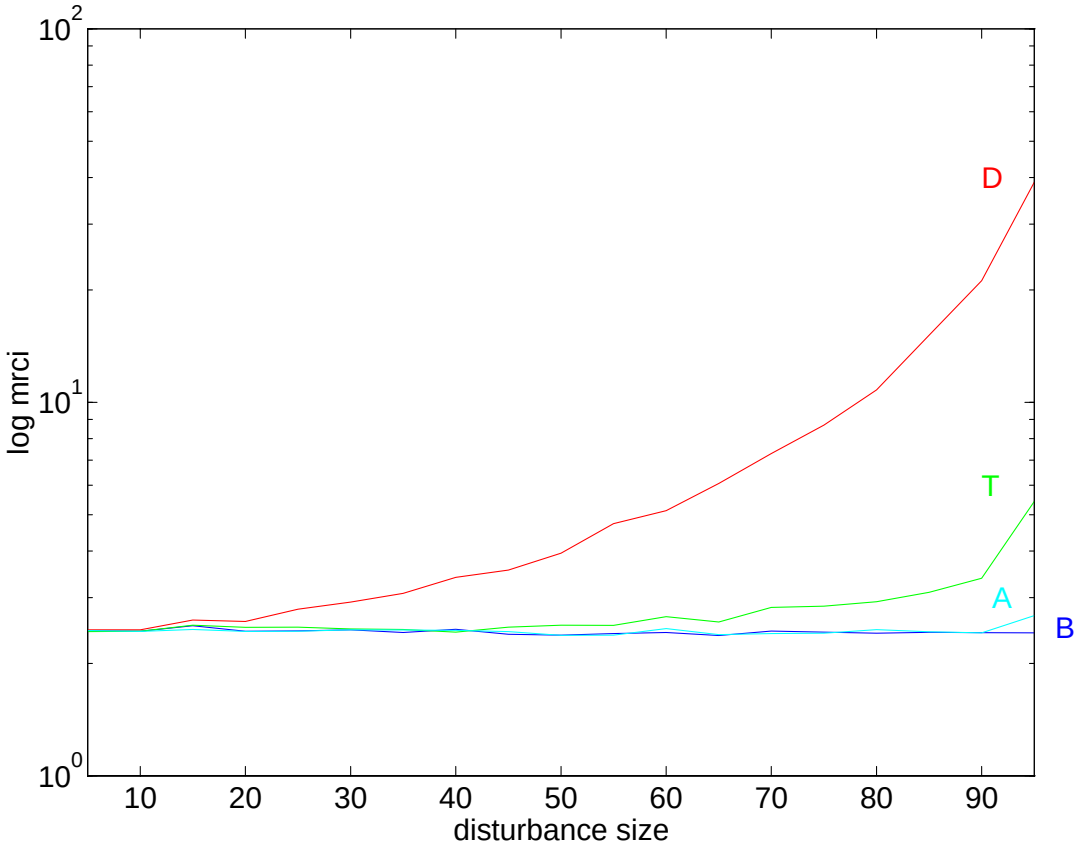

Figure 64: Logarithm of mean relative clumping indices (MRCI) for the mosaic cycle CA model as a function of disturbance size: **B** 1000 iterations before disturbance (but after initial transients) (blue); **D** 1000 iterations during disturbance (red); **T** 1000 iterations during transience of disturbance (green); **A** 1000 iterations after transience of disturbance (cyan).

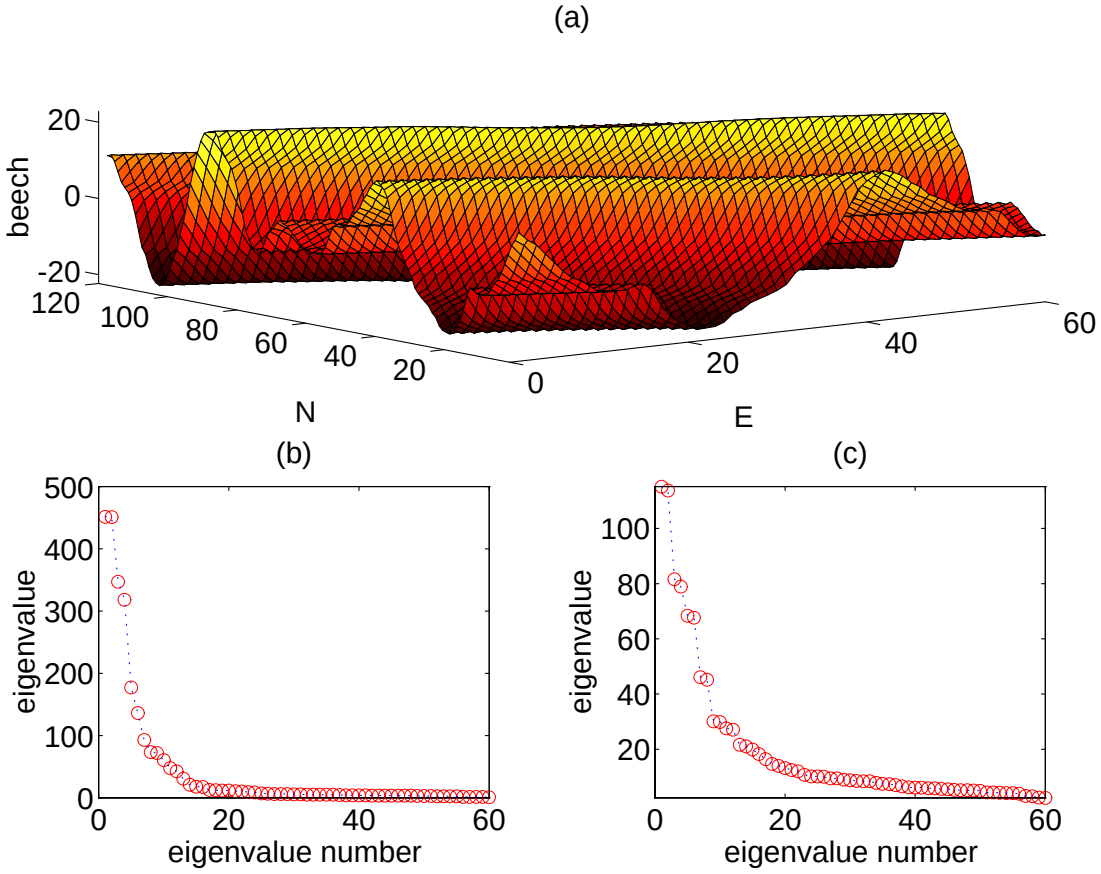

Figure 65: Embedding analysis of the mosaic cycle CA model. (a) Time-delayed matrix with embedding dimension $E = 60$ for the number of beech cells in the full model. (b) - (c) Singular values for the time-delayed matrix for the number of beech cells. (b) The full memory/radiation model; (c) the no memory/radiation model.

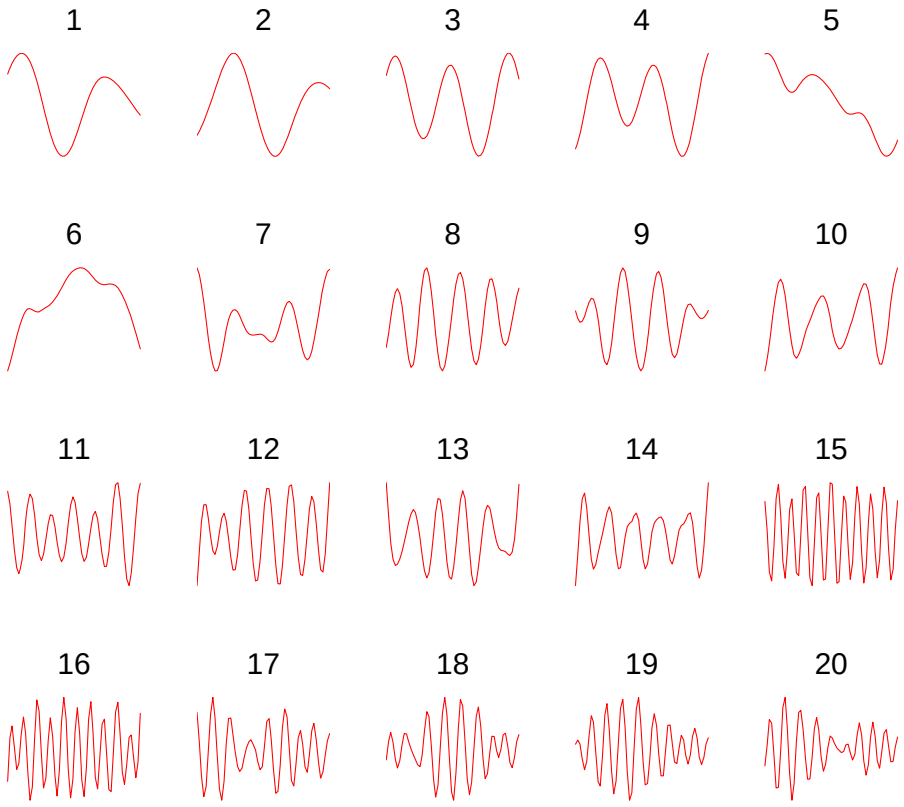

Figure 66: Representation of the embedded singular vectors for the mosaic cycle CA model: the first 20 vectors of the time-delayed matrix with embedding dimension E = 60 for the number of beech cells.

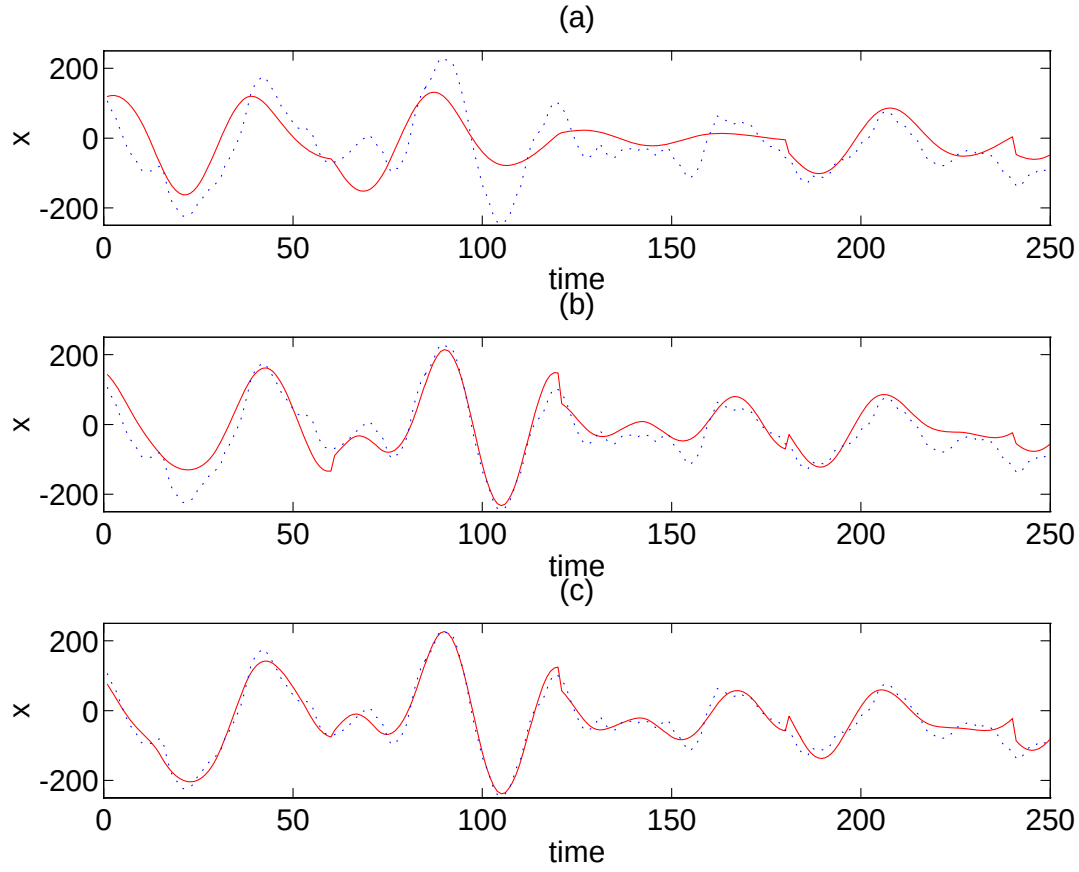

Figure 67: Projection of the time series for the mosaic cycle CA model onto the first d singular vectors of the time-delayed matrix with embedding dimension $E = 60$ for the number of beech cells in the full model: projection (red —), original time series (blue $\cdots$). (a) d = 2 (b) d = 4 (c) d = 6.

singular values that are larger than the remainder, so the fundamental dimension of this system is not less than 8, which is significantly larger than the *memory* model.

7.6.4. Summary.

The full beech forest model has a coherence length scale of around 30 and an averaging length scale of around 150. A lattice above 150×150 shows constant state frequencies, which provides minimal information about the system dynamics, whereas a 30×30 lattice should allow maximal observation of the deterministic dynamics without the complication of local stochasticity. The no radiation model has a larger coherence length, above the lattice size used by Wissel, which may also have contributed to his failure to observe patches. The no memory/no radiation model has a very small coherence length scale, which agrees with the observation from the Markovian model that the spatial effects have minimal impact in this case.

Consideration of transience demonstrates that the coherence length scale is not a universally optimal scale for studying spatial systems. At this scale, transients are not apparent, whereas they are clearly observable around the averaging length scale. An alternative technique for viewing transients is the evolution of trajectories of the clumping indices for the dominant species. The path of the clumping index converges throughout the transient period onto a final value (which fluctuates slightly because of noise in the system). This method therefore provides a graphic illustration of the length and form of transience and allows comparison of the four models.

The clumping index also dynamically illustrates of the relative levels of aggregation in the different models. There is only a slight decrease in clumping levels when the radiation mechanism is removed from the mosaic cycle, whereas absence of the memory mechanism leads to near random index values. This supports the claim that *memory* is vital in the mosaic ecosystem.

A basic investigation of stability studied the effect, on both state frequencies and spatial structure, of perturbations at various spatiotemporal scales. All but the smallest disturbances cause large oscillations in species distributions and considerably increase the aggregation, since the

range of spatial coupling is temporarily increased. Thus the system is not at all resistant to perturbation. However, even massive disturbances of long duration do not prevent return to the original dynamical equilibria, so the system is extremely resilient. The clumping index proved useful for exhibiting the phases of disturbance phenomena. It therefore appears to be a practical and insightful statistic for a wide range of spatial models, as well as other applications such as image processing.

Lyapunov exponents were used to investigate whether this model is chaotic, despite the high levels of noise which make evaluation of the exponents difficult. An extension to the standard method of evaluating maximum positive Lyapunov exponents suggests that the mosaic cycle is chaotic. Removal of memory removes the chaos (this does not apply to radiation), so memory fundamentally affect the nature of the dynamics. However, the no memory model has a large stochastic element and does not have a significantly greater level of global predictability that the chaotic model, as shown by the much simpler average Lyapunov exponent. However, the average exponent does not fully characterise the dynamics, as it fails to predict the chaotic nature of the full model.

The full model was shown, by techniques of embedding and SVD, to have underlying dynamics of low dimension. A four-dimensional projection of the time series for beech was seen to represent the full model well, while the no memory model has a higher dimension. Hence simpler models need not correspond to lower-dimensional dynamical systems. An alternative use of the SVD technique, for the evaluation of the singular values of a replication matrix demonstrated substantial robustness of the model simulation.

7.7. Extension of the Memory Concept to Epidemiology.

7.7.1. Introduction to the SIR Model.

The forest CA belongs to a class of models - effectively spatially-explicit Markov chains - which is applicable to other areas of biology. The importance of *memory* can therefore be extended and illustrated more widely. The CA is adjusted to model an SIR (*Susceptible Infected Recovered*)

epidemic (Anderson & May, 1979; Anderson & Nokes, 1991; Anderson, 1993). The population is assumed to consist of individuals which are *Susceptible* to a viral or bacterial infection. Transmission of the infection is assumed to occur by contact with an *Infected* neighbour with a transmissibility τ. Infected individuals remain infectious for a certain period before becoming *Recovered*. Recovered individuals are assumed to be immune to the infection, but are eventually replaced by more Susceptibles, via assumed implicit birth-death processes.

The basic model with memory consists of 29 states: 1 Susceptible, 14 Infected and 14 Recovered with a maximum transmissibility of $\tau = \frac{1}{2}$. There is a transition probability between Susceptible and Infected proportional to the number n of Infected cells in an eight cell Moore neighbourhood. All other states progress with probability 1 at each iteration, so that the evolution of the states is:

$$S \overset{n/16}{\rightarrow} I_1 \overset{1}{\rightarrow} \cdots \overset{1}{\rightarrow} I_{14} \overset{1}{\rightarrow} R_1 \overset{1}{\rightarrow} \cdots \overset{1}{\rightarrow} R_{14} \overset{1}{\rightarrow} S.$$

The *no memory* model has 3 states: Susceptible, Infected and Recovered. The transition between Susceptible and Infected is the same as above. The other two transition probabilities are both $\frac{1}{14}$, so that the model is:

$$S \overset{n/16}{\rightarrow} I \overset{1/14}{\rightarrow} R \overset{1/14}{\rightarrow} S.$$

Figure 68 shows the memory and no memory CA after transients have passed. The memory model exhibits a striking ringed pattern, whereas the no memory model is a near random distribution. The results specifically contradict the claim by Durrett (1993a) that *universality* implies that an exponential duration of infection (equivalent to the no memory case) has similar qualitative behaviour to a more realistic (memory) model.

7.7.2. Implications of Memory for an Epidemic.

The proportions of the Susceptible, Infected and Recovered states in a 100×100 CA are shown

(a)

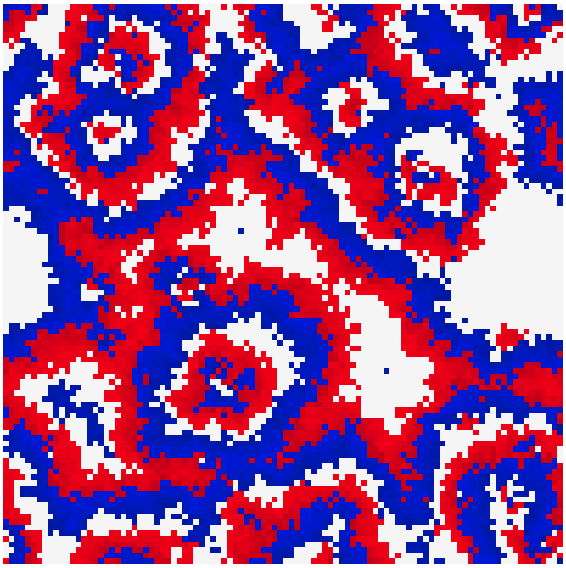

(b)

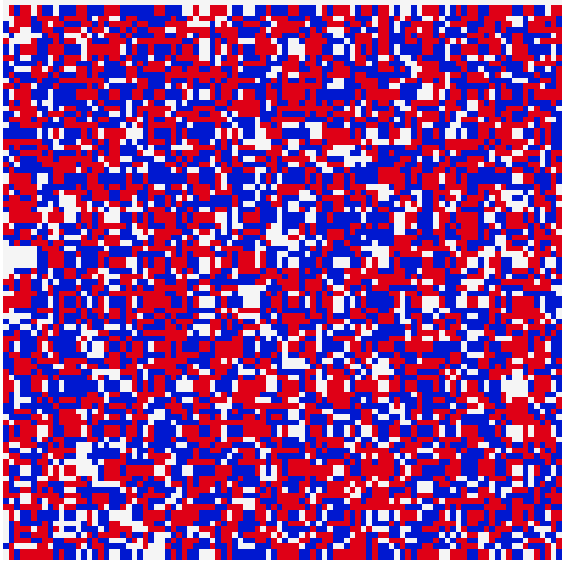

Figure 68: Spatial pattern in the SIR epidemic CA model after transience. (a) With memory; (b) without memory. White - Susceptible, red - Infected; blue - Recovered.

as time series for the memory and no memory cases in figure 69a. There is some oscillation in the memory case, but the mean proportions of each class of cell are similar for the two types of CA.

Markov matrices may be constructed as in section 7.4.4 for the SIR model. For the no memory case, the 3×3 transition matrix $\mathbf{P}$ is given by equation (48), where n_I and n_R are the times spent respectively in the Infected and Recovered states, which in the previous section are given by $n_I = n_R = 14$. The mean number of Infecteds in the eight cell neighbourhood of a cell is approximated in the mean field by π_2, where $\boldsymbol{\pi}$ is the vector of mean occupancies of the Susceptible, Infected and Recovered states.

$$\boldsymbol{P} = \begin{pmatrix} 1 - \frac{\pi_2}{2} & \frac{\pi_2}{2} & 0 \\ 0 & 1 - \frac{1}{n_I} & \frac{1}{n_I} \\ \frac{1}{n_R} & 0 & 1 - \frac{1}{n_R} \end{pmatrix} \tag{48}$$

The proportions of each of the states are found from the solution of $\boldsymbol{\pi P} = \boldsymbol{\pi}$ as:

$$\boldsymbol{\pi} = \left(\frac{2}{n_I}, \frac{n_I - 2}{n_I + n_R}, \frac{n_R}{n_I} \frac{n_I - 2}{n_I + n_R} \right).$$

The memory model has an $(n_I + n_R + 1) \times (n_I + n_R + 1)$ transition matrix (equation (49)) which gives a frequency vector $\boldsymbol{\pi}$ identical to the no memory case (equation (50)). Thus memory has no effect on the SIR system in the mean field, as well as little effect on the state frequencies of the CA (figure 69a). Memory therefore primarily has an impact on the spatial structure of a system.

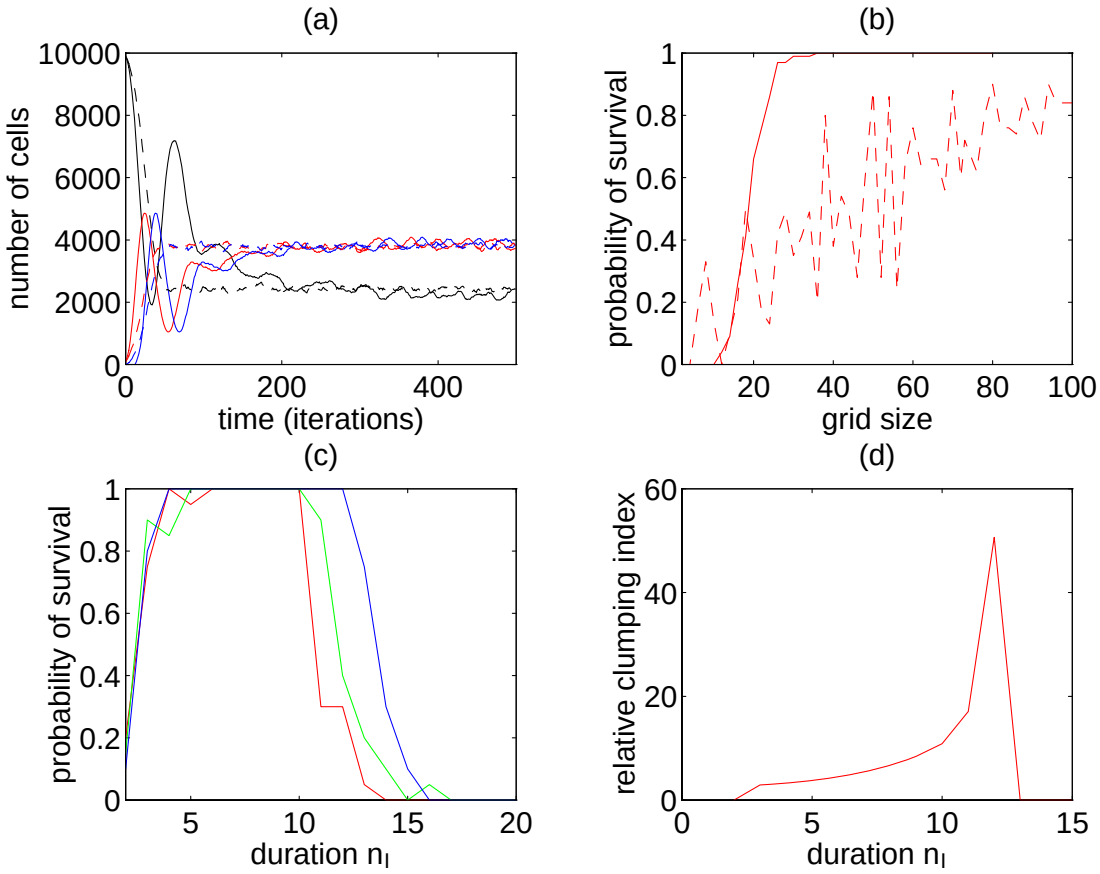

Figure 69: Investigation of the SIR epidemic CA model. (a) Numbers of the different cell types in the SIR CA on a 100×100 grid with memory (—) and without memory (- - -): Susceptibles (black), Infecteds (red) and Recovereds (blue). (b) Probability of survival of the epidemic for 10000 iterations as the size of the CA varies for the memory (—) and no memory models, given a random initial distribution. (c) Probability of survival of the epidemic for 10000 iterations as the duration of infection and immunity varies on 50×50 (red), 100×100 (green) and 200×200 (blue) grids. (d) Relative clumping index of the SIR model as the duration of infection and immunity varies on a 50×50 grid.

$$\boldsymbol{P} = \begin{pmatrix} 1-\frac{1}{2}\sum_{i=2}^{n_I+1}\pi_i & \frac{1}{2}\sum_{i=2}^{n_I+1}\pi_i & 0 & \cdots & 0 & 0 \\ 0 & 0 & 1 & \cdots & 0 & 0 \\ \vdots & \vdots & \vdots & \ddots & \vdots & \vdots \\ 0 & 0 & 0 & \cdots & 1 & 0 \\ 0 & 0 & 0 & \cdots & 0 & 1 \\ 1 & 0 & 0 & \cdots & 0 & 0 \end{pmatrix} \tag{49}$$

$$\boldsymbol{\pi} = \left(\frac{2}{n_I}, \frac{n_I-2}{n_I(n_I+n_R)}, \frac{n_I-2}{n_I(n_I+n_R)}, \cdots, \frac{n_I-2}{n_I(n_I+n_R)}\right) \tag{50}$$

Spatial structure has implications for the long term behaviour of an epidemic, so the CA was run fifty times for both memory scenarios for 10000 iterations and for a range of grid sizes up to 100×100 (figure 69b).

With memory, a small grid causes the epidemic to wipe itself out. If a single Infected cell is placed at the centre of a grid of Susceptibles, a wave of infection will propagate outwards from the initial site of infection. This is followed by a wave of immune Recovered sites, which blocks the Infecteds from the following wave of Susceptibles. The epidemic can only persist if at least one Infected cell can break through the ring of Recovereds and infect a Susceptible. The speed of the epidemic wave is roughly constant, as is the probability that the epidemic will break through to the new Susceptibles. Therefore in a small (toroidal) system the epidemic is very likely to reach the edge of the grid and disappear with the ring of Recovereds remaining unbroken, whereas a large system allows sufficient opportunity for the infection to break through so the epidemic can persist. This is shown by the relatively sharp increase in the survival probability of the epidemic from near zero below about a 10×10 grid to near 1 above 20×20 (figure 69b). The system thus exhibits a type of threshold phenomenon.

In contrast, although the no memory system shows greater survival of the epidemic as the grid size increases, the variation of survival probability is extremely erratic. The random structure of the no memory system mean that the infection disappears from any cell with probability

$\frac{1}{n_I}$, thus there is always a chance that all Infected cells become Recovered at a given instant in time. Similarly it is possible that the infection will spread to none of the Susceptibles at that iteration, so there is always a finite probability that the epidemic will disappear immediately. However, this probability will decrease as the number of grid cells increases, hence the survival probability rises with the grid size (figure 69b). The system is very noisy, so the functional form of the variation of survival probability with system size is not clear.

7.7.3. Duration of Infection and Immunity.

The long term dynamics of the epidemic critically depend on the ability of the infection to penetrate the wave of immunity that follows the epidemic. The width of this ring of Recovereds clearly depends on the duration of immunity (n_R), so the role of the parameters n_I and n_R in determining the structure of the system is investigated here.

Figure 69c shows the probability that a single Infected site will lead to an epidemic lasting at least 10000 iterations, as n_I ($= n_R$) varies. Results are shown for grids of sizes 50×50, 100×100 and 200×200. For low values of n_I the epidemic sometimes disappears via stochastic effects as there is limited structure in the system (figure 70a). At intermediate values ($6 \leq n_I = n_R \leq 10$) the epidemic always survives, as the pattern is not noisy enough to cause random extinction, while the wavefronts are sufficiently narrow to allow the infection to spread to new Susceptibles. Above $n_I = n_R = 17$ extinction always occurs as the ring of immune Recovered cells is impenetrable to the infection. Between $n_I = 10$ and 17 the epidemic persists with a positive probability for as much as 10000 iterations. The probability of survival is higher for large grids, as there is more time for the infection to break the ring of immunity before the wave reaches the edge of the grid.

The structure of the epidemic before extinction is shown in figure 70 for four values of n_I. Spatial structure clearly becomes more pronounced as n_I and n_R, and hence the width of the wavefronts, increase. Thus the longevity of states is critical to the production of structure in systems with memory and there is a continuous spectrum from the randomness of no memory (or $n_I = n_R = 1$) through to the strong patterns of high values of n_I and n_R. The patterns

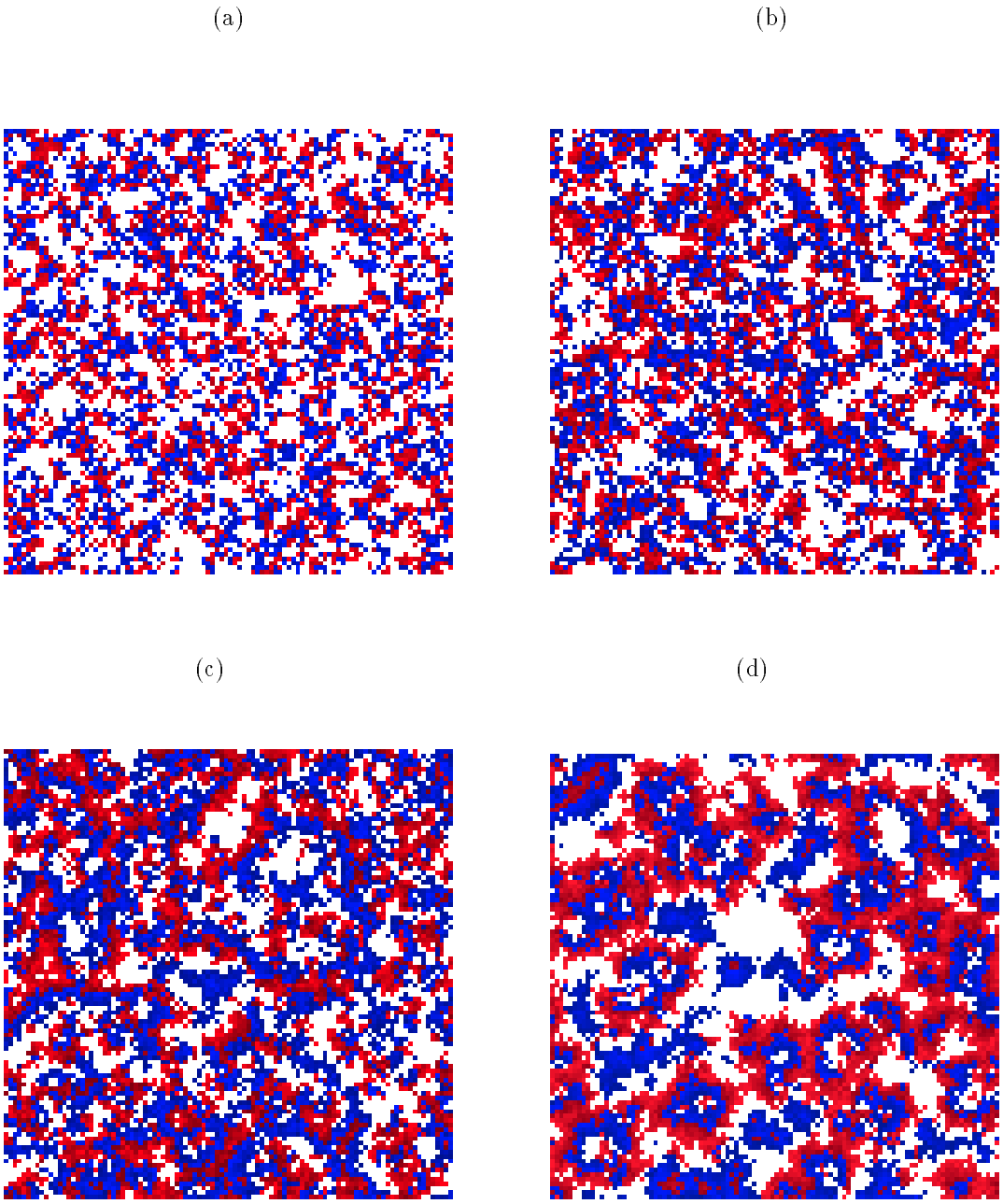

Figure 70: Spatial pattern in the SIR epidemic CA model as duration of infection varies on a 100×100 grid with memory: (a) $n_I = n_R = 5$; (b) $n_I = n_R = 7$; (c) $n_I = n_R = 9$; (d) $n_I = n_R = 11$. White - Susceptible, red - Infected; blue - Recovered.

are quantified in figure 69d by the mean relative clumping index of the Infected states, which rises sharply with n_I, as long as the epidemic persists and settles to a pattern for a long enough period.

The effect of memory in the SIR epidemic can also be investigated analytically using a simple representation in a single dimension. The epidemic can be assumed to spread outwards from an initial site of infection at the origin. The direction of propagation is denoted by x, which could represent a radial vector in two dimensions or else linear vectors (positive and negative) in one dimension. The epidemic spreads outwards towards an asymptotic shape (Durrett, 1993a) at a relatively constant speed S, which is independent of n_I and n_R (figure 71a): the speed is about 0.6 cells per iteration. In the memory case the wavefront of Infecteds is at $x = St$ at time t and the fronts of Recovereds and Susceptibles are at $x = S(t - n_I)$ and $x = S(t - n_I - n_R)$ respectively (figure 71b). The proportion of Susceptibles, Infecteds and Recovereds are given at time t and position x by $\rho_S(x,t)$, $\rho_I(x,t)$ and $\rho_R(x,t)$:

$$\rho_S(x,t) = \begin{cases} 1 & 0 \leq x \leq S(t - n_I - n_R) \\ 0 & \text{otherwise} \end{cases}$$

$$\rho_I(x,t) = \begin{cases} 1 & S(t - n_I) \leq x \leq St \\ 0 & \text{otherwise} \end{cases}$$

$$\rho_R(x,t) = \begin{cases} 1 & S(t - n_I - n_R) \leq x \leq S(t - n_I) \\ 0 & \text{otherwise.} \end{cases}$$

The average proportions of each type over their range are $\bar{\rho}_S(t) = \bar{\rho}_I(t) = \bar{\rho}_R(t) = 1$. In the no memory case the transitions from Susceptible to Infected and from Infected to Recovered are both exponential processes with parameters $\frac{1}{n_I}$ and $\frac{1}{n_R}$ respectively. Given that the probability density function of an exponential random variable with parameter λ is:

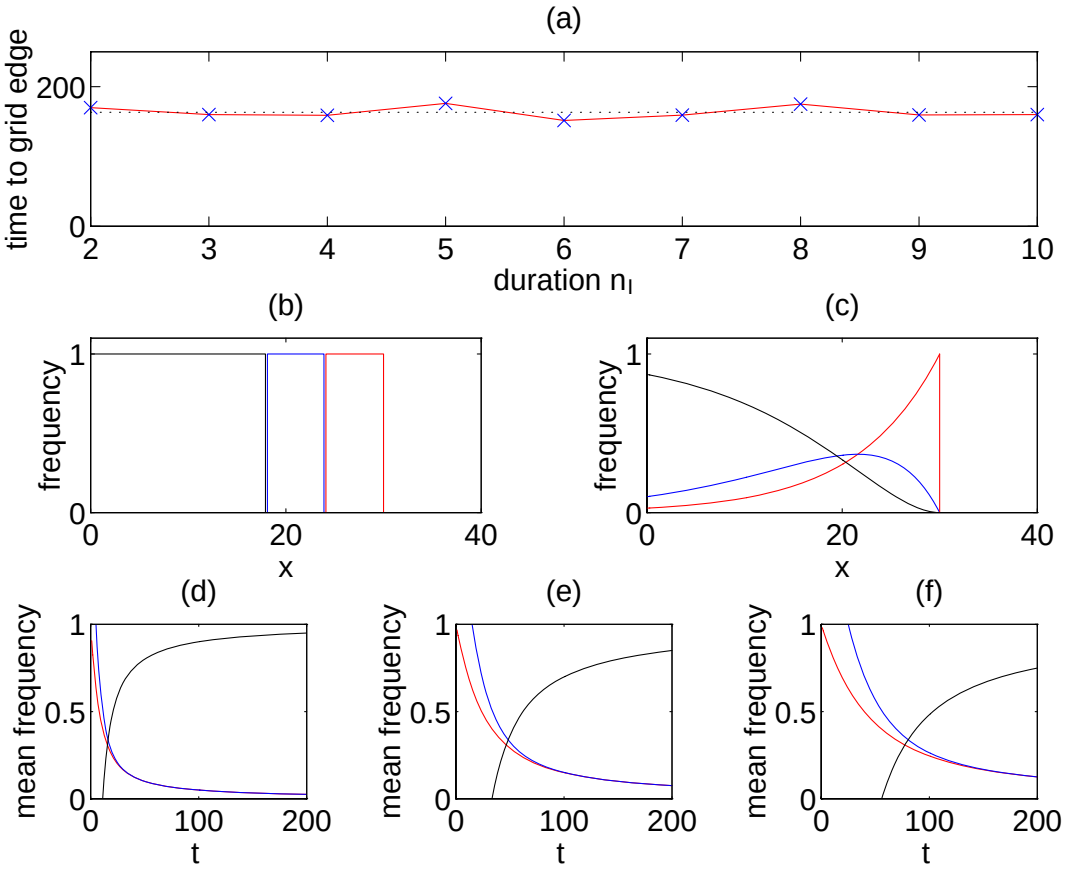

Figure 71: Analysis of a one-dimensional simplification of the SIR epidemic CA model. (a) Time for an epidemic to reach the edge of the grid for a 100×100 CA SIR model as the duration of infection (n_I) and immunity (n_R) varies (—) and mean time ($\cdots$). (b) - (c) Frequency of Susceptibles (black), Infecteds (red) and Recovereds (blue) in a simple one-dimensional SIR model as distance (x) from the initial site of infection varies: (b) with memory; (c) with no memory. (d) - (f) Mean frequency averaged over space of Susceptibles (black), Infecteds (red) and Recovereds (blue) as time (t) varies from the initial time of infection for (d) $n_I = 5$; (e) $n_I = 15$; (f) $n_I = 25$.

$$f(\lambda) \quad = \quad \begin{cases} \lambda e^{-\lambda x} & x \geq 0 \\ 0 & x < 0 \end{cases},$$

the proportion of Infecteds at x at time t is given by:

$$\rho_I(x,t) \quad = \quad \int_0^{t-\frac{x}{S}} \frac{1}{n_I} e^{-\frac{t'}{n_I}} dt',$$

since site x first becomes infected at time $\frac{x}{S}$. Thus:

$$\rho_I(x,t) \quad = \quad e^{-\frac{St-x}{Sn_I}}$$

and:

$$\bar{\rho}_I(t) \quad = \quad \int_0^{St} \rho_I(x,t)dx \quad = \quad Sn_I\left(1 - e^{-\frac{t}{n_I}}\right).$$

Likewise the proportion of Susceptibles, assuming $n_I \equiv n_R$, is:

$$\begin{aligned} \rho_S(x,t) \quad &= \quad \int_0^{t-\frac{x}{S}} dt'' \frac{1}{n_I} e^{-\frac{t''}{n_I}} \int_0^{t-t'-t''} dt' \frac{1}{n_I} e^{-\frac{t'}{n_I}} \\ &= \quad 1 - e^{-\frac{St-x}{Sn_I}} - \frac{St-x}{Sn_I} e^{-\frac{St-x}{Sn_I}}. \end{aligned}$$

The remaining fraction is therefore Recovered, so that:

$$\begin{aligned} \rho_R(x,t) \quad &= \quad 1 - \rho_I(x,t) - \rho_S(x,t) \\ &= \quad \frac{St-x}{Sn_I} e^{-\frac{St-x}{Sn_I}}. \end{aligned}$$

The average densities of Recovereds and Susceptibles are therefore:

$$\bar{\rho}_S(t) \quad = \quad S(t-2n_I) - Ste^{\frac{-}{t}n_I}$$

and:

$$\bar{\rho}_R(t) \quad = \quad Sn_I + S(t-n_I)e^{\frac{-}{t}n_I}.$$

These spatial distributions are shown in figure 71c and the spatially-averaged proportions in figures 71d - f for a range of values of n_I. It is clear that even for very long infection times (figure 71f) the average frequency of Infecteds and Recovereds is far below one. The average frequency provides a good indication of the degree of aggregation in the system, as a simplified alternative to the clumping index. Thus figures 71b - f show that the no memory SIR model has far less aggregation and spatial structure than the memory model.

8. Analysis of a One-dimensional Cellular Automaton.

Chapter Summary

The forest and epidemic models of chapter 7 are reduced to a simple one-dimensional cellular automaton model, which is a discrete time contact process on two states. A mapping is constructed between the n-site cellular automaton and a 2^n-state Markov process.

A Sierpiński Matrix is defined to be a matrix with the same geometric scaling properties as the fractal object called a Sierpiński Gasket. In the case of zero transmission, the Markov transition matrix and all its iterates are shown to be of the Sierpiński form and hence fractal in the limit of $n \to \infty$, with respect to a geometric mapping to the unit square. In the case of zero recovery, the transition matrix is shown to be a subset of a Sierpińksi Matrix.

For the full model, the complex structure of the transition matrix is fully described and is shown to have a fractal dimension below 2 in the limit of $n \to \infty$. The fractal dimension is found numerically by two alternative methods.

'Et harum scientarum porta et clavis est Mathematica.' - Roger Bacon

8.1. Introduction.

A one-dimensional simplification of the forest CA model is examined here, which is a basic contact process[66] defined on a finite one-dimensional n-vector. The CA is treated as a Markov process and analysed via the Markov transition matrix, which is shown to have a characteristic neo-fractal structure.

[66] Harris, 1974; Durrett, 1980; Durrett, 1981; Durrett & Liu, 1988; Durrett & Schonmann, 1988; Durrett et al., 1989.

The CA states are confined to the space $\mathbb{N}_2 = \{0, 1\}$, so that a configuration $\mathbf{X}^t = (x_1^t, x_2^t, \ldots, x_n^t)$ can be considered to be a binary number of length n. The automaton rules describe a simple contact process, dependent only on the nearest neighbours. If the model is treated as a simple *Susceptible-Infected-Susceptible* (SIS) epidemic, then states 0 and 1 can considered respectively to be 'Susceptible' and 'Infected'. Alternatively, it could be viewed as the spread of a plant population by localised dispersive mechanisms. An individual at cell i becomes 'Infected' with probability $n_i p$, where n_i is the number of nearest neighbours that are infected, so that $n_i \in \mathbb{N}_3 = \{0, 1, 2\}$. An individual loses infection and returns to susceptibility with probability q. The transition probabilities are therefore as follows:

$$\begin{aligned}
\mathbb{P}(x_i^{t+1} = 0 | x_i^t = 0, x_{i-1}^t = 0, x_{i+1} = 0) &= 1 \\
\mathbb{P}(x_i^{t+1} = 1 | x_i^t = 0, x_{i-1}^t = 1, x_{i+1} = 0) &= p \\
\mathbb{P}(x_i^{t+1} = 1 | x_i^t = 0, x_{i-1}^t = 0, x_{i+1} = 1) &= p \\
\mathbb{P}(x_i^{t+1} = 1 | x_i^t = 0, x_{i-1}^t = 1, x_{i+1} = 1) &= 2p \\
\mathbb{P}(x_i^{t+1} = 0 | x_i^t = 1) &= q.
\end{aligned}$$

The boundary conditions for the automaton are toroidal so that the neighbourhood of x_1^t is $\{x_n^t, x_2^t\}$ and the neighbourhood of x_n^t is $\{x_{n-1}^t, x_1^t\}$. The speed with which an infection dies out is dependent on the parameters p and q. Figure 72a shows the probability that there are no infected sites left at iteration 100 for the case $n = 10$; persistence generally rises with $\frac{p}{q}$. The spatial structure of the CA also varies with p and q. The relative clumping index (chapter 2, figure 72b) shows that intermediate values of $\frac{p}{q}$ lead to highly aggregated patterns.

8.2. The Cellular Automaton as a Markov Process.

The set of configurations $\{\mathbf{X}^t\}$ of the CA can be considered to be the random variables of a discrete stationary finite *Markov chain*. For an n-site CA on the state space $\mathbb{N}_2$, the size of the configuration space Ω_n will be 2^n, so that there will be a corresponding 2^n-state Markov process, with a $2^n \times 2^n$ stochastic matrix $\mathbf{P}$ representing the stationary Markov transition probabilities.

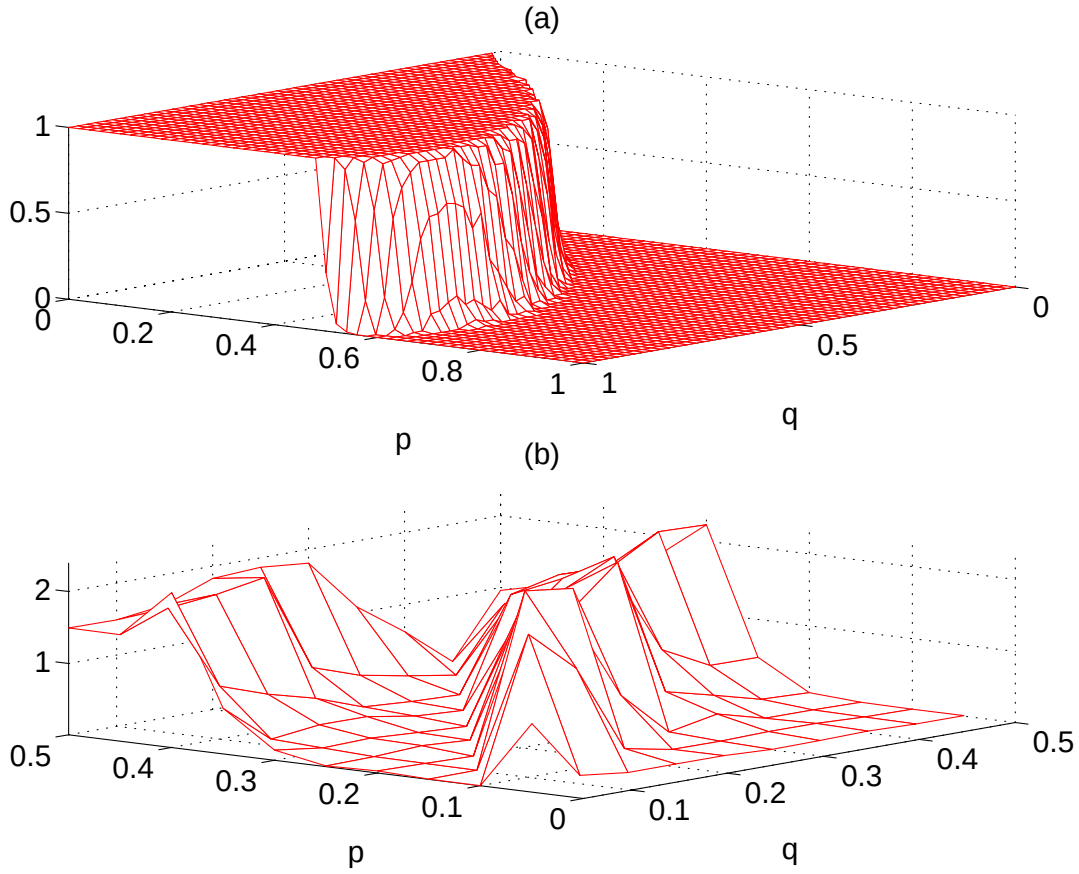

Figure 72: Numerical investigation of the one-dimensional contact CA model. (a) Probability that infection persists for at least 100 iterations in a 10-site one-dimensional CA as a function of the CA parameters p and q. (b) Relative clumping index in a 10-site one-dimensional CA as a function of the CA parameters p and q.

A map $\Phi : \Omega_n \rightarrow \{1, \ldots, 2^n\}$ can be defined between the automaton configuration $\mathbf{X}^t \in \Omega_n$ and the Markov state $N^t \in \{1, \ldots, 2^n\}$. Since configuration $\mathbf{X}^t$ is equivalent to a binary number of length n digits, the Markov state N^t may be expressed as the corresponding denary number. Thus Φ is given by:

$$\Phi(\mathbf{X}^t) \quad = \quad 1 + \sum_{i=1}^{n} 2^{n-i} x_i^t.$$

The inverse map $\Phi^{-1} : \{1, \ldots, 2^n\} \rightarrow \Omega_n$ may be calculated recursively on the sites $\{x_i^t\}$ as follows:

$$\begin{aligned} (\Phi^{-1}(N^t))_n &= (N^t - 1) \pmod 2 \\ (\Phi^{-1}(N^t))_i &= \left(\frac{(N^t - 1)}{2^{n-i}} - \sum_{j=i+1}^{n} \frac{x_j^t}{2^{j-i}} \right) \pmod 2. \end{aligned}$$

The transition matrix $\mathbf{P}$ for the Markov process can be calculated explicitly from the automaton rules for any $n \in \mathbb{N}$. The structure of the matrix initially will be investigated in the following section for the simple case of $p = 0$ or *zero transmission*.

8.3. The Case of Zero Transmission.

If $p = 0$ and $q > 0$ then no new infections can occur, while the expected time to loss of infection is $\frac{1}{q} < \infty$ for any site $i \in \{1, \ldots, n\}$. Thus the totally uninfected configuration $(0, \ldots, 0)$ corresponds to Markov state $N^t = 1$, which is an *absorbing state*. Denoting matrix $\mathbf{P}$ by $\mathbf{A}$ in this special case, and the elements by a_{ij}, this means that $a_{11} = 1$ and $a_{1j} = 0 \; \forall \, j > 1$. A few lemmas now investigate the structure of $\mathbf{A}$ for this special case of $p = 0$. The transition matrix is denoted here by $\mathbf{A}(n)$ for the n-site automaton, with elements $a(n)_{ij}$.

LEMMA 1.

$\mathbf{A}(n)$ is lower triangular.

Since $p = 0$, the only feasible transitions are $0 \rightarrow 0$, $1 \rightarrow 0$ and $1 \rightarrow 1$, so that:

$$x_i^{t+1} \quad \leq \quad x_i^t$$

and therefore:

$$N^{t+1} \quad = \quad \sum_{i=1}^{n} 2^{n-i} x_i^{t+1} \quad \leq \quad \sum_{i=1}^{n} 2^{n-i} x_i^t \quad = \quad N^t.$$

Hence for $i < j$:

$$\mathbb{P}(N^{t+1} \quad = \quad j | N^t = i) = 0$$

and:

$$a(n)_{ij} \quad = \quad 0 \qquad \forall \quad i < j,$$

that is, $\mathbf{A}$ is lower triangular $\square$

The structure of the transition matrix $\mathbf{A}$ is shown in figure 73b and exhibits a characteristic pattern, which has the same scaling behaviour as a Sierpiński gasket (Stewart, 1995). The Sierpiński gasket is a fractal object, with Hausdorff dimension $\frac{\log 3}{\log 2}$, which is constructed by removing a triangle from the centre of a triangle with twice the linear dimensions. The finite nature of the transition matrix $\mathbf{A}$ means that the scaling relations only occur over a finite range, not down to the infinitesimal scales of the true Sierpiński gasket, so it can be considered to be a *truncated Sierpiński gasket*. Such a matrix will here be described as a *Sierpiński matrix*.

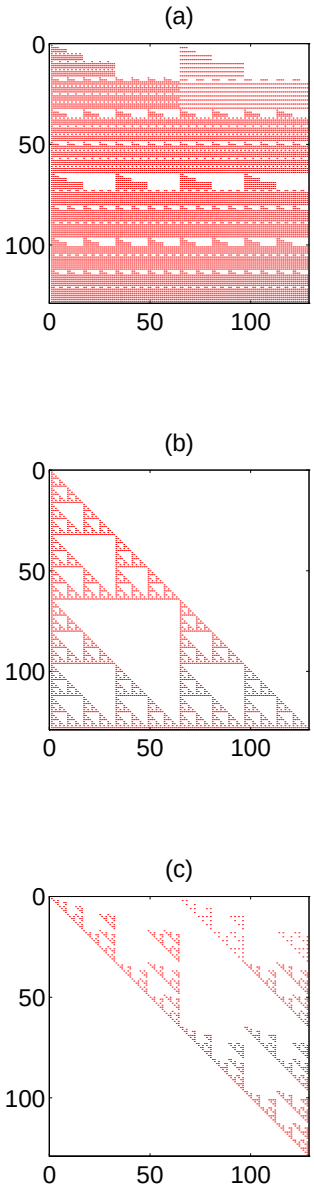

Figure 73: Structure of the transition matrices for the one-dimensional contact CA model: structure of the positive elements for the 7-site one-dimensional CA: (a) full model; (b) zero transmission ($q = 0$); (c) zero recovery ($p = 0$).

DEFINITION.

A matrix $\mathbf{M}$ *is a Sierpiński matrix if the non-zero elements of the matrix satisfy the same geometric scaling properties as the Sierpiński gasket.*

LEMMA 2.

$\mathbf{A}$ *is a Sierpiński matrix.*

For $n = 1$ and $n = 2$ the transition matrices are:

$$\mathbf{A}(1) = \begin{pmatrix} 1 & 0 \\ q & 1-q \end{pmatrix}$$

and:

$$\mathbf{A}(2) = \begin{pmatrix} 1 & 0 & 0 & 0 \\ q & 1-q & 0 & 0 \\ q & 0 & 1-q & 0 \\ q^2 & q(1-q) & q(1-q) & (1-q)^2 \end{pmatrix}.$$

This illustrates a primitive truncated Sierpiński structure, whereby the three 2×2 submatrices covering the lower triangle of $\mathbf{A}(2)$ are each lower triangular.

Assuming that $\mathbf{A}(n)$ is a Sierpiński matrix, the structure of $\mathbf{A}(n+1)$ can be determined in terms of $\{a(n)_{ij}\}$. Suppose Markov states i and j correspond to configurations $\mathbf{Y}_n(i)$ and $\mathbf{Z}_n(j)$ of the n-site CA:

$$\begin{aligned} \mathbf{Y}_n(i) &= (y_1, \ldots, y_n) \\ \mathbf{Z}_n(j) &= (z_1, \ldots, z_n). \end{aligned}$$

Then for the $(n+1)$-site CA:

$$\begin{aligned}\mathbf{Y}_{n+1}(i) &= (0, y_1, \ldots, y_n) \\ \mathbf{Z}_{n+1}(j) &= (0, z_1, \ldots, z_n).\end{aligned}$$

For $p = 0$ the CA states are independent random variables so that

$$a(n)_{ij} = \prod_{k=1}^{n} \mathbb{P}(x_k^{t+1} = z_k | x_k^t = y_k).$$

Given that:

$$\mathbb{P}(x_i^{t+1} = 0 | x_i^t = 0) = 1,$$

the probability in the $(n+1)$-site CA for the transition $i \rightarrow j$ is:

$$p(n+1)_{ij} = 1.a(n)_{ij}\,.$$

Similarly:

$$\begin{aligned}\mathbf{Y}_{n+1}(i+2^n) &= (1, y_1, \ldots, y_n) \\ \mathbf{Z}_{n+1}(j+2^n) &= (1, z_1, \ldots, z_n),\end{aligned}$$

so noting that:

$$\begin{aligned}\mathbb{P}(x_i^{t+1} = 1 | x_i^t = 0) &= q \\ \mathbb{P}(x_i^{t+1} = 1 | x_i^t = 1) &= 1 - q,\end{aligned}$$

the transition probabilities for the two lower $2^n \times 2^n$ submatrices are given by:

$$\begin{aligned} a(n+1)_{i+2^n j} &= q.a(n)_{ij} \\ a(n+1)_{i+2^n j+2^n} &= (1-q).a(n)_{ij}\,. \end{aligned}$$

Using lemma 1 to provide the remaining submatrix, the structure of $\mathbf{A}(n+1)$ is:

$$\left(\begin{array}{c|c} \mathbf{A}(n) & \mathbf{0} \\ \hline q\mathbf{A}(n) & (1-q)\mathbf{A}(n) \end{array}\right).$$

Thus the structure of the top left submatrix is preserved in the lower two submatrices and hence by induction $\mathbf{A}(n)$ shares the scaling properties of a truncated Sierpiński gasket and therefore $\mathbf{A}(n)$ is a Sierpiński matrix for all n $\square$

If the matrix is assigned dimensions in space of one unit by one unit, and each element of the matrix is assumed to fill a $\frac{1}{2^n} \times \frac{1}{2^n}$ square, the matrix can be treated as a geometric object. Thus as the transition matrix increases in size, as $n \rightarrow \infty$, the matrix approaches the structure of the Sierpiński gasket. Given this interpretation of the geometrical structure of the matrix, the following lemmas may be stated as corollaries to lemma 1. However, it must be noted that the positive elements of $\mathbf{A}$ tend towards zero as the matrix and CA become infinitely large.

COROLLARY 1.

$\mathbf{A}(\infty) = \lim_{n\rightarrow\infty} \mathbf{A}(n)$ *is a Sierpiński gasket.*

COROLLARY 2.

$$\mathbf{A}(\infty) = \lim_{n\to\infty} \mathbf{A}(n) \text{ is fractal.}$$

The following two lemmas show that the structure of the transition matrix is preserved as it is iterated, which is equivalent to multiple generations of the underlying CA.

LEMMA 3.

An iterated lower triangular matrix is lower triangular.

Consider an $n \times n$ lower triangular matrix $\mathbf{M}$ with elements m_{ij} and denote the rth iterate of $\mathbf{M}$ by $\mathbf{M}^r$ with elements m^r_{ij}:

$$m^{r+1}_{ij} = \sum_{k=1}^{n} m_{ik} m^r_{kj}.$$

By assumption, $m^r_{ij} = 0$ for $i < j$, hence:

$$m^{r+1}_{ij} = \sum_{k=j}^{i} m_{ik} m^r_{kj} = 0 \qquad \forall\, i < j.$$

Thus by induction $\mathbf{M}^r$ is lower triangular for all r □

LEMMA 4.

An iterated Sierpiński matrix is a Sierpiński matrix.

Consider a $2^n \times 2^n$ truncated Sierpiński matrix $\mathbf{M}(n)$ with elements $m(n)_{ij}$ and denote the rth iterate of $\mathbf{M}(n)$ by $\mathbf{M}(n)^r$ with elements $m(n)^r_{ij}$. $\mathbf{M}(1) = \mathbf{M}(1)^1$ is lower triangular so by lemma 3 $\mathbf{M}(1)^2$ is lower triangular and trivially Sierpiński for all r. Consider $\mathbf{M}(n+1)^2$ and take i, $j \in \{1, \ldots, 2^n\}$, so that:

$$
\begin{aligned}
m(n+1)^2_{ij} &= \sum_{k=1}^{2^{n+1}} m(n+1)_{ik} m(n+1)_{kj} \\
&= \sum_{k=1}^{2^n} m(r+1)_{ik} m(n+1)_{kj} + \sum_{k=2^n+1}^{2^{n+1}} m(n+1)_{ik} m(n+1)_{kj} \\
&= \sum_{k=1}^{2^n} m(n)_{ik} m(n)_{kj} + 0 \\
&= m(n)^2_{ij} ,
\end{aligned}
$$

using lemma 2 and the fact that $\mathbf{M}(1)^r$ is lower triangular. Similarly, if $i \in \{2^n+1, \ldots, 2^{n+1}\}$ and $j \in \{1, \ldots, 2^n\}$ then:

$$
\begin{aligned}
m(n+1)^2_{ij} &= \sum_{k=1}^{2^n} m(r+1)_{ik} m(n+1)_{kj} + \sum_{k=2^n+1}^{2^{n+1}} m(n+1)_{ik} m(n+1)_{kj} \\
&= \sum_{k=1}^{2^n} q m(n)_{ik} m(n)_{kj} + \sum_{k=2^n+1}^{2^{n+1}} (1-q) m(n)_{ik} q m(n)_{kj} \\
&= q(2-q) m(n)^2_{ij} ,
\end{aligned}
$$

and if $i, j \in \{2^n+1, \ldots, 2^{n+1}\}$ then:

$$
\begin{aligned}
m(n+1)^2_{ij} &= \sum_{k=1}^{2^n} m(r+1)_{ik} m(n+1)_{kj} + \sum_{k=2^n+1}^{2^{n+1}} m(n+1)_{ik} m(n+1)_{kj} \\
&= 0 + \sum_{k=2^n+1}^{2^{n+1}} (1-q) m(n)_{ik} (1-q) m(n)_{kj} \\
&= (1-q)^2 m(n)^2_{ij} .
\end{aligned}
$$

Thus the structure of $\mathbf{M}(n+1)^2$ is:

$$\left(\begin{array}{c|c} \mathbf{M}(n)^2 & \mathbf{0} \\ \hline q(2-q)\mathbf{M}(n)^2 & (1-q)^2\mathbf{M}(n)^2 \end{array}\right),$$

which is Sierpiński by induction for all n. It remains to show that $\mathbf{M}(n)^r$ is also Sierpiński for any r. By lemma 3, $\mathbf{M}(1)^r$ is lower triangular and trivially Sierpiński for all r. Also, $\mathbf{M}(n)^r$ is lower triangular for all n and r. Suppose that $\mathbf{M}(n)^r$ is Sierpiński. Thus by a straightforward extension of the argument above:

$$\begin{aligned} m(n+1)^r_{ij} &= m(n)^r_{ij} && i,j \in \{1,\ldots,2^n\} \\ m(n+1)^r_{ij} &= q(2-q)m(n)^r_{ij} && i \in \{2^n+1,\ldots,2^{n+1}\}, j \in \{1,\ldots,2^n\} \\ m(n+1)^r_{ij} &= (1-q)^2 m(n)^r_{ij} && i,j \in \{1,\ldots,2^n\}, \end{aligned}$$

so that the structure of $\mathbf{M}(n+1)^r$ is:

$$\left(\begin{array}{c|c} \mathbf{M}(n)^{r+1} & \mathbf{0} \\ \hline q(2-q)\mathbf{M}(n)^{r+1} & (1-q)^2\mathbf{M}(n)^{r+1} \end{array}\right).$$

Thus by induction on n all iterates of a Sierpiński matrix are also Sierpiński matrices □

COROLLARY 3.

All iterates of $\mathbf{A}(n)$ *have an invariant structure and are Sierpiński matrices.*

The following lemma is a simplification of a theorem in Doob (1953) and shows that if a Markov matrix $\mathbf{M}$ has a column with all entries strictly positive, the iterated matrix $\mathbf{M}^r$ will tend towards having all rows identical as $n \to \infty$.

LEMMA 5.

Given an $n \times n$ Markov matrix $\mathbf{M}$ containing a column $\tilde{j}$ with all elements strictly positive, such that:

$$\min_{1 \le i \le n} m_{i\tilde{j}} \quad = \quad \delta \quad > \quad 0,$$

then there exist numbers $m_1, \ldots, m_n$ such that:

$$\lim_{r \to \infty} m_{ij}^r \quad = \quad m_j \qquad \forall\, i, j \in \{1, \ldots, n\}.$$

The following lemma demonstrates that all infection eventually dies out for all initial conditions, for the case $p = 0$.

LEMMA 6.

$\mathbf{A}(n)^\infty = \lim_{r \to \infty} \mathbf{A}(n)^r$ *is given by:*

$$a(n)_{ij}^\infty \quad = \quad \begin{cases} 1 & j = 1 \\ 0 & j \neq 1. \end{cases}$$

$\mathbf{A}(n)$ has been shown to be lower triangular (lemma 1), so that $a(n)_{11} = 1$ and $a(n)_{ij} = 0$ for $j > 1$. Also:

$$a(n)_{1j}^{r+1} \quad = \quad \sum_{k=1}^{2^n} a(n)_{1k} a(n)_{kj}^r \quad = \quad \sum_{k=1}^{2^n} \delta_{1k} a(n)_{kj}^r \quad = \quad a(n)_{1j}^r \,,$$

so that for all r:

$$a(n)^r_{1j} \quad = \quad \begin{cases} 1 & j = 1 \\ 0 & j > 1. \end{cases}$$

Now consider the elements of the first column of $\mathbf{A}(n)$:

$$a(n)_{i1} \quad = \quad q^s,$$

where s is the number of sites of the automaton in state 1:

$$s \quad = \quad \sum_{k=1}^{n} (\Phi^{-1}(i))_k .$$

Since $s \in \{0, ..., n\}, 0 < a(n)_{i1} \leq 1$, for all i and the conditions of lemma 5 are satisfied, which means that all the rows of $\mathbf{A}(n)^r$ become identical in the limit $r \to \infty$. Since the first row is known for any r, all rows must have this form. Thus at large times the iterated matrix tends towards having all elements zero except the first column where all elements are unity. Thus Markov state 1, equivalent to CA configuration $(0, \ldots, 0)$, is absorbing □

8.4. The Case of Zero Recovery.

If $q = 0$ and $p > 0$ then no infection can die out, so there is zero recovery. However, the totally uninfected configuration $(0, \ldots, 0)$ or Markov state $N^t = 1$ is still an absorbing state. Denoting the elements of the transition matrix for $q = 0$ by $\mathbf{Q}$ and the elements by b_{ij}, this means that $b_{11} = 1$ and $b_{1j} = 0 \; \forall \, j > 1$. The following lemmas investigate the structure of $\mathbf{B}$ and show that an infection will eventually spread through the entire population, assuming that at least one cell is initially infected. The structure of $\mathbf{B}$ is a subset of a Sierpiński matrix, as shown in figure 73c.

LEMMA 7.

$\mathbf{B}(n)$ *is upper triangular.*

Since $q = 0$, the only feasible transitions are $0 \rightarrow 0$, $0 \rightarrow 1$ and $1 \rightarrow 1$, so that:

$$x_i^{t+1} \quad \geq \quad x_i^t$$

and therefore:

$$N^{t+1} \quad = \quad \sum_{i=1}^{n} 2^{n-i} x_i^{t+1} \quad \geq \quad \sum_{i=1}^{n} 2^{n-i} x_i^t \quad = \quad N^t.$$

Hence for $i > j$:

$$\mathbb{P}(N^{t+1} = j | N^t = i) \quad = \quad 0$$

and:

$$b(n)_{ij} \quad = \quad 0 \qquad \forall \quad i > j,$$

that is, $\mathbf{B}$ is upper triangular □

The following lemma demonstrates that $\mathbf{B}(n)$ has no column with all elements strictly positive, but sufficient iterations of $\mathbf{B}(n)$ produce a column that has all entries strictly positive, except in the first row.

LEMMA 8.

There exists an r_0 such that:

$$\begin{array}{lcll} b(n)^r_{ij} & = & 0 & \text{for some } \tilde{\imath},\ \forall\ j \qquad r < r_0 \\ b(n)^r_{i2^n} & > & 0 & \forall\ i > 1 \qquad\qquad\quad r \geq r_0 . \end{array}$$

By an identical argument to lemma 6:

$$b(n)^r_{1j} \quad = \quad \begin{cases} 1 & j = 1 \\ 0 & j > 1 \end{cases}$$

for all r. Thus the only column of $\mathbf{B}(n)$ that could have all elements strictly positive is column 1. But, by lemmas 3 and 7, $\mathbf{B}(n)$ is upper triangular, so that:

$$b(n)^r_{i1} \quad = \quad 0 \qquad i > 1$$

for all r. Therefore no column has all elements strictly positive in any iterate of $\mathbf{B}(n)$. However, the above observations mean that the structure of $\mathbf{B}(n)^r$ is as follows:

$$\left(\begin{array}{c|c} 1 & 0 \cdots 0 \\ \hline 0 & \\ \vdots & \tilde{\mathbf{B}}(n,r) \\ 0 & \end{array}\right),$$

where $\tilde{\mathbf{B}}(n,r)$ is upper triangular. Denote $\tilde{\mathbf{B}}(n,1)$ by $\hat{\mathbf{B}}(n)$ and suppose that $\tilde{\mathbf{B}}(n,r) = \hat{\mathbf{B}}(n)^r$. Then if $i,j > 1$:

$$\begin{aligned} b(n)_{ij}^{r+1} &= \sum_{k=1}^{2^n} b(n)_{ik} b(n)_{kj}^r \\ &= b(n)_{i1} b(n)_{1j}^r + \sum_{k=2}^{2^n} b(n)_{ik} b(n)_{kj}^r \\ &= \delta_{i1}\delta_{1j} + \sum_{k=1}^{2^n-1} \hat{q}(n)_{ik} \hat{q}(n)_{kj}^r \\ &= 0 \quad + \quad \hat{q}(n)_{ij}^{r+1}, \end{aligned}$$

so by induction on r, $\tilde{\mathbf{B}}(n,r) = \hat{\mathbf{B}}(n)^r$ for all r. It has already been shown that $\hat{\mathbf{B}}(n)^r$ is upper triangular, so all columns except the last must always have at least one zero element. The structure of the last column is now investigated. Column $j = 2^n - 1$ of $\hat{\mathbf{B}}(n)^r$ represents transitions to the state of total infection, $(1,\ldots,1)$. Firstly, consider initial configurations where there is a single infected state, so that the Markov state N_i is:

$$N_i \quad = \quad 1 + 2^{n-i}$$

for any $i \in \{1,\ldots,n\}$. It is possible for the infection to move out from the initial site of infection at a rate of one site per iteration in each direction, but this is the maximum speed of transmission. Thus the probability that there are $(2r-1)$ infected sites at iteration r is p^{2r}, but the probability that there are more than $(2r-1)$ infected sites is zero. Thus:

$$\hat{b}(n)^r_{N,2^n-1} = \begin{cases} 0 & r < \frac{n+1}{2} \quad n \text{ odd} \\ p^{n+1} & r = \frac{n+1}{2} \quad n \text{ odd} \\ 0 & r < \frac{n}{2}+1 \quad n \text{ even} \\ 2p^{n+1} & r = \frac{n}{2} \quad n \text{ even}, \end{cases}$$

so that the final column of $\hat{\mathbf{B}}(n)^{r_0}$ has all elements strictly positive, where:

$$r_0 = \begin{cases} \frac{n+1}{2} & n \text{ odd} \\ \frac{n}{2}+1 & n \text{ even}, \end{cases}$$

but there is at least one non-zero element for $r < r_0$. It remains to show that this structure of the final column of $\hat{\mathbf{B}}(n)^r$ is preserved for all $r > r_0$. First consider the diagonal elements of $\hat{\mathbf{B}}(n)$, which represent zero change in the automaton, so that:

$$\hat{b}(n)_{ii} = f(i) > 0,$$

since it is always possible for the automaton to remain unchanged, given $p < 1$, which means that the transmission is not perfect and automaton is non-deterministic. Assuming $r > r_0$ and $\hat{\mathbf{B}}(n)^r$ has all elements of the last column non-zero, then the last column of $\hat{\mathbf{B}}(n)^{r+1}$ is given by:

$$\begin{aligned} \hat{b}(n)^{r+1}_{i2^n-1} &= \sum_{k=1}^{2^n-1} \hat{b}(n)_{ik}\hat{b}(n)^r_{k2^n-1} \\ &= \hat{b}(n)_{ii}\hat{b}(n)^r_{i2^n-1} + \sum_{k=1}^{i-1} \hat{b}(n)_{ik}\hat{b}(n)^r_{k2^n-1} + \sum_{k=i+1}^{2^n-1} \hat{b}(n)_{ik}\hat{b}(n)^r_{k2^n-1} \end{aligned}$$

$$\begin{aligned} &\geq \quad \hat{b}(n)_{ii}\hat{b}(n)^r_{i2^n-1} \quad + \quad 0 \\ &= \quad f(i).\hat{b}(n)^r_{i2^n-1} \\ &> \quad 0. \end{aligned}$$

Thus by induction on r, the lemma holds □

LEMMA 9.

$\mathbf{B}(n)^\infty = \lim_{r\to\infty} \mathbf{B}(n)^r$ *is given by:*

$$b(n)^\infty_{ij} \quad = \quad \begin{cases} 1 & i = 1 \quad and \quad i = 2^n, j > 1 \\ 0 & otherwise \end{cases}$$

Since $\hat{\mathbf{B}}(n)$ is upper triangular, $\hat{b}(n)^r_{2^n 2^n} = 1$ for all r. Applying lemma 6 to $\hat{\mathbf{B}}(n)^r$ and using the results of lemma 8:

$$\hat{b}(n)^r_{ij} \quad \equiv \quad b(n)^r_{i+1j+1} \quad = \quad \begin{cases} 1 & j = 2^n \\ 0 & j < 2^n \end{cases}$$

Thus:

$$\lim_{r\to\infty} \mathbf{B}(n)^r \quad = \quad \begin{pmatrix} 1 & 0 & \cdots & 0 & 0 \\ 0 & 0 & \cdots & 0 & 1 \\ \vdots & \vdots & & \vdots & \vdots \\ 0 & 0 & \cdots & 0 & 1 \end{pmatrix}$$

□

8.5. The Full Model.

The following lemma describes the general structure of the transition matrix $\mathbf{P}$(n) for $p, q > 0$, which exhibits a complex iterative structure, shown in figure 73a.

LEMMA 10.

If some of the $2^{n-2} \times 2^{n-2}$ *submatrices of* $\mathbf{P}(n)$ *are denoted by* **A** - **G** *as follows:*

$$\mathbf{P}(n) \quad = \quad \begin{pmatrix} \mathbf{A} & \mathbf{B} & \mathbf{C} & \mathbf{D} \\ \mathbf{E} & & & \\ \mathbf{F} & & & \\ \mathbf{G} & & & \end{pmatrix},$$

then the structure of the matrix $\mathbf{P}(n+1)$ *is given by:*

$$\mathbf{P}(n) \quad = \quad \begin{pmatrix} \mathbf{A} & \mathbf{B} & \mathbf{0} & \mathbf{0} & \mathbf{C} & \mathbf{D} & \mathbf{0} & \mathbf{0} \\ \mathbf{E} & \mathbf{E} & \mathbf{E} & \mathbf{E} & \mathbf{E}^* & \mathbf{E}^* & \mathbf{E}^* & \mathbf{E}^* \\ \mathbf{A} & \mathbf{A} & \mathbf{A} & \mathbf{A} & \mathbf{A} & \mathbf{A} & \mathbf{A} & \mathbf{A} \\ \mathbf{E} & \mathbf{E} & \mathbf{E} & \mathbf{E} & \mathbf{E} & \mathbf{E} & \mathbf{E} & \mathbf{E} \\ \mathbf{F} & \mathbf{F}^* & \mathbf{F} & \mathbf{F}^* & \mathbf{F} & \mathbf{F}^* & \mathbf{F} & \mathbf{F}^* \\ \mathbf{G} & \mathbf{G} & \mathbf{G} & \mathbf{G} & \mathbf{G} & \mathbf{G} & \mathbf{G} & \mathbf{G} \\ \mathbf{F} & \mathbf{F} & \mathbf{F} & \mathbf{F} & \mathbf{F} & \mathbf{F} & \mathbf{F} & \mathbf{F} \\ \mathbf{G} & \mathbf{G} & \mathbf{G} & \mathbf{G} & \mathbf{G} & \mathbf{G} & \mathbf{G} & \mathbf{G} \end{pmatrix},$$

where $\mathbf{E}^* = \mathbf{E}$ *with rows* $\{1, 3, \ldots, 2^{n-2} - 1\}$ *replaced by zeros and* $\mathbf{F}^* = \begin{pmatrix} \mathbf{0} \\ \mathbf{F}_2 \end{pmatrix}$

given that $\mathbf{F} = \begin{pmatrix} \mathbf{F}_1 \\ \mathbf{F}_2 \end{pmatrix}$.

Assuming Markov states $i, j \in \{1, \ldots, 2^{n-2}\}$, then the corresponding automaton states may be

denoted by:

$$\begin{aligned}\mathbf{Y}_n(i) &= (0,0,y_1,\ldots,y_{n-2})\\ \mathbf{Z}_n(j) &= (0,0,z_1,\ldots,z_{n-2})\end{aligned}$$

and the various $2^{n-2}\times 2^{n-2}$ submatrices of $\mathbf{P}(n+1)$ may be analysed in turn. The following functions are defined to allow simplification of transition probabilities:

$$\begin{aligned}f(\alpha,y_i) &= (1-2\alpha)(1+y_i)p+1-\alpha\\ g(\alpha) &= (1-2\alpha)q+\alpha\\ h(\alpha) &= (2\alpha-1)p+1-\alpha\end{aligned}$$

for which it should be noted that $f(\alpha,y_i)>0$, $g(\alpha)>0$ and $h(\alpha)>0$ for $\alpha,\beta,y_i\in\{0,1\}$, given that $0<p<\frac{1}{2}$ and $0<q<1$, as assumed for the full model. The Markov states of $\mathbf{P}(n+1)$ are given by automata $\mathbf{Y}_{n+1}$ and $\mathbf{Z}_{n+1}$ and the transition probabilities for each submatrix of $\mathbf{P}(n+1)$ are found in terms of the submatrices of $\mathbf{P}(n)$.

(i) Submatrix $\mathbf{A}$.

$$\begin{aligned}\mathbf{Y}_{n+1}(i) &= (0,0,0,y_1,\ldots,y_{n-2})\\ \mathbf{Z}_{n+1}(j) &= (0,0,0,z_1,\ldots,z_{n-2})\end{aligned}$$

$$\begin{aligned}p(n+1)_{ij} &= \mathcal{P}^{n+1}(1,0,0)\mathcal{P}^{n+1}(2,0,0)\mathcal{P}^{n+1}(3,0,0)\prod_{k=1}^{n-2}\mathcal{P}^{n+1}(k+3,z_k,y_k)\\ &= \mathcal{P}^{n}(1,0,0).1.\mathcal{P}^{n}(2,0,0)\prod_{k=1}^{n-2}\mathcal{P}^{n}(k+3,z_k,y_k)\\ &= p(n)_{ij}\end{aligned}$$

where $\mathbb{P}^n$ indicates probability in an n-site automaton and $\mathcal{P}^n(a,b,c)$ represents $\mathbb{P}^n(x_a^{t+1} = b | x_a^t = c)$. Also:

$$\begin{aligned}
\mathbf{Y}_{n+1}(i + 2^{n-1}) &= (0, 1, 0, y_1, \ldots, y_{n-2}) \\
\mathbf{Z}_{n+1}(j + \kappa 2^{n-1}) &= (\alpha, \beta, \gamma, z_1, \ldots, z_{n-2})
\end{aligned}$$

where: $\kappa \in \{0, \ldots, 7\}$; $\alpha = \alpha(\kappa)$, $\beta = \beta(\kappa)$ and $\gamma = \gamma(\kappa)$; $\alpha, \beta, \gamma \in \{0, 1\}$. Thus:

$$\begin{aligned}
p(n+1)_{i+2^{n-1}j+\kappa 2^{n-1}} &= \mathcal{P}^{n+1}(1, \alpha, 0)\mathcal{P}^{n+1}(2, \beta, 1)\mathcal{P}^{n+1}(3, \gamma, 0) \prod_{k=1}^{n-2} \mathcal{P}^{n+1}(k+3, z_k, y_k) \\
&= f(\alpha, y_{n-2}) g(\beta) f(\gamma, y_1) \prod_{k=1}^{n-2} \mathcal{P}^n(k+3, z_k, y_k) \\
&= \frac{f(\alpha, y_{n-2}) g(\beta) f(\gamma, y_1)}{(1 - p y_1)(1 - p y_{n-2})} p(n)_{ij} \\
&> 0 \qquad \text{if} \qquad p(n)_{ij} > 0
\end{aligned}$$

(ii) Submatrix $\mathbf{B}$.

$$\begin{aligned}
\mathbf{Y}_{n+1}(i) &= (0, 0, 0, y_1, \ldots, y_{n-2}) \\
\mathbf{Z}_{n+1}(j + 2^{n-2}) &= (0, 0, 1, z_1, \ldots, z_{n-2})
\end{aligned}$$

$$\begin{aligned}
p(n+1)_{ij+2^{n-2}} &= \mathcal{P}^{n+1}(1, 0, 0)\mathcal{P}^{n+1}(2, 0, 0)\mathcal{P}^{n+1}(3, 1, 0) \prod_{k=1}^{n-2} \mathcal{P}^{n+1}(k+3, z_k, y_k) \\
&= \mathcal{P}^n(1, 0, 0).p.\mathcal{P}^n(2, 1, 0) \prod_{k=1}^{n-2} \mathcal{P}^n(k+3, z_k, y_k) \\
&= p.p(n)_{ij} \\
&> 0 \qquad \text{if} \qquad p(n)_{ij} > 0
\end{aligned}$$

(iii) Submatrix $\mathbf{C}$.

$$\begin{aligned}\mathbf{Y}_n(i) &= (0,0,y_1,\ldots,y_{n-2})\\ \mathbf{Z}_n(j+2^{n-1}) &= (0,1,z_1,\ldots,z_{n-2})\end{aligned}$$

$$\begin{aligned}\mathbf{Y}_{n+1}(i) &= (0,0,0,y_1,\ldots,y_{n-2})\\ \mathbf{Z}_{n+1}(j+2^n) &= (1,0,0,z_1,\ldots,z_{n-2})\end{aligned}$$

$$\begin{aligned}p(n+1)_{ij+2^n} &= \mathcal{P}^{n+1}(1,1,0)\mathcal{P}^{n+1}(2,0,0)\mathcal{P}^{n+1}(3,0,0)\prod_{k=1}^{n-2}\mathcal{P}^{n+1}(k+3,z_k,y_k)\\ &= \mathcal{P}^n(1,1,0).1.\mathcal{P}^n(2,0,0)\prod_{k=1}^{n-2}\mathcal{P}^n(k+3,z_k,y_k)\\ &= p(n)_{ij+2^{n-1}}\end{aligned}$$

(iv) Submatrix $\mathbf{D}$.

$$\begin{aligned}\mathbf{Y}_n(i) &= (0,0,y_1,\ldots,y_{n-2})\\ \mathbf{Z}_n(j+2^{n-2}+2^{n-1}) &= (1,1,z_1,\ldots,z_{n-2})\end{aligned}$$

$$\begin{aligned}\mathbf{Y}_{n+1}(i) &= (0,0,0,y_1,\ldots,y_{n-2})\\ \mathbf{Z}_{n+1}(j+2^{n-1}+2^n) &= (1,0,1,z_1,\ldots,z_{n-2})\end{aligned}$$

$$\begin{aligned}p(n+1)_{ij+2^{n-1}+2^n} &= \mathcal{P}^{n+1}(1,1,0)\mathcal{P}^{n+1}(2,0,0)\mathcal{P}^{n+1}(3,1,0)\prod_{k=1}^{n-2}\mathcal{P}^{n+1}(k+3,z_k,y_k)\\ &= \mathcal{P}^n(1,1,0).1.\mathcal{P}^n(2,1,0)\prod_{k=1}^{n-2}\mathcal{P}^n(k+3,z_k,y_k)\\ &= p(n)_{ij+2^{n-2}+2^{n-1}}\end{aligned}$$

(v) Submatrix **E**.

$$\begin{aligned}\mathbf{Y}_n(i+2^{n-2}) &= (0,1,y_1,\ldots,y_{n-2})\\ \mathbf{Z}_n(j) &= (0,0,z_1,\ldots,z_{n-2})\end{aligned}$$

$$\begin{aligned}\mathbf{Y}_{n+1}(i+2^{n-2}) &= (0,0,1,y_1,\ldots,y_{n-2})\\ \mathbf{Z}_{n+1}(j+\kappa 2^{n-2}) &= (0,\beta,\gamma,z_1,\ldots,z_{n-2})\end{aligned}$$

where $\kappa \in \{0,\ldots,3\}$.

$$\begin{aligned}p(n+1)_{i+2^{n-2}j+\kappa 2^{n-2}} &= \mathcal{P}^{n+1}(1,0,0)\mathcal{P}^{n+1}(2,\beta,0)\mathcal{P}^{n+1}(3,\gamma,1)\prod_{k=1}^{n-2}\mathcal{P}^{n+1}(k+3,z_k,y_k)\\ &= (1-py_{n-2})h(\beta)g(\gamma)\prod_{k=1}^{n-2}\mathcal{P}^{n}(k+3,z_k,y_k)\\ &= \frac{(1-py_{n-2})h(\beta)g(\gamma)}{[1-p(1+y_{n-2})]q}p(n)_{i+2^{n-2}j}\\ &> 0 \qquad \text{if} \qquad p(n)_{i+2^{n-2}j}>0\end{aligned}$$

$$\begin{aligned}\mathbf{Y}_{n+1}(i+2^{n-2}+2^{n-1}) &= (0,1,1,y_1,\ldots,y_{n-2})\\ \mathbf{Z}_{n+1}(j+\kappa 2^{n-2}) &= (\alpha,\beta,\gamma,z_1,\ldots,z_{n-2})\end{aligned}$$

where $\kappa \in \{0,\ldots,7\}$.

$$p(n+1)_{i+2^{n-2}+2^{n-1}j+\kappa 2^{n-2}} = \mathcal{P}^{n+1}(1,\alpha,0)\mathcal{P}^{n+1}(2,\beta,1)\mathcal{P}^{n+1}(3,\gamma,1)\prod_{k=1}^{n-2}\mathcal{P}^{n+1}(k+3,z_k,y_k)$$

$$
\begin{aligned}
&= f(\alpha, y_{n-2})g(\beta)g(\gamma)\prod_{k=1}^{n-2}\mathcal{P}^n(k+3, z_k, y_k) \\
&= \frac{f(\alpha, y_{n-2})g(\beta)g(\gamma)}{[1-p(1+y_{n-2})]q}p(n)_{i+2^{n-2}j} \\
&> 0 \qquad \text{if} \qquad p(n)_{i+2^{n-2}j} > 0
\end{aligned}
$$

(vi) Submatrix $\mathbf{E}^*$.

$$
\begin{aligned}
\mathbf{Y}_{n+1}(i+2^{n-2}) &= (0,0,1,y_1,\ldots,y_{n-2}) \\
\mathbf{Z}_{n+1}(j) &= (0,0,0,z_1,\ldots,z_{n-2})
\end{aligned}
$$

$$
\begin{aligned}
\mathbf{Y}_{n+1}(i+2^{n-2}) &= (0,0,1,y_1,\ldots,y_{n-2}) \\
\mathbf{Z}_{n+1}(j+\kappa 2^{n-2}) &= (1,\beta,\gamma,z_1,\ldots,z_{n-2})
\end{aligned}
$$

where $\kappa \in \{4,\ldots,7\}$.

$$
\begin{aligned}
p(n+1)_{i+2^{n-2}j+\kappa 2^{n-2}} &= \mathcal{P}^{n+1}(1,1,0)\mathcal{P}^{n+1}(2,\beta,0)\mathcal{P}^{n+1}(3,\gamma,1)\prod_{k=1}^{n-2}\mathcal{P}^{n+1}(k+3,z_k,y_k) \\
&= py_{n-2}.p.g(\gamma)\prod_{k=1}^{n-2}\mathcal{P}^n(k+3,z_k,y_k) \\
&= \begin{cases} 0 & \text{if} \quad y_{n-2}=0 \\ \frac{p^2 g(\gamma)}{(1-p)q}p(n+1)_{i+2^{n-2}j} & \\ > 0 & \text{if} \quad y_{n-2}=1,\ p(n)_{i+2^{n-2}j}>0 \end{cases}
\end{aligned}
$$

(vii) Submatrix $\mathbf{F}$.

$$
\begin{aligned}
\mathbf{Y}_n(i+2^{n-1}) &= (1,0,y_1,\ldots,y_{n-2}) \\
\mathbf{Z}_n(j) &= (0,0,z_1,\ldots,z_{n-2})
\end{aligned}
$$

$$\begin{aligned}
\mathbf{Y}_{n+1}(i+2^n) &= (1,0,0,y_1,\ldots,y_{n-2}) \\
\mathbf{Z}_{n+1}(j+\kappa 2^{n-2}) &= (\alpha,\beta,0,z_1,\ldots,z_{n-2})
\end{aligned}$$

where $\kappa \in \{0,2,4,6\}$.

$$\begin{aligned}
p(n+1)_{i+2^n j+\kappa 2^{n-2}} &= \mathcal{P}^{n+1}(1,\alpha,1)\mathcal{P}^{n+1}(2,\beta,0)\mathcal{P}^{n+1}(3,0,0)\prod_{k=1}^{n-2}\mathcal{P}^{n+1}(k+3,z_k,y_k) \\
&= g(\alpha)h(\beta)(1-py_1)\prod_{k=1}^{n-2}\mathcal{P}^{n}(k+3,z_k,y_k) \\
&= \frac{g(\alpha)h(\beta)(1-py_1)}{qp(1+y_1)}p(n)_{i+2^{n-1}j} \\
&> 0 \qquad \text{if} \qquad p(n)_{i+2^{n-1}j} > 0
\end{aligned}$$

$$\begin{aligned}
\mathbf{Y}_{n+1}(i+2^{n-1}+2^n) &= (1,1,0,y_1,\ldots,y_{n-2}) \\
\mathbf{Z}_{n+1}(j+\kappa 2^{n-2}) &= (\alpha,\beta,\gamma,z_1,\ldots,z_{n-2})
\end{aligned}$$

where $\kappa \in \{0,\ldots,7\}$.

$$\begin{aligned}
p(n+1)_{i+2^{n-1}+2^n j+\kappa 2^{n-2}} &= \mathcal{P}^{n+1}(1,\alpha,1)\mathcal{P}^{n+1}(2,\beta,1)\mathcal{P}^{n+1}(3,\gamma,0)\prod_{k=1}^{n-2}\mathcal{P}^{n+1}(k+3,z_k,y_k) \\
&= g(\alpha)g(\beta)f(\gamma,y_1)\prod_{k=1}^{n-2}\mathcal{P}^{n}(k+3,z_k,y_k) \\
&= \frac{g(\alpha)g(\beta)f(\gamma,y_1)}{qp(1+y_1)}p(n)_{i+2^{n-1}j} \\
&> 0 \qquad \text{if} \qquad p(n)_{i+2^{n-1}j} > 0
\end{aligned}$$

(viii) Submatrix $\mathbf{F}^*$.

$$\begin{aligned}
\mathbf{Y}_n(i+2^{n-1}) &= (1,0,y_1,\ldots,y_{n-2}) \\
\mathbf{Z}_n(j) &= (0,0,z_1,\ldots,z_{n-2})
\end{aligned}$$

$$\begin{aligned}
\mathbf{Y}_{n+1}(i+2^n) &= (1,0,0,y_1,\ldots,y_{n-2}) \\
\mathbf{Z}_{n+1}(j+\kappa 2^{n-2}) &= (\alpha,\beta,1,z_1,\ldots,z_{n-2})
\end{aligned}$$

where $\kappa \in \{1,3,5,7\}$.

$$\begin{aligned}
p(n+1)_{i+2^n j+\kappa 2^{n-2}} &= \mathcal{P}^{n+1}(1,\alpha,1)\mathcal{P}^{n+1}(2,\beta,0)\mathcal{P}^{n+1}(3,1,0)\prod_{k=1}^{n-2}\mathcal{P}^{n+1}(k+3,z_k,y_k) \\
&= g(\alpha)h(\beta)py_1)\prod_{k=1}^{n-2}\mathcal{P}^{n}(k+3,z_k,y_k) \\
&= \begin{cases}
0 & \text{if} \quad y_1=0 \quad (i\in\{1,\ldots,2^{n-3}\}) \\
\frac{pg(\alpha)h(\beta)}{2pq}p(n)_{i+2^{n-1}j} & \\
>0 & \text{if} \quad y_1=1 \quad (i\in\{2^{n-3}+1,\ldots,2^{n-2}\}) \\
 & \quad p(n)_{i+2^{n-1}j}>0
\end{cases}
\end{aligned}$$

(ix) Submatrix $\mathbf{G}$.

$$\begin{aligned}
\mathbf{Y}_n(i+2^{n-2}+2^{n-1}) &= (1,1,y_1,\ldots,y_{n-2}) \\
\mathbf{Z}_n(j) &= (0,0,z_1,\ldots,z_{n-2})
\end{aligned}$$

$$\begin{aligned}
\mathbf{Y}_{n+1}(i+2^{n-2}+\kappa' 2^{n-1}+2^n) &= (1,\beta',1,y_1,\ldots,y_{n-2}) \\
\mathbf{Z}_{n+1}(j+\kappa 2^{n-2}) &= (\alpha,\beta,\gamma,z_1,\ldots,z_{n-2})
\end{aligned}$$

where $\kappa \in \{0, \ldots, 7\}$ and $\kappa' \in \{0, 1\}$.

$$\begin{aligned} p(n+1)_{i+2^{n-2}+\kappa' 2^{n-1}+2^n j+\kappa 2^{n-2}} &= \mathcal{P}^{n+1}(1,\alpha,1)\mathcal{P}^{n+1}(2,\beta,\beta')\mathcal{P}^{n+1}(3,\gamma,1)\prod_{k=1}^{n-2}\mathcal{P}^{n+1}(k+3,z_k,y_k) \\ &= g(\alpha)\left[\beta' g(\beta)+(1-\beta')2p\right]g(\gamma)\prod_{k=1}^{n-2}\mathcal{P}^{n}(k+3,z_k,y_k) \\ &= \frac{g(\alpha)\left[\beta' g(\beta)+(1-\beta')2p\right]g(\gamma)}{q^2}p(n)_{i+2^{n-2}+2^{n-1}j} \\ &> 0 \qquad \text{if} \qquad p(n)_{i+2^{n-2}+2^{n-1}j} > 0 \end{aligned}$$

(x) Zero submatrix $\mathbf{0}$.

$$\begin{aligned} \mathbf{Y}_{n+1}(i) &= (0,0,0,y_1,\ldots,y_{n-2}) \\ \mathbf{Z}_{n+1}(j+\kappa 2^{n-2}+2^{n-1}+\kappa' 2^n) &= (\alpha,1,\gamma,z_1,\ldots,z_{n-2}) \end{aligned}$$

where $\kappa, \kappa' \in \{0, 1\}$.

$$\begin{aligned} p(n+1)_{ij+\kappa 2^{n-2}+2^{n-1}+\kappa' 2^n} &\propto \mathcal{P}^{n+1}(1,1,0) \\ &\equiv 0 \end{aligned}$$

□

From lemma 10 the invariant structure of the matrix $\mathbf{P}$(n) can be described, for $n > 2$.

COROLLARY 4.

The structure of $\mathbf{P}(n)$ *can be given by:*

$$\mathbf{P}(n) \quad = \quad \begin{pmatrix} \mathbf{A} & \mathbf{B} & \mathbf{C} & \mathbf{D} \\ \mathbf{E} & \mathbf{E} & \mathbf{E} & \mathbf{E} \\ \mathbf{F} & \mathbf{F} & \mathbf{F} & \mathbf{F} \\ \mathbf{G} & \mathbf{G} & \mathbf{G} & \mathbf{G} \end{pmatrix}.$$

The following lemma shows that all infected sites eventually die out, so any epidemic persists for a finite time only.

LEMMA 11.

$\mathbf{P}(n)^{\infty} = \lim_{r \to \infty} \mathbf{P}(n)^r$ *is given by:*

$$p(n)_{ij}^{\infty} \quad = \quad \begin{cases} 1 & j = 1 \\ 0 & j \neq 1. \end{cases}$$

By the same argument used in lemma 6, the first row of $\mathbf{P}(n)^r$ is:

$$p(n)_{1j}^{r} \quad = \quad \begin{cases} 1 & j = 1 \\ 0 & j > 1, \end{cases}$$

for all r, so that Markov state 1 (no infection) is an absorbing state. The elements of the first column of $\mathbf{P}(n)$ can be expressed as:

$$p(n)_{i1} \quad = \quad (1-p)^{s_{0,1}}(1-2p)^{s_{0,2}}q^{s_1},$$

where $s_{0,u}$ is the number of sites of the automaton in state 0 with u neighbours in state 1

$(u = 1, 2)$ and s_1 is the number of sites of the automaton in state 1. Thus $0 < p(n)_{i1} \leq 1$, for all i and the conditions of lemma 5 are satisfied, so all the rows of $\mathbf{P}(n)^r$ become identical in the limit $r \to \infty$ □

By defining the geometric structure of matrices $\mathbf{P}(n)$ in the same way as $\mathbf{A}(n)$, the box-counting dimension of $\mathbf{P}(n)$ in the limit as $n \to \infty$ is fractional, so that as a geometric object the matrix if fractal. The following intuitive lemma (12) is used in the inductive derivation of expressions for the box-counting dimensions.

LEMMA 12.

In limit $n \to \infty$ the number of zero submatrices of a given size within a Sierpiński matrix is constant.

LEMMA 13.

$\mathbf{P}(\infty) = \lim_{n \to \infty} \mathbf{P}(n)$ *has a fractional box-counting dimension.*

The box-counting fractal dimension of the matrix $\mathbf{P}(\infty)$ is given by the scaling with m of the number of submatrices of size $2^m \times 2^m$ which are needed to cover all of the non-zero elements of $\mathbf{P}(\infty)$.

Firstly $\mathbf{P}(n)$ is considered for $n < \infty$. Since it is clear that there are no $2^n \times 2^n$, $2^{n-1} \times 2^{n-1}$ or $2^{n-2} \times 2^{n-2}$ zero submatrices, let the number of total zero submatrices in $\mathbf{P}(n)$ of size $2^{n-m-2} \times 2^{n-m-2}$ be denoted by $\psi(m)$. The total number of $2^{n-m-2} \times 2^{n-m-2}$ submatrices is 4^{m+2}, so the number of submatrices needed to cover all of the non-zero elements is $4^{m+2} - \psi(m)$. Similarly, let $\psi_A(m), \psi_B(m), \ldots$ denote the number of $2^{n-m-2} \times 2^{n-m-2}$ zero submatrices in the submatrices $\mathbf{A}, \mathbf{B}, \ldots$, as shown in lemma 10. Then in general $\psi_Z(m)$ is four times $\psi_Z(m-1)$ plus the number of $2^{n-m-2} \times 2^{n-m-2}$ zero submatrices that are not part of a larger zero submatrix. For $m = 1$ and $m = 2$ new zero submatrices are created, as shown by the structure given in lemma 10. For $m > 1$, $2^{n-m-2} \times 2^{n-m-2}$ zero submatrices of $\mathbf{P}(n)$ are equivalent to $2^{n-m-1} \times 2^{n-m-1}$ zero submatrices of $\mathbf{P}(n-1)$. However, in the infinite limit, it can be

assumed by lemma 12 that ψ is the same for $\mathbf{P}(n)$ and $\mathbf{P}(n-1)$. Thus for $m > 2$:

$$\begin{aligned}
\psi_A(m) &= \psi_A(m-1) + \psi_B(m-1) + 2\psi_E(m-1) \\
\psi_B(m) &= 2\psi_E(m-1) \\
\psi_C(m) &= \psi_C(m-1) + \psi_D(m-1) + 2\psi_{E^*}(m-1) \\
\psi_D(m) &= 2\psi_{E^*}(m-1) \\
\psi_E(m) &= 2\psi_A(m-1) + 2\psi_E(m-1) \\
\psi_F(m) &= \psi_F(m-1) + \psi_{F^*}(m-1) + 2\psi_G(m-1) \\
\psi_G(m) &= 2\psi_F(m-1) + 2\psi_G(m-1) \\
\psi_{E^*}(m) &= 2\psi_C(m-1) + 2\psi_{E^*}(m-1) \\
\psi_{F^*}(m) &= 2\psi_G(m-1) \\
\psi(m) &= 4\psi(m-1) + \psi_A(m) + \psi_B(m) + \psi_C(m) + \psi_D(m) + (\psi_E(m) + \psi_F(m) + \psi_G(m)) .
\end{aligned}$$

The fractal dimension F_B is then given by:

$$F_B = \lim_{m\to\infty} \frac{\log\left(4^{m+2} - \psi(m)\right) - \log\left(4^{m+1} - \psi(m-1)\right)}{\log 2}.$$

Now, a lower bound can be put on $\psi(m)$ by noting that:

$$\psi_A(m) \geq \psi_A(m-1) \geq \cdots \geq \psi_A(2) = 2$$

and:

$$\psi(m) \geq \psi_A(m) + 4\psi(m-1) > 4\psi(m-1).$$

Thus:

$$4^{m+2} - \psi(m) \quad < \quad 4\left[4^{m+1} - \psi(m-1)\right],$$

so that:

$$\begin{aligned} \log\left(4^{m+2} - \psi(m)\right) - \log\left(4^{m+1} - \psi(m-1)\right) &\equiv \log\left[\frac{4^{m+2} - \psi(m)}{4^{m+1} - \psi(m-1)}\right] \\ &< \log 4 \\ &= 2\log 2 \end{aligned}$$

and hence $F_B < 2$ □

The use of lemma 12 may be verified numerically, by evaluating F_B firstly directly from the structure of a sample (finite) matrix and secondly using the expressions for ψ derived above. Such methods both yield a value of 1.93 for F_B, so the approaches are equivalent. The initial values for ψ are:

$$\begin{array}{llll} \psi_A(1) = 0 & & \psi_A(2) = 2 \\ \psi_B(1) = 2 & & \psi_B(2) = 0 \\ \psi_C(1) = 0 & & \psi_C(2) = 2 \\ \psi_D(1) = 2 & & \psi_D(2) = 0 \\ \psi_E(1) = 0 & & \psi_E(2) = 0 \\ \psi_F(1) = 0 & & \psi_F(2) = 2 \\ \psi_G(1) = 0 & & \psi_G(2) = 0 \\ \psi_{E^*}(1) = 0 & & \psi_{E^*}(2) = 0 \\ \psi_{F^*}(1) = 0 & & \psi_{F^*}(2) = 0 \\ \psi(1) = 4 & & \psi(2) = 28. \end{array}$$

8.6. Extensions.

The one-dimensional CA model is still being investigated further and in particular the rela-

tionship between the mean field approximation, a pairwise approximation and the full spatially extensive model is being studied analytical and numerical techniques, along with the observation that fluctuations from the mean field predictions are typically Gaussian. Many of the results that exist in the literature for continuous time models, such as the Contact Process, are being extended to the discrete time case presented here (I. Mezic, personal communication). Particularly noteworthy results are the exponential dependence of mean survival time with system size (n) and the catastrophic nature of the death process.

9. Conclusions.

'Many of earth's habitats, animals and plants that we know as rare may not be known at all by future generations. We have the capability and the responsibility. We must act before it is too late.' - The Dalai Lama 1990

The approach of spatially explicit ecological models has been shown to be both necessary and useful in many circumstances because of the range of insights and empirically testable results that have been obtained. The majority of the models presented here have concerned plant communities; single and multiple species systems have been investigated using a variety of numerical and graphical techniques.

Both short and long term systems have been modelled, with the former providing qualitatively distinctive results that can potentially be tested in field conditions (chapters 3 to 5) and the latter adding to the understanding of long term ecological processes where experiments cannot feasibly be undertaken (chapters 5 and 7). Throughout, the aim has been to construct simple mechanistic models which are able to promote understanding of the processes and dynamics involved (section 1.3.2).

A CML model of a single plant species has been described and simulated, using a discrete spatial extension of the mapping of local interactions presented by Aikman & Watkinson (1980) (chapter 3). Simulations of the system demonstrate the presence of competitive interference and exhibit the size structures which subsequently develop in the population. Asymmetric competition between neighbouring plants is observed to give rise to increased size variability compared with symmetric competition. This result favours the assertion of Miller & Weiner (1989) that higher size variation at higher density implies greater competitive asymmetry, at the expense of Bonan's (1988; 1991) claim that such observations arise by local spatial effects alone. Thus plant population size variation can be used as evidence for discriminating between asymmetric and symmetric competition. It is not being suggested, however, that spatial effects are unimportant. On the contrary, the local spatial interactions are fundamental to the growth patterns of the individual plants and hence profoundly influence the population statistics. It is

the interaction of the spatial processes with the asymmetric competition that gives rise to the characteristic response of the size structure to the stand density.

A lattice-based data set was obtained from a field experiment on carrot plants which is a suitable application of the CML model. The single, double and triple cohorts of seedlings sown in checkerboard configurations are easily mimicked by the model and artificial harvests can be 'taken' numerically to correspond to the available data. The plant CML model provides a clear indication that carrot plants grown in monoculture experience predominantly asymmetric competition, resulting in high levels of suppression of later cohorts of plants. The presence of asymmetry means that even-aged monocultures at high densities which are not grown on a completely regular lattice are likely to develop high levels of size variation, which is unsuitable in many agricultural applications. Thus, having established asymmetry in a crop, there is a balance to be found between the desirable high yields of a high density stand and the commercial undesirability of excessive size variability.

The relationship of long- and short-lived species has been investigated by a complex extension of the CML from a single growing season in monoculture to multiple years in a two species system (chapter 4). In particular, various spatial analyses have demonstrated the impact of perennial plants on annual species. Visual inspection, back up by numerical analysis, of the CML patterns shows that the perennial species imposes an aggregation pattern to a greater extent than the annuals regardless of the presence or absence of the annuals. The perennials are also seen to induce a complex scaling or multifractal character in the annuals. This provides a quantitative representation of processes acting over a range scales, with different patterns of mass distribution corresponding to different biological mechanisms. This leads to the need to ask new biological questions about the relationships of mass distributions and mechanistic processes within plant communities.

The annual-perennial system is thus asymmetrical with the perennials influencing the annuals to a far greater extent than the annuals influence the perennials. This has also been shown empirically, for example by transplantation experiments with analyses of of selection pressures,

that annuals have restricted success when placed within areas of established perennial vegetation (Davy & Smith, 1988). The conclusions of this model point to a potential problem in both empirical and theoretical plant community studies. The time scales involved must not solely correspond to a particular species of interest, but must also take into account any longer-lived species that form part of the local environment. Thus a model may require time scales substantially in excess of the life expectancy of the target species. This will often impose a severe computational penalty on plant community models.

In spite of the asymmetrical annual-perennial relationship, the evolution of the annual type of life history strategy and the presence of annual species in association with perennial species across a broad range of habitats provides a clear indication of advantages to the annual strategy. In some situations perennial vegetation structures will provide protection for the annuals, while the annuals are sometimes better adapted to deal with spatiotemporal environmental stochasticity. Therefore, despite the asymmetry of the interspecific interactions in the annual-perennial system, as quantified by the techniques presented here, a frequently successful and ubiquitous plant community structure is seen.

The vital role of spatial dimension in plant ecosystems has been further emphasised by the annual-perennial model. Although a mean field analytical approximation provides a fair prediction of the coexistence of annual and perennial species at intermediate reproductive rates, it is wholly inadequate towards the extremes of reproductive rates. Thus spatial extensiveness plays a key part in the species interactions via either a refuge effect or a restriction of dispersal depending on the part of the parameter range.

The widespread occurrence of environmental heterogeneity at many scales in ecological systems prompts the inclusion of an explicit resource base in the plant CML model (chapter 5). This allows the impact of resource heterogeneity on plant growth to be assessed and, just as importantly, the extent of alteration of the environment by plants can be studied. The two way relationship between a species and its environment is all too often overlooked. In general, a plant will profoundly influence both its biotic and physical surroundings by direct and in-

direct competitive effects, including crowding, allelopathy, depletion of mineral nutrients and the mediation of herbivore and pathogen effects. The CML model certainly is able to display this complex interdependence of organism and environment as different mechanisms and model parameters are investigated.

In its simplest form of one species, a homogeneous resource supply and a single growing season, the resource CML demonstrates suppression of growth by high resource depletion and crowding. Positive and negative feedback processes interact to affect the extent of size hierarchy development in the plant population. The increase of size variation at high densities indicates asymmetry of competitive interactions, verifying the conclusions of chapter 3. The coefficient of variation of resources levels provides a good - and in some circumstances better - indicator of asymmetry than mass variation.

Heterogeneous resource distributions can be imposed on the lattice using an algorithm developed here for generating patchy patterns. The scale of patches is clearly a significant factor in the response of a system, so it is imperative that the grain of the resource patterns can be controlled. The grain determines whether there is any difference between the environment experienced at the level of individual plants and in the population as a whole. For example, in an environment with large contrasting patches, an individual must usually rely on a single resource patch type, while the population may have access to all patch types. A small grain, on the other hand, allows each individual to exploit all patch types.

In monocultures, patchy resource distributions lead to suppressed stand yields and enhanced population variability, which demonstrates the importance of environmental heterogeneity in crops, where yield and size constancy are both important economically. An interesting phenomenon is exhibited whereby fine scale variation allows greater yields under highly contrasting patches than under intermediate contrasts. Competitive mechanisms and neighbourhood interactions lead to a differentiation in size between small suppressed plants and large dominant individuals, so a resource environment echoing this distribution may be optimal. This observation supports the idea that community and environment coevolve, as the biota both adapt to

and modify the physical environment.

The inference of competitive asymmetry from increases in mass variation with density (chapter 3) is dependent on relative homogeneity of resource distribution. The increase in size variability at high density becomes less marked as the contrast between rich and poor patches rises, but is only substantially obscured when the poor patches are deprived of virtually all resources. Thus the absence of increasing mass variation with rising density cannot be taken to imply symmetry of competitive interference, as it may alternatively be due to the confounding influence of resource heterogeneity. The environmental factor must therefore always be considered before an inference of competitive asymmetry is made. In the case of the carrot plants studied in chapter 3, the experimental conditions are controlled, so resources are likely to be largely homogeneous and the conclusions remain valid.

The selection of different characteristics over periods of many years can be studied using an extension to the resource-based CML to longer time scales. Although a constant environmental pattern means that a single species produces a higher yield with localised seed dispersal, in competition wider dispersal is favoured. The central role played by environmental predictability is highlighted by the extinction of species with overly-restricted dispersal in a randomly-changing environment. A second observation is that community behaviour cannot in general be inferred from the dynamics of a single species. This is another aspect of the argument that community and environment evolve together, as the environment of a single species can be considered to be not only the physical factors involved but also all the other species in the same system.

The resource environment is the key system feature investigated in the final part of chapter 5, which makes a preliminary exploration of the ecology of seed sizes. There is a long-held and widespread belief in agricultural science that identifying an optimal seed size is a significant factor in maximising crop yield, but there is no consensus as to whether small or large seeds are best.

From a more ecological viewpoint, there is also a lack of agreement on the relationship of seed size and environment. There is much evidence that large seeds - with their intrinsic nutrient

reserves - are adapted to tolerate adverse conditions such as drought or shade. It is likewise asserted that these reserves give a large seed a competitive head start in areas of intense competition, which are likely to correspond to rich resources. Thus there are very different environmental types which appear to impose selective forces in favour of larger seeds. It can, however, be argued that the richest environments provide adverse conditions, as competition also leads to nutrient deprivation, the difference between this and the former case of the poorest environments being that the disadvantages arise respectively from biotic and physical (or indirect biotic) sources.

The fact that seeds vary widely in size, by many orders of magnitude, implies that there must also be selective pressures acting in favour of small seeds. One such is the possibility of wide dispersal, although it must be noted that dispersal distance and propagule size have a far from simple relationship. This is an interesting feature, but the large range of spatial scales involved is not immediately suited to this type of model, which is restricted to scales ranging over only two orders of magnitude or so. A second feature of small-seeded species, concerns relative growth rates: negative correlations of seed size and relative growth rates have been reported in many studies and provide the mechanism whereby small seeds counter the head start of large seeds. Resource supply and growth rates are easily studied using the resource CML making seed size ecology a suitable application of this model.

Assuming these features and pairwise competition in a homogeneous environment, low resource levels favour small seeds and high resource levels favour large seeds, with the preferred type driving the other to extinction. An elegant transitional behaviour is seen in intermediate environments where the two species types coexist, with an increasing proportion of the large-seeded species as the resource levels rise.

A heterogeneous environment adds an extra dimension to the competitive interactions. Coexistence of large- and small-seeded species is seen if sufficiently large patches of high and low resources are imposed on the system. As would be expected, large-seeded plants monopolise the high resource patches. Although small-seeded plants are dominant in poorer environments,

they naturally perform better in monoculture on the high resource regions, so they are seen to cluster around the edges of the high resource patches.

These observations are, however, dependent on the grain of the system. If the patches are small and the high and low resources are closely intermingled, then large seeds always fall sufficiently near high resource supplies and the small-seeded species is excluded. Thus, while a homogeneous landscape sees a transition of species' dominance as resource levels varies, heterogeneity witnesses a transition between single species dominance and coexistence as the grain of the resource patterns changes. This reflects back on the earlier observation that an individual may experience an environmental type different from that of the whole population. In this way, the CML model exhibits qualitative changes in community structure as assumptions of the model system are varied, which are potentially observable in real systems.

The plant lattice model has thus already been shown to have several applications in both theoretical and more empirical plant communities. The models are eminently usable in widely ranging areas of ecology and would feasibly make particularly strong contributions where associated empirical studies could be carried out. One proposed experimental project would obtain data from populations of chrysanthemums. These crops are grown commercially in lattice configurations and so could potentially provide ideal data for validation of a version of the lattice model. Optimisation of planting patterns could be investigated by a combination of theoretical and field work. The CML can, for example, be used to select from the myriads of possible plant configurations those which are most likely to produce maximal crop yields.

At the other end of the scale from such detailed and specific cases, the lattice model can continue to be developed for the purpose of addressing general ecological issues and promoting broader understanding of ecosystems functioning. If a basic model with minimal assumptions can produce significantly different empirical outcomes from different suggested mechanisms, then these predictions can be tested in real systems. There is good capability to combine these modelling approaches with laboratory work in simple controlled ecosystems, such as the 'Ecotron' at Silwood Park (Lawton et al., 1993) and the controlled microcosms at the NERC

Unit of Comparative Plant Ecology (U.C.P.E., 1995). Different conditions in simplified real systems can be examined in conjunction with different assumptions in the model systems, thus promoting understanding of the fundamental controlling mechanisms of real systems.

The lattice model has the capacity to be extended beyond the plant community itself to associated organisms and issues such as herbivory, seed predation and the effects of changes in climate and land use.

Herbivory can have a strong effect on the abundance, spatial distribution and size distribution of single plant species and communities (Louda et al., 1990). Selective consumption and modification of competitive ability of different plant species by herbivores can alter the outcome of competition in multispecies communities. The CML could be adapted in a straightforward manner for herbivory, for example by imposing dynamical patterns of mass reduction of the individual plants in the lattice cells. In possible conjunction with a strong size-dependence of reproductive output, the impact of various types of herbivory on one or more species of plants can be investigated.

The explicit treatment of the seed dispersal stage in the lattice model, at the level of the individual seeds, means that the model lends itself to the study of topics such as seed predation (*granivory*). The high numbers of seeds that are often produced by single plants point to high potential selective forces on seed attributes, so that predation can be a significant mediating factor in a plant community (Crawley, 1992). The lattice model could usefully be applied to such issues as the effects of pre- and post-dispersal predation and the impact of different spatiotemporal patterns of predation on persistence and distribution of plant species.

The CML could also be developed to investigate mechanisms at a more fundamental level, using a more explicitly physiological approach. Resources could be partitioned into above ground (photosynthate) and below ground (mineral nutrient) sources and the relative importance of these investigated under a range of conditions. The size of the neighbourhood over which a plant assimilates resources could be extended beyond the four cells used here. This could allow different resources to be treated over different spatial ranges, as a representation of different

foraging characteristics. In particular, it would be insightful to provide a model intermediate between the simple lattice used here and the detailed translocation model used by Colasanti (U.C.P.E., 1995). In this way the interdependence of plant population structure and resource dynamics could be investigated.

All of the above issues - resource dynamics, herbivory, physiological response - will interact with changing environmental conditions as climate and land use are modified by natural or anthropological forces. Small scale empirical work is being carried out on the effect of such factors as changes in temperature and atmospheric composition, but large scale predictions are inevitably restricted to modelling techniques. These lattice models are a good basis for such models and could easily incorporate simple physiological mechanisms to allow the effects of temperature, carbon dioxide level and other components to be investigated at the level of individual plants, single species and more complex multispecies communities. As described above, collaboration of these modelling methods with existing experimental microcosm studies will provide an good basis for studying and eventually predicting the change in plant dynamics as their environmental background evolves.

The red grouse model of chapter 6 establishes the alternative methodology required by animal rather than plant ecosystems. The motile nature of the red grouse adds to the complexity and encourages the use of the discrete state CA type of mode, an artificial ecology. Computational intensity is clearly a problem in this system and places a restriction on the length of simulations and number of replicates. Nonetheless, different processes for producing the characteristic cyclic population dynamics observed in field data are able to be implemented and tested. This allows some suggestions to be dismissed and others to be identified as possible mechanisms. This example illustrates both the benefits and disadvantages of spatially explicit modelling techniques in ecosystem analysis.

The difference of approach needed to study systems with longer temporal and spatial scales is illustrated in the final part of this thesis, including Appendix A. As with the complex grouse model, larger scale systems need simpler modelling procedures to be practicable. The CA

of chapter 7 demonstrates the use of simple discrete state models for assessing the relative importance of different processes in a mosaic ecosystem.

The dominant role of *memory* or *longevity* (Remmert, 1991) as a mechanism in ecological pattern formation is clearly demonstrated. A beech forest mosaic cycle displays spatial structure if memory is present in the system, but has random distributions otherwise. This contradicts the claim of Wissel (1991; 1992a) that the formation of the mosaic depends critically on local synchronisation by radiation death, but his failure to observe patches in the absence of radiation death may be attributed to insufficient allowance for transience. Although the memory does not in itself cause the emergence of structure from the model's interactions, it amplifies other aggregating mechanisms within systems. This conclusion is supported by comparison with a non-spatial (Markovian) analytical model, which demonstrates that the spatial dimensions are not important in the absence of memory.

The role of the explicit longevity of the species can be understood by considering pattern formation as a balance of aggregating and randomising processes. The radiation and early colonisation mechanisms provide pattern aggregation, while death through senility tends to break down spatial structure. In the *memory* case, death in old age is restricted to a few of the beech states, so there is only a weak randomising effect and clumped patterns emerge. In the *no memory* case, all beech trees are susceptible to this mortality, which leads to a widespread breakdown of spatial structure.

A variety of techniques are used to illustrate further the part played by memory within the beech forest system. The aggregation of different versions of the model is quantified numerically and confirms that the memory mechanism is the main promoter of a clumped spatial pattern. Memory in the system is linked both to chaotic behaviour and to low dimensionality of the system dynamics, so the character of the dynamics is fundamentally altered by the inclusion of memory. However, the no memory case is very noisy and offers little more global predictability than the chaotic memory case.

The vital role of memory is further illustrated using a second CA model in a different area -

epidemiology. In this case memory refers to the duration of infectious and immune phases in an SIR epidemic, so that this CA is stage-structured rather than age-structured. This supports the use of the general term 'memory' rather than 'age-structured'. Memory amplifies the local synchronisation induced by the infection process and leads to marked ring patterns in the CA grid. The memory plays a key part in determining the behaviour of the system, as an enforced delay in recovery from infection and in return to susceptibility means that the susceptibles are kept separated from the epidemic waves for significant periods. Memory can thus cause the epidemic to wipe itself out completely below a certain threshold lattice size, as well as leading to the emergence of characteristic spatiotemporal patterns. A very simple one-dimensional model verifies these conclusions analytically.

The spatial pattern formation in such large scale artificial ecosystems, such as the forest model, is ideally suited to comparison with real systems using modern data collection techniques, primarily satellite imagery. Data on vegetation patterns are now increasingly available over wide spatial scales by the interpretation of radiation maps gathered by satellites. Configurations of reflected radiation from different vegetational types can be combined with ground-truthing studies to obtain patterns for comparison with artificial ecology output. Some of the numerical techniques developed here for the lattice models are equally applicable to grid-based satellite data. In this way the real and artificial ecosystems can be compared and underlying mechanisms explored further into the future.

The primary drawback of satellite data is the restricted time scale: although wide spatial scales are being surveyed, the time scale is limited by the real time that has elapsed since the technique of satellite imagery was first developed. This does, however, again point to the invaluable role played by the development of models. Although it is possible to find current examples of ecosystems at all stages of succession - which may be cyclic - data on long term dynamical progression is simply not available and cannot be produced in the foreseeable future. Therefore modelling must be combined with the snapshots of ecological structures that are available at this particular moment in time, in an attempt to describe and understand the entire course of dynamical ecosystems. This understanding can then eventually lead to reliable prediction

of the future of the Earth's major ecosystems and thus to the implementation of appropriate protection and management schemes for the entire biosphere.

Lattice models are thus widely applicable in theoretical plant (and animal) ecology and have great potential for further development in conjunction with experimental spatial studies.

Appendix A. A Cellular Automaton Model for Juvenile Selection in Plant Species.

Chapter Summary

An artificial ecology version of the plant coupled map lattice of chapters 3 to 5 similar to a cellular automaton, is constructed. It is presented as an illustration of the spatial modelling techniques used throughout this thesis, although spurious results are obtained; in particular the necessity of computational simplification is shown for situations where longer time scales are required.

The conjecture of Salisbury that important selection occurs at the juvenile stage of a plant's life history is studied, along with the rejection of the idea by Fisher on the grounds of low reproductive value of juvenile plants.

Probability tables are drawn up to provide a mapping between the coupled map lattice of chapter 3 and the growth phase for selected discrete automaton states. Alleles are described which allow for the bias of a plant's success at either the adult or juvenile stage. No genetic selection operates in a mean field version of the model, but the spatial model demonstrates selection for a varied life history, favouring the allele for juvenile bias, but allowing the allele for adult bias to coexist with it at lower levels.

'The aims of scientific though are to see the general in the particular and the eternal in the transitory' - Alfred North Whitehead

1. Introduction.

A CA version of the plant CML of chapters 4 - 5 is presented here. Some of the results obtained appear to be spurious and for this reason the model is confined to an appendix. Nonetheless, the

approach taken highlights the relationship between CA and CML and demonstrates a method of overcoming the unfeasible computational intensity that would result from modelling this system with a CML.

The specific issue of genetic selection in plant species is addressed here.

In 1930, Salisbury suggested in a short article in Nature that selection acts at the seedling stage of the life cycle of a plant (Salisbury, 1930). He justified this claim with the observation that the greatest mortality occurs at this early stage, hence there is the most opportunity for stronger genotypes to gain an advantage. However, in the same year, Fisher replied with a letter which rejected Salisbury's conjecture, on the basis that seedlings have very low *reproductive value* (Fisher, 1930). This was a theoretical concept which means that while a large number of seedlings contribute to the gene pool, they each have very low importance, compared with the adult plants.

The ideas of Salisbury and Fisher are re-examined here via a CA model.

2. Reduction of the Coupled Map Lattice to a Cellular Automaton.

It is noted in chapter 3 that under absolutely asymmetric competition the hierarchy of plant sizes generated by the plant CML is limited to five discrete classes (figure 10). Consideration of crop data (section 3.10) shows that a substantial degree of asymmetry is present in plant monocultures. The CML distribution is bimodal: most plants are either large or small, while a few take one of three intermediate sizes. The different size classes can be mapped to CA states, the three intermediate classes being aggregated to form a single CA state, to reduce the complexity of the model and hence limit the computation. The adult sizes are therefore restricted to *small*, *medium* and *large*, denoted here by $k = 1, 2$ and 3 respectively.

The CML was run $\sim 10^3$ times for a complete range of densities to construct a mapping from the seedling neighbourhood type to the adult size distribution. The neighbourhood type of a plant was initially classified by the number of plants in the first, second and third neighbourhoods (figure 74a). Probability tables were drawn up for the mapping from seedling neighbourhood

to adult size using the CML data. The third neighbourhood was found to have relatively little effect on the mapping, so only the first two neighbourhoods are used in the CA.

The probability of getting an adult of size k if there are i and j plants in the first and second neighbourhoods respectively is given by p_{ijk}. p_{ijk} therefore provides the CA rules, by giving the transition probabilities between juvenile and adult states. The probability mapping is illustrated in figures 74b - d.

It now remains to specify the transition between adults and the juveniles of the following season. The adults produce a number of seeds in proportion to their sizes, which are scattered into the surrounding four cells. At most one seed per cell is then able to grow into a seedling and hence survive into the next generation of adults, according to the seedling neighbourhood configurations. There are therefore three phases of the model: seedling $\rightarrow$ adult, adult $\rightarrow$ seeds and seeds $\rightarrow$ seedling. This is therefore not strictly a CA and is more accurately termed an AE.

3. Incorporation of Genetics in the Artificial Ecology.

There are three stages in the life history: *seed*, *seedling* and *adult*, with three corresponding transition mechanisms: *growth*, *reproduction* and seed *survival*. The plants are assumed to have a single locus **A**, with three alleles, expressed at the survival and reproduction stages. The alleles are arranged as follows:

- **A1** favours reproduction at the expense of seed survival
- **A2** is neutral to reproduction and seed survival
- **A3** favours seed survival at the expense of reproduction.

The CA thus has two state variables. The first describes the plant *phenotype*: presence/absence at the seedling stage; size (small/medium/large) at the adult stage; the number of seeds at the seed stage. The second variable describes the *genotype* as **A1**, **A2** or **A3**.

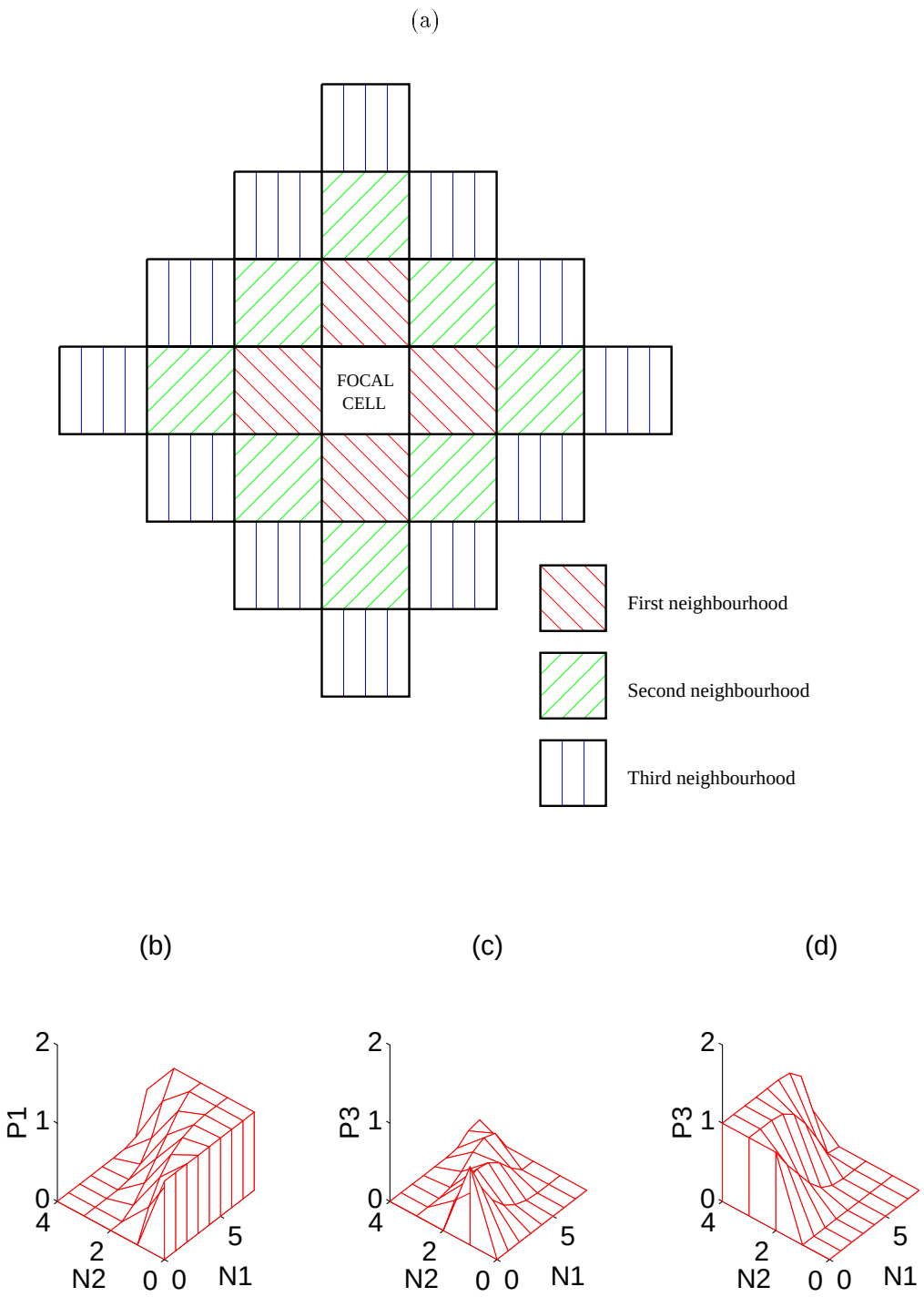

Figure 74: Construction of the genetic CA model from the CML model. (a) Representation of the CML neighbourhoods. (b) - (d) Probabilities $P1$, $P2$, $P3$ of getting (a) small (b) medium and (c) large focal plants given $N1$ neighbours in the first neighbourhood and $N2$ neighbours in the second neighbourhood.

(a) Growth.

The growth mechanism acts on the seedlings. The grid cells contain either 0 or 1 seedlings. Each seedling assesses the number of nearest neighbours and grows to a small, medium or large plant according to the probability tables described in the previous section.

(b) Reproduction.

Two factors affect the production of seeds by adults: the adult size (phenotype) and the **A** locus (genotype). The number of seeds is weighted by a *size factor*, depending on parental size, and by a *gene factor*, determined by the allele at locus **A**. The weighting factors are simply applied multiplicatively. When the number of seeds has been determined by the phenotype and genotype, the seeds are redistributed into the parent's focal cell and four nearest neighbour cells. The genotype of each scattered seed is noted, so that the number of seeds of each genotype in each cell is ascertained.

(c) Seed survival.

One seed in each cell is chosen to have the potential to survive to a seedling. The seed is chosen randomly, in proportion to the numbers of seeds of each genotype present in each cell. These seed numbers are weighted by genetic factors controlled by the **A** locus. Thus some genotypes may be chosen preferentially over others. The chosen seed is then given a fixed chance of surviving, which results in either an empty cell (juvenile state 0) or a seedling of the chosen genotype (juvenile state 1).

4. A Mean Field Approximation.

The mean field approximation to the AE follows the proportion of seedlings in the population, as this is the simplest life stage. The proportion of cells with a seedling of genotype α is j_α, where α represents the allele at locus **A**. Thus the total density of seedlings, as a proportion of cells occupied, is given by ρ:

$$\rho = \sum_\alpha j_\alpha .$$

The probabilities of having i seedlings in neighbourhood 1 and j seedlings in neighbourhood 2 are approximated respectively by $\pi_i^{(1)}$ and $\pi_i^{(2)}$, assuming a sufficiently large grid:

$$\pi_i^{(1)} = \left(\begin{array}{c} 4 \\ i \end{array} \right) \rho^i (1-\rho)^{4-i}$$

$$\pi_i^{(2)} = \left(\begin{array}{c} 8 \\ i \end{array} \right) \rho^i (1-\rho)^{8-i} .$$

The probability that an adult is of size k and genotype α is given by $P_{\alpha k}$ (equation (51)), where p_{ijk} is the probability that seedling neighbourhood types i, j lead to a size k adult.

$$P_{\alpha k} = \sum_{ij} j_\alpha \pi_i^{(1)} \pi_i^{(2)} p_{ijk} \tag{51}$$

The expected number of seeds from an adult of type α and size k is S_α (equation (52)). σ_k is the size factor which gives the phenotypic dependence of seed production on parent size. r_α is the gene factor which gives the dependence of seed production on locus **A**.

$$S_\alpha = \sum_k \sigma_k P_{\alpha k} r_\alpha \tag{52}$$

The probability that a cell has a surviving seed of type α is therefore:

$$\frac{P_g S_\alpha s_\alpha}{\sum_{\alpha'} S_{\alpha'} s_{\alpha'}},$$

where P_g is the probability any chosen seed survives and s_α is the weighting factor for survival at locus **A**. This is therefore equal to the proportion of seedlings of type α in the next generation, that is, j'_α. The generation may therefore be described fully in the mean field by:

$$j'_\alpha = \frac{P_g \sum_{ijk} \begin{pmatrix} 4 \\ i \end{pmatrix} \begin{pmatrix} 8 \\ i \end{pmatrix} \{\sum_{\alpha'} j_{\alpha'}\}^{i+j} \{\sum_{\alpha'} (1 - j_{\alpha'})\}^{12-i-j} \sigma_k p_{ijk} r_\alpha s_\alpha j_\alpha}{\sum_{\alpha'' ijk} \begin{pmatrix} 4 \\ i \end{pmatrix} \begin{pmatrix} 8 \\ i \end{pmatrix} \{\sum_{\alpha'} j_{\alpha'}\}^{i+j} \{\sum_{\alpha'} (1 - j_{\alpha'})\}^{12-i-j} \sigma_k p_{ijk} r_{\alpha''} s_{\alpha''} j_{\alpha''}}.$$

If the reproduction/survival weighting factors are balanced so that the **A** locus is *'compensated'* then:

$$r_\alpha s_\alpha = 1.$$

Therefore the evolution reduces to:

$$j'_\alpha = \frac{P_g F j_\alpha}{\sum_{\alpha'} F j_{\alpha'}},$$

where F is independent of α. Hence the mean field model exhibits no selection in the case of a compensated **A** locus.

5. Results of the Artificial Ecology.

5.1. Length Scale Analysis.

Error analysis (section 2.1.5) of the genotypes in the model is illustrated in figure 75, from

which a coherence length scale of $n_c \simeq 80$ can be identified. At scales below n_c the system shows negative spatial coherence, with an aggregating tendency as n increases. Thus an 80×80 AE grid is used throughout.

5.2. Selection for Different Life History Strategies.

Figure 76 illustrates the structure of the model at early stages of invasion (figures 76a - b) and in a later near-equilibrium phase (figures 76c - d). There is a near random distribution of plant sizes (figures 76a, c) but the spatial distribution of genotypes is structured (figures 76b, d).

If the **A** locus is compensated ($r_\alpha s_\alpha = 1$ for all α) then the mean field model predicts that no selection occurs. The AE, however, shows selection in favour of the **A1** and **A3** alleles and rapid elimination of the **A2** (neutral) allele, for a range of values of $r_\alpha \equiv \frac{1}{s_\alpha}$ (figure 77a). Allele **A3**, which favours the seedling stage, is present in the polymorphic population at a considerably higher level that the **A1** allele, which favours the adult stage. (If the **A** locus is not compensated, then selection takes place towards whichever allele has the highest $r_\alpha s_\alpha$ value.) Thus the system shows clear selection towards genotypes which are expressed at different life stages, with a bias towards those genotypes favour selection at the juvenile stage. These results cannot be predicted by mean field theory and must arise via local interactions in space.

5.3. Competition Between Constant and Varied Life Strategy Genotypes.

Selection towards $r_\alpha \neq s_\alpha$, that is, varied life strategies, has been demonstrated in the presence of a constant neutral genotype $r_\alpha = s_\alpha = 1$. It is therefore interesting to see how much bias must be given to the constant strategy $r_\alpha = s_\alpha > 1$ before this allele is selected above the varied strategy. Figure 77b shows the probability of extinction of allele **A2** within 500 years, as a function of $r_{A2} = s_{A2}$. The varied strategy alleles take the values $r_{A1} = \frac{1}{s_{A1}} = \frac{1}{r_{A3}} = s_{A3} = 2$, so that $r_{A1}s_{A1} = r_{A3}s_{A3} = 1$. A clear threshold is seen where there is a switch between the varied and constant strategies.

Thus, in summary, the AE version of the plant CML has allowed sufficiently long time scales to be used that selection of life history strategies can be modelled (Davy & Smith, 1988). The

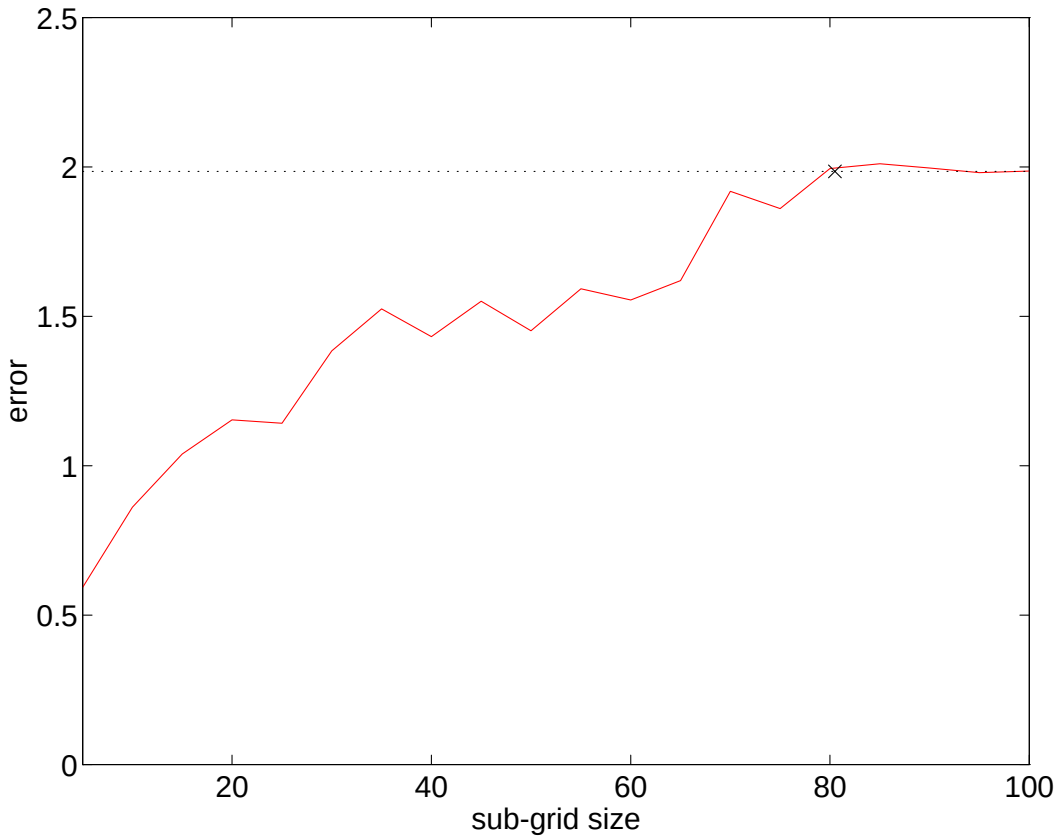

Figure 75: Error analysis for the genetic CA model: numerical error $n\mathcal{E}_n$ for the model (—) and theoretical error $n\mathcal{E}'_n$ $(\cdots)$.

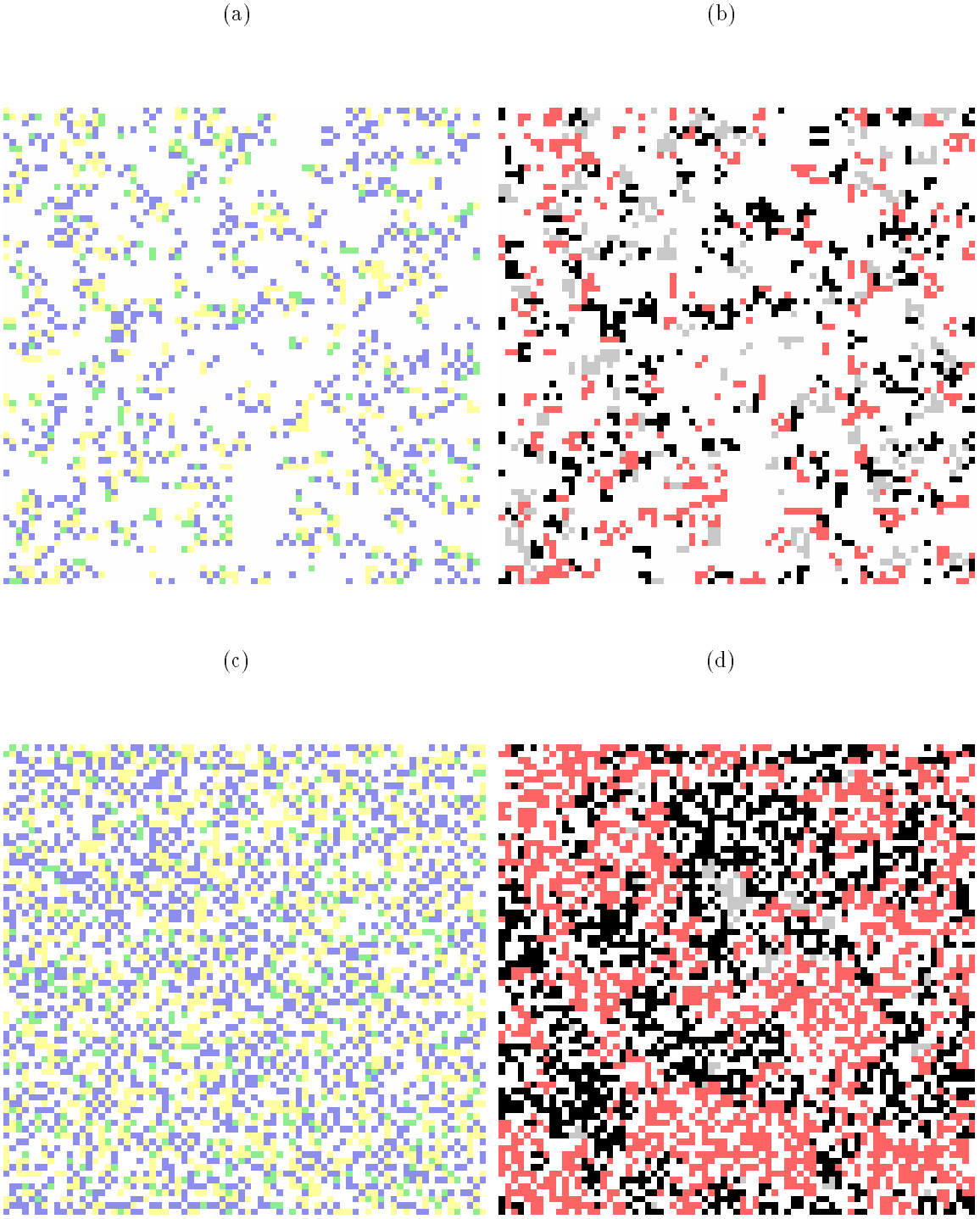

Figure 76: Spatial pattern in the genetic CA model: (a) - (b) early invasion phase; (c) - (d) later equilibrium phase. (a), (c) Adult plant sizes: small (yellow), medium (green) and large (blue). (b), (d) Genotype: **A1** favours adults (red), **A2** neutral (grey) and **A3** favours juveniles (black).

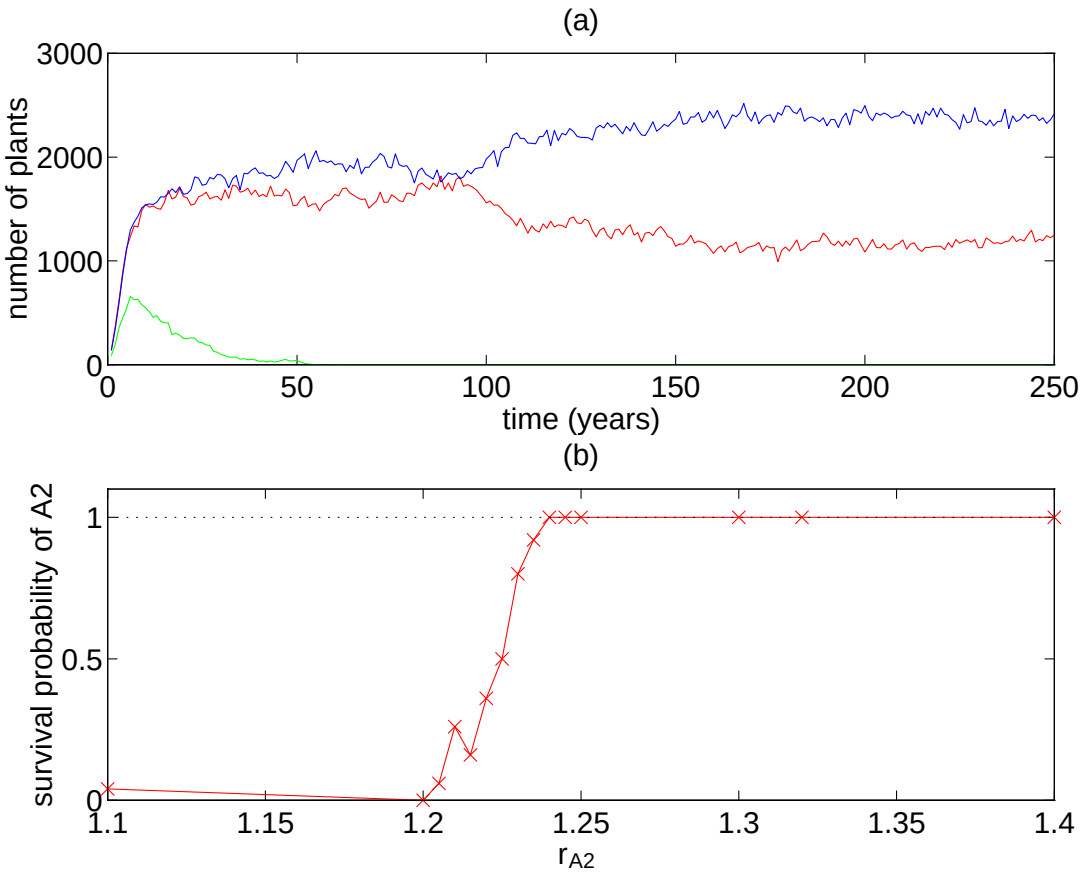

Figure 77: Time series and threshold behaviour for the genetic CA model. (a) Time series for number of plants of genotypes **A1** (red), **A2** (green) and **A3** (blue). (b) Probability that a constant strategy allele **A2** survives for 500 years as a function of its gene factors $r_{A2} = s_{A2}$, given the varied strategies **A1** and **A3** with $r_{A1} = \frac{1}{s_{A1}} = s_{A3} = \frac{1}{r_{A3}}$.

AE provides evidence that selection occurs in favour of variable life history strategies and in particular in favour of selection at the juvenile life stage.

Appendix B. Technical Details for the Grouse Model.

'Nessuna humana investigazione si pio dimandara vera scienzia s'essa non passa per le matematiche dimonstrazione. (No human investigation can be called real science if it cannot be demonstrated mathematically.)' - Leonardo da Vinci

Parameter	**Description**	**Typical value(s)**
L	grid size	100
$NoYears$	duration of simulation	50
$density$	initial density of birds	0.001
μ_{brood}	mean brood size	3.6
σ_{brood}	standard deviation of brood size	2.0
p_{fail}	proportion of broods which fail	0.1
p_{die}	summer mortality of adult birds	0.1 - 0.3
N_{disp}	number of dispersal attempts	0 - 8
ΔP	pressure difference tolerated before boundary moves	0.005
$kindp$	factor by which kin neighbours increase ΔP	10
$\overline{CTS}$	basic critical minimum territory size	25 - 50
ΔTol	effect of kin neighbours on minimum critical territory size	0.1 - 0.25
δ_{Tol}	change in tolerance behaviour (Model I)	0.0 - 1.0
δ_{disp}	change in dispersal behaviour (Model II)	1 - 4

Table 13: Parameters for the two-dimensional red grouse model.

Variable	**Description**
N	population size
X_i	bird present in cell i
T_i	territory owner of cell i
K_{mn}	relatedness of birds m and n
F_n	father of bird n
Tol_n	tolerance/intolerance of bird n
FRS_n	fighting rank strength of bird n
P_n	pressure exerted by bird n
TS_n	territory size of bird n
CTS_n	critical minimum territory size of bird n
NN_n	number of kin neighbours of bird n
$resid$	"residual" - number of site changes in one iteration
nw	number of failed recruiters

Table 14: Variables in the two-dimensional red grouse model.

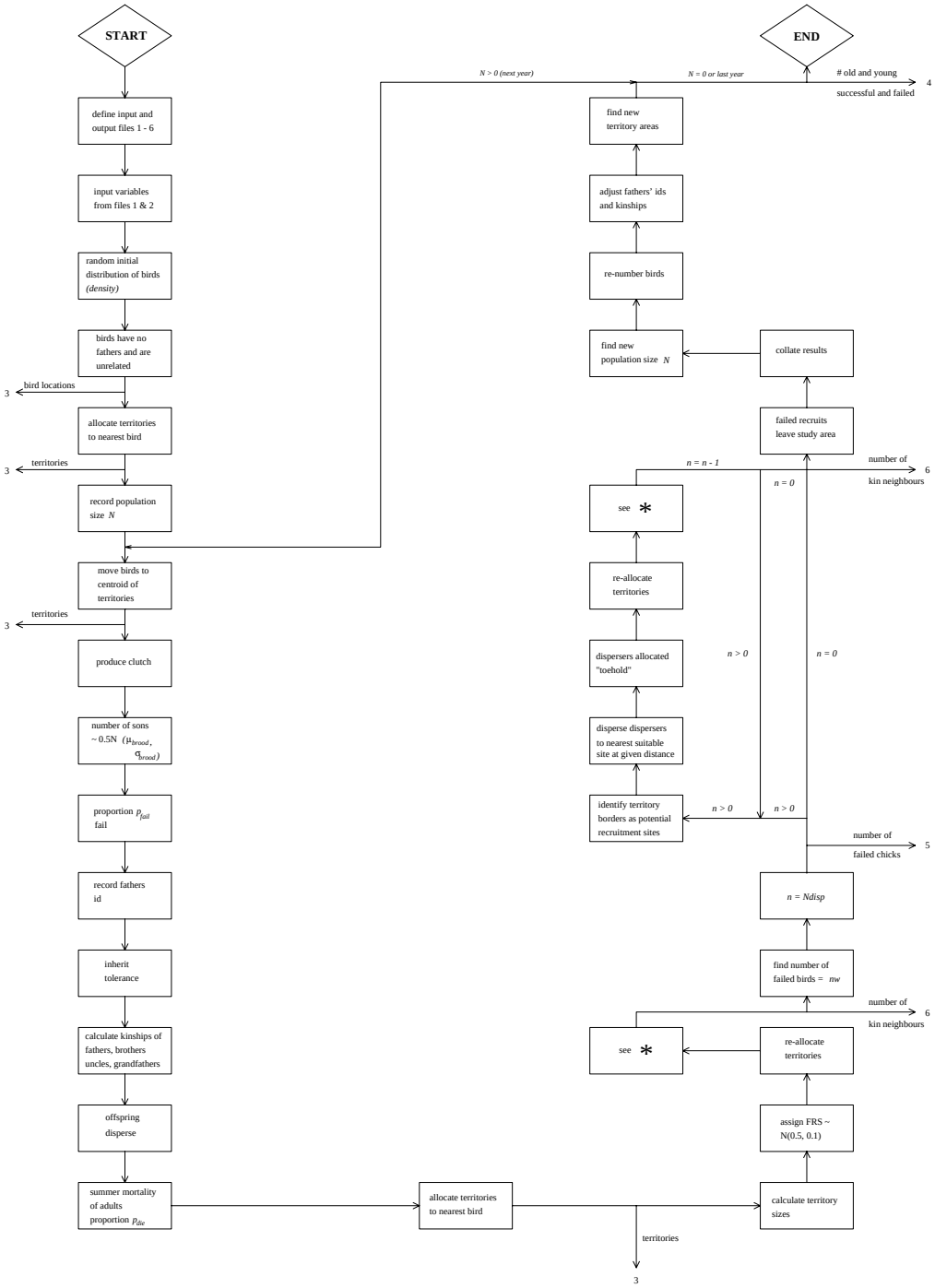

Figure 78: Flow chart of the two-dimensional red grouse model (Model 0).

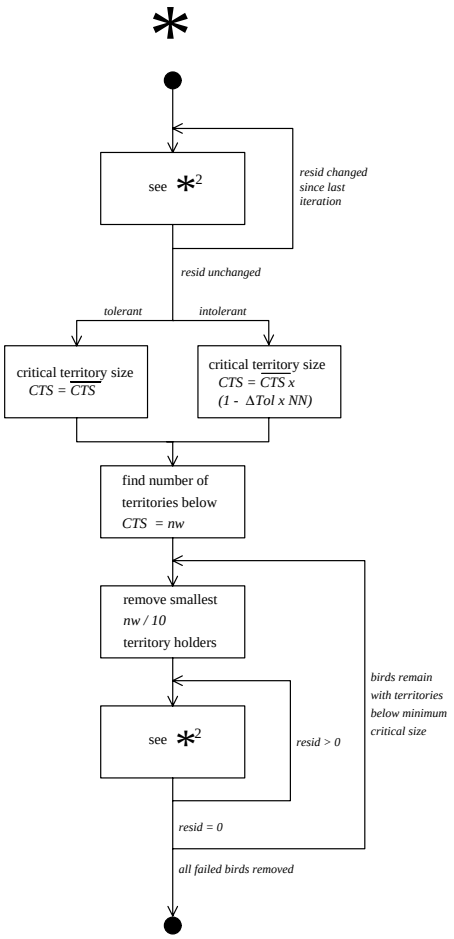
*
see *2
resid changed since last iteration
resid unchanged
tolerant
intolerant
critical territory size CTS = CTS
critical territory size CTS = CTS x (1 - ΔTol x NN)
find number of territories below CTS = nw
remove smallest nw / 10 territory holders
see *2
resid > 0
resid = 0
birds remain with territories below minimum critical size
all failed birds removed

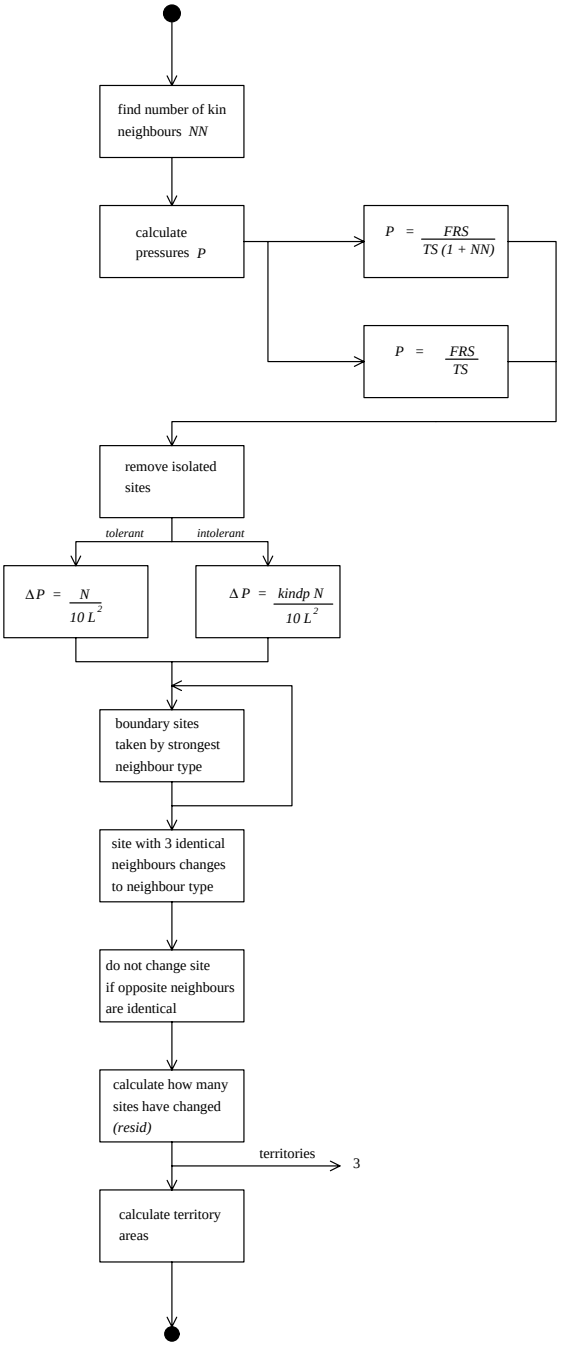
*2
find number of kin neighbours NN
calculate pressures P
P = FRS / TS (1 + NN)
P = FRS / TS
remove isolated sites
tolerant
intolerant
ΔP = N / 10 L2
ΔP = kindp N / 10 L2
boundary sites taken by strongest neighbour type
site with 3 identical neighbours changes to neighbour type
do not change site if opposite neighbours are identical
calculate how many sites have changed (resid)
territories
3
calculate territory areas

References

Abrams, P.A. 1988 Resource productivity - consumer species diversity: simple models of competition in spatially homogeneous environments. *Ecology* 69:1418-1433.

Acquaah, G. 1992 A factor analysis of plant variables associated with architecture and seed size in dry bean. *Euphytica* 60:171-177.

Addicott, J.F., Aho, J.M., Antolin, M.F., Padilla, D.K., Richardson, J.S. & Soluk, D.A. 1987 Ecological neighbourhoods: scaling environmental patterns. *Oikos* 49:340-346.

Adler, F.R. & Nuernberger, B. 1994 Persistence in patchy irregular landscapes. *Theoretical Population Biology* 45:41-75.

Aharony, A. 1990 Multifractals in physics: successes, dangers and challenges. *Physica* 168A:479-489.

Aikman, D.P. & Watkinson, A.R. 1980 A model for growth and self-thinning in even-aged monocultures of plants. *Annals of Botany* 45:419-427.

Albrecht, K.-F. 1992 Problems of modelling and forecasting on the basis of phenomenological investigations. *Ecological Modelling* 63:45-69.

a Allen, J.C. 1990 Factors contributing to chaos in population feedback systems. *Ecological Modelling* 51:281-298.

Allsopp, N. & Stock, W.D. 1995 Relationships between seed reserves, seedling growth and mycorrhizal responses in 14 related shrub (Rosidae) from a low-nutrient environment. *Functional Ecology* 9:248-254.

Anderson, R.M. 1993 Epidemiology. In: *Modern parasitology* ed. Cox, F.E.G. pp. 75-116. Blackwell, Oxford.

Anderson, R.M. & May, R.M. 1979 Population biology of infectious diseases: part I. *Nature*

280:361-366.

Anderson, R.M. & May, R.M. 1992 *Infectious diseases of humans.* Oxford University Press, Oxford.

Anderson, R.M. & Nokes, D.J. 1991 Mathematical models of transmission and control. In: *Oxford textbook of public health* Vol. 2 ed. Holland, W.W., Detals, R., Knox, G., Fitzsimmons, B. & Gardner L. pp. 225-252. Oxford Medical Publications, Oxford.

Arfken, G. 1970 *Mathematical methods for physicists.* Academic Press, New York.

Argoul, F., Arnéodo, A., Grasseau, G., Gagne, Y., Hopfinger, E.J. & Frisch, U. 1989 Wavelet analysis of turbulence reveals the multifractal nature of the Richardson cascade. *Nature* 338:51-53.

Armesto, J.J., Pickett, S.T.A. & McDonnell, M.J. 1991 Spatial heterogeneity during succession: a cyclic model of invasion and exclusion. In: *Ecological heterogeneity* ed. Kolasa, J. & Pickett, S.T.A. pp. 256-269. *Springer Ecological Studies* Vol. 86, Berlin.

Armstrong, D.P. & Westoby, M. 1993 Seedlings from large seeds tolerate defoliation better: a test using phylogenetically independent contrasts. *Ecology* 74:1092-1110.

Armstrong, R.A. 1976 Fugitive species: experiments with fungi and some theoretical considerations. *Ecology* 57:953-963.

Armstrong, R.A. 1993 A comparison of index-based and pixel-based neighbourhood simulations of forest growth. *Ecology* 74:1707-1712.

Auld, B.A. & Coote, B.G. 1980 A model of a spreading plant population. *Oikos* 34:287-292.

Bak, P. & Chen, K. 1989 The physics of fractals. *Physica* 38D:5-12.

Bak, P. & Chen, K. 1990 A forest fire model and some thoughts on turbulence. *Physics Letters* A 147:297-300.

Baker, H.G. 1972 Seed weight in relation to environmental conditions in California. *Ecology* 53:997-1010.

Ballaré, C.L., Scopel, A.L., Jordan, E.T. & Vierstra, R.D. 1994 Signaling among neighbouring plants and the development of size inequalities in plant populations. *Proceedings of the National Academy of Science USA* 91:10094-10098.

Bard, J.B.L. 1981 A model for generating aspects of zebra and other mammalian coat patterns. *Journal of Theoretical Biology* 93:363-385.

Barkham, J.P. & Hance, C.E. 1982 Population dynamics of the wild daffodil *(Narcissus pseudo-narcissus)*. III. Implications of a computer model of 1000 years of population change. *Journal of Ecology* 70:323-344.

Bartlett, M.S. 1957 On theoretical models for competitive and predatory biological systems. *Biometrika* 44:27-42.

Bartlett, M.S. 1990 Chance or chaos? *Journal of the Royal Statistical Society* A 153:321-347.

Bascompte, J. & Solé, R.V. 1994 Spatially-induced bifurcations in single-species population dynamics. *Journal of Animal Ecology* 63:256-264.

a Bebawi, F.F., Mutwali, E.M. & Neugebohrn, L. 1991 Influence of seed size and growth stage on forage sorghum-sudangrass hybrid cultivar P988 grown on *Striga* infested soil. *Journal of Agronomy and Crop Science* 167:8-22.

Beddington, J.R., Free, C.A. & Lawton, J.H. 1975 Dynamic complexity in predator-prey models framed in difference equations. *Nature* 255:58-60.

Bence, J.R. & Nisbet, R.M. 1989 Space-limited recruitment in open systems: the importance of time delays. *Ecology* 70:1434-1441.

Bendel, R.B., Higgins, S.S., Teberg, J.E. & Pyke, D.A. 1989 Comparison of skewness coefficient, coefficient of variation and Gini coefficient as inequality measures within populations. *Oecologia*

78:394-400.

Bengtsson, J. 1989 Interspecific competition increases local extinction rate in a metapopulation system. *Nature* 340:713-715.

Benjamin, L.R. 1988 A single equation to quantify the hierarchy in plant size induced by competition within monocultures. *Annals of Botany* 62:199-214.

Benjamin, L.R. 1993 Experimental discrimination between contrasting models of neighbourhood competition. *Journal of Ecology* 81:417-423.

Benjamin, L.R. & Hardwick, R.C. 1986 Sources of variation and measurement of variability in even-aged stands of plants. *Annals of Botany* 58:757-778.

a Benjamin, L.R. & Sutherland, R.A. 1992 Control of mean root weight in carrots *(Daucus carota)* by varying within- and between-row spacing. *Journal of Agricultural Sciences* 119:59-70.

a Bergelson, J. 1993 Details of local dispersion improve the fit of neighborhood competition models. *Oecologia* 95:299-302.

a Berntson, G.M. & Weiner, J. 1990 Size structure of populations within populations: leaf number and size in crowded and uncrowded *Impatiens pallida* individuals. *Oecologia* 85:327-331.

Berryman, A.A. & Millstein, J.A. 1989a Are ecological systems chaotic - and it not, why not? *Trends in Evolution and Ecology* 4:26-28.

Berryman, A.A. & Millstein, J.A. 1989b Avoiding chaos - reply. *Trends in Evolution and Ecology* 4:240.

s Bewick, T. 1826 *A history of British birds.* Vol. II. Longman, London.

Bignone, F.A. 1993 Cells-gene interactions - simulations on a coupled map lattice. *Journal of Theoretical Biology* 161:231-249.

Birch, C.P.D. & Hutchings, M.J. 1994 Exploitation of patchily distributed soil resources by the

clonal herb *Glechoma Hederaceae*. *Journal of Ecology* 82:653-664.

Block, A., von Bloh, W. & Schnellnhuber 1990 Efficient box-counting determination of generalised fractal dimensions. *Physical Review* A 42:1869-1874.

Blumenfeld, R., Meir, Y., Aharony, A. & Harris, A.B. 1987 Resistance fluctuations in randomly diluted networks. *Physical Review* B 35:3524-3535.

a Bolker, B.M. & Grenfell, B.T. 1993 Chaos and biological complexity in measles dynamics. *Proceedings of the Royal Society of London* B 251:75-81.

Bonan, G.B. 1988 The size structure of theoretical plant populations: spatial patterns and neighbourhood effects. *Ecology* 69:1721-1730.

Bonan, G.B. 1991 Density effects on the size structure of annual plant populations: an indication of neighbourhood competition. *Annals of Botany* 68:341-347.

Bonan, G.B. 1993 Analysis of neighbourhood competition among annual plants: implications of a plant growth model. *Ecological Modelling* 65:123-136.

Bradshaw, G.A. & Spies, T.A. 1992 Characterising canopy gap structure in forests using wavelet analysis. *Journal of Ecology* 80:205-215.

Breckling, B. 1992 Uniqueness of ecosystems versus generalizability and predictability in ecology. *Ecological Modelling* 63:13-27.

Britton, N.F. 1982a Threshold phenomena and solitary traveling waves in a class of reaction-diffusion systems. *SIAM Journal of Applied Mathematics* 42:188-217.

Britton, N.F. 1982b A model for suppression and dominance in trees. *Journal of Theoretical Biology* 97:691-698.

Broomhead, D.S. & King, G.P. 1986 Extracting qualitative dynamics from experimental data. *Physica* 20D:217-236.

'*s* Bronowski, J. 1956 *Science and human values.* Hutchinson, London.

Bullock, J. 1994 Individual-based models. *Trends in Evolution and Ecology* 9:299.

Burdon, J.J. & Harper, J.L. 1980 Relative growth rates of individual members of a plant population. *Journal of Ecology* 68:953-957.

Burks, C. & Farmer, D. 1984 Towards modeling DNA sequences. *Physica* 10D:157-167.

Burrough, P.A. 1981 Fractal dimensions of landscapes and other environmental data. *Nature* 294:240-242.

Cannell, M.G.R., Rothery, P. & Ford, E.D. 1984 Competition within stands of *Picea Sitchensis* and *Pinus Contorta*. *Annals of Botany* 53:349-362.

Caraco, T. & Kelly, C.K. 1991 On the adaptive value of physiological integration in clonal plants. *Ecology* 72:81-93.

Caro, T.M. & Laurenson, M.K. 1994 Ecological and genetic factors in conservation: a cautionary tale. *Science* 263:485-486.

Carter, R.N. & Prince, S.D. 1988 Distribution limits from a demographic viewpoint. In: *Plant population ecology* ed. Davy, A.J., Hutchings, M.J. & Watkinson, A.R. pp. 165-184. Blackwell Scientific Publications, Oxford.

Cartwright, M.L. & Littlewood, J.E. 1945 On non-linear differential equations of the second order. *Journal of the London Mathematical Society* 20:180-189.

Casdagli, M. 1991 Chaos and deterministic versus stochastic non-linear modelling. *Journal of the Royal Statistical Society* B 54:303-328.

Caswell, H. & Etter, R.J. 1993 Ecological interactions in patchy environments: from patch-occupancy models to cellular automata. In: *Patch Dynamics* ed. Levin, S.A., Powell, T.M. & Steele, J.H. pp. 93-108. *Springer lecture notes in biomathematics* Vol. 96, Berlin.

Caswell, H. & John, A.M. 1992 From the individual to the population in demographic models. In: *Individual-based models and approaches in ecology: populations, communities and ecosystems* ed. DeAngelis, D.L. & Gross, L.J. pp. 36-61. Chapman & Hall, New York.

a Chandra-Babu, R., Muralidharan, V., Seetha-Rani, M., Nagarajan, M., Sree-Rangasamy, S.R. & Pallikonda-Perumal, R.K. 1990 Effect of seed size on germination and seedling growth in green gram (*Vigna radiate* L. Wilczek) and blackgram (*Vigna mungo* L. Hepper) cultivars. *Journal of Agronomy and Crop Science* 164:213-216.

Chaplain, M. 1993 Mathematical models of cancer growth. Fontevraud, workshop on pattern formation in Medicine and Biology.

Chaplain, M. 1994 The roles of endothelial cell proliferations and migration in tumour angiogenesis. University of Sheffield, British Applied Mathematics Conference.

Char, B.W., Geddes, K.O., Gonnet, G.H. & Watt, S.M. 1985 *Maple user's guide.* Watcom publications, Waterloo, Ontario.

Chaté, H. & Manneville, P. 1992 Collective behaviours in spatially extended systems with local interactions and synchronous updating. *Progress in Theoretical Physics* 87:1-60.

Chesson, P.L. 1981 Models for spatially distributed populations: the effect of within-patch variability. *Theoretical Population Biology* 19:288-325.

Chesson, P.L. 1982 The stabilising effect of a random environment. *Journal of Mathematical Biology* 15:1-36.

Chesson, P.L. 1985 Coexistence of competitors in spatially and temporally varying environments: a look at the combined effects of different sorts of variability. *Theoretical Population Biology* 28:263-287.

Chesson, P. 1991 A need for niches? *Trends in Evolution and Ecology* 6:26-28.

Clark, J.S. 1991 Disturbance and population structure on the shifting mosaic landscape. *Ecology*

72:1119-1137.

Clark, P.J. & Evans, F.C. 1955 On some aspects of spatial pattern in biological populations. *Science* 121:397-398.

Clements, F.E. 1936 *Nature* and structure of the climax. *Journal of Ecology* 24:252-284.

Clifford, P. & Sudbury, A. 1973 A model for spatial conflict. *Biometrika* 60:581-97.

Cocho, G., Péréz-Pascual, R., Rius, J.L. & Soto, F. 1987 Discrete systems, cell-cell interactions and color pattern of animals II. Clonal theory and cellular automata. *Journal of Theoretical Biology* 125:437-447.

Coffin, D.P. & Lauenroth, W.K. 1988 The effects of disturbance size and frequency on a short-grass plant community. *Ecology* 69:1609-1617.

Cohen, D. 1971 Maximising final yield when growth is limited by time or by limiting resources. *Journal of Theoretical Biology* 33:299-307.

Cohen, D. & Levin, S.A. 1991 Dispersal in patchy environments: the effects of temporal and spatial structure. *Theoretical Population Biology* 39:63-99.

Cohen, D.S. & Murray, J.D. 1981 A generalised diffusion model for growth and dispersal in a population. *Journal of Mathematical Biology* 12:237-249.

Cohen, J. & Stewart, I. 1991 Chaos, contingency and convergence. *Nonlinear Science Today* 1:9-13.

Cohen, J. & Stewart, I. 1994 *The collapse of chaos.* Viking Penguin, London.

Colasanti, R.L. & Grime, J.P. 1993 Resource dynamics and vegetation processes: a deterministic model using two-dimensional cellular automata. *Functional Ecology* 7:169-176.

Cole, B.J. 1991 Is animal behaviour chaotic? Evidence from the activity of ants. *Proceedings of the Royal Society of London* B 244:253-259.

Comins, H.N. & Blatt, D.W.E. 1974 Predator-prey models in spatially heterogeneous environments. *Journal of Theoretical Biology* 48:75-83.

a Comins, H.N., Hassell, M.P. & May, R.M. 1992 The spatial dynamics of host-parasitoid systems. *Journal of Animal Ecology* 61:735-748.

Coniglio, A., DeArcangelis, L. & Herrmann, H.J. 1989 Fractals and multifractals: applications in Physics. *Physica* 157A:21-30.

Coniglio, A., Stauffer, D. & Jan, N. 1987 Search for multifractality in damage spreading for Kauffman cellular automata. *Journal of Physics* A 20:1103-1106.

Coniglio, A. & Zannetti, M. 1989 Multiscaling and multifractality. *Physica* 38D:37-40.

Cousens, R. 1995 Can we determine the intrinsic dynamics of real plant populations? *Functional Ecology* 9:15-20.

Cox, J.T. & Griffeath, D. 1986 Diffusive clustering in the two dimensional voter model. *Annals of Probability* 14:347-370.

Crawley, M.J. 1990a The population dynamics of plants. *Philosophical Transactions of the Royal Society of London* B 330:125-1240.

Crawley, M.J. 1990b The response of terrestrial ecosystems to global climate change. In: *Global climate and ecosystem change* ed. MacDonald, G.J. & Sertorio, L. pp. 141-164. NATO ASI Series B: Physics Vol. 240, Plenum, New York.

Crawley, M.J. 1992 Seed predators and plant populations dynamics. In: *Seeds - the ecology of regeneration in plant communities* ed. Fenner, M. pp. 157-191. CAB International, Wallingford, UK.

Crawley, M.J. & May, R.M. 1987 Population dynamics and plant community structure: competition between annuals and perennials. *Journal of Theoretical Biology* 125:475-489.

a Crawley, M.J. & Weiner, J. 1991 Plant size variation and vertebrate herbivory: winter wheat grazed by rabbits. *Journal of Applied Ecology* 28:154-172.

Crowley, P.H. 1977 Spatially distributed stochasticity and the constancy of ecosystems. *Bulletin of Mathematical Biology* 39:157-166.

Crutchfield, J.P. & Kaneko, K. 1988 Are attractors relevant to turbulence? *Physics Review Letters* 60:2715-2718.

Cruywagen, G.C., Maini, P.K. & Murray, J.D. 1994 Travelling waves in a tissue interaction model for skin pattern formation. *Journal of Mathematical Biology* 33:193-210.

Czárán, T. & Bartha, S. 1992 Spatiotemporal dynamic models of plant populations and communities. *Trends in Evolution and Ecology* 7:38-42.

Davis, F.W. 1993 Introduction to spatial statistics. In: *Patch Dynamics* ed. Levin, S.A., Powell, T.M. & Steele, J.H. pp. 16-26. *Springer lecture notes in biomathematics* Vol. 96, Berlin.

Davy, A.J. & Smith, H. 1988 Life-history variation and environment. In: *Plant population ecology* ed. Davy, A.J., Hutchings, M.J. & Watkinson, A.R. pp. 1-22. Blackwell Scientific Publications, Oxford.

DeAngelis, D.L. & Gross, L.J. 1992 *Individual-based models and approaches in ecology: populations, communities and ecosystems.* Chapman & Hall, New York.

DeAngelis, D.L. & Rose, K.A. 1992 Which individual-based approach is most appropriate for a given problem? In: *Individual-based models and approaches in ecology: populations, communities and ecosystems* ed. DeAngelis, D.L. & Gross, L.J. pp. 67-87. Chapman & Hall, New York.

DeAngelis, D.L., Travis, C.C. & Post, W.M. 1979 Persistence and stability of seed-dispersed species in a patchy environment. *Theoretical Population Biology* 16:107-125.

DeArcangelis, L., Redner, S. & Coniglio, A. 1985 Anomalous voltage distribution of random

resistor networks and a new model for the backbone at the percolation threshold. *Physical Review* B 31:4725-4727.

DeRoos, A.M., McCauley, E. & Wilson, W.G. 1991 Mobility versus density-limited predator-prey dynamics on different spatial scales. *Proceedings of the Royal Society of London* B 246:117-122.

Deutschman, D.H., Bradshaw, G.A., Childress, W.M., Daly, K.L., Grünbaum, D., Pascual, M., Schumaker, N.H. & Wu, J. 1993 Mechanisms of patch formation. In: *Patch Dynamics* ed. Levin, S.A., Powell, T.M. & Steele, J.H. pp. 184-209. *Springer lecture notes in biomathematics* Vol. 96, Berlin.

Diggle, P.J. 1976 A spatial stochastic model of inter-plant competition. *Journal of Applied Probability* 13:662-671.

Diggle, P.J. 1977 The detection of random heterogeneity in plant populations. *Biometrics* 33:390-394.

Dixon, P.M., Weiner, J., Mitchell-Olds, T. & Woodley, R. 1987 Bootstrapping the Gini coefficient of inequality. *Ecology* 68:1548-1551.

Doak, D.F., Marino, P.C. & Kareiva, P.M. 1992 Spatial scale mediates the influence of habitat fragmentation on dispersal success: implications for conservation. *Theoretical Population Biology* 41:315-336.

Dolan, R.W. & Sharitz, R.R. 1984 Population dynamics of *Ludwigia Leptocarpo* (Onograceae) and some factors affecting size hierarchies in a natural population. *Journal of Ecology* 72:1031-1041.

Doob, J.L. 1953 *Stochastic processes.* John Wiley, Chichester.

a Douglas, G.B., Gordon, I.L., Chu, A.C.P. & Robertson, A.G. 1993 Effect of genotype and seed size on early vegetative growth of sheep's burnet. *New Zealand Journal of Agricultural*

Research 36:109-116.

Du, Y. & Ott, E. 1993 Fractal dimensions of fast dynamo magnetic fields. *Physica* 67D:387-417.

Dunbar, S.R. 1983 Travelling wave solutions of diffusive Lotka-Volterra equations. *Journal of Mathematical Biology* 17:11-32.

Durrett, R. 1980 On the growth of one dimensional contact processes. *Annals of Probability* 8:890-907.

Durrett, R. 1981 An introduction to infinite particle systems. *Stochastic Processes and their Applications* 11:109-150.

Durrett, R. 1988 Crabgrass, measles, and gypsy moths: an introduction to interacting particle systems. *The Mathematical Intelligencer* 10:37-47.

Durrett, R. 1993a Spatial epidemic models. *Manuscript.*

Durrett, R. 1993b Stochastic models of growth and competition. In: *Patch Dynamics.* ed. Levin, S.A., Powell, T.M. & Steele, J.H. pp. 176-183. *Springer lecture notes in biomathematics* Vol. 96, Berlin.

Durrett, R. & Levin, S.A. 1994a The importance of being discrete (and spatial). *Theoretical Population Biology* 46:363-394.

Durrett, R. & Levin, S.A. 1994b Stochastic spatial models - a user's guide to ecological applications. *Philosophical Transactions of the Royal Society of London* B 343:329-350.

Durrett, R. & Liu, X.-F. 1988 The contact process on a finite set. *Annals of Probability* 16:1158-1173.

Durrett, R. & Schonmann, R.H. 1988 The contact process on a finite set. II. *Annals of Probability* 16:1570-1583.

Durrett, R., Schonmann, R.H. & Tanaka, N.I. 1989 The contact process on a finite set. III.

The critical case. *Annals of Probability* 17:1303-1321.

Durrett, R. & Swindle, G. 1991 Are there bushes in a forest? *Stochastic Processes and their Applications* 37:19-31.

Dytham, C. 1994 Habitat destruction and competitive coexistence: a cellular model. *Journal of Animal Ecology* 63:490-491.

a Dytham, C. & Shorrocks, B. 1992 Selection, patches and genetic variation: a cellular automaton modelling Drosophila populations. *Evolutionary Ecology* 6:342-351.

Eckmann, J.-P. & Ruelle, D. 1992 Fundamental limitations for estimating dimensions and Lyapunov exponents in dynamical systems. *Physica* 56D:185-187.

Ehrlich, P.R. 1961 Intrinsic barriers to dispersal in Checkerspot butterfly. *Science* 134:108-109.

Elderkin, R.H. 1982 Seed dispersal in a patchy environment with global age dependence. *Journal of Mathematical Biology* 13:283-303.

Ellison, A.M. 1987 Density-dependent dynamics of *Salicornia europa* monocultures. *Ecology* 68:737-741.

Ellison, A.M., Dixon, P.M., Ngai, J. 1994 A null model for neighbourhood models of plant competitive interactions. *Oikos* 71:225-238.

Ellison, A.M. & Rabinowitz, D. 1989 Effects of plant morphology and emergence time on size hierarchy formation in experimental populations of two varieties of cultivated peas *(Pisum sativum). American Journal of Botany* 76:427-436.

Ellner, S. & Turchin, P. 1995 Chaos in a noisy world: new methods and evidence from time series analysis. *American Naturalist* 145:343-375.

af Elrahman, N.A. & Bourdu, R. 1986 The effect of seed size and shape on early development in maize. *Agronomie* 6:181-186.

Ermentrout, G.B. & Edelstein-Keshet, L. 1993 Cellular automata approaches to biological modelling. *Journal of Theoretical Biology* 160:97-133.

Evans, G.T. 1980 Diffusive structure: counterexamples to any explanation? *Journal of Theoretical Biology* 82:313-315.

Facelli, J.M. & Pickett, S.T.A. 1990 Markovian chains and the role of history in succession. *Trends in Evolution and Ecology* 5:27-29.

Fahrig, L., Coffin, D.P., Lauenroth, W.K. & Shugart, H.H. 1994 The advantage of long-distance clonal spreading in highly disturbed habitats. *Evolutionary Ecology* 8:172-187.

Fahrig, L. & Merriam, G. 1985 Habitat patch connectivity and population survival. *Ecology* 66:1762-1768.

Falconer, K. 1990 *Fractal geometry: mathematical foundations and applications.* John Wiley, Chichester.

Feder, J. 1988 *Fractals.* Plenum, New York.

Ferrara, L.S. & Quinn, J.A. 1987 Environment and seed size effects on germination and growth in *Polygala Paucifolia*, a perennial forest herb. *American Journal of Botany* 74:649-650.

Ferrière, R. & Gatto, M. 1994 The evolution of oscillations and chaos in population dynamics. University of Manchester, VIth International Congress of Ecology.

Fielding, A. 1991 Chaotic biology. *The Biologist* 38:185-188.

Finerty, J.P. 1980 *The population ecology of cycles in small mammals.* Yale University Press, Newhaven.

Firbank, L.G. & Watkinson, A.R. 1985 A model of interference within plant monocultures. *Journal of Theoretical Biology* 116:291-311.

Firbank, L.G. & Watkinson, A.R. 1987 On the analysis of competition at the level of the

individual plant. *Oecologia* 71:308-317.

Firbank, L.G. & Watkinson, A.R. 1990 On the effects of competition: from monocultures to mixtures. In: *Perspectives on plant competition.* ed. Grace, J.B. & Tilman, D. pp. 165-192. Academic Press, San Diego.

Fischer, R.A. & Miles, R.E. 1973 The role of spatial pattern in the competition between crop plants and weeds. A theoretical analysis. *Mathematical Biosciences* 18:335-350.

Fisher 1930 Mortality amongst plants and its bearing on natural selection. *Nature* 125:

Ford, E.D. 1975 Competition and stand structure in some even-aged plant monocultures. *Journal of Ecology* 63:311-333.

Ford, E.D. & Diggle, R.J. 1981 Competition for light in a plant monoculture modelled as a spatial stochastic process. *Annals of Botany* 48:481-500.

Ford, E.D. & Sorrensen, K.A. 1992 Theory and models of inter-plant competition as a spatial process. In: *Individual-based models and approaches in ecology: populations, communities and ecosystems* ed. DeAngelis, D.L. & Gross, L.J. pp. 363-407. Chapman & Hall, New York.

Foster, S.A. & Janson, C.H. 1985 The relationship between seed size and establishment conditions in tropical woody plants. *Ecology* 66:773-780.

Fowler, N.L. 1984 The role of germination date, spatial arrangement, and neighbourhood effects in competitive interactions in *Linum. Journal of Ecology* 72:307-318.

Fowler, N. 1988 The effects of environmental heterogeneity in space and time on the regulation of populations and communities. In: *Plant population ecology* ed. Davy, A.J., Hutchings, M.J. & Watkinson, A.R. pp. 249-269. Blackwell Scientific Publications, Oxford.

Gadgil, M. 1971 Dispersal: population consequences and evolution. *Ecology* 52:253-261.

Galiano, E.F. 1982 Pattern detection in plant populations through the analysis of plant-to-all-

plants distances. *Vegetatio* 49:39-43.

Galitsky, V.V. 1990 Dynamic 2-d models of plant communities. *Ecological Modelling* 50:95-105.

a Ganeshaiah, K.N. & Uma-Shaanker, R. 1991 Seed size optimization in a wind dispersed tree *Butea monosperma*: a trade off between seedling establishment and pod dispersal efficiency. *Oikos* 60:3-6.

Garcia-Moliner, G., Mason, D.M., Greene, C.H., Lobo, A., Li, B., Wu, J. & Bradshaw, G.A. 1993 Description and analysis of spatial patterns. In: *Patch Dynamics* ed. Levin, S.A., Powell, T.M. & Steele, J.H. pp. 70-89. *Springer lecture notes in biomathematics* Vol. 96, Berlin.

Gardner, M. 1970 Mathematical games: the fantastic combinations of John Conway's new solitaire game 'Life'. *Scientific American* 223:120-123.

Gardner, M. 1971 Mathematical games: on cellular automata, self-reproduction, the Garden of Eden and the game 'Life'. *Scientific American* 224:112-117.

Gates, D.J. 1978 Bimodality in even-aged plant monocultures. *Journal of Theoretical Biology* 71:525-540.

Gates, D.J. 1980a Competition between two types of plants located at random on a lattice. *Mathematical Biosciences* 48:157-194.

Gates, D.J. 1980b Competition between two types of plants with specified neighbour configurations. *Mathematical Biosciences* 48:195-209.

Gates, D.J. 1982a Competition and skewness in plantations. *Journal of Theoretical Biology* 94:909-922.

Gates, D.J. 1982b Analysis of some equations of growth and competition in plantations. *Mathematical Biosciences* 59:17-32.

Gates, D.J., O'Connor, A.J. & Westcott, M. 1979. Partitioning the union of disks in plant

competition models. *Proceedings of the Royal Society of London* A 367:59-79.

Gates, D.J. & Westcott, M. 1981 Negative skewness and negative correlations in spatial competition models. *Journal of Mathematical Biology* 13:159-171.

Gatto, M. 1993 The evolutionary optimality of oscillatory and chaotic dynamics in simple population models. *Theoretical Population Biology* 43:310-336.

Geber, M.A. 1989 Interplay of morphology and development on size inequality: a *Polygonum* greenhouse study. *Ecological Monographs* 59:267-288.

Giles, B.E. 1990 The effects of variation in seed size on growth and reproduction in the wild barley *Hordeum vulgare* ssp. *spontaneum*. *Heredity* 64:239-250.

Gleason, H.A. 1926 The individualistic concept of the plant association. *Bulletin of the Torrey Botanical Club* 53:7-26.

Gleick, J. 1987 *Chaos - making a new science.* Cardinal, London.

Godfray, H.C.J. & Blythe, S.P. 1990 Complex dynamics in multispecies communities. *Philosophical Transactions of the Royal Society of London* B 330:221-233.

Goldberg, D.E. 1987 Neighbourhood competition in an old-field plant community. *Ecology* 68:1211-1223.

Goldberg, D.E. & Fleetwood, L. 1987 Competitive effect and response in four annual plants. *Journal of Ecology* 75:1131-1143.

Goldbeter, A. 1993 Patterns in time: modelling biochemical and cellular rhythms II. Fontevraud, workshop on pattern formation in Medicine and Biology.

a Gonzales, J.E. 1993 Effect of seed size on germination and seedling vigor of *Virola koschnyi* Warb. *Forest Ecology and Management* 57:275-281.

Gonzales-Andujar, J.L. & Perry, J.N. 1993 Chaos, metapopulations and dispersal. *Ecological*

Modelling 65:255-263.

Grace, J.B. 1990 On the relationship between plant traits and competitive ability. In: *Perspectives on plant competition.* ed. Grace, J.B. & Tilman, D. pp. 51-65. Academic Press, San Diego.

Grace, J.B. & Tilman, D. 1990 Perspectives on plant competition: some introductory remarks. In: *Perspectives on plant competition.* ed. Grace, J.B. & Tilman, D. pp. 3-7. Academic Press, San Diego.

Grassberger, P. 1983 Generalised dimensions of strange attractors. *Physics Letters* A 97:227-230.

a Graven, L.M. & Carter, P.R. 1990 Seed size/shape and tillage system effect on corn growth and grain yield. *Journal of Production Agriculture* 3:445-452.

Green, D.G. 1989 Simulated effects of fire, dispersal and spatial pattern on competition within forest mosaics. *Vegetatio* 82:139-153.

Green, D.M. 1991 Chaos, fractals and nonlinear dynamics in evolution and phylogeny. *Trends in Evolution and Ecology* 6:333-337.

Grenfell, B.T. 1992 Chance and chaos in measles dynamics. *Journal of the Royal Statistical Society* B 54:383-398.

Grenfell, B.T., Bolker, B.M. & Kleczkowski, A. 1995 Seasonality and extinction in chaotic metapopulations. *Proceedings of the Royal Society of London* B 259:97-103.

Grieve, C.M. & François, L.E. 1992 The importance of initial seed size in wheat - response to salinity. *Plant and Soil* 147:197-205.

Grimm, V., Schmidt, E. & Wissel, C. 1992 On the application of stability concepts in ecology. *Ecological Modelling* 63:143-161.

Grindod, P., Murray, J.D. & Sinha, S. 1989 Steady-state spatial patterns in a cell-chemotaxis model. *IMA Journal of Mathematics Applied in Medicine and Biology* 6:69-79.

a Gross. K.L. 1986 Patterns and predictions of differences in seed size. *American Journal of Botany* 76:658.

Gross. K.L., Pregitzer, K. & Burton, A.J. 1995 Spatial variation in nitrogen availability in three successional plant communities. *Journal of Ecology* 83:357-367.

Grussbach, H. & Schreiber, M. 1993 Spatial multifractal properties of wave packets in the Anderson model of localisation. *Physical Review* B 48:6650-6653.

Guckenheimer, J., Oster, G. & Ipaktchi, A. 1977 The dynamics of density dependent population models. *Journal of Mathematical Biology* 4:101-147.

a Gunji, Y. 1990 Pigment color patterns of molluscs as an autonomous process generated by asynchronous automata. *Biosystems* 23:317-334.

Gurevitch, J., Wilson, P., Stone, J.L., Teese, P. & Stoutenburgh, R.J. 1990 Competition among old-field perennials at different levels of soil fertility and available space. *Journal of Ecology* 78:727-744.

Haefner, J.W., Poole, G.C., Dunn, P.V. & Decker, R.T. 1991 Edge effects in computer models of spatial competition. *Ecological Modelling* 56:221-244.

Hagan, P.S. 1982 Spiral waves in reaction-diffusion equations. *SIAM Journal of Applied Mathematics* 42:762-786.

Halley, J.M., Comins, H.N., Lawton, J.H. & Hassell, M.P. 1994 Competition, succession and pattern in fungal communities - towards a cellular automaton model. *Oikos* 70:435-442.

Halsey, T.C., Jensen, M.H., Kadanoff, L.P., Procaccia, I. & Shraiman, B.I. 1986 Fractal measures and their singularities: the characterisation of strange sets. *Physical Review* A 33:1141-1151.

Hanski, I. 1983 Coexistence of competitors in a patchy environment. *Ecology* 64:493-500.

Hanski, I. 1989 Metapopulation dynamics: does it help to have more of the same? *Trends in Evolution and Ecology* 4:113-114.

Hanski, I. 1994a Spatial scale, patchiness and population dynamics on land. *Philosophical Transactions of the Royal Society of London* B 343:19-25.

Hanski, I. 1994b A practical model of metapopulation dynamics. *Journal of Animal Ecology* 63:151-162.

Hanski, I. & Gilpin, M. 1991 Metapopulation dynamics: brief history and conceptual domain. *Biological Journal of the Linnean Society* 42:3-16.

Hanski, I., Turchin, P., Korpimaki, E. & Henttoren, H. 1993 Population oscillations of borel rodents: regulation by mustelid predators leads to chaos. *Nature* 363:232-235.

Hanski, I. & Zhang, D.-Y. 1993 Migration, metapopulation dynamics and fugitive co-existence. *Journal of Theoretical Biology* 163:491-504

Hara, T. 1988 Dynamics of size structure in plant populations. *Trends in Evolution and Ecology* 3:129-133.

Harper, J.L. 1977 *Plant population ecology.* Academic Press, London.

Harris, T.E. 1974 Contact iterations on a lattice. *Annals of Probability* 2:969-988.

Hartnett, D.C. & Bazzaz, F.A. 1983 Physiological integration among intraclonal ramets in *Solidago canadensis*. *Ecology* 64:779-788.

a Hartnett, D.C. & Bazzaz, F.A. 1985 The integration of neighbourhood effects by clonal genets in *Solidago canadensis*. *Journal of Ecology* 73:415-428.

Hassell, M.P., Comins, H.N. & May, R.M. 1991 Spatial structure and chaos in insect population dynamics. *Nature* 353:255-258.

Hassell, M.P., Comins, H.N. & May, R.M. 1994 Species coexistence and self-organising spatial dynamics. *Nature* 370:290-292.

a Hassell, M.P., Lawton, J.H. & May, R.M. 1976 Patterns of dynamical behaviour in single-species populations. *Journal of Animal Ecology* 45:471-486.

Hastings, A. 1977 Spatial heterogeneity and the stability for predator-prey systems. *Theoretical Population Biology* 12:37-48.

Hastings, A. 1978a Spatial heterogeneity and the stability of predator-prey systems: predator-mediated coexistence. *Theoretical Population Biology* 14:380-395.

Hastings, A. 1978b Global stability in Lotka-Volterra systems with diffusion. *Journal of Mathematical Biology* 6:163-168.

Hastings, A. 1980 Disturbance, coexistence, history, and competition for space. *Theoretical Population Biology* 98:363-373.

Hastings, A. 1992 Age dependent dispersal is not a simple process: density dependence, stability, and chaos. *Theoretical Population Biology* 41:388-400.

Hastings, A. 1993 Complex interactions between dispersal and dynamics: lessons from coupled logistic equations. *Ecology* 74:1362-1372.

Hastings, A. & Higgins, K. 1994 Persistence of transients in spatially structured ecological models. *Science* 263:1133-1136.

Hastings, A. & Wolin, C.L. 1989 Within-patch dynamics in a metapopulation. *Ecology* 70:1261-1266.

Heather, D.W. & Sieczka, J.B. 1991 Effect of seed size and cultivar on emergence and stand establishment of broccoli in crusted soil. *Journal of the American Society of Horticultual Science* 116:946-949.

Hegazy, A.K. 1994 Trade-off between sexual and vegetative reproduction of the weedy *Heliotropium curappariсum*. *Journal of Arid Environments* 27:209-270.

Heltshe, J.F. & Ritchey, T.A. 1984 Spatial pattern detection using quadrat samples. *Biometrics* 40:877-885.

Hentschel, H.G.E. & Procaccia, I. 1983 The infinite number of generalised dimensions of fractals and strange attractors. *Physica* 8D:435-444.

Herman, G.T. 1969 Computing ability of a developmental model for filamentous organisms. *Journal of Theoretical Biology* 25:421-435.

Hobbs, R.J. & Hobbs, V.J. 1987 Gophers and grassland: a model of vegetation response to patchy soil disturbance. *Vegetatio* 69:141-146.

Hochberg, M.E., Menaut, J.C. & Gignoux, J. 1994 The influences of tree biology and fire in the spatial structure of the West African savannah. *Journal of Ecology* 82:217-226.

Hocking, P.J. & Steer, B.T. 1989 Effects of seed size, cotyledon removal and nitrogen stress on growth and yield components of oilseed sunflower. *Field Crops Research* 22:59-75.

Höfer, T., Sherratt, J.A. & Maini, P.K. 1995 *Dictyostelium discoideum*: cellular self-organisation in an excitable biological medium. *Proceedings of the Royal Society of London* B 259:249-257.

Hogeweg, P. 1988 Cellular automata as a paradigm for ecological modelling. *Applied Mathematics and Computation* 27:81-100.

a Holbrook, N.M. & Putz, F.E. 1989 Influence of neighbors on tree form: effects of lateral shade and prevention of sway on the allometry of *Liquidambar styraciflua* (sweet gum). *American Journal of Botany* 76:1740-1749.

Holmes, E.E., Lewis, M.A., Banks, J.E. & Veit, R.R. 1994 Partial differential equations in ecology: spatial interactions and population dynamics. *Ecology* 75:17-29.

Holsinger, K.E. & Roughgarden, J. 1985 A model for the dynamics of an annual plant population. *Theoretical Population Biology* 28:288-313.

Holt, R.D. 1992 A neglected facet of island biogeography: the role of internal spatial dynamics in area effects. *Theoretical Population Biology* 41:354-371.

Horn, H.S. 1975 Forest succession. *Scientific American* 232:90-98.

Horn, H.S. & MacArthur, R.H. 1972 Competition among fugitive species in a harlequin environment. *Ecology* 53:749-752.

a Houssard, C. & Escarre, J. 1991 The effects of seed weight on growth and competitive ability of *Rumex acetosella* from two successional old-fields. *Oecologia* 86:236-242.

Hudson, P.J. 1989 Territorial status and survival in a low density grouse population: preliminary observations and experiments. In: *Red grouse population processes* ed. Lance, A.N. & Lawton, J.H. pp. 20-28. Sandy: Royal Society for the Protection of Birds.

Hudson, P.J. & Dobson, A.P. 1989 Red grouse population cycles and the population dynamics of the caecal nematode *Trichostrongylus tenuis*. In: *Red grouse population processes* ed. Lance, A.N. & Lawton, J.H. pp. 5-19. Sandy: Royal Society for the Protection of Birds.

Hunter, M.D. & Price, P.W. 1992 Playing chutes and ladders: heterogeneity and the relative roles of bottom-up and top-down forces in natural communities. *Ecology* 73:724-732.

Huston, M. 1986 Size bimodality in plant populations: an alternative hypothesis. *Ecology* 67:265-269.

Huston, M., DeAngelis, D.L. & Post, W. 1988 New computer models unify ecological theory. *Bioscience* 38:682-691.

Hutchings, M.J. & Budd, C.S.J. 1981 Plant competition and its course through time. *Bioscience* 31:640-645.

Hutchings, M.J. & Slade, A.J. 1988 Morphological plasticity, foraging and integration in clonal perennial herbs. In: *Plant population ecology* ed. Davy, A.J., Hutchings, M.J. & Watkinson, A.R. pp. 83-109. Blackwell Scientific Publications, Oxford.

Huyghe, C. 1993 Growth of white lupin seedlings during the rosette stage as affected by seed size. *Agronomie* 13:145-153.

Inghe, O. 1989 Genet and ramet survivorship under different mortality regimes - a cellular automata model. *Journal of Theoretical Biology* 138:257-270.

Inouye, R.S. & Tilman, D. 1988 Convergence and divergence of old-field plant communities along experimental nitrogen gradients. *Ecology* 69:995-1004.

Ives, A.R. 1991 Chaos in time and space. *Nature* 353:214-215.

Iwasa, Y., Satō, K. & Nakashima, S. 1991 Dynamics modelling of wave regeneration (Shimagare) in subalpine Abies forests. *Journal of Theoretical Biology* 152:143-158.

Jackson, R.B. & Caldwell, M.M. 1992 Shading and the capture of localized soil nutrients - nutrient contents, carbohydrates, and root uptake kinetics of a perennial tussock grass. *Oecologia* 91:457-462.

Jackson, R.B. & Caldwell, M.M. 1993 The scale of nutrient heterogeneity around individual plants and its quantification with geostatistics. *Ecology* 74:612-614.

Jenkins, D., Watson, A. & Miller, G.R. 1963 Population studies on red grouse, *Lagopus lagopus scoticus* (Lath.) in North-east Scotland. *Journal of Animal Ecology* 32:317-376.

Jenkins, D., Watson, A. & Miller, G.R. 1967 Population fluctuations in the red grouse *Lagopus lagopus scoticus*. *Journal of Animal Ecology* 36:97-122.

Jensen, M.H., Paladin, G. & Vulpiani, A. 1991 Multiscaling in multifractals. *Physics Review Letters* 67:208-211.

Jetschke, G. 1992 Stochastic population models and their relevance for the conservation of species. *Ecological Modelling* 63:71-89.

Judson, O.P. 1994a The rise of the individual-based model in ecology. *Trends in Evolution and Ecology* 9:9-14.

Judson, O.P. 1994b Individual-based models - reply. *Trends in Evolution and Ecology* 9:299-300.

a Jurado, E. & Westoby, M. 1992 Seedling growth in relation to seed size among species of arid Australia. *Journal of Ecology* 80:407-416.

Kadmon, R. 1995 Plant competition along soil moisture gradients: a field experiment with the desert annual *Stipa capensis*. *Journal of Ecology* 83:253-262.

Kadmon, R. & Schmida, A. 1990 Spatiotemporal demographic processes in plant populations: an approach and a case study. *American Naturalist* 135:382-397.

Kaneko, K. 1984 Period-doubling of kink-antikink patterns, quasiperiodicity in antiferro-like structures and spatial intermittency in coupled logistic lattices. *Progress in Theoretical Physics* 72:480-486.

Kaneko, K. 1985 Spatiotemporal intermittency in coupled map lattices. *Progress in Theoretical Physics* 74:1033-1044.

Kaneko, K. 1986 Lyapunov analysis and information flow in coupled map lattices. *Physica* 23D:436-447.

Kaneko, K. 1989 Spatiotemporal chaos in 1- and 2-dimensional coupled map lattices. *Physica* 37D:60-82.

Kaneko, K. 1990 Supertransients, spatiotemporal intermittency and stability of fully developed spatiotemporal chaos. *Physics Letters* A 149:105-112.

Kareiva, P. 1987 Habitat fragmentation and the stability of predator-prey interactions. *Nature*

326:388-390.

Kareiva, P. 1990 Population dynamics in spatially complex environments: theory and data. *Philosophical Transactions of the Royal Society of London* B 330:175-190.

Kareiva, P. 1994 Space: the final frontier for ecological theory. *Ecology* 75:1.

Kareiva, P. & Andersen, M. 1988 Spatial aspects of species interactions: the wedding of models and experiments. In: *Community ecology* ed. Hastings, A. pp. 35-50. *Springer lecture notes in biomathematics* Vol. 77, New York.

Karlson, R.H. & Jackson, J.B.C. 1981 Competitive networks and community structure: a simulation study. *Ecology* 62:670-678.

Kauffman, S.A. 1969 Metabolic stability and epigenesis in randomly constructed genetic nets. *Journal of Theoretical Biology* 22:437-467.

Keeling, M.J. 1995 Doctoral thesis, University of Warwick. *Manuscript.*

Keeling, M.J., Hendry, R.J., McGlade, J.M., & Rand, D.A. 1995 Characteristic length scales of discrete spatial models in ecology. *Manuscript.*

Keeling, M.J. & Sheppard, C.R.C. 1994 A cellular automaton model for coral dynamics and the implications for biodiversity. *Manuscript.*

Keller, E.F. & Segel, L.A. 1970 Initiation of slime mold aggregation viewed as an instability. *Journal of Theoretical Biology* 26:399-415.

Kelly, V.R. & Canham, C.D. 1992 Resource heterogeneity in oldfields. *Journal of Vegetation Science* 3:545-552.

a Kelly, C.K. & Purvis, A. 1993 Seed size and establishment conditions in tropical trees: on the use of taxonomic relatedness in determining ecological patterns. *Oecologia* 94:356-360.

Kenkel, N.C. 1988 Patterns of self-thinning in jack pine: testing the random mortality hypoth-

esis. *Ecology* 69:1017-24.

Kenkel, N.C., Hoskins, J.A. & Hoskins, W.D. 1989a Local competition in a naturally established jack pine stand. *Canadian Journal of Botany* 67:2630-2635.

Kenkel, N.C., Hoskins, J.A. & Hoskins, W.D. 1989b Edge effects in the use of polygons to study competition. *Ecology* 70:272-274.

Kingsland, S.E. 1991 Defining ecology as a science. In: *Foundations of ecology* ed. Real, L.A. & Brown, J.H. pp. 1-13. University of Chicago Press, London.

Kishimoto, 1981 Instability of non-constant equilibrium solutions of a system of competition diffusion equations. *Journal of Mathematical Biology* 13:105-114.

Kishimoto, 1982 The diffusive Lotka-Volterra system with three species can have a stable non-constant equilibrium solution. *Journal of Mathematical Biology* 16:103-112.

Kitagawa, T. 1974 Cell space approaches in biomathematics. *Mathematical Biosciences* 19:27-71.

a Klinkhamer, P.G.L., Meelis, E., De Jong, T.J. & Weiner, J. 1992 On the analysis of size-dependent reproductive output in plants. *Functional Ecology* 6:308-316.

Knox, R.G., Peet, R.K. & Christensen, N.L. 1989 Population dynamics in loblolly pine stands: changes in skewness and size inequality. *Ecology* 70:1153-1166.

Kolasa, J. & Pickett, S.T.A. 1991 *Ecological heterogeneity. Springer Ecological Studies* Vol. 86, Berlin.

Kotliar, N.B. & Wiens, J.A. 1990 Multiple scales of patchiness and patch structure: a hierarchical framework for the study of heterogeneity. *Oikos* 59:253-260.

a Kougias, Ch. F. & Schulte, J. 1990 Simulating the immune response to the HIV-1 virus with cellular automata. *Journal of Statistical Physics* 60:263-273.

Krannitz, P.G., Aarssen, L.W. & Dow, J.M. 1991 The effect of genetically based differences in seed size on seedling survival in *Arabidopsis Thaliana* (Brassicaceae). *American Journal of Botany* 78:446-450.

Kretzschmar, M. & Adler, F.R. 1993 Aggregated distributions in models for patchy populations. *Theoretical Population Biology* 43:1-39.

Krishna Iyer, P.V. 1949 The first and second moments of some probability distributions arising from points on a lattice and their application. *Biometrika* 36:135-141.

Krishna Iyer, P.V. 1950 The theory of probability distributions of points on a lattice. *Annals of Mathematical Statistics* 21:198-217.

Lafond, G.P. & Baker, R.J. 1986 Effects of genotype and seed size on speed of emergence and seedling vigor in 9 spring wheat cultivars. *Crop Science* 26:341-346.

Lance, A.N. 1978 Survival and recruitment success of individual young cock red grouse *Lagopus L. scoticus* tracked by radio-telemetry. *Ibis* 120:369-378.

Lance, A.N. & Lawton, J.H. 1989 *Red grouse population processes.* Sandy: Royal Society for the Protection of Birds.

Langton, C.G. 1990 Computation at the edge of chaos: phase transitions and emergent computation. *Physica* 42D:12-37.

Lavorel, S., O'Neill, R.V. & Gardner, R.H. 1994 Spatio-temporal dispersal strategies and annual plant species coexistence in a structured landscape. *Oikos* 71:75-88.

Lawton, J.H. 1989 Red grouse populations and moorland management. In: *Red grouse population processes* ed. Lance, A.N. & Lawton, J.H. pp. 84-99. Sandy: Royal Society for the Protection of Birds.

Lawton, J.H., Naeem, S., Woodfin, R.M., Brown, V.K., Gange, A., Godfray, H.J.C., Heads, P.A., Lawler, S., Magda, D., Thomas, C.D., Thompson, L.J. & Young, S. 1993 The Ecotron -

a controlled environmental facility for the investigation of population and ecosystem processes. *Philosophical Transactions of the Royal Society of London* B 341:181-194.

Legendre, P. & Fortin, M.-J. 1989 Spatial pattern and ecological analysis. *Vegetatio* 80:107-138.

Leishman, M.R. & Westoby, M. 1994a The role of seed size in seedling establishment in dry soil conditions - experimental evidence from semi-arid species. *Journal of Ecology* 82:249-258.

a Leishman, M.R. & Westoby, M. 1994b Hypotheses on seed size - test using the semiarid flora of Western New South Wales, Australia. *American Naturalist* 143:890-906.

a Leishman, M.R. & Westoby, M. 1994c The role of large seed size in shaded conditions - experimental evidence. *Functional Ecology* 8:205-214.

Leishman, M.R., Westoby, M. & Jurado E. 1995 Correlates of seed size variation: a comparison among five temperate flora. *Journal of Ecology* 83:517-530.

Lepš, J. & Kindlmann, P. 1987 Models of the development of spatial pattern of an even-aged plant population over time. *Ecological Modelling* 39:45-57.

Leung, A. 1978 Limiting behaviour for a prey-predator model with diffusion and crowding effects. *Journal of Mathematical Biology* 6:87-93.

Levi, B.G. 1986 New global fractal formalism describes paths to turbulence. *Physics Today* 39:17-18.

Levin, D.A. 1988 Plasticity, canalization and evolutionary stasis in plants. In: *Plant population ecology* ed. Davy, A.J., Hutchings, M.J. & Watkinson, A.R. pp. 35-45. Blackwell Scientific Publications, Oxford.

Levin, S.A. 1974 Dispersion and population interactions. *American Naturalist* 108:207-227.

Levin, S.A. 1990 Physical and biological scales and the modelling of predator-prey interactions in large marine ecosystems. In: *Large patterns, marine processes, ecosystems and yield* ed.

Sherman, K., Alexander, L.M. & Gold, B.D. American Association for the Advancement of Science, Washington.

Levin, S.A. 1988 Pattern, scale and variability: an ecological perspective. In: *Community ecology* ed. Hastings, A. pp. 1-12. *Springer lecture notes in biomathematics* Vol. 77, New York.

Levin, S.A. 1992 The problem of pattern and scale in ecology. *Ecology* 73:1943-1967.

Levin, S.A., Cohen, D. & Hastings, A. 1984 Dispersal strategies in patchy environments. *Theoretical Population Biology* 26:165-191.

Levin, S.A. & Paine, R.T. 1974 Disturbance, patch formation and community structure. *Proceedings of the National Academy of Science USA* 71:2744-2747.

Levin, S.A., Powell, T.M. & Steele, J.H. 1993 *Patch dynamics. Springer lecture notes in biomathematics* Vol. 96, Berlin.

Levin, S.A. & Segel, L.A. 1976 Hypothesis for origin of planktonic patchiness. *Nature* 259:659.

Levin, S.A. & Segel, L.A. 1985 Pattern generation in space and aspect. *SIAM Review* 27:45-67.

Lewis, M.A. 1994 Spatial coupling of plant and herbivore dynamics: the contribution of herbivore dispersal to transient and persistent 'waves' of damage. *Theoretical Population Biology* 45:277-312.

Liddle, M.J., Budd, C.S.J. & Hutchings, M.J. 1982 Population dynamics and neighbourhood effects in establishing swards of *Festuca rubra*. *Oikos* 38:52-59.

Liebovitch, L.S. & Toth, T. 1989 A fast algorithm to determine fractal dimensions by box counting. *Physics Letters* A 141:386-390.

Lieffers, V.J. & Titus, S.J. 1989 The effects of stem density and nutrient status on size inequality. *Canadian Journal of Botany* 67:2900-2903.

Lindenmayer, A. 1968a Mathematical models for cellular interactions in development. I Fila-

ments with one-sided inputs. *Journal of Theoretical Biology* 18:280-299.

Lindenmayer, A. 1968b Mathematical models for cellular interactions in development. II Simple and branching filaments with two-sided inputs. *Journal of Theoretical Biology* 18:300-315.

Lloyd, A.L. 1994 Chaos and forecasting. *Trends in Evolution and Ecology* 9:244-245.

Lloyd, A.L. 1995 The coupled logistic map: a simple model for the effects of spatial heterogeneity on population dynamics. *Journal of Theoretical Biology* 173:217-230.

Lomnicki, A. 1989 Avoiding chaos. *Trends in Evolution and Ecology* 4:239.

Lomnicki, A. 1992 Population ecology from the individual perspective. In: *Individual-based models and approaches in ecology: populations, communities and ecosystems* ed. DeAngelis, D.L. & Gross, L.J. pp. 3-17. Chapman & Hall, New York.

Lorenz, E.M. 1963 Deterministic nonperiodic flow. *Journal of Atmospheric Sciences* 20:130-141.

Lotka, A.J. 1920 Analytical note on certain rhythmic relations in organic systems. *Proceedings of the National Academy of Science USA* 6:410-415.

Louda, S.M., Keeler, K.H. & Holt, R.D. 1990 Herbivore influences on plant performance and competitive interactions. In: *Perspectives on plant competition.* ed. Grace, J.B. & Tilman, D. pp. 414-444. Academic Press, San Diego.

Ludwig, D., Aronson, D.G. & Weinberger, H.F. 1979 Spatial patterning of the spruce budworm. *Journal of Mathematical Biology* 8:217-258.

Ludwig, D. & Levin, S.A. 1991 Evolutionary stability of plant communities and the maintenance of multiple dispersal types. *Theoretical Population Biology* 40:285-307.

Mack, R.N. & Harper, J.L. 1977 Interference in dune annuals: spatial pattern and neighbourhood effects. *Journal of Ecology* 65:345-363.

MacKenzie, J.M.D. 1952 Fluctuations in the numbers of British Tetraonids. *Journal of Animal*

Ecology 21:128-153.

s Mackinder, H.J. 1887 *Proceedings of the Royal Geographical Society* 9:141-150.

Maginu, K. 1975 Reaction-diffusion equation describing morphogenesis. I. Waveform stability of stationary wave solutions in a one dimensional model. *Mathematical Biosciences* 27:17-98.

Maini, P.K. 1993a The role of boundary conditions and background environment on patterns in reaction diffusion systems. Fontevraud, workshop on pattern formation in Medicine and Biology.

Maini, P.K. 1993b A tissue-interaction model for skin organ morphogenesis. Fontevraud, workshop on pattern formation in Medicine and Biology.

Maini, P.K. 1994 Sequential pattern formation in a model for skin morphogenesis. University of Manchester, VIth International Congress of Ecology.

Mandelbrot, B.B. 1974 Intermittent turbulence in self-similar cascades: divergence of high moments and dimensions of the carrier. *Journal of Fluid Mechanics* 62:331-358.

Mangel, M. & Tier, C. 1993 Dynamics of metapopulations with demographic stochasticity and environmental catastrophes. *Theoretical Population Biology* 44:1-31.

Mani, G.S. 1989 Avoiding chaos. *Trends in Evolution and Ecology* 4:239-240.

Marañon, T. & Grubb, P.J. 1993 Physiological basis and ecological significance of the seed size and relative growth rate relationship in Mediterranean annuals. *Functional Ecology* 7:591-599.

Markus, M. 1992 Are one-dimensional maps of any use in ecology? *Ecological Modelling* 63:243-259.

Marshall, D.L. 1986 Effect of seed size on seedling success in 3 species of *Sesbania* (Fabaceae). *American Journal of Botany* 73:457-464.

Martiel, J.-P. 1993 A model for cyclic AMP signalling in *Dictyostelium discoideum* cells: from

oscillations to chaos. Fontevraud, workshop on pattern formation in Medicine and Biology.

The Maths Works Inc., 1992 *MATLAB User's Guide for Unix workstations.* The Maths Works Inc., Massachussetts.

Mauchamp, A., Rambal, S. & Lepart, J. 1994 Simulating the dynamics of a vegetation mosaic: a spatialized functional model. *Ecological Modelling* 71:107-130.

May, R.M. 1974 Biological populations with non-overlapping generations: stable points, stable cycles and chaos. *Science* 186:645-647.

May, R.M. 1975 Biological populations obeying difference equations: stable points, stable cycles and chaos. *Journal of Theoretical Biology* 51:511-524.

May, R.M. 1976 Simple mathematical models with very complicated dynamics. *Nature* 261:459-467.

May, R.M. 1981 The role of theory in ecology. *American Zoologist* 21:903-910.

May, R.M. 1986 The search for patterns in the balance of nature: advances and retreats. *Ecology* 67:1115-1126.

May, R.M. 1987 Chaos and the dynamics of biological populations. *Proceedings of the Royal Society of London* A 413:27-44.

May, R.M. 1995 Spatial chaos and its role in ecology and evolution. In: *Frontiers of theoretical biology* ed. Levin, S.A. *Springer lecture notes in biomathematics* Vol. 100, Berlin.

May, R.M. & Oster, G.F. 1976 Bifurcations and dynamic complexity in simple ecological models. *American Naturalist* 110:573-599.

Maynard Smith, J. 1974 *Models in ecology.* Cambridge University Press, Cambridge.

McCauley, E., Wilson, W.G. & DeRoos, A.M. 1993 Dynamics of age-structured and spatially structured predator-prey interactions: individual-based models and population-level formula-

tions. *American Naturalist* 142:412-442.

McConnaughay, K.D.M. & Bazzaz, F.A. 1987 The relationship between gap size and performance of several colonizing annuals. *Ecology* 68:411-416.

McGlade, J.M. 1993 Alternative ecologies. *New Scientist* suppl. 137:14-16.

McGlade, J.M. 1994 Chaos and its implications for marine resources science. *Marine Environmental Management Review of Events in 1993 and Future Trends* 1:57-60.

McGlade, J.M., Hendry, R.J. & Keeling, M.J. 1994 Dynamics of cumulative and cascading effects. *Manuscript.*

McLauglin, J.F. & Roughgarden, J. 1991 Pattern and stability in predator-prey communities: how diffusion in spatially variable environments affects the Lotka-Volterra model. *Theoretical Population Biology* 40:148-172.

McMurtrie, R. 1981 Suppression and dominance of trees with overlapping crowns. *Journal of Theoretical Biology* 89:151-174.

Mead, R. 1966 A relationship between individual plant-spacing and yield. *Annals of Botany* 30:301-309.

Mead, R. 1967 A mathematical model for the estimation of inter-plant competition. *Biometrics* 23:189-205.

Mead, R. 1974 A test for spatial pattern at several scales using data from a grid of contiguous quadrats. *Biometrics* 30:295-307.

a Mehlman, D.W. 1993 Seed size and seed packaging variation in *Baptisia lanceolata* (Fabaceae). *American Journal of Botany* 80:735-742.

a Meinhardt, H. & Klingler, M. 1987 A model for pattern formation on the shells of molluscs. *Journal of Theoretical Biology* 126:63-89.

Meisel, L.V., Johnson, M. & Cole, P.J. 1992 Box-counting multifractal analysis. *Physics Review Letters* A 45:6989-6996.

Menge, B.A. & Olson, A.M. 1990 Role of scale and environmental factors in regulation of community structure. *Trends in Evolution and Ecology* 5:52-57.

Mian, M.A.R. & Nafziger, E.D. 1994 Seed size and water potential effects on germination and seedling growth of winter wheat. *Crop Science* 34:169-171.

Miller, T.E. & Weiner, J. 1989 Local density variation may mimic effects of asymmetric competition on plant size variability. *Ecology* 70:1188-1191.

Milosevic, M., Rajnpreht, J. & Dokic, P. 1992 Effect of different seed size fractions on germination in sugar beet (*Beta vulgaris* L.). *Seed Science and Technology* 20:703-710.

Mimura, M. & Kawasaki, K. 1980 Spatial segregation in competitive interaction diffusion equations. *Journal of Mathematical Biology* 9:49-64.

Mimura, M. & Murray, J.D. 1978 On a diffusive prey-predator model which exhibits patchiness. *Journal of Theoretical Biology* 75:249-262.

Minnich, R.A. 1983 Fire mosaics in Southern California and Northern Baja California. *Science* 219:1287-1294.

Mitchell-Olds, T. 1987 Analysis of local variation in plant size. *Ecology* 68:82-87.

Mitchison, G.J. 1980 A model for vein formation in higher plants. *Proceedings of the Royal Society of London* B 207:79-109.

Mithen, R., Harper, J.L. & Weiner, J. 1984 Growth and mortality of individual plants as a function of 'available area'. *Oecologia* 62:57-60.

Moilanen, A. & Hanski, I. 1994 Habitat destruction and coexistence of competitors in a spatially realistic population model. *Journal of Animal Ecology* 64:141-144.

a Molofsky, J. 1994 Population dynamics and pattern formation in theoretical populations. *Ecology* 75:30-39.

Moloney, K.A. 1988 Fine-scale spatial and temporal variation in the demography of a perennial bunchgrass. *Ecology* 69:1588-1598.

Moloney, K.A. 1993 Determining process through pattern: reality or fantasy? In: *Patch dynamics* ed. Levin, S.A., Powell, T.M. & Steele, J.H. pp. 61-69. *Springer lecture notes in biomathematics* Vol. 96, Berlin.

Moloney, K.A., Levin, S.A., Chiarello, N.R. & Buttel, L. 1992 Pattern and scale in a serpentine grassland. *Theoretical Population Biology* 41:257-276.

Monk, P.B. & Othmer, H.G. 1989 Cyclic AMP oscillations in suspensions of *Dictyostelium discoideum*. *Philosophical Transactions of the Royal Society of London* B 323:185-224.

Moore, P.D. 1977 Restating the self-thinning rule. *Nature* 265:295.

Moore, P.D. 1993 For richer, for poorer. *Nature* 366:515.

Moran, P.A.P. 1948 The interpretation of statistical maps. *Journal of the Royal Statistical Society* B 10:243-251.

Moran, P.A.P. 1952 The statistical analysis of game-bird records. *Journal of Animal Ecology* 21:154-158.

Morris, W.F. 1990 Problems in detecting chaotic behaviour in natural populations by fitting simple discrete models. *Ecology* 71:1846-1862.

Morse, D.R., Lawton, J.H., Dodson, M.M. & Williamson, M.H. 1985 Fractal dimension of vegetation and the distribution of arthropod body lengths. *Nature* 314:731-733.

Moss, R., Parr, R. & Lambin, X. 1994 Effects of testosterone on breeding density, breeding success and survival of red grouse. *Proceedings of the Royal Society of London* B 258:175-180.

Moss, R., Rothery, P. & Trenholm, I.B. 1985 The inheritance of social dominance rank in red grouse *(Lagopus lagopus scoticus). Aggressive Behaviour* 11:253-259.

Moss, R., Shaw, J.L., Watson, A. & Trenholm, I.B. 1989 Role of the caecal threadworm *Trichostrongylus tenuis* in the population dynamics of red grouse. In: *Red grouse population processes* ed. Lance, A.N. & Lawton, J.H. pp. 62-71. Sandy: Royal Society for the Protection of Birds.

Moss, R., Trenholm, I.B., Watson, A. & Parr, R. 1990 Parasitism, predation and survival of hen red grouse *Lagopus lagopus scoticus* in spring. *Journal of Animal Ecology* 59:631-642.

Moss, R. & Watson, A. 1985 Adaptive value of spacing behaviour in population cycles of red grouse and other animals. *Symposia of the British Ecological Society* 25:275-294.

Moss, R. & Watson, A. 1989a Population regulation in red grouse. A theoretical outline. In: *Red grouse population processes* ed. Lance, A.N. & Lawton, J.H. pp. 29-34. Sandy: Royal Society for the Protection of Birds.

Moss, R. & Watson, A. 1989b Red grouse numbers in relation to their resources. In: *Red grouse population processes* ed. Lance, A.N. & Lawton, J.H. pp. 53-61. Sandy: Royal Society for the Protection of Birds.

Moss, R. & Watson, A. 1989c Predicting, manipulating and understanding red grouse population fluctuations. In: *Red grouse population processes* ed. Lance, A.N. & Lawton, J.H. pp. 72-77. Sandy: Royal Society for the Protection of Birds.

Moss, R. & Watson, A. 1991 Population cycles and kin selection in Red Grouse *Lagopus lagopus scoticus. Ibis* 133 suppl. 1:113-120.

Moss, R. & Watson, A. 1994 Population dynamics of red grouse. In: *Individuals, populations and patterns in ecology* ed. Leather, S.R., Watt, A.D., Mills, N.J. & Walters, K.F.A. pp. 87-96. Intercept, Andover.

Moss, R., Watson, A. & Rothery, P. 1984 Inherent changes in the body size, viability and behaviour of a fluctuating red grouse *Lagopus lagopus scoticus* population. *Journal of Animal Ecology* 53:171-189.

Moss, R., Watson, A., Trenholm, I.B. & Parr, R. 1993 Caecal threadworms *Trichostrongylus tenuis* in red grouse *Lagopus lagopus scoticus*: effects of weather and host density upon estimated worm burdens. *Parasitology* 107:199-209.

Motro, U. 1982a Optimal rates of dispersal. I. Haploid populations. *Theoretical Population Biology* 21:394-411.

Motro, U. 1982b Optimal rates of dispersal. II. Diploid populations. *Theoretical Population Biology* 21:412-429.

Mountford, M.D., Watson, A., Moss, R., Parr, R. & Rothery, P. 1989 Land inheritance and population cycles of red grouse. In: *Red grouse population processes* ed. Lance, A.N. & Lawton, J.H. pp. 78-83. Sandy: Royal Society for the Protection of Birds.

Mueller, L.D. & Ayala, F.J. 1981 Dynamics of single-species population growth: stability or chaos? *Ecology* 62:1148-1154.

Müller, F., Windhorst, W. & Jorgensen, S.E. 1992 Recent problems in ecosystem theory - conclusions of the workshop. *Ecological Modelling* 63:325-331.

Müller-Dombois, D. 1991 The mosaic theory and the spatial dynamics of natural dieback and regeneration in the Pacific forest. In: *The mosaic-cycle concept of ecosystems* ed. Remmert, H. pp. 46-60. *Springer Ecological Studies* Vol. 85, New York.

Murdoch, W.W., McCauley, E., Nisbet, R.M., Gurney, W.S.C. & DeRoos, A.M. 1992 Individual-based models: combining testability and generality. In: *Individual-based models and approaches in ecology: populations, communities and ecosystems* ed. DeAngelis, D.L. & Gross, L.J. pp. 18-35. Chapman & Hall, New York.

Murray, G.A., Swensen, J.B. & Auld, D.L. 1984 Influence of seed size and planting date on the performance of Austrian winter field peas. *Agronomy Journal* 76:595-598.

Murray, J.D. 1975 Non-existence of wave solutions for the class of reaction-diffusion equations given by the Volterra interacting-population equation with diffusion. *Journal of Theoretical Biology* 52:459-469.

Murray, J.D. 1981 A pre-pattern formation mechanism for animal coat markings. *Journal of Theoretical Biology* 88:161-199.

Murray, J.D. 1982 Parameter space for Turing instability in reaction diffusion mechanisms: a comparison of models. *Journal of Theoretical Biology* 98:143-163.

Murray, J.D. 1988 How the leopard gets its spots. *Scientific American* 258:62-69.

Murray, J.D. 1989 *Mathematical biology.* Springer Biomathematics Vol. 19, Berlin.

Murray, J.D. 1993a Spatial pattern formation with reaction-diffusion and cell-chemotaxis systems. Fontevraud, workshop on pattern formation in Medicine and Biology.

Murray, J.D. 1993b Modelling epidermal wound healing. Fontevraud, workshop on pattern formation in Medicine and Biology.

Murray, J.D. 1993c Mechanochemical theory of morphogenesis. Fontevraud, workshop on pattern formation in Medicine and Biology.

Murray, J.D. & Oster, G.F. 1984 Generation of biological pattern and form. *IMA Journal of Mathematics Applied in Medicine and Biology* 1:51-75.

Murray, J.D., Oster, G.F. & Harris, A.K. 1983 A mechanical model for mesenchymal morphogenesis. *Journal of Mathematical Biology* 17:125-129.

Murray, J.D. & Sperb, R.P. 1983 Minimum domains for spatial patterns in a class of reaction diffusion equations. *Journal of Mathematical Biology* 18:169-184.

Murray, J.D., Stanley, E.A. & Brown, D.L. 1986 On the spatial spread of rabies by foxes. *Proceedings of the Royal Society of London* B 229:111-150.

Naeem, S. 1990 Patterns of the distribution and abundance of competing species when resources are heterogeneous. *Ecology* 71:1422-1429.

a Nafziger, E.D. 1992 Seed size effects on yields of two corn hybrids. *Journal of Production Agriculture* 5:538-540.

Nagai, T. & Mimura, M. 1983 Asymptotic behaviour for a nonlinear degenerate diffusion equation in population dynamics. *SIAM Journal of Applied Mathematics* 43:449-464.

Nagao, R.T., Kimpel, J.A., Vierling, E. & Key, J.L. 1986 The heat shock response: a comparative analysis. In *Oxford surveys of plant molecular & cell biology* Vol. 3 ed. B.J. Miflin pp. 384-438. Oxford University Press, Oxford.

Nagatani, T. 1993 Scaling and multifractality in a river network model with flow-dependent meandering. *Journal of Physics* A 26:4273-4279.

Namba, T. 1980 Density-dependent dispersal and spatial distribution of a population. *Journal of Theoretical Biology* 86:351-363.

a Naylor, R.E. 1993 The effect of parent plant nutrition on seed size, viability and vigour and on germination of wheat and triticale at different temperatures. *Annals of Applied Biology* 123:379-390.

a Nee, S. & May, R.M. 1992 Dynamics of metapopulations: habitat destruction and competitive coexistence. *Journal of Animal Ecology* 61:37-40.

Nisbet, R., Blythe, S., Gurney, W., Metz, H. & Stokes, K. 1989 Avoiding chaos. *Trends in Evolution and Ecology* 4:238-239.

Nowak, M.A. & May, R.M. 1992 Evolutionary games and spatial chaos. *Nature* 359:826-829.

Oborny, B. 1994a Growth rules in clonal plants and environmental predictability - a simulation study. *Journal of Ecology* 82:341-351.

a Oborny, B. 1994b Spacer length in clonal plants and the efficiency of resource capture in heterogeneous environments - a Monte Carlo simulation. *Folia Geobotanica & Phytotaxonomica* 29:139-158.

Okubo, A. & Levin, S.A. 1989 A theoretical framework for data analysis of wind dispersal of seed and pollen. *Ecology* 70:329-338.

Okubo, A., Maini, P.K., Williamson, M.H. & Murray, J.D. 1989 On the spatial spread of the grey squirrel in Britain. *Proceedings of the Royal Society of London* B 238:113-125.

Olsen, L.F. & Schaffer, W.M. 1990 Chaos versus noisy periodicity: alternative hypotheses for childhood epidemics. *Science* 249:499-504.

Olsen, L.F., Truty, G.L. & Schaffer, W.M. 1988 Oscillations and chaos in epidemics: a nonlinear dynamic study of six childhood diseases in Copenhagen, Denmark. *Theoretical Population Biology* 33:344-370.

Othmer, H.G. & Scriven, L.E. 1971 Instability and dynamic pattern in cellular networks. *Journal of Theoretical Biology* 32:507-537.

Othmer, H.G. & Scriven, L.E. 1974 Non-linear aspects of dynamic pattern in cellular networks. *Journal of Theoretical Biology* 43:83-112.

Pacala, S.W. 1986 Neighbourhood models of plant population dynamics. 2. Multi-species models of annuals. *Theoretical Population Biology* 29:262-292.

Pacala, S.W. 1987 Neighbourhood models of plant population dynamics. 3. Models with spatial heterogeneity in the physical environment. *Theoretical Population Biology* 31:359-392.

a Pacala, S.W. & Crawley, M.J. 1994 Herbivores and plant diversity. *American Naturalist* 140:243-260.

Pacala, S.W., Hassell, M.P. & May, R.M. 1990 Host-parasitoid associations in patchy environments. *Nature* 344:150-153.

Pacala, S.W. & Roughgarden, J. 1982 Spatial heterogeneity and interspecific competition. *Theoretical Population Biology* 21:92-113.

Pacala, S.W. & Silander, J.A. 1985 Neighbourhood models of plant population dynamics. I. Single species models of annuals. *American Naturalist* 125:385-411.

Pacala, S.W. & Silander, J.A. 1987 Neighbourhood interference among velvet leaf, *Abutilon theophrasti*, and pigweed, *Amaranthus retroflexus*. *Oikos* 48:217-224.

Pacala, S.W. & Silander, J.A. 1990 Field tests of neighbourhood population dynamic models of two annual weed species. *Ecological Monographs* 60:113-134.

Pacala, S.W. & Tilman, D. 1994 Limiting similarity in mechanistic and spatial models of plant competition in heterogeneous environments. *American Naturalist* 143:222-257.

Pacala, S.W. & Weiner, J. 1991 Effects of competitive asymmetry on a local density model of plant interference. *Journal of Theoretical Biology* 149:165-179.

Packard, N.H., Crutchfield, J.P., Farmer, J.D. & Shaw, R.S. 1980 Geometry from a time series. *Physics Review Letters* 45:712-716.

Packard, N.H. & Wolfram, S. 1984 Two-dimensional cellular automata. *Journal of Statistical Physics* 38:901-946.

Palmer, T.N., Buizza, R., Molteni, F., Chen, Y.-C. & Corti, S. 1994 Singular vectors and the predictability of weather and climate. *Philosophical Transactions of the Royal Society of London* A 348:459-475.

Pawelzik, K. & Schuster, H.G. 1987 Generalised dimensions and entropies from a measured time series. *Physical Review* A 35:481-484.

a Pearson, C.H. & Miklas, P.N. 1992 Seed size and planting depth effects on emergence and yield of pinto bean. *Journal of Production Agriculture* 5:103-106.

Peart, D.R. 1985 The quantitative representation of seed and pollen dispersal. *Ecology* 66:1081-1083.

Penridge, L.K. & Walker, J. 1986 Effect of neighbouring trees on eucalypt growth in a semi-arid woodland in Australia. *Journal of Ecology* 74:925-936.

Percival, I. 1989 Chaos: a science for the real world. *New Scientist* 124:42-47.

Perry, J.N. 1995 Spatial analysis by distance indices. *Journal of Animal Ecology* 64:303-314.

Pet, G. & Garretsen, F. 1983 Genetic and environmental factors influencing seed size of tomato (*Lycopersican esculentum* mill.) and the effect of seed size on growth and development of tomato plants. *Euphytica* 32:711-718.

Phillips, D.L. & MacMahon, J.A. 1981 Competition and spacing patterns in desert shrubs. *Journal of Ecology* 69:97-115.

Pielou, E.C. 1960 A single mechanism to account for regular, random and aggregated populations. *Journal of Ecology* 48:575-584.

Pimm, S.L. & Hyman, J.B. 1987 Ecological stability in the context of multispecies fisheries. *Canadian Journal of Fisheries and Aquatic Sciences* 44 suppl. 2:84-94.

Pons, T.L. 1992 Seed response to light. In: *Seeds - the ecology of regeneration in plant communities* ed. Fenner, M. pp. 259-284. CAB International, Wallingford, UK.

Pool, R. 1989a Is it chaos, or is it just noise? *Science* 243:25-28.

Pool, R. 1989b Ecologists flirt with chaos. *Science* 243:310-313.

Power, M.E. 1992 Top-down and bottom-up forces in food webs - do plants have primacy? *Ecology* 73:733-746.

Procaccia, I. 1988 Complex or just complicated? *Nature* 333:498-499.

Pyke, K.A. & Hedley, C.L. 1983 The effect of foliage phenotype and seed size on the crop growth of *Pisum Sativum* (L). *Euphytica* 32:193-203.

Qi, A.-S., Zheng, X., Du, C.-Y. & An, B.-S. 1993 A cellular automaton model of cancerous growth. *Journal of Theoretical Biology* 161:1-12.

Rabinowitz, D. 1979 Bimodal distributions of seedling weight in relation to density of *Festuca paradoxa* Desv. *Nature* 277:297-298.

Rand, D.A., Keeling, M. & Wilson, H.B. 1995 Invasion, stability and evolution to criticality in spatially extended, artificial host-pathogen ecologies. *Proceedings of the Royal Society of London* B 259:55-63.

Rand, D.A. & Wilson, H.B. 1991a Chaotic stochasticity: a ubiquitous source of unpredicatability in epidemics. *Proceedings of the Royal Society of London* B 246:179-184.

Rand, D.A. & Wilson, H.B. 1991b Detecting chaos: a critique of the Sugihara-May approach to time-series analysis. *Warwick preprint.*

Rand, D.A. & Wilson, H.B. 1995 Using spatio-temporal chaos and intermediate scale determinism in artificial ecologies to quantify spatially extended ecosystems. *Proceedings of the Royal Society of London* B 259:111-117.

Rand, D.A., Wilson, H.B. & McGlade, J.M. 1994 Dynamics and evolution - evolutionarily stable attractors, invasion exponents and phenotype dynamics. *Philosophical Transactions of the Royal Society of London* B 343:261-283.

Rapp, P.E. 1993 Chaos in the neurosciences: cautionary tales from the frontier. *The Biologist* 40:89-94.

Raynal, D.J. & Bazzaz, F.A. 1975 Interference of winter annuals with *Ambrosia artemisiifolia* in early successional fields. *Ecology* 56:35-49.

Reddy, P.N., Reddy, K.N., Rao, S.K. & Singh, S.P. 1989 Effect of seed size on qualitative traits in soybean (*Glycine* max (L.) Merrill). *Seed Science and Technology* 17:289-295.

Rees, M. & Crawley, M.J. 1991 Do plant populations cycle? *Functional Ecology* 5:580-582.

Reeve, J.D. 1990 Stability, variability, and persistence in host-parasitoid systems. *Ecology* 71:422-426.

Reise, K. 1991 Mosaic cycles in the marine benthos. In: *The mosaic-cycle concept of ecosystems* ed. Remmert, H. pp. 61-82. *Springer Ecological Studies* Vol. 85, New York.

g Remmert, H. 1985 Was geschieht in Klimax-Stadium? Ökologisches Gleichgewicht durch Mosaik aus desynchronen Zyklen. *Naturwissenschaften* 72:505-512.

Remmert, H. 1991 The mosaic-cycle concept of ecosystems - an overview. In: *The mosaic-cycle concept of ecosystems* ed. Remmert, H. pp. 1-21. *Springer Ecological Studies* Vol. 85, New York.

Renshaw, E. 1984 Competition experiments for light in a plant monoculture: an analysis based on two-dimensional spectra. *Biometrics* 40:717-728.

Renshaw, E. 1994 Chaos in biometry. *IMA Journal of Mathematics Applied in Medicine and Biology* 11:17-44.

Ricklefs, R.E. 1990 Scaling pattern and process in marine ecosystems. In: *Large patterns, marine processes, ecosystems and yield* ed. Sherman, K., Alexander, L.M. & Gold, B.D. American Association for the Advancement of Science, Washington.

Ripley, B.D. 1977 Modelling spatial patterns. *Journal of the Royal Statistical Society* B 39:172-212.

Robertson, G.P., Crum, J.R. & Ellis, B.G. 1993 The spatial variability of soil resources following long-term disturbance. *Oecologia* 96:451-456.

Robertson, G.P., Huston, M.A., Evans, F.C. & Tiedje, J.M. 1988 Spatial variability in a suc-

cessional plant community: patterns of nitrogen availability. *Ecology* 69:1517-1524.

Robinson, J.V. & Edgemon 1988 An experimental evaluation of the effect of invasion history on community structure. *Ecology* 69:1410-1417.

Rohlf, F.J. & Davenport, D. 1969 Simulation of simple models of animal behavior with a digital computer. *Journal of Theoretical Biology* 23:400-425.

Rosanov, Y.A. 1977 *Probability theory: a concise course.* Dover, New York.

Rothe, F. 1976 Convergence to the equilibrium state in the Volterra-Lotka diffusion equations. *Journal of Mathematical Biology* 3:319-324.

Rothery, P., Moss, R. & Watson, A. 1984 General properties of predictive population models in red grouse *Lagopus lagopus scoticus*. *Oecologia* 62:382-386.

Roux, J.C., Rossi, A., Bachelart, S. & Vidal, C. 1981 Experimental observations of complex dynamical behaviour during a chemical reaction. *Physica* 2D:395-403.

Ruxton, G.D. 1995 Temporal scales and the occurrence of chaos in coupled populations. *Trends in Evolution and Ecology* 10:141-143.

Salisbury, E. 1930 Mortality amongst plants and its bearing on natural selection. *Nature* 125:817.

s Salisbury, E.J. 1942 *The reproductive capacity of plants.* London.

Salisbury, E. 1974 Seed size and mass in relation to environment. *Proceedings of the Royal Society of London* B 186:83-88.

Salski, A. 1992 Fuzzy-based models in ecological research. *Ecological Modelling* 63:103-112.

Sano, M. & Sawada, Y. 1985 Measurement of the Lyapunov spectrum from a chaotic time series. *Physics Review Letters* 55:1082-1085.

Satō, K., Matsuda, H. & Sasaki, A. 1994 Pathogen invasion and host extinction in lattice structured populations. *Journal of Mathematical Biology* 32:251-268.

Savić, D. 1995 Model of pattern formation in animal coatings. *Journal of Theoretical Biology* 172:299-303.

Sawyer, S. 1979 A limit theorem for patch sizes in a selectively-neutral migration model. *Journal of Applied Probability* 16:482-495.

Schaffer, W.M. 1984 Stretching and folding in lynx fur returns: evidence for a strange attractor in nature? *American Naturalist* 124:798-820.

Schaffer, W.M. 1985a Order and chaos in ecological systems. *Ecology* 66:93-106.

Schaffer, W.M. 1985b Can nonlinear dynamics elucidate mechanism in ecology and epidemiology. *IMA Journal of Mathematics Applied in Medicine and Biology* 2:221-252.

Schaffer, W.M. & Kot, M. 1985 Nearly one-dimensional dynamics in an epidemic. *Journal of Theoretical Biology* 112:403-427.

Schindler, D.W. & Holling, C.S. 1992 Biodiversity in the functioning of boreal shield ecosystems. Stockholm, The Beijer International Institute of Ecological Economics, second conference on the ecology and economics of biodiversity loss.

Schmid, B. 1986 Spatial dynamics and integration within clones of grassland perennials with different growth forms. *Proceedings of the Royal Society of London* B 228:173-186.

Schmitt, J., Ehrhardt, D.W. & Cheo, M. 1986 Light-dependent dominance and suppression in experimental radish populations. *Ecology* 67:1502-1507.

Schmitt, J., Eccleston, J. & Ehrhardt, D.W. 1987 Dominance and suppression, size-dependent growth and self-thinning in a natural *Impatiens capiensis* population. *Journal of Ecology* 75:651-665.

Segel, L.A. & Jackson, J.L. 1972 Dissipative structure: an explanation and an ecological example. *Journal of Theoretical Biology* 37:545-559.

Seiwa, K. & Kikuzawa, K. 1991 Phenology of tree seedlings in relation to seed size. *Canadian Journal of Botany* 69:532-538.

Sexton, P.J., White, J.W. & Boote, K.J. 1994 Yield-determining processes in relation to cultivar seed size of common bean. *Crop Science* 34:84-91.

Shalev, E., Klafter, J., Plusquellic, D.F. & Pratt, D.W. 1992 Scaling properties of molecular spectra. *Physica* 191A:186-189.

Shanmuganathan, V. & Benjamin, L.R. 1992 The influence of sowing depth and seed size on seedling emergence time and relative growth rate in spring cabbage (*Brassica Oleraceae* var. Capitata L.). *Annals of Botany* 69:273-276.

Shigesada, N., Kawasaki, K. & Teramoto, E. 1979 Spatial segregation of interacting species. *Journal of Theoretical Biology* 79:83-99.

Shigesada, N. & Roughgarden, J. 1982 The role of rapid dispersal in the population dynamics of competition. *Theoretical Population Biology* 21:353-372.

a Shipley, B. & Parent, M. 1991 Germination responses of 64 wetland species in relation to seed size, minimum time to reproduction and seedling relative growth rate. *Functional Ecology* 5:111-118.

Shorrocks, B. 1991 A need for niches? Letter to the editor. *Trends in Evolution and Ecology* 6:262-263.

Sidorowich, J.J. 1992 Repellors attract attention. *Nature* 355:583-585.

Sieburg, H.B., McCutchan, J.A., Clay, O.K., Cabelerro, L. & Ostlund, J.J. 1990 Simulation of HIV infection in artificial immune systems. *Physica* D 45:208-227.

Silander, J.A. & Pacala, S.W. 1985 Neighbourhood predictors of plant performance. *Oecologia* 66:256-302.

Silander, J.A. & Pacala, S.W. 1990 The application of plant population dynamic models to understanding plant competition. In: *Perspectives on plant competition.* ed. Grace, J.B. & Tilman, D. pp. 67-91. Academic Press, San Diego.

Silberschmidt, V.V. 1993 On the multifractal character of load distribution near the cracks. *Europhysics Letters* 23:593-598.

Silvertown 1988 The demographic and evolutionary consequences of seed dormancy. In: *Plant population ecology* ed. Davy, A.J., Hutchings, M.J. & Watkinson, A.R. pp. 205-219. Blackwell Scientific Publications, Oxford.

Silvertown, J., Holtier, S., Johnson, J. & Dale, P. 1992 Cellular automaton models of interspecific competition for space - the effect of pattern on process. *Journal of Ecology* 80:527-534.

Simberloff, D. 1979 Nearest neighbour assessments of spatial configurations of circles rather than points. *Ecology* 60:679-685.

Sinclair, D.F. 1985 On tests of spatial randomness using mean nearest neighbor distance. *Ecology* 66:1084-1085.

Singh, A.R. & Makne, V.G. 1985 Correlation studies on seed viability and seedling vigor in relation to seed size in *Sorghum (Sorghum bicolor). Seed Science and Technology* 13:139-142.

a Singh, K. 1992 Effect of seed size and seed rate on growth and yield of potato *(Solanum tuberosum)* in hills. *Indian Journal of Agronomy* 37:506-509.

Skellam, J.G. 1951 Random dispersal in theoretical populations. *Biometrika* 38:196-218.

Slatkin, M. 1974 Competition and regional coexistence. *Ecology* 55:128-134.

Slatkin, M. & Anderson, D.J. 1984 A model of competition for space. *Ecology* 65:1840-1845.

Smith, L.A. 1994 Local optimal prediction: exploiting strangeness and the variation of sensitivity to initial condition. *Philosophical Transactions of the Royal Society of London* A 348:371-381.

Smith, S.A., Watt, R.C. & Hameroff, S.R. 1984 Cellular automata in cytoskeletal lattices. *Physica* 10D:168-174.

Smith, T.M. & Goodman, P.S. 1986 The effect of competition on the structure and dynamics of acacia savannas in Southern Africa. *Journal of Ecology* 74:1031-1044.

Solé, R.V. & Bascompte, J. 1993 Chaotic Turing structures. *Physics Letters* A 179:325-331.

Solé, R.V. & Bascompte, J. 1994 Measuring chaos from spatial information. *Manuscript.*

Solé, R.V., Bascompte, J. & Valls, J. 1992a Nonequilibrium dynamics in lattice ecosystems: chaotic stability and dissipative structures. *Chaos* 2:387-395.

Solé, R.V., Lopez, D., Ginovart, M. & Valls, J. 1992b Self-organised criticality in Monte Carlo simulated ecosystems. *Physics Letters* A 172:56-61.

Solé, R.V. & Manrubia, S.C. 1995 Are rainforests self-organized in a critical state? *Journal of Theoretical Biology* 173:31-40.

Solé, R.V., Manrubia, S.C. & Luque, B. 1994 Multifractals in rainforest ecosystems - modelling and simulation. *IFIP Transactions* A 41:397-407.

Solé, R.V. & Valls, J. 1991 Order and chaos in a 2D Lotka-Volterra coupled map lattice. *Physics Letters* A 153:330-336.

Solé, R.V. & Valls, J. 1992a On structural stability and chaos in biological systems. *Journal of Theoretical Biology* 155:87-102.

Solé, R.V. & Valls, J. 1992b Nonlinear phenomena and chaos in a Monte Carlo simulated microbial system. *Bulletin of Mathematical Biology* 54:939-955.

Solé, R.V., Valls, J. & Bascompte, J. 1992c Spiral waves, chaos and multiple attractors in lattice models of interacting populations. *Physics Letters* A 166:123-128.

a Spilde, L.A. 1989 Influence of seed size and test weight on several agronomic traits of barley and hard red spring wheat. *Journal of Production Agriculture* 2:169-172.

Stamp. N.E. 1990 Production and effect of seed size in a grassland annual (*Erodium Brachycarpum*, Geraniaceae). *American Journal of Botany* 77:874-882.

Stanley, H.E. & Meakin, P. 1988 Multifractal phenomena in physics and chemistry. *Nature* 335:405-409.

Stanton, M.L. 1984 Seed variation in wild radish: effect of seed size on components of seedling and adult fitness. *Ecology* 65:1105-1112.

Stauffer, D. 1991 Computer simulations of cellular automata. *Journal of Physics* 24A:909-927.

Steele, J.H. & Henderson, E.W. 1994 Coupling between physical and biological scales. *Philosophical Transactions of the Royal Society of London* B 343:5-9.

Sterner, R.W., Ribic, C.A. & Schatz, G.E. 1986 Testing for life historical changes in spatial patterns of four tropical tree species. *Journal of Ecology* 74:621-633.

Stewart, I. 1989a *Does God play dice? The new mathematics of chaos.* Penguin, London.

Stewart, I. 1989b Portraits of chaos. *New Scientist* 124:42-47.

Stewart, I. 1995 Four encounters with Sierpiński's gasket. *The Mathematical Intelligencer* 17:52-64.

Stock, W.D., Pate, J.S. & Delfs, J. 1990 Influence of seed size and quality on seedling development under low nutrient conditions in five Australian and South African members of the Proteaceae. *Journal of Ecology* 78:1005-1020.

a Stoll, P., Weiner, J. & Schmid, B. 1994 Growth variation in a naturally established popu-

lation of *Pinus sylvestris*. *Ecology* 75:660-670.

Sugihara, G., Grenfell, B. & May, R.M. 1990 Distinguishing error from chaos in ecological time series. *Philosophical Transactions of the Royal Society of London* B 330:235-251.

Sugihara, G. & May, R.M. 1991 Nonlinear forecasting as a way of distinguishing chaos from measurement error in time series. *Nature* 344:734-741.

Sung, F.J.M. 1992 Field emergence of edible soybean seeds differing in seed size and emergence strength. *Seed Science and Technology* 20:527-532.

a Sutherland, R.A. & Benjamin, L.R. 1993 The influence of the arrangement of neighbours on the spatial components of resource capture by an individual plant in even-aged monocultures. *Annals of Botany* 71:131-134.

Swindale, N.V. 1980 A model for the formation of ocular dominance stripes. *Proceedings of the Royal Society of London* B 208:243-264.

Symonides, E. 1988 Population dynamics of annual plants. In: *Plant population ecology* ed. Davy, A.J., Hutchings, M.J. & Watkinson, A.R. pp. 221-248. Blackwell Scientific Publications, Oxford.

Takahashi, S. 1990 Cellular automata and multifractals: dimension spectra of linear cellular automata. *Physica* 45D:36-48.

Taylor, A.D. 1990 Metapopulations, dispersal, and predator-prey dynamics: an overview. *Ecology* 71:429-433.

Tekrony, D.M., Bustamam, T., Egli, D.B. & Pfeiffer, T.W. 1987 Effects of soybean seed size, vigor and maturity on crop performance in row and hill plots. *Crop Science* 27:1040-1045.

Thiéry, J.M., D'Herbès, J.-M. & Valentin, C. 1995 A model simulating the genesis of banded vegetation patterns in Niger. *Journal of Ecology* 83:497-507.

Thomas, M. 1951 Some tests for randomness in plant populations. *Biometrika* 38:102-111.

Thomas, S.C. & Weiner, J. 1989a Including competitive asymmetry in measures of local interference in plant populations. *Oecologia* 80:349-355.

Thomas, S.C. & Weiner, J. 1989b Growth, death and size distribution change in an *Impatiens Pallida* population. *Journal of Ecology* 77:524-536.

Thomas, W.R., Pomerantz, M.J. & Gilpin, G.E. 1980 Chaos, asymmetric growth and group selection for dynamical stability. *Ecology* 61:1312-1320.

a Thompson, B.K., Weiner, J. & Warwick, S.I. 1991 Size-dependent reproductive output in agricultural weeds. *Canadian Journal of Botany* 69:442-446.

a Thompson, K., Band, S.R. & Hodgson, J.G. 1993 Seed size and shape predict persistence in soil. *Functional Ecology* 7:236-241.

a Thrall, P.H., Pacala, S.W. & Silander, J.A. 1989 Oscillatory dynamics in populations of an annual weed species *Abutilon theophrasti*. *Journal of Ecology* 77:1135-1149.

Tilman, D. 1990 Mechanisms of plant competition for nutrients: the elements of a predictive theory of competition. In: *Perspectives on plant competition.* ed. Grace, J.B. & Tilman, D. pp. 117-141. Academic Press, San Diego.

Tilman, D. 1994 Competition and biodiversity in spatially structured habitats. *Ecology* 75:2-16.

Tilman, D. & Wedin, D. 1991a Plant traits and resource reduction for five grasses growing on a nitrogen gradient. *Ecology* 72:685-700.

Tilman, D. & Wedin, D. 1991b Oscillations and choas in the dynamics of a perennial grass. *Nature* 353:653-655.

Tinius, C.N., Burton, J.W. & Carter, T.E. 1991 Recurrent selection for seed size in soybean. 1. Response to selection in replicate populations. *Crop Science* 31:1137-1141.

Tinius, C.N., Burton, J.W. & Carter, T.E. 1992 Recurrent selection for seed size in soybean. 2. Indirect effects on seed growth rate. *Crop Science* 32:104-112.

a Tinius, C.N., Burton, J.W. & Carter, T.E. 1993 Recurrent selection for seed size in soybean. 3. Indirect effects on seed composition. *Crop Science* 33:959-962.

Tollenaar, H. 1992 Reinterpretation and evaluation of some simple descriptive models for weed-crop interference in terms of one-sided and two-sided competition. *Oikos* 65:256-264.

Tsonis, A.A., Elsner, J.B. & Tsonis, P.A. 1989 On the dynamics of a forced reaction-diffusion model for biological pattern formation. *Proceedings of the National Academy of Science USA* 86:4938-4942.

Turchin, P. & Taylor, A.D. 1992 Complex dynamics in ecological time series. *Ecology* 73:289-305.

Turing, A.M. 1952 The chemical basis of morphogenesis. *Philosophical Transactions of the Royal Society of London* B 237:37-72.

Turner, M.D. & Rabinowitz, D. 1983 Factors affecting frequency distribution of plant mass: the absence of dominance and suppression in competing monocultures of *Festuca paradoxa*. *Ecology* 64:469-475.

U.C.P.E., 1995 *Report of the Unit of Comparative Plant Ecology 1992-94.* NERC Publishing Services, Swindon.

Vail, S.G. 1993 Scale-dependent responses to resource spatial pattern in simple-models of consumer movements. *American Naturalist* 141:199-216.

Vance, R.R. 1980 The effect of dispersal on population size in a temporally varying environment. *Theoretical Population Biology* 18:343-362.

van Tongeren, O. & Prentice, I.C. 1986 A spatial simulation model for vegetation dynamics. *Vegetatio* 65:163-173.

a Venable, D.L. 1986 Dormancy, dispersal and the evolution of seed size. *American Journal of Botany* 73:659.

a Venable, D.L. 1987 The evolutionary ecology of seed banks - fitness interactions with dispersal and seed size as adaptations for reducing risk.

Vicsek, T. 1990 Mass multifractals. *Physica* 168A:490-497.

Vicsek, T. & Szalay, A.S. 1987 Fractal distribution of galaxies modelled by a cellular-automaton-type stochastic process. *Physics Review Letters* 58:2818-2821.

Villa, F. 1992 New computer architectures as tools for ecological thought. *Trends in Evolution and Ecology* 7:179-183.

Volterra, V. 1926 Fluctuations in the abundance of a species considered mathematically. *Nature* 118:558-560.

Waddington, C.H. & Cowe, R.J. 1969 Computer simulation of a molluscan pigmentation pattern. *Journal of Theoretical Biology* 25:219-225.

Waller, D.M. 1981 Neighbourhood competition in several violet populations. *Oecologia* 51:116-122.

Waller, D.M. 1985 The genesis of size hierarchies in seedling populations of *Impatiens capiensis* Meerb. *New Phytologist* 100:243-260.

Watkinson, A.R. 1980a Density-dependence in single-species populations of plants. *Journal of Theoretical Biology* 83:345-357.

Watkinson, A.R. 1980b Factors affecting the density response of *Vulpia fasciculata*. *Journal of Ecology* 70:149-161.

Watkinson, A.R., Lonsdale, W.M. & Firbank, L.G. 1983 A neighbourhood approach to self-thinning. *Oecologia* 56:381-384.

Watson, A. 1968 Social status and population control in the red grouse. *Proceedings of the Royal Society of Medicine* 61:161.

Watson, A. 1985 Social class, socially-induced loss, recruitment and breeding of red grouse. *Oecologia* 67:493-498.

Watson, A. & Jenkins, D. 1968 Experiments on population control by territorial behaviour in red grouse. *Journal of Animal Ecology* 37:595-614.

Watson, A. & Miller, G.R. 1971 Territory size and aggression in a fluctuating red grouse population. *Journal of Animal Ecology* 40:367-383.

Watson, A. & Moss, R. 1972 A current model of population dynamics in red grouse. *Proceedings of the International Ornithological Congress* 15:134-149.

Watson, A. & Moss, R. 1980 Advances in our understanding of the population dynamics of red grouse from a recent fluctuation in numbers. *Ardea* 68:103-111.

Watson, A. & Moss, R. 1989 Spacing behaviour and winter loss in red grouse. In: *Red grouse population processes* ed. Lance, A.N. & Lawton, J.H. pp. 35-52. Sandy: Royal Society for the Protection of Birds.

Watson, A., Moss, R., Parr, R., Trenholm, I.B. & Robertson, A. 1988 Preventing a population decline of red grouse *Lagopus lagopus scoticus* by manipulating density. *Experientia* 44:274-275.

Watson, A., Moss, R., Rothery, P. & Parr, R. 1984 Demographic causes and predictive models of population fluctuations in red grouse. *Journal of Animal Ecology* 53:639-662.

Watson, A., Moss, R., Parr, R., Mountford, M.D. & Rothery, P. 1994 Kin landownership, differential aggression between kin and non-kin, and population fluctuations in red grouse. *Journal of Animal Ecology* 63:39-50.

Watt, A.S. 1947 Pattern and process in the plant community. *Journal of Ecology* 35:1-22.

Weiner, J. 1982 A neighbourhood model of annual-plant interference. *Ecology* 63:1237-1241.

Weiner, J. 1984 Neighbourhood interference amongst *Pinus Rigida* individuals. *Journal of Ecology* 72:183-195.

Weiner, J. 1985 Size hierarchies in experimental populations of annual plants. *Ecology* 66:743-752.

Weiner, J. 1986 How competition for light and nutrients affects size variability in *Ipomoea tricolor* populations. *Ecology* 67:1425-1427.

Weiner, J. 1988 Variation in the performance of individuals in plant populations. In: *Plant Population Ecology* ed. Davy, A.J., Hutchings, M.J. & Watkinson, A.R. pp. 59-81. Blackwell Scientific Publications, Oxford.

Weiner, J. 1990 Asymmetric competition in plant populations. *Trends in Evolution and Ecology* 5:360-364.

a Weiner, J. 1993 Competition, herbivory and plant size variability: *Hypochaeris radicata* grazed by snails (*Helix aspersa*). *Functional Ecology* 7:47-53.

Weiner, J. 1995 On the practice of ecology. *Journal of Ecology* 83:153-158.

Weiner, J., Berntson, G.M. & Thomas, S.C. 1990a Competition and growth form in a woodland annual. *Journal of Ecology* 78:459-469.

Weiner, J. & Conte, P.T. 1981 Dispersal and neighbourhood effects in an annual plant competition model. *Ecological Modelling* 13:131-147.

a Weiner, J. & Fishman, L. 1994 Competition and allometry in *Kochia scoparia*. *Annals of Botany* 73:263-271.

a Weiner, J., Mallory, E.B. & Kennedy, C. 1990b Growth and variability in crowded and uncrowded populations of dwarf marigolds *(Tagetes patula)*. *Annals of Botany* 65:513-524.

Weiner, J. & Solbrig, O.T. 1984 The meaning and measurement of size hierarchies in plant populations. *Oecologia* 61:334-336.

Weiner, J. & Thomas, S.C. 1986 Size variability and competition in plant monocultures. *Oikos* 47:211-222.

a Weiner, J. & Thomas, S.C. 1992 Competition and allometry in three species of annual plants. *Ecology* 73:648-656.

Weiner, J. & Whigham, D.F. 1988 Size variability and self-thinning in wild rice *(Zizania aquatica). American Journal of Botany* 75:445-458.

Welch, W.J. 1993 How cells respond to stress. *Scientific American* 268:34-41.

Westoby, M. 1977 Self-thinning driven by leaf area not by weight. *Nature* 265:330-331.

Westoby, M. 1984 The self-thinning rule. *Advances in Ecological Research* 14:167-225.

Westoby, M., Rice, B. & Howell, J. 1990 Seed size and plant growth as factors in dispersal spectra. *Ecology* 71:1307-1315.

a White, J.W. & Gonzales, A. 1990 Characterization of the negative association between seed yield and seed size among genotypes of common bean. *Field Crops Research* 23:159-176.

White, J.W., Singh, S.P., Pino, C., Rios, M.J. & Buddenhagen, I. 1992 Effects of seed size and photoperiod response on crop growth and yield of common bean. *Field Crops Research* 28:295-307.

Whittaker, R.H. & Levin, S.A. 1977 The role of mosaic phenomena in natural communities. *Theoretical Population Biology* 12:117-139.

Wiens, J.A. 1989 Spatial scaling in ecology. *Functional Ecology* 3:385-397.

Williams, J. 1985 Statistical analysis of fluctuations in red grouse bag data. *Oecologia* 65:269-272.

Willson, M.F. 1992 The ecology of seed dispersal. In: *Seeds - the ecology of regeneration in plant communities* ed. Fenner, M. pp. 61-85. CAB International, Wallingford, UK.

Wilson, D.S. 1992 Complex interactions in metacommunities, with implications for biodiversity and higher levels of selection. *Ecology* 73:1984-2000.

Wilson, H.B. 1994 Applications of dynamical systems in ecology. Doctoral thesis, University of Warwick.

Wilson, H.B. & Rand, D.A. 1993 Detecting chaos in a noisy time series. *Proceedings of the Royal Society of London* B 253:239-244.

Wilson, J.B. 1988 The effect of initial advantage on the course of plant competition. *Oikos* 51:19-24.

Wilson, W.G., DeRoos, A.M. & McCauley, E. 1993 Spatial instabilities within the diffusive Lotka-Volterra system: individual-based simulation results. *Theoretical Population Biology* 43:91-127.

Winfree, A.T. 1974 Rotating chemical reactions. *Scientific American* 230:82-95.

Winn, A.A. 1988 Ecological and evolutionary consequences of seed size in *Prunella vulgaris*. *Ecology* 69:1537-1544.

Wissel, C. 1991 A model for the mosaic-cycle concept. In: *The mosaic-cycle concept of ecosystems* ed. Remmert, H. pp. 22-45. *Springer Ecological Studies* Vol. 85, New York.

Wissel, C. 1992a Modelling the mosaic cycle of a middle European beech forest. *Ecological Modelling* 63:29-43.

Wissel, C. 1992b Aims and limits of ecological modelling exemplified by island theory. *Ecological Modelling* 63:1-12.

Wixley, R.A.J. 1983 An elliptical zone of influence model for uneven-aged row crops. *Annals*

of Botany 51:77-84.

Wolf, A., Swift, J.B., Swinney, H.L. & Vastano, J.A. 1985 Determining Lyapunov exponents from time series. *Physica* 16D:285-317.

Wolfram, S. 1983 Statistical mechanics of cellular automata. *Reviews of Modern Physics* 55:601-644.

Wolfram, S. 1984a Universality and complexity of cellular automata. *Physica* 10D:1-35.

Wolfram, S. 1984b Cellular automata as models of complexity. *Nature* 311:419-424.

Wolfram, S. 1986 *Theory and applications of cellular automata.* Advanced series on complex systems Vol. 1, World Scientific, Singapore

Wu, H.-I., Sharpe, P.J.H., Walker, J. & Penridge, L.K. 1985 Ecological field theory: a spatial analysis of resource interference among plants. *Ecological Modelling* 29:215-243.

a Yakowitz, S., Gani, J. & Hayes, R. 1990 Cellular automaton modeling of epidemics. *Applied Mathematics and Computation* 40:41-54.

Yorke, J. 1989 In: Pool, R. Chaos theory: how big an advance? *Science* 243:26-28.

Zaikin, A.N. & Zhabotinsky, A.M. 1970 Concentration wave propagation in two-dimensional liquid-phase self-oscillating system. *Nature* 225:535-537.

a Zammit, C. & Zedler, P.H. 1990 Seed yield, seed size and germination behavior in the annual *Pogoyne abramsii*. *Oecologia* 84:24-28.

Zeigler, B.P. 1977 Persistence and patchiness of predator-prey systems induced by discrete event population exchange mechanisms. *Journal of Theoretical Biology* 67:687-713.

Zeng, X., Eykholt, R. & Pielke, R.A. 1991 Estimating the Lyapunov-exponent spectrum from short time series of low precision. *Physics Review Letters* 66:3229-3232.

a Zhang, J. & Maun, M.A. 1990 Seed size variation and its effects on seedling growth in *Agropyron psammophilum*. *Botanical Gazette* 151:106-113.

University of Warwick Guide to examinations for higher degree by research.

(*a* abstract only)

(*f* in French)

(*g* in German)

(*s* secondary source only)